

STRESS ANALYSIS OF STEAM TURBINE BLADE DURING START-UP

A PROJECT REPORT

SUBMITTED IN PARTIAL FULFILLMENT OF THE
REQUIREMENTS FOR THE AWARD OF THE DEGREE
OF

MASTER OF

TECHNOLOGY IN

COMPUTATIONAL DESIGN

Submitted by:

KUNAL POPLI

(2K18/CDN/04)

Under the supervision of

Prof. A K AGRAWAL



DEPARTMENT OF MECHANICAL ENGINEERING

DELHI TECHNOLOGICAL UNIVERSITY

(Formerly Delhi College of

Engineering) Bawana Road, Delhi-

110042

JUNE, 2020

CANDIDATE'S DECLARATION

I, Kunal Popli, Roll No. - 2K18/CDN/04 student of M.Tech (Computational Design), hereby declare that the project dissertation titled “Stress Analysis of Steam Turbine Blade during a Start-Up” which is submitted by us to the Department of Mechanical Engineering, Delhi Technological University, Delhi in partial fulfillment of the requirement for the award of the degree of Master of Technology, is original and not copied from any source without proper citation. This work has not previously formed the basis for the award of any degree, diploma associateship, fellowship or other similar title or recognition.

Place: New Delhi

Date: 30/06/2020

Kunal Popli

(2K18/CDN/04)

CERTIFICATE

I hereby certify that the Project Dissertation titled “Stress Analysis of Steam Turbine Blade during a Start-Up” which was submitted by Kunal Popli, Roll No.- 2K18/CDN/04, Department of Mechanical Engineering, Delhi Technological University, New Delhi in partial fulfillment of the requirement for the award of the degree of Master of Technology, is a record of the project carried out by the student under my supervision. To the best of my knowledge this work has not been submitted in part or full for any Degree or Diploma in this University or elsewhere.

Place: Delhi

Date: 30/06/2020

Dr. A K AGRAWAL

SUPERVISOR

Professor

Department of Mechanical Engineering

Delhi Technological University

ABSTRACT

In this report, we have performed fluid structure interaction (FSI) simulation for a steam turbine blade. Steam turbine blade geometry is created on CAD software with aerofoil shape. Then the geometry is imported into Ansys R18.1 software from CAD software. After this, CFD analysis of the turbine blade is performed with hot steam passing over the blade and cold water passing through the hollow section of the blade for cooling purposes. Thermal load, pressure load and centrifugal load is considered in CFD analysis. After the CFD analysis, FEA analysis is performed for the same geometry. Pressure load, thermal load, centrifugal load and gravitational load are considered in FEA analysis. Pressure load and thermal load are extracted from CFD software to FEA software. Von mises stress and deformation of the blade are obtained as results from FEA analysis. This entire FSI analysis is performed on turbine blade for two operating conditions of turbine, namely, steady state and transient state (start-up). After obtaining FSI results for both the analysis, results are compared and conclusions are made.

ACKNOWLEDGEMENT

The efficient and effective completion of the project is unfinished without giving the acknowledgement to everyone who made it feasible and the person whose guidance and support was very crucial.

I owe a lot to my supervisor, Dr. Atul Kumar Agrawal, Professor, Department of Mechanical Engineering, for supporting and guiding to explore the depth in the search of knowledge and creativity. I would like to thank him for all the assistance and being a source of motivation whenever needed.

I am obliged to everyone who directly or indirectly lent his/her support for successful completion the task. I would like to thank the Department of Mechanical Engineering for providing us advanced computational lab facilities for producing efficient work.

In the end, I thank my parents for always being supportive.

CONTENTS

Candidate's Declaration	ii
Certificate	iii
Acknowledgement	iv
Abstract	v
Contents	vi
List of Tables	vii
List of Figures	viii
List of Symbols, abbreviations	ix
CHAPTER 1 INTRODUCTION	1
1.1 Steam Turbine	2
1.2 Turbine Blade	3
1.3 Computational Fluid Dynamics and Finite Element Analysis	5
1.3.1 Computational Fluid Dynamics	5
1.3.2 Finite Element Analysis	6
CHAPTER 2 LITERATURE REVIEW	8
2.1 Studies on Operating Conditions	8
2.2 Studies on Failure Modes and Transient Analysis	10
2.3 Motivation	24
CHAPTER 3 STEDAY STATE FSI ANALYSIS	26
3.1 Steady State Condition	26
3.2 Types of Stress	27
3.3 Types of Failure	29
3.4 Turbine Cooling	31
3.5 FSI Simulation	32
3.5.1 Methodology	34
3.5.2 Problem Formulation	36
3.5.3 CAD Model	36
3.5.4 Meshing	40
3.5.5 CFD Analysis	41

3.5.5.1	Methodology	41
3.5.5.2	Setup	42
3.5.5.3	Solution	44
3.5.5.4	Results	47
3.5.6	FEA Analysis	52
3.5.6.1	Methodology	52
3.5.6.2	Engineering Data	53
3.5.6.3	Geometry	53
3.5.6.4	Model	54
3.5.6.5	Setup	55
3.5.6.6	Solution and Results	57
CHAPTER 4 TRANSIENT FSI ANALYSIS		67
4.1	Transient Condition	67
4.2	Start-up	68
4.3	Types of Stress	70
4.4	Types of Damage	72
4.5	FSI Simulation	73
4.5.1	Meshing	74
4.5.2	CFD Analysis	75
4.5.2.1	Setup	75
4.5.2.2	Solution	77
4.5.2.3	Results	80
4.5.3	FEA Analysis	85
4.5.3.1	Methodology	85
4.5.3.2	Setup	86
4.5.3.3	Solution and Results	87
4.5.3.3.1	At t = 108s	90
4.5.3.3.2	At t = 1080 s	91
4.5.3.3.3	At t = 4428s	93
4.5.3.3.4	At t = 8100s	94
4.5.3.3.5	At t = 10800s	95
CHAPTER 5 RESULTS		97

5.1	Steady State Analysis	97
5.1.1	CFD Results	98
5.1.2	FEA Results	98
5.2	Transient State Analysis	99
5.2.1	CFD Results	99
5.2.2	FEA Results	99
5.3	Comparison of Results	100
CHAPTER 6 CONCLUSION		102
APPENDIX		106
A.1 PROBLEMS SOLVED ON ANSYS R18.1		106
A.2 PROBLEMS SOLVED AND IMPORTANT CONCEPTS		128
REFERENCES		130

List of Tables

Table no.	Table name	Page no.
4.1	Rotational velocity magnitude for transient analysis	75
4.2	Rotational velocity magnitude for transient analysis	87
4.3	Force reaction vs time	96
4.4	Moment reaction vs time	97
5.1	Total deformation vs time during start-up	101
5.2	Von mises stress vs time during start-up	101
5.3	Maximum force reaction vs time during start-up	102
5.4	Maximum moment reaction vs time during start-up	102
A.1	Problems vs. concepts	128

List of Figures

Figure No.	Figure Name	Page No.
1.1	Block Diagram of a power plant	3
1.2	Velocity triangle of turbine blade	5
1.3	Results obtained on CFD software	6
1.4	Meshing of problem domain	7
2.1	Original enlarged view of blade root and rim interface	13
2.2	Optimized design of the blade root and rim interface	13
2.3	Contour obtained for hollow shaft after structural analysis	15
2.4	Peak stress reduced at root of the blade after design optimization	16
2.5	Maximum von mises stress for blade root at various speeds	18
2.6	Loading cycle for turbine blade	18
2.7	Fully coupled approach	20
2.8	CHT solution approach	20
2.9	Temperature distribution on turbine rotor after unloading	21
2.10	Relative stress and fatigue life contour for a) original and b) optimized blade groove	23
3.1	Block diagram of an ideal turbine	27
3.2	Internal blade cooling	31
3.3	a) Internal convection cooling and b) Internal impingement cooling	32
3.3	c) Discrete film cooling and d) Full blade cooling	32
3.3	e) Full blade transpiration cooling	32
3.4	Methodology of the problem	35
3.5	Problem domain and its components	36
3.6	CAD model of the problem	37
3.7	Cold domain and its properties	37
3.8	Hot domain and its properties	38

3.9	Blade and its properties	38
3.10	CAD model and its properties	39
3.11	Meshing of model	40
3.12	Named selections in geometry	40
3.13	Ansys R18.1 CFX methodology	41
3.14	Inlet and outlet boundary condition for steam	42
3.15	Inlet and outlet boundary condition for cold water	43
3.16	Setup module of the problem	44
3.17	Momentum and mass residuals for cold water	45
3.18	Momentum and mass residuals for steam	45
3.19	Heat transfer for cold water and heat fluid	46
3.20	Turbulence kinetic energy for cold water	46
3.21	Turbulent kinetic energy residuals for steam	47
3.22	Temperature contour upper surface	49
3.23	Temperature contour lower surface	50
3.24	Temperature gradient upper surface	50
3.25	Temperature gradient lower surface	51
3.26	Pressure on upper surface contour	51
3.27	Pressure on lower surface contour	52
3.28	Line location on blade surface in z direction	52
3.29	Pressure vs z curve along z direction on blade surface	53
3.30	Line along x direction on blade surface	53
3.31	Pressure vs chart count along the line in x direction on upper blade surface	54
3.32	Pressure vs chart count along the line in x direction on lower blade surface	54
3.33	Pressure on a plane	55
3.34	Ansys R18.1 Static Structural methodology	56
3.35	Engineering data module	57
3.36	Distributed mass applied to blade	58
3.37	Meshed geometry for FEA analysis	59
3.38	Rotational velocity applied to turbine blade	60

3.39	Fixed boundary condition at cold inlet surface	60
3.40	Pressure on upper surface	61
3.41	Pressure on lower surface	61
3.42	Total deformation contour on blade's upper surface	62
3.43	Total deformation contour on blade's lower surface	63
3.44	Equivalent stress contour on upper surface of blade	63
3.45	Equivalent stress contour on lower surface of blade	64
3.46	Line location along z direction	64
3.47	Stress vs z graph along line in z direction	65
3.40	Force reaction direction and magnitude	65
3.41	Moment reaction direction and magnitude	66
4.1	Start-up curve	70
4.2	Meshed model	74
4.3	Transient blade row model settings	77
4.4	Residual target of mass and momentum for cold water	79
4.5	Residual target of mass and momentum for steam	79
4.6	Residual target of heat transfer for steam and cold water	80
4.7	Residual target of turbulence kinetic energy and turbulence frequency for cold water	80
4.8	Residual target of turbulence kinetic energy and turbulence frequency for steam	81
4.9	Temperature contour on upper surface	82
4.10	Temperature contour on lower surface	82
4.11	Temperature gradient contour on upper surface	83
4.12	Temperature gradient contour on lower surface	83
4.13	Pressure on upper surface contour	84
4.14	Pressure on lower surface contour	84
4.15	Pressure on a plane	85
4.16	Line location on blade surface in z direction	85
4.17	Pressure vs z graph along line in z direction on Upper surface and lower surface	86
4.18	Line location on blade surface in x direction	86

4.19	Pressure vs x graph along line in x direction on Upper surface	87
4.20	Pressure vs x graph along line in x direction on Lower surface	87
4.21	Pressure vs time during start-up	88
4.22	Temperature vs time during start-up	88
4.23	Methodology of FEA analysis	89
4.24	Meshed model for FEA analysis	90
4.25	Graph of rotational velocity for transient analysis	91
4.26	Rotational velocity boundary condition	92
4.27	Pressure on upper surface	92
4.28	Pressure on lower surface	93
4.29	Total deformation contour at $t = 108s$	94
4.30	Equivalent stress on upper surface contour	94
4.31	Equivalent stress contour on lower surface	95
4.32	Line location on upper blade surface in z direction	95
4.33	Stress vs z graph along line in z direction	96
4.34	Force reaction direction and magnitude at remote point	96
4.35	Moment reaction direction and magnitude at remote point	97
4.36	Total deformation contour	97
4.37	Von mises stress contour on upper surface	98
4.38	Von mises stress contour on lower surface	98
4.39	Stress vs z graph along line in z direction	99
4.40	Force reaction direction and magnitude at remote point	99
4.41	Moment reaction direction and magnitude at remote point	100
4.42	Total deformation contour	100
4.43	Von mises stress contour on upper surface	101
4.44	Von mises stress contour on lower surface	101
4.45	Von mises stress vs z graph along line in z direction	102
4.46	Force reaction direction and magnitude	102
4.47	Moment reaction direction and magnitude	103
4.48	Total deformation contour at $t = 8100$	103

4.49	Von mises stress contour on upper surface	104
4.50	Von mises stress contour on lower surface	104
4.51	Von mises stress vs z graph on upper surface	105
4.52	Force reaction direction and magnitude	105
4.53	Moment reaction direction and magnitude	106
4.54	Total deformation contour at $t = 10800$ s	106
4.55	Von mises stress contour on upper surface	107
4.56	Von mises stress contour on lower surface	107
4.57	Von mises stress vs z graph along line in z direction	108
4.58	Force reaction direction and magnitude	108
4.59	Moment reaction direction and magnitude	109
4.60	Von mises stress vs time during start-up	109
A.1	Schematic diagram	106
A.2	Boundary condition	107
A.3	Velocity contour in Y direction	107
A.4	Velocity magnitude vector	107
A.5	Schematic diagram	109
A.6	Pressure contour	109
A.7	Velocity contour	110
A.8	Velocity vector	110
A.9	Velocity profile	111
A.10	Skin friction coefficient along the length of pipe	111
A.11	Schematic diagram	112
A.12	Boundary condition	112
A.13	Meshed model	113
A.14	Velocity vector	113
A.15	Pressure contour	114
A.16	Velocity in Y direction	114
A.17	Normalised velocity in Y direction	115
A.18	Schematic diagram	115
A.19	Meshed model	116
A.20	Mach number vector	116

A.21	Static pressure vs position along axis and nozzle wall	117
A.22	Schematic diagram	117
A.23	Boundary condition	118
A.24	Velocity contour on half cross section of the pipe	118
A.25	Total deformation contour	119
A.26	Total mesh displacement contour	119
A.27	Schematic diagram	120
A.28	Boundary condition	120
A.29	Contour on half cross section of pipe	121
A.30	Pressure contour	121
A.31	Temperature along length of the pipe	122
A.32	Temperature across the cross section	122
A.33	Schematic diagram	123
A.34	Boundary condition	123
A.35	Velocity vector	124
A.36	Velocity along length of pipe	124
A.37	Stream function across the pipe	125
A.38	Schematic diagram	125
A.39	Boundary condition	126
A.40	Meshed model	126
A.41	Pressure contour	127
A.42	Turbulence kinetic energy contour	127
A.43	Velocity contour	128
A.44	Velocity streamline	128

List of Symbols, Abbreviations

Symbol	Interpretation
F	Load (Vertical)
R	Radius
m	Metre
N	Newton
MPa	Mega Pascal
s	Second
mm	Milli Metre
mJ	Milli Joule
FSI	Fluid Structure Interaction
ω	Angular Speed
σ	Stress
ϵ	Strain

CHAPTER 1: INTRODUCTION

In present world, turbine is used in large number of applications; few of them include electricity generation, jet engines, turbochargers, motors etc. Whether the electricity is produced from wind energy, burning fluid, steam or water; it is generated with the help of a turbine [29]. A turbine consists of a shaft passing through centre of the turbine disk. The periphery of the disk is covered with blades. In power plants, this turbine is further connected to a generator for producing electricity. A heated fluid is passed through the turbine at high velocity. The running fluid hits the turbine blades and the turbine starts rotating. At this point, the energy of the fluid is converted into the rotating energy of the turbine, by which the principle of conservation of energy is followed. As the turbine starts rotating, the shaft also starts rotating. The shaft of the turbine is connected to the shaft of a generator. So, the shaft of the generator also rotates and electricity is produced. Hence, the energy of the fluid is exploited to produce electricity.

There are different types of turbines based on different classifications. One category is of axial flow turbine and radial flow turbine. In axial flow turbines, the fluid flow strikes the turbine along the shaft line whereas in radial flow turbines, the fluid flow smoothly moves around the turbine perpendicular to the shaft axis. Another classification of turbines is impulse turbine and reaction turbine. With the increasing demand of electricity at global level, it becomes important to produce more efficient turbines. A fluid flow consists of kinetic energy and pressure energy. The impulse turbine utilizes the kinetic energy of the fluid flow whereas the radial turbine utilizes the pressure energy of the fluid flow [33]. Another type of classification includes pressure compounded turbine, velocity compounded turbine and pressure velocity compounded turbine. This classification is based on the manner in which thermal energy of the fluid is converted into mechanical energy. The pressure compounded turbine splits the pressure in different stages of turbine, velocity compounded turbine splits the velocity in different stages and pressure velocity compounded turbine combines the above two types of turbines. Finally, depending on the

type of applications, the turbines are classified as steam turbine, fluid turbine, water turbine, mercury vapour turbine, screw turbine, wind turbine, bladeless turbine, shroudless turbine, shrouded turbine, ceramic turbine, statorless turbine and contra rotating turbine. The turbine blade that we have analyzed in this report is of a reaction type, single stage, high pressure, axial flow steam turbine.

1.1 STEAM TURBINE

A steam turbine is a turbine operated with steam as fluid. Steam flows through the turbine, by which the turbine rotates so as to produce mechanical energy. In coal power plants, steam turbines are deployed to generate electricity. The modern form of steam turbine was invented by Charles Parsons in 1884 [34]. Modern day steam turbines are used in variety of applications like in mechanical drives for pumps, compressors and shaft driven equipments, electricity generation etc.

Thermodynamically, the steam turbine follows an isentropic expansion process. That is, Expansion of the steam takes place in the process at constant entropy. The assembly of the steam turbine consists of turbine disk, rotor, blades, shaft, casing and nozzle. Firstly, the working fluid, in this case steam passes through a nozzle with increased velocity before striking the blades of the turbine. When the steam hits the turbine blade, it slides over the blade from one end of the blade to another. This sliding action of steam over the blade results in the application of force on blades. Therefore, the blades start rotating and hence the rotor, disk and shaft start rotating. After gliding over the blade, the steam passes through the turbine from exhaust. Now, more the outlet pressure of the steam, lesser will be the turbine efficiency (thermodynamically). Hence, the pressure of the steam at outlet is kept around 0.1 bars in power plants. Also, higher the inlet temperature of the steam, higher will be the efficiency of the turbine (thermodynamically). But, there are some limitations to which the temperature of the inlet steam can be increased.

One of the most important applications of steam turbine is electricity generation in power

plants. Steam turbines are used as prime movers in producing about 80% of world's electricity. Reheaters and regenerators are used in power plants for redistributing steam's enthalpy and use it in a more efficient manner.

The advantage of steam turbine over other internal combustion engines is that it does not have any reciprocating masses. Hence, there is no issue of unbalancing of components. It also means that there will be less wear and tear in steam turbines. Also, since there are no sliding members in steam turbines, there is less friction than other prime movers and engines. In reciprocating engines, the limiting speed is around 300rpm whereas in steam turbines, the limiting speed is around 40000rpm. Lubrication required in steam turbines is very less.

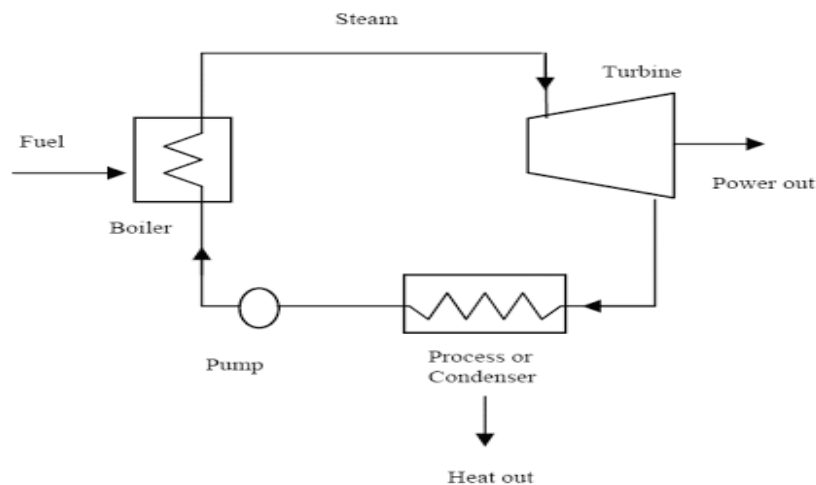


Fig 1.1: Block diagram of a power plant

1.2 TURBINE BLADE

Turbine blade is one of the most important components of a turbine. It is fitted around the periphery of the rotor and also along the axis of the rotor. There are two types of disks, one is the rotor and the other is the stator. The rotor rotates and the stator remains stationary. Both the rotor and stator consists of blades around their periphery. The blades of rotor and

stator are designed differently due to different operation requirements.

During working of steam turbine, the fluid glides along the surface of turbine blades, providing required angular motion to the turbine. In case of steam turbine, high pressure and high temperature steam hits the turbine blades during the operation. This creates high stress conditions for the turbine blade. Hence, reducing its life. This is the reason that the turbine blade is the component that limits the life of the turbine. As we have discussed in section 1.1, as the temperature of inlet steam increase, the thermodynamic efficiency of the steam turbine increases. As the electricity demand is increasing globally, the researchers are continuously looking to increase the efficiency of the steam turbines. With increasing inlet temperature, the stress condition on the turbine blade becomes more severe. In order to tackle this problem, suitable material is used for manufacturing turbine blades, which are called as super alloys. Examples of such materials are U-500, Rene 77, Rene N5, Rene N6, PWA 1484, Inconel, Nimonic 80a, Nimonic 90, Nimonic 105 etc. Apart from using such materials, thermal coatings are done on the surface of the turbine blades and different methods of turbine cooling are deployed.

During the operation of steam turbine, the turbine blade experiences four types of loads, namely, centrifugal loads, thermal load, pressure load and self weight. The major types of failure modes that occur in turbine blades are fatigue, creep and damage due to resonance condition. In order to prevent damage due to vibrations, friction dampers are also used [35]. Another type of failure is corrosion failure, which takes place due to availability of both steam and air on the surface of the turbine blade.

For different types of turbines, the profile of the turbine blade varies. The profile of the turbine blade used is aerofoil and rectangular for reaction and impulse turbines respectively. For calculating blade efficiency, velocity triangles are used as shown in fig 1.2. The maximum blade efficiency depends on the inlet guide vane angle (α_1) as shown in fig 1.2. Equations (1.1 and 1.2) represent the maximum blade efficiency of reaction and impulse turbine respectively.

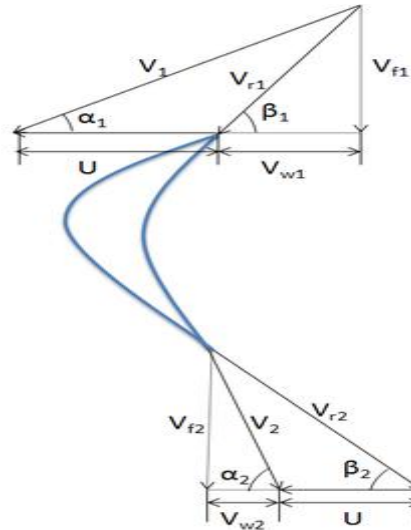


Fig 1.2: Velocity triangle of turbine blade (Saksham grover13, 2012)

$$\eta_{\text{REACTION}} = 2\cos^2\alpha_1/(1 + \cos^2\alpha_1) \quad (1.1)$$

$$\eta_{\text{IMPULSE}} = \cos^2\alpha_1 \quad (1.2)$$

1.3 COMPUTATIONAL FLUID DYNAMICS AND FINITE ELEMENT ANALYSIS

1.3.1 Computational Fluid Dynamics (CFD)

Computational fluid dynamics is the branch of fluid dynamics in which problems of fluid dynamics are solved on computers with the help of software. Such software utilizes principles of fluid mechanics to solve problems. It is used in various fields such as aerodynamics, heat transfer, biology, power systems, piping systems, combustion analysis etc. The software works on fundamental principles of fluid mechanics, like continuity equation, energy equation, momentum equation, navier stokes equation etc. On the backend, the software follows a procedure called as finite volume method. It is a numerical procedure in which the problem is divided into small number of problems using a mesh.

Then the fundamental equations of fluid mechanics are solved in conservative form over discretized volumes. At the end, all the discretized solutions are combined to form a final solution. Other methods are also used at the backend, such as finite element method, boundary element method etc. But, finite volume method is the more predominant one in CFD software. Some commercial packages used in CFD.

The advantage of solving problems using CFD is that it reduces the cost of experimental processes. It can provide results at any point in the domain whereas in experimental analysis, one can only achieve results at places where measurement units are setup. Another important advantage of CFD is its speed of doing the calculations. Higher the computational power of the system, quicker will be the calculations. Since, the calculations are quicker, time is saved. Also, CFD analysis is more flexible, as the parameters like material properties, boundary conditions can be changed at a click. Finally, CFD is able to create an almost exact environment as of real world providing approximate but accurate results.

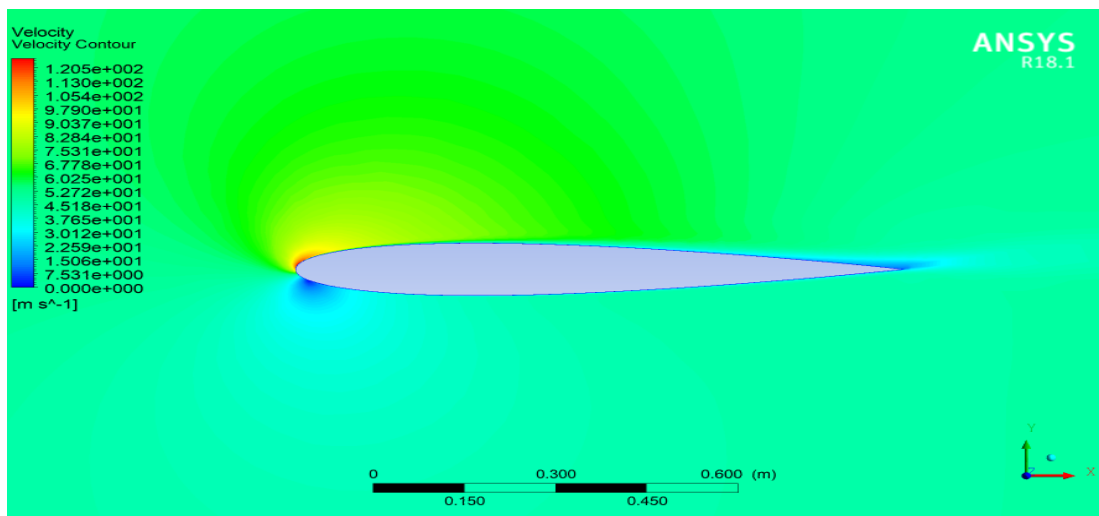


Fig1.3: Results obtained on CFD software

1.3.2 Finite Element Analysis (FEA)

Finite Element Analysis is the procedure to solve physical problems related to specific fields on computer following a certain algorithm. The basic idea behind finite element method is to break the problem domain into smaller parts and then solve each part. At last, combine the solutions of smaller parts to obtain the solution of the complete problem domain. It is used to solve problems in the field of structural analysis, heat transfer analysis, modal analysis, dynamic and static analysis, electromagnetic, biomechanics etc.

For any physical problem, the problem domain is first meshed (divided into smaller parts). The mesh creates elements and nodes out of the domain. The equations representing the physical problem are solved at the nodes. Then, with the help of shape functions, equations are solved across the elements. Finally, the solution at element level is converted into assembly level and unknown variables are calculated.

The advantages of FEA include increased speed, time is saved, money is saved and almost exact environment of the real world is created in FEA software. Another advantage is that one can also simulate such problems which in real world would not be possible. Some of the commercial FEA software packages are Abaqus CAE, Ansys R18.1 Transient Structural, Ansys R18.1 Static Structural, Altair Hypermesh etc.

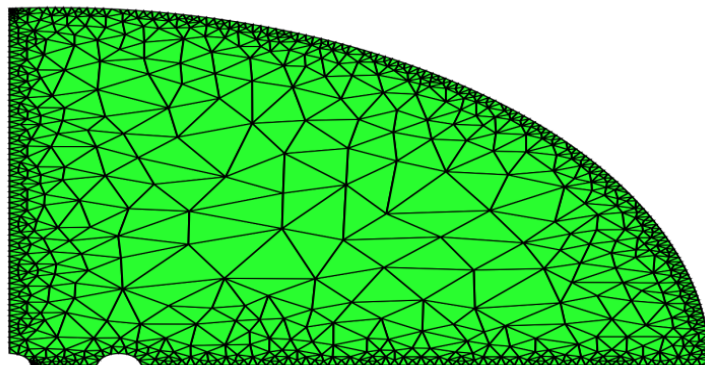


Fig1.4: Meshing of problem domain

CHAPTER 2: LITERATURE REVIEW

Literature survey is done in three sections, which are detailed below.

2.1 STUDIES ON OPERATING CONDITIONS

Banaszkiewicz et. al. [25] has presented a study on one of the important stages of working of a steam turbine which is start-up. First of all, the principle of a start-up is explained. The procedure of a start-up needs to be followed strictly in view of safety and reliability of steam turbine. The start-up phase in working of steam, turbine is a transient phase and involves handling of various systems and equipments of a turbine. Hence, this stage requires safety and experience. There are three phases during a steam turbine start up are turbine preparation to start up, running up to idle run and synchronization and loading. During first phase, turning gear is started to rotate the turbine at a very low speed and bring it to dynamic state from static state. During second phase, steam flows through the turbine at a pressure and temperature less than the normal working pressure and temperature, till the required speed of synchronization is reached. In the third phase, the turbine is synchronized with the power grid to produce electrical power. After the third phase, the turbine operates at steady state conditions.

There are three types of start up, namely, cold start, warm start and hot start. When the turbine inner casing temperature is lower or equal to 170°C , then cold start up procedure is used. When the turbine inner casing temperature is lower or equal to 430°C , then warm start up procedure is used. When the turbine inner casing temperature is greater than 430°C , then hot start up procedure is used. During a start up, the fluid parameters are not constant. The hot steam is in contact with the outer surface of the turbine blade. Due to thermal coating, heat transfer is less cross the blade. Hence a thermal gradient is created across the body of the turbine blade. This leads to thermal stress generation. Also, lower the time period of start up, more are the thermal stresses generated due to fast temperature

changes. Another damage mechanism during a start up is the vibrations produced in different parts of the turbine. Also, one has to quickly pass through the resonant frequency of rotating components during the start up. Also, the vibrations damage the path of steam. Frequent startups leads to increased thermal stress which may even cross the yield point of the material and lead to crack initiation. The internal thermal stress also leads to thermal expansion of turbine components such as rotor and casing. The various parameters such as steam parameters, rotational speeds etc that are need to be taken care of during a startup are given in startup curves. Startup curves are designed for an individual turbine with an aim to reduce the thermal stresses and take optimum time.

Mali et. al. [19] presented the study of cold start, hot start and warm start for high pressure turbine and intermediate pressure turbine. The experiments are performed for a 125MW steam turbine. It is observed that low pressure turbines are more prone to failure during transient events than high pressure and intermediate pressure turbines. Firstly, two graphs are taken as reference which are speed vs. time and load vs. time during a start up. Then two graphs are plotted with the help of experiments conducted for each case of cold start, warm start and hot start. The two graphs are also plotted for both HP turbine and IP turbine. The two graphs are pressure vs. time and temperature vs. time. The first observation is that the turbine takes 240 min, 120 min and 60 min to reach full load of 125 MW for cold, warm and hot start respectively. The second observation is that the turbine speed reaches from 0 to 3000rpm in 60 min, 15 min and 10 min for cold, warm and hot start condition respectively. The final observation is that it is better to start the turbine from hot start than warm start and also better to start with warm start than cold start, but the startup procedure also depends on the turbine inner casing temperatures.

Chow et. al. [21] states that we need a safe and economical operating procedure for steam turbine startup. At the same time, we have to look for shortest possible time for loading and unloading so as to reduce the thermal stresses. The following points need to be taken care of during a startup:

- The steam temperature should be 50-100⁰F above the turbine metal temperature.

- The hot start should take less than 6-7 minutes to make turbine attain steady speed and warm start should take 20-30 minutes for the same.
- At cold start, the temperature and pressure of the steam should be kept as low as possible.

2.2 STUDIES ON FAILURE MODES AND TRANSIENT ANALYSIS

Moroz et. al. [1] has presented a study on the process of developing an online setup to monitor the thermal stress produced in steam turbine blade. The operational flexibility of the steam turbine needs to be increased in order to meet the power demands. But, the thermal stresses produced, limits the operational flexibility of a steam turbine. The thermal stress induced leads to damage of the components. The various damage mechanisms that take place are low cycle fatigue, high cycle fatigue, creep-fatigue interactions, corrosion, erosion, stress corrosion cracking and thermal aging.

The thick walled components like rotor, valve steam chest, nozzle boxes, casings and casing rings are affected by thermal fatigue due to varying temperature gradients during transient events. The stress in the rotor is produced by thermal load, pressure load and centrifugal loads. During a start up, out of these three loads, thermal stress accounts for 95% of the total stress.

Abu et. al. [36] presented a steady state analysis of a turbine blade using a finite element model. A simplified geometry is taken and accumulation of three damage mechanisms is considered, namely, creep, corrosion and fatigue. This accumulation is represented by Neu-Sehitoglu thermo mechanical fatigue formula. In this analysis, the predicted life of turbine blade is two times less in comparison to analysis where the damage mechanisms occur separately. The drawback of this analysis is the requirement of 19 material data which is difficult to gather accurately.

Moroz et. al. [2] presented a thermo-mechanical analysis of complete steam turbine considering some key aspects like steam condensation and psychometric properties of steam during the operation. The author got motivation from the fact that with increase of operational flexibility of steam turbine, the thermal stresses on primary components is increasing and hence, the demand of more accurate LCF simulations has increased. The conclusions are that the author's approach resulted in better accuracy of the results. The psychometric properties, condensation effect and the windage effect were all captured in the analysis.

Badshah et. al. [6] presented a fluid structure interaction analysis for a tidal turbine with fluid flow following a specific velocity profile. In this analysis, Ansys R18.1 CFX software is coupled with Ansys R18.1 Transient Structural software. A turbulent flow was considered with velocity following $1/7^{\text{th}}$ power velocity profile. In order to reduce the computation time required to solve the problem, first a steady state analysis is performed on uncoupled Ansys R18.1 CFX software. Then the results of this analysis are taken as initial value in transient analysis performed on uncoupled Ansys R18.1 CFX software. Finally, the results obtained from this analysis are taken as initial values in coupled Ansys R18.1 CFX software. This process results in fast convergence of the coupled FSI analysis. After this following the standard CFD procedure, the problem domain is divided into small control volumes. Then, the continuity equation and momentum equation are solved over these control volumes.

The SST (Shear Stress Transport) model is used as turbulent flow model. This model uses $k-\omega$ turbulence model near the walls and $k-\epsilon$ turbulence model away from the walls. A turbulent intensity of 5% and viscosity ratio of 10 is taken in this analysis. At the outlet, relative static pressure is 0. On some faces of the fluid domain, no-slip boundary condition is applied, which means that velocity of fluid flow on these faces will be zero. The Ansys R18.1 CFX software is loosely coupled with the Ansys R18.1 Transient Structural software. The CFD analysis is performed independently on Ansys R18.1 CFX and FEA Structural analysis performed on Ansys R18.1 Transient Structural separately. The

coupling system transfers data between the two software. Structural steel is taken as the material of the turbine, as composite material makes the analysis more complex. The same geometry model is used for both CFD and FEA analysis. The angular velocity of the turbine is set to 0.7 rad/s. The setting for CFD and FEA analysis is set to transient analysis. The FEA system is solved first and then the CFD system is solved. The accuracy of this simulation depends on the mesh and mapping procedure. Mesh verification is done in this paper to obtain a mesh independent solution.

Zhu et. al. [11] has performed a FEA simulation to analyze blade root and then has provide an optimized design of the blade root. The turbine blade consists of three parts, namely, blade leaf, root and tip. All the parts are designed according to the operation requirements. The turbine blade is under a multi-axial state of stress during its operation. In this paper, the root and rim of the blade of a marine turbine is analyzed and then optimized for design. Firstly, the factors affecting the turbine blade design are discussed.

The parameters on which design of a turbine blade depends are blade material, centrifugal bending stress, load and dynamic pressure. First talking about material, the material of turbine blade varies with the type of the turbine. If the turbine is HP turbine or IP turbine, then the material used is stainless steel with 12Cr, with stainless steel above 450⁰C. If the turbine is LP turbine, then the material used is titanium alloys (Ti-6Al-4V). The nature of material used determines the elasticity, corrosion resistance, pressure resistance and tensile strength, and hence the life of a turbine blade. Talking of centrifugal bending stress, if the centre of gravity of blade and leaf and centre of gravity of blade root are not in straight line, then centrifugal bending stress is generated during working of the turbine. The designers design the blade in such a way so as to counter the aerodynamic force with the centrifugal force. Talking of load, the aerodynamic force is only 10% of the centrifugal force. Airflow bending is most prominent in HP turbine, since the pressure difference across the blade is high in HP turbine. But, airflow bending is also prominent in LP turbine, because LP turbine has much more section area than HP and IP turbine. The last parameter affecting the turbine blade design is dynamic pressure. The dynamic pressure

means the vibration generated in the turbine blade, which leads to fluctuation of stress in the blade. If the amplitude of vibrations is large, the stress generated does not cross the limit of stress material can bear. But, if the Amplitude is large, then the stress generated can cross the limit of stress material can bear. Generally, due to dynamic pressure, the failure of blade takes place due to HCF rather than LCF. In HCF, the material fails suddenly at large number of cycles.

The FEA analysis of turbine blade model is carried out for stress analysis. As the centrifugal force is greater on the blade root and flange, the mesh is refined there and rest of the model, grid is thicker. The total number of elements created is 94079 and the number of nodes created is 344324. Radial displacement constraint is applied to inner surface of the rim. Axial displacement constraint is applied to both sides of the rim. Only centrifugal load is considered in the model. A rotational velocity of 7300r/min is applied to the model. The material of the blade is Cr17Ni4Cu4Nb and the material of the rim is 30Cr2Ni4MoV.

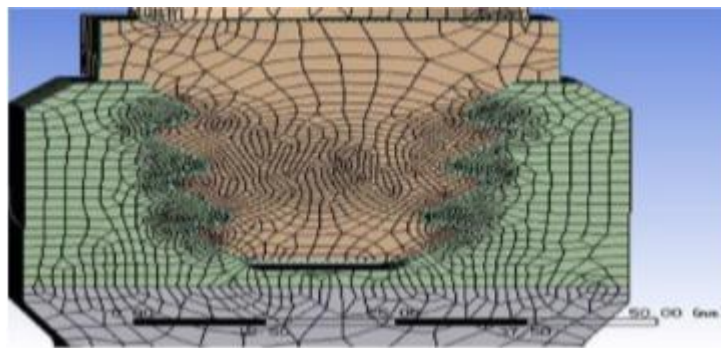


Fig2.1: Original enlarged view of blade root and rim interface (Zhu M., 2019, p. 3)

During post-processing of FEA analysis, von-mises stress contour is obtained. It is observed that the maximum stress for blade root is at the root of the first tooth, which is equal to 758MPa. The maximum stress of the rim is at the root of the lowermost part, equal

to 1150MPa. The maximum stress produced in rim has exceeded the strength limit of the material. Hence, we require providing modification in the design of turbine blade and rim, in order to make a safe model. Because of structural constraints, the blade leaf cannot be modified. Hence, to reduce loads, the width of the blade and weight of the blade is reduced.

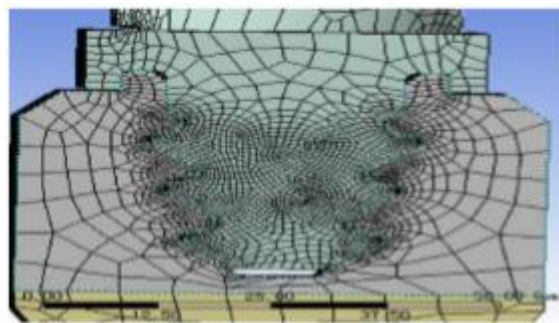


Fig2.2: Optimized design of the blade root and rim interface (Zhu M., 2019, p. 5)

After design optimization of the turbine blade, in order to calculate maximum stresses in the model, FEA analysis is performed. All the parameters and settings of the analysis are same as the previous analysis. Only difference is that the number of nodes this time is 346537 and the number of elements is 95658. During post-processing, it is observed that the maximum equivalent stress in the rim is 743MPa. This stress is 53% lower than the stress obtained during previous analysis. It is also concluded, that the titanium alloy is very well suited to the turbine blade applications as it reduces the weight of the blade, improves its efficiency and is a onetime change for the blade. A onetime change is cheaper than altering power plant units for long life development.

Somashekar et. al. [12] has performed static structural FEA analysis on a turbine blade model for two different materials, in order to predict the best material for a steam turbine blade. The 3D modeling of turbine blade is done using CAD software, which is CATIA V5 R20. First, a blade profile is imported, then a curved 3D surface is formed out of it and

finally blade root and cooling holes are modeled. Now, using FEA software, Ansys R18.1 15.0 Static Structural, FEA analysis is performed. First, the blade geometry is imported from CATIA software to Ansys R18.1 software. Then, meshing is performed, forces are applied on the blade leaf and fixed support is created on the blade root. The materials taken are structural steel and inconel 600. Then simulation is performed. In post-processing, maximum principal stress, von mises stress, total deformation, shear stress and maximum principal elastic strain contours were studied for both the materials. All the parameters studied are lower for inconel 600 in comparison to structural steel. The maximum principal stress is less than the stress limit for both the materials but the total deformation is less for inconel 600 materials. Hence, it is concluded that inconel 600 is better suited for turbine blade in comparison to structural steel.

Jojappa et. al. [13] has performed static structural analysis, modal analysis, thermal analysis and fatigue analysis for different materials for a hollow steam turbine shaft and a solid steam turbine shaft. The author got motivation from the fact that the analysis has been performed earlier for different materials but it has not been done for a hollow steam turbine shaft. Firstly, 3D models of solid and hollow steam turbine shaft are created on CAD software. The calculations for self weight load and pressure load is performed before the analysis. Two materials are taken, one is AISI 4130 Steel (super alloy steel) and other is Haynes Hastelloy C-276 alloy. All the analysis are performed are stated above. Equivalent stress, total heat flux, total deformation, safety factor and life contours are obtained from the analysis. Another geometry is taken with hollow shaft having centered bearing for support and analysis is performed.

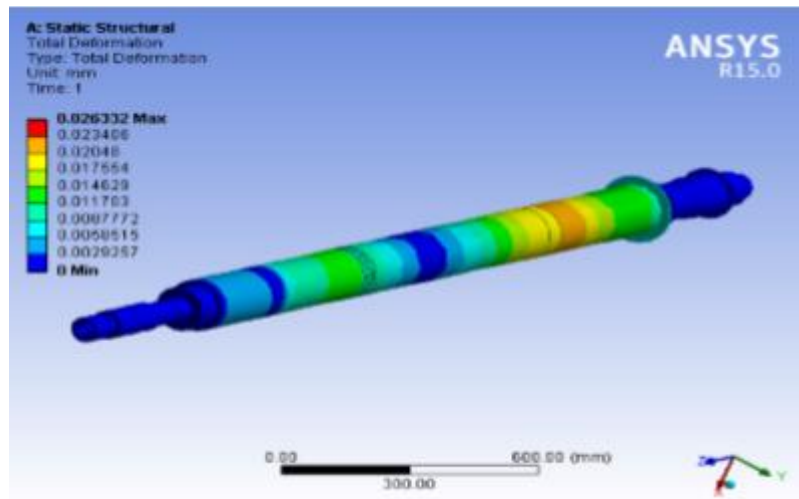


Fig2.3: Contour obtained for hollow shaft after structural analysis
(Jojappa D. et. al., 2016, p. 196)

It is concluded that stress and deformation for hollow shaft is larger than solid shaft but it is under the maximum limits if the material considering the factor of safety. For the hollow shaft with centered bearing, the stresses were reduced for the hollow shaft. Finally, it is concluded that hollow shaft with centered bearing for C-276 material is well suited for steam turbine shaft. Also, using this geometry, the weight of the shaft is reduced by 16% and hence mechanical efficiency of the turbine is increased.

Gowda et. al. [16] is a joint study between Triveni Engineering and Industries Ltd. and Ansys R18.1 India. In this paper, a FEA analysis is performed for a LP turbine blade under centrifugal load at constant rpm and then design optimization is performed. During operation of the turbine, the turbine blade root gets stressed in the disk slot. At some contact points, the stress may reach yield point and deformation may enter into the plastic region leading to crack initiation. Generally, the life prediction analysis that are performed for turbine blade does not take into account the geometry deformation of the blade root, providing results with errors. In the analysis performed by the author, Pro/ENGINEER CAD geometry of LP turbine blade disk assembly is imported to Ansys R18.1 Mechanical

software. The meshing is performed using SOLID185 elements. Contact pair is formed at the mating surfaces using augmented lagrangian algorithms. A safety factor of 1.5 is taken for the blade and of 1.25 is taken for the disk. The rpm of the turbine is taken 6000rpm and 7200 rpm. The linear analysis is performed with the above parameters. In post-processing, the results showed that the maximum stress at the mating surface reached a maximum value of 585 MPa. Now, another analysis was run with elastic-plastic material properties. In order to reduce the computational time and power required for the analysis, Neuber formula was deployed which predicts the plastic stress-strain rates from linear runs. In this analysis, the maximum stress reached to 1904 MPa and gave very poor LCF life of the model. In order to reduce the stress levels, design optimization is performed using Ansys R18.1 Design Language (APDL). After design optimization, the peak stress in blade root reduced from 1904 MPa to 1153 MPa and the peak stress in blade disk reduced from 1660 MPa to 1102 MPa. Also, the stress concentration factor was reduced from 10.4 to 6.

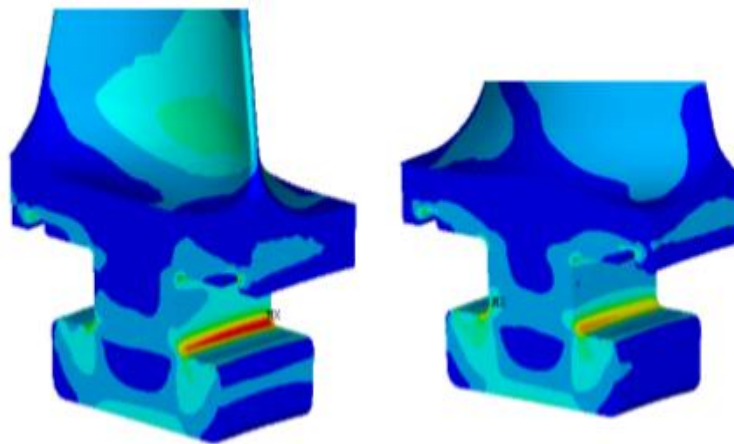


Fig 2.4: Peak stress reduced at root of the blade after design optimization

(Gowda K.K. et. al., p. 2)

Tulsidas et. al. [18] has performed LCF analysis of steam turbine blade with goal to predict its useful life. The author has performed linear elastic FEA analysis and elasto-plastic FEA analysis using Neuber's formula. In low cycle fatigue case, when the stresses

are high, the part of the model initiates cracks in less number of cycles. In such cases, one has to consider both elastic strain and plastic strain. To predict LCF life, ‘Mason-Coffin’ equation is used. This equation relates life to total strain.

$$\Delta\epsilon_t = MN_f + G/E(N_f) \quad (2.1)$$

The coefficient ‘M’ is governed by ductility and ‘G’ by strength.

There is another method for calculating useful life using total strain. This method is called universal slope method. This method utilizes results obtained from tensile testing rather than LCF testing. LCF testing is expensive and takes a lot of time. This method gives an approximate result for useful life, but is found to be a useful tool. For performing the non linear FEA analysis, the author has used Neuber’s formula, which is basically used to make the computational requirements lesser for non linear FEA analysis.

The inlet temperature of the fluid for analysis is taken as 450⁰C. Static pressure is taken as 0.1 bars and the rated speed of turbine is 8650rpm. Factor of Safety is also considered for all types of stresses considering operating conditions, manufacturing, assembly and other parameters. The problem is formulated in order to estimate the stresses at different cross sections of the blade, with turbine running at 121% over speed. Then neuber’s formula is applied in order to calculate the total strain for non linear analysis. Lastly, universal slope method is applied for calculating LCF life. The blade and disk assembly model is generated using CAD software. Exploiting the cyclic symmetry of the model, only one cyclic sector is utilized for analysis. Surface to surface contact pair is formed between the mating surfaces of disk and blade. A matching node pattern is formed at the mating surfaces for accurate load transfer. The blade and disk are assigned chrome steel as material. The yield stress of the material is 585 MPa, young’s modulus is 210 GPa, density is 7900 kg/m³ and poisson’s ratio is 0.3. The linear analysis is performed with the above material properties and boundary conditions. The linear peak stress is observed at blade root fillet of 2978 MPa and at the disk root fillet, of 2968 MPa. Both the magnitudes of

stress are above the yield strength of the material. But, these are elastic stresses and no plasticity is considered in the model, which is not the actual case. Now, using two techniques, bilinear analysis and Neuber's formula, linear stress is converted into non linear stress. The peak stress observed after the non linear analysis is 446 MPa, which is below the yield strength of the material. Also, the stresses evaluated by both the techniques are almost same. Since, the maximum stress value for disk is less than that of blade, we can conclude that disk is stiffer than blade. The weaker section of the assembly can be replaced in case of failure.

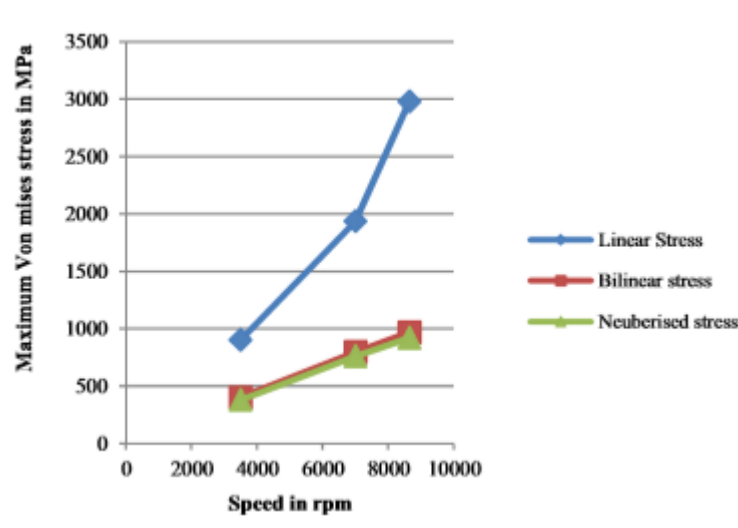


Fig 2.5: Maximum von mises stress for blade root at various speeds

(Tulsidas D. et. al., 2014, p. 2398)

Now, the fatigue analysis is performed in order to determine the useful life for turbine blade-disk assembly. Generally, the disk and blade fillets undergo the peak stresses during cycling loading. The maximum stress is produced during transient events such as start up and shut down cycle.

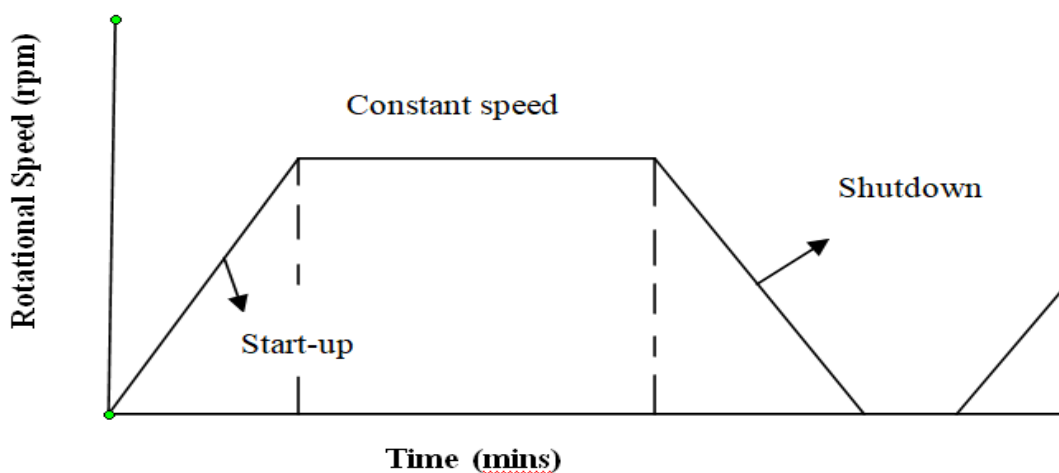


Fig 2.6: Loading cycle for turbine blade

The same material properties and boundary conditions are used in the fatigue analysis as used in previous analysis. Life contours are obtained from the analysis. Aligning with the expectations, the lowest life is observed at blade and disk fillets, which is equal to 10834 cycles. This result is in accordance with the life obtained from analytical method and USM method. The analytical method predicts life as 10486 cycles and the USM method predict life as 10500 cycles.

The author's target was to achieve a minimum of 5000 lifecycles as fatigue life. The life cycle obtained from Ansys R18.1 Fatigue tool, analytical method and graphical method, all complies with each other and are much greater than 5000 life cycles which was the target. Also, in this paper, a correlation is established between the bilinear analysis and Neuber's rule for performing non linear FEA analysis. This can now be used for analysis industrial blades in future.

Ubulom et. al. [20] has performed a fully coupled fluid-thermal and structure interaction simulation for steam turbine blade in order to predict fatigue life and creep life for the same. In this analysis, heat flux, temperature, displacement and aerodynamic forces were updated for every iteration. Another analysis is also performed in which a single software

is used, which is termed as Conjugate heat Transfer Method. The computational resources required for CHT method is much lower than the fully coupled analysis. Then analysis is performed to determine fatigue life and creep life. There are three approaches for solving the above problem, namely, conjugate heat transfer, uncoupled and fully coupled. In CHT method, a subroutine code of metal conduction is incorporated with fluid flow code, to achieve blade temperature. In uncoupled approach, first the CFD part is solved and then the data is transferred to software to solve the FEA part. In the fully coupled approach, both the CFD and FEA parts are solved simultaneously, updating the required variables for each other in every iteration.

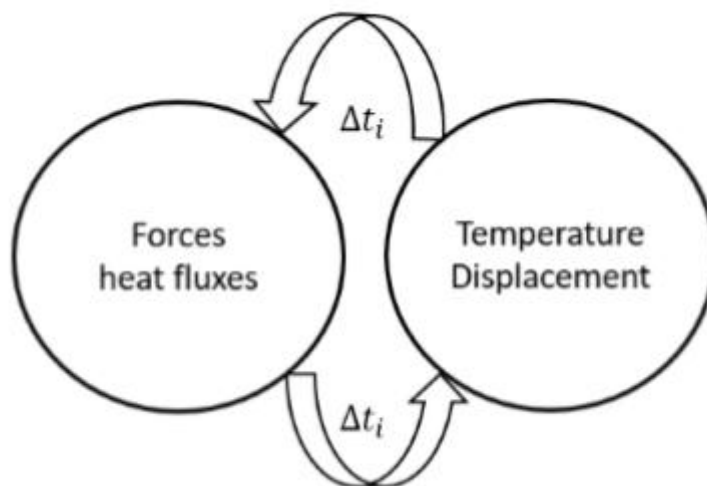


Fig 2.7: Fully coupled approach (Ubulom I.A., 2019, p. 142)

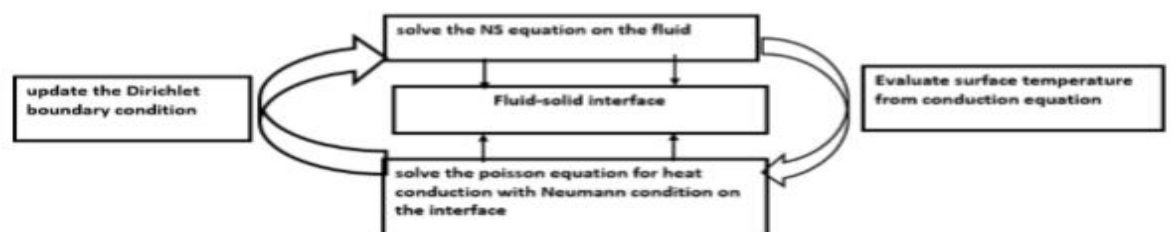


Fig 2.8: CHT solution approach (Ubulom I.A. et. al., 2019, p. 162)

Two analyses are performed for the same problem, one with fully coupled approach and other with CHT approach. All the boundary conditions are same for the two approaches except the inlet fluid temperature. The inlet temperature was 900K for CHT method and 784K for the fully coupled approach. This was done keeping in mind the computational resources required. The temperature contours are compared for both the analysis after normalization. The temperature ratio for fully coupled case is greater than CHT method. The fatigue life is calculated using Coffin-Manson's equation separately for elastic strain, plastic strain and total strain. The dominant mode of creep taking place in turbine blade is tertiary creep. A tertiary creep model is proposed by Hayhurst and Leckie based on continuum damage mechanics theory. It is observed that the creep strain increase at very slow rate from 0 to 1000 hours. After this time period, the creep strain increases exponentially with time. From the fully coupled analysis and CHT analysis, it is concluded that the blade temperature obtained from fully coupled analysis is greater than the CHT analysis, but the temperature difference is greater for CHT analysis, leading to more thermal stress.

Chow et. al. [21] has performed a transient analysis on steam turbine rotor using a digital computer by writing a raw code. A complete cycle of loading and unloading is considered during the analysis that is, shutdown, loading and starts up. Further, two start ups were considered separately, one after 6 hours shutdown and one after 36 hours shutdown. From the temperature contours obtained after the analysis, it can be concluded that section 10 needs future study as thermal gradient is maximum at this section.

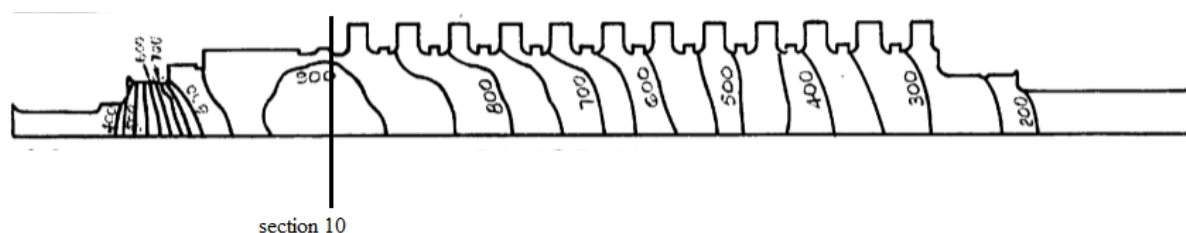


Fig 2.9: Temperature distribution on turbine rotor after unloading (Chow C., 1965, p. 103)

After the calculation of temperature contours, the thermal stress is calculated using raw code on digital computer. It is observed that the thermal gradient is high near the periphery and decreases towards the bore of the rotor for section 10. The maximum shear stress in radial direction is 1.1tons/in^2 . The maximum shear strain energy comes out to be 6.28 in-lb/in^3 . The maximum thermal stress is developed at the periphery of the rotor.

Banaskeiwicz et. al. [26] has presented an advance procedure of life prediction of steam turbine components. In this procedure, the author has performed thermo-mechanical analysis of a steam turbine rotor along with a computer program generating creep fatigue damage by taking long term operating data as input. In earlier lifetime assessment studies, the data obtained from turbine operators was a representative data, which worked for base load machines. But, now we require more detailed data for modern day turbines. Characteristic strain model of creep developed by Bolton is used for creep calculations. Neuber's rule is used for calculation of non linear stresses and strains using linear stresses and strains. If the Neuber's rule predicts high damage due to LCF, then more accurate FE calculations are performed using elastic-plastic material model with Prager-Ziegler linear kinematic hardening. For creep-fatigue damage evaluation, linear theory of damage accumulation is used.

The analysis is performed for a steam turbine rotor with operating data of around 78 months. Using the computer program, it is concluded that the rotor has undergone 267 start ups and a total operating period of 43387 hours. Further, it is obtained that 267 start ups include 31 cold starts, 214 warm starts and 22 hot starts. Thermal analysis is performed on Abaqus CAE software to obtain temperature distribution during steady state and cold start. In post-processing, it was observed that during cold start, radial temperature gradient dominates and during steady state, axial temperature gradient dominates. For steady state, creep strain contour is obtained and it was observed that creep strain is highest at places where temperature is highest, which is at heat relief groove. Creep strain was less during part load in comparison to full load. Fatigue load contour is also obtained and it is

observed that fatigue damage is also more at places with higher temperature and thermal gradient. Also thermal stress and minimum number of cycles to crack initiation contours are also obtained which shows that maximum stress concentration is at the left bottom part of first blade groove. The geometry was optimized at high stress concentration area and the most damaged part was machined. Analysis was again run with new geometry, and it was observed that the maximum stress value dropped by 50% and fatigue increased by seven times.

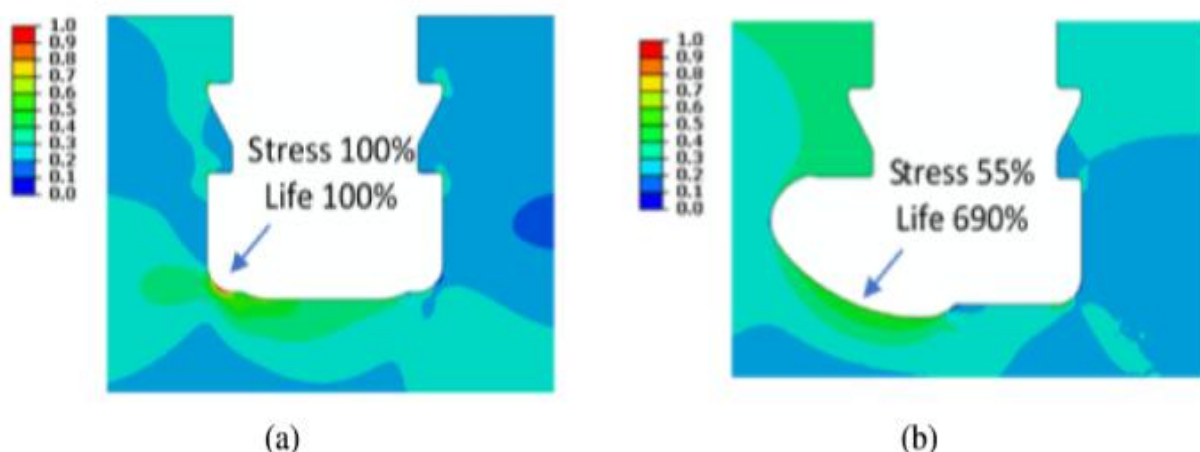


Fig 2.10: Relative stress and fatigue life contour for a) original and b) optimized blade groove (Banaszkiewicz M. et. al., 2018, p. 593)

It has been observed that old lifetime assessment method provides varying results, when results are compared with an analytical method. The method proposed in this paper has been developed in response to the market demands and has been found to be the most accurate method till date.

Patil et. al. [37] has given a lecture on thermo mechanical fatigue and how it can be analysed on Ansys R18.1 software. Thermo mechanical damage may be due to the following reasons:

- Thermal expansion induced stress
- Material strength decreases with increase in temperatures
- Material resistance to fatigue damage decreases with increase in temperature
- Materials creep at high temperature and creep voids accelerates fatigue cracking
- Oxidation accelerates fatigue damage

Different applications where thermo mechanical fatigue occurs include exhaust manifold, exhaust mufflers, fluid turbines, steam turbines, turbocharger etc. Ansys R18.1 nCode Design Life software can be used for performing thermo mechanical fatigue analysis. It evaluates four types of thermo mechanical fatigue approaches namely, multi-temperature method, chaboche method, chaboche transient method and creep rupture. For applications like steam turbine blade, first stress analysis should be performed considering elastic-plastic material models in FEA software. Then chaboche transient method plus creep rupture method should be deployed for damage analysis.

Trevino et. al. [39] has performed a static structural analysis of a steam turbine blade with Nb₅Si₃ as the material. Niobium Silicides, Nb₅Si₃ is being tested as a potential material for steam turbine blade. The required microstructure of Nb₅Si₃ is obtained by a process called as MASHS (Mechanically Activated Self Propagating High temperature Synthesis). The properties of Nb₅Si₃ include high melting point, low density and high fracture toughness. α -phase of Nb₅Si₃ is being used for testing. Standard material used for steam turbine blades is Ti6Al4V. The CAD model is generated for the steam turbine blade. It is then imported in Ansys R18.1 Static Structural software for analysis. The boundary conditions of force, temperature and fixed support is provided to the model. After this, meshing of the model is generated. In post processing, the max deformation contours were obtained for Ti6Al4V and Nb₅Si₃. The maximum deformation for Ti alloy is found to be 0.9038mm and for Nb₅Si₃, it is found to be 0.2456mm. Hence, it can be concluded that Nb₅Si₃ can be thought of as an alternative material for steam turbine blades. Further research can be done on the manufacturing process for Nb₅Si₃.

2.3 MOTIVATION

As studied in introduction, steam turbines are used in various applications across different industries. It is a power generator used in different ways. With increasing population and increasing technology, the demand for power is on its peak. In order to produce more power, one of the foremost activities is to modify the main power generating component for better efficiency, flexibility and life. Steam turbine is one of the widely used power generator globally and its blades are one of the most important components of the turbine. According to the thermodynamic cycle on which steam turbines operate, increasing the inlet temperature of the fluid increases efficiency of the turbine. This has led to even more rise in the severe conditions under which turbines work. Turbine blades are the components of turbines which are directly and continuously attacked by the high temperature steam entering the turbine. Turbine blades are made up of super alloys in order to sustain the severe conditions. Also, turbine cooling methods are deployed in order to prevent the blades from excessive damage. But still, the turbine blades operate under severe conditions.

As written in literature review, during complete cycle of turbine operation, there are steady state and transient state events. A turbine blade faces majorly four types of loads, namely, centrifugal load, thermal load, pressure load and self weight. Except the self weight of the blade, all other loads vary with varying conditions. The stresses produced by these loads leads to different types of damage mechanisms in the blade, reducing their useful life and ultimately, reducing the turbine life. These stresses are more during transient events than steady state events. Hence, it becomes more important to study stress analysis of turbine blades during transient events. The transient events can be start ups, shut downs, speed change events, load change events etc. In this report, we have performed stress and strain analysis of steam turbine blades during steady state and during transient event in order to identify the severe conditions tackled by the turbine blades. By studying the stress and strains acting on turbine blades, we can work on technologies to reduce the stress and strains on turbine blades.

CHAPTER 3: STEADY STATE FSI ANALYSIS

This chapter deals with the fluid structure simulation of steam turbine blade during steady state using Ansys R18.1 CFX and Ansys R18.1 Static Structural software. We have first talked about steady state conditions. Then we have moved onto types of stress faced by turbine blade and types of damage mechanism occurring. Then, we have discussed about turbine cooling and finally the methodology and procedure used for performing the FSI simulation on steam turbine blade.

3.1 STEADY STATE CONDITION

Steady state events are those events during which input parameters do not change with time. The output may or may not change with time. In some systems, the steady state is achieved after a series of transient events. Hence, steady state condition can also be called as time independent event. Generally, these events are easier to understand, formulate and solve both analytically and computationally. When a transient state is reached after steady state in a system, first steady state is studied and then the solution of steady state is considered as initial value for transient state.

In steam turbine operation, for a larger period of cycle, it runs on steady state conditions. In case of power plant, at that time, it is connected to a generator for producing electricity of required frequency. At steady state condition, turbine operator needs to pay very less attention on the system. In steady state condition, the steam parameters or the inlet parameters remain constant in time. Steady inlet conditions in steam turbine means that the inlet steam has constant parameters. All fluid at constant parameters follow an equation called as steady flow energy equation (Equation 3.1).

$$\dot{m}_1(h_1 + V_1^2/2 + Z_1g) + dQ/dT = \dot{m}_2(h_2 + V_2^2/2 + Z_2g) + dW/dT \quad (3.1)$$

where \dot{m} is the mass flow rate, h is specific enthalpy, V is velocity, Z is elevation from datum, dQ/dT is the rate of heat transfer and dW/dT is the rate of work transfer. For an ideal turbine, the change in kinetic energy is zero; change in elevation is zero, mass flow rate remains same and there is no heat transfer. The steady flow energy equation for an ideal turbine becomes as stated in Equation 3.2.

$$W = H_1 - H_2 \quad (3.2)$$

where H_1 and H_2 are the enthalpy of steam at inlet and outlet respectively.

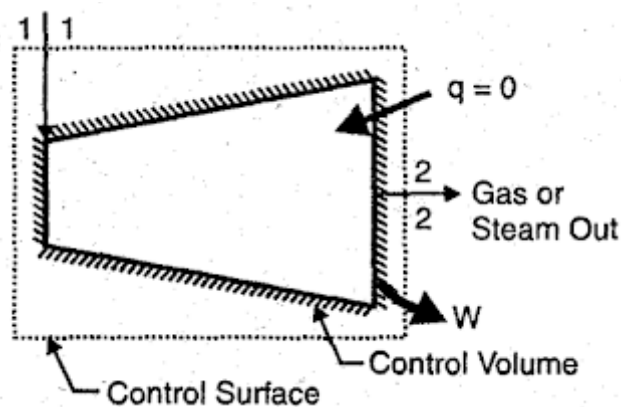


Fig 3.1: Block diagram of an ideal turbine

Along with the fluid being in steady state, the turbine components also operate at steady conditions. Initially, for some time, the turbine might operate in transient state, but then it operates in steady state. The steady state of turbine means that the rotational speed of turbine is constant, the turning gear is rotating at constant speed, power output is constant etc. As shown in Fig 2.6, the constant speed line in the graph represents the steady state of a steam turbine.

3.2 TYPES OF STRESS

In this section, the types of loads and stresses acting on a steam turbine blade during steady state operation are discussed. Loads are basically the forces acting on the body. Stresses are the internal resistance of the body acting against the external loads. Force and stress is defined by Equation 3.3 and Equation 3.4 respectively.

$$F = dP/dt \quad (3.3)$$

$$\sigma = F/A \quad (3.4)$$

where F is the load, P is the momentum and t is the time in Equation 3.3. In Equation 3.4, σ is the stress, F is the load and A is the cross sectional area. The stress may further be of different types depending on various classifications. Some important types of stresses are normal stress, shear stress, tensile stress, compressive stress, thermal stress, hydrodynamic stress, static stress, dynamic stress etc.

In case of a steam turbine, during steady state conditions, there are five types of stresses acting on steam turbine blades. These are thermal stress, centrifugal stress, pressure, stress due to self weight and vibratory stresses. Thermal load is due to the thermal gradient produced on steam turbine blade, as the temperature of the steam varies as it moves from leading edge to trailing edge of the blade. Since, the inlet temperature of the steam is constant in steady state conditions, the thermal gradient produced is less and hence, the thermal stresses are less. Centrifugal stresses are due to the rotation of the turbine. Centrifugal load is given by Equation 3.5.

$$F = m.r.\omega^2 \quad (3.5)$$

Where F is the centrifugal load, m is the mass, r is the radius of rotation and ω is the rotational velocity. More the rotational speed more is the centrifugal load and hence, more

is the centrifugal stress. Since, during steady state condition, rotational speed of turbine remains constant, the centrifugal stresses are constant. When the steam hits the turbine blades, pressure load is produced on the blades. To counter this external load, internal stresses are produced within the blades. Since, the mass flow rate of steam is constant during steady state condition, the pressure load is constant. Pressure load is given by Equation 3.6.

$$F = \rho \cdot A \cdot V^2 \quad (3.6)$$

where F is the pressure load, ρ is the density of the fluid, A is the area and V is the velocity of the fluid. Another type of stress acting on turbine blade is stress due to the blade itself. Depending on the power output, size of turbines and hence blades varies. The last type of stress acting on turbine blade is vibratory stresses. The blades are embedded or fitted on the turbine rotor. This fitment leads to vibrations produced in the turbine blades. Also, other turbine components of turbine such as shaft, rotor, disk, casing etc are very heavy in comparison to individual blades. This also leads to vibratory stresses.

All these stresses are kept in mind while designing a turbine blade. In general self weight is not considered during the analysis, as this load is negligible in comparison to other loads. In general, thermal stresses cause damage to body over a long period of time as this stress is not above the yield strength of the material for turbine blades. Centrifugal stress and pressure load causes damage over a shorter period of time to blades. Modal analysis is performed to skip the resonance condition that can occur when the rotational speed of the turbine becomes equal to the vibrating frequency of the blade. Resonance condition due to vibratory stresses can be very dangerous for the complete turbine. In the next section, we have discussed the damage caused due to these stresses.

3.3 TYPES OF FAILURE

Failure is the damage caused in the body due to stresses induced. As discussed in previous section, stresses are induced due to external loads. Hence, failure or damage is caused due to external loads. Failure is the damage caused to the body by external loads acting on it in any form. Failure is a type of damage which prevents the body from performing its function as defined, in the system. The damage caused to the body may be external, internal, on the surface, at the microstructure level or at the macrostructure level. Depending on type of damage caused, failures are classified as fatigue, yielding, fracture, elastic deformation, wear, buckling, corrosion, stress concentration, etc. These failures takes place due to different reasons, but common reason for all types of failure is stress induced in the body. The reasons for failure at material level can be dislocations of slip planes, absorption, lattice breaking etc. Different types of failure theories are present to estimate and study the failure in the field of material mechanics. Some common failure theories are as follows:

- Maximum principal stress theory or Rankine's theory
- Maximum shear stress theory or Guest and Tresca's theory
- Maximum principal strain theory or St. Venant's theory
- Total strain energy theory or Haigh's theory
- Maximum distortion energy theory or VonMises and Hencky's theory

Apart from above mentioned theories of failure, there are also other theories of failure which are valid for specific conditions, namely, Bolton model for creep, linear damage of accumulation for fatigue-creep damage, Manson-Coffin equation for fatigue, Larson-Miller parameter for creep etc. All the above mentioned theories of failure have well defined numerical models, which are used to predict the failure of the body under load.

Failure occurs due to stresses induced in the body due to external loads. In case of steam turbine, the loads acting on turbine blades are thermal load, self weight, centrifugal load,

pressure load and vibratory load as mentioned in section 3.2. The failure mechanisms occurring in turbine blades are fatigue, resonance, creep, elastic deformation, yielding and stress concentration. While designing of a turbine blade, the CAE engineer has to study all the failure mechanisms possible and perform in detail analysis for each of them. Various analysis are performed in order to study failure mechanisms occurring in turbine blades which are modal analysis, fatigue analysis, creep analysis, fatigue-creep analysis, stress analysis, strain analysis etc. The best method to perform these analyses is by using computational resources. The analysis performed using computational methods makes the work easy, saves time and provides detailed analysis. These analyses are also performed to predict the useful life of the turbine blade under the failure mechanisms occurring during its operation. This prediction provides an approximate idea to the turbine operators about the life of turbine components, which helps them to prepare its maintenance schedule and operating conditions.

3.4 TURBINE COOLING

The concept of turbine cooling came from the fact that as we keep on increasing the inlet fluid temperature for a steam turbine blade, the output of the turbine will keep on increasing. Hence, with greater energy demands, inlet temperature increased for the turbine and therefore, turbine cooling became an integral part of the turbine system. The major part of heat transfer from fluid to blade takes place through conduction and convection. The radiation heat transfer is negligible. The maximum heat transfer takes place at the stagnation point of the leading edge.

In 1960, blade was reengineered for providing cooling. Internal passages are provided through the turbine in order to transfer the heat from blade surface to the cooling fluid. This is called as distributed internal cooling. This method of cooling further has two types; one is called internal convection cooling and other is internal impingement cooling. Also,

there are other types of cooling methodologies, namely, discrete film cooling and full blade film cooling. There is another most efficient method of turbine cooling and it is called full blade transpiration cooling. This method is under research and is not in practical use till now. In this report for analysis purposes, instead of internal cooling passages, hollow turbine blade has been considered.

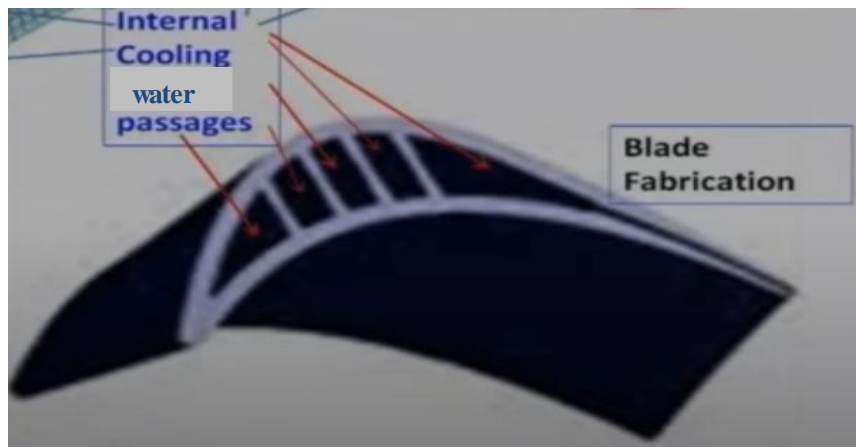


Fig 3.2: Internal blade cooling (Roy B., 2015)

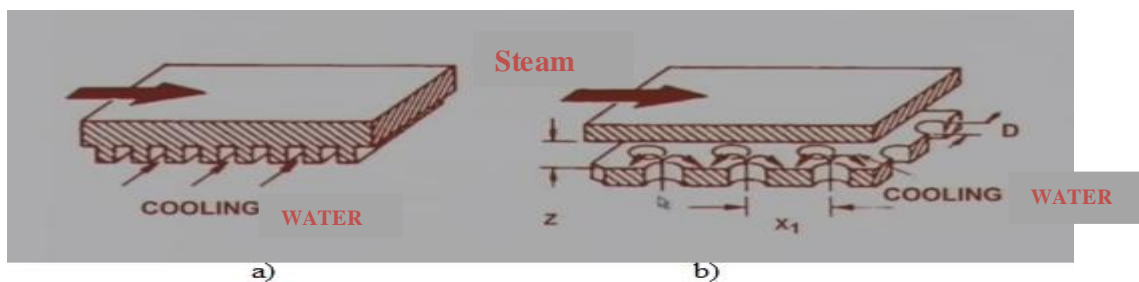


Fig 3.3: a) Internal convection cooling and b) Internal impingement cooling (Roy B., 2015)

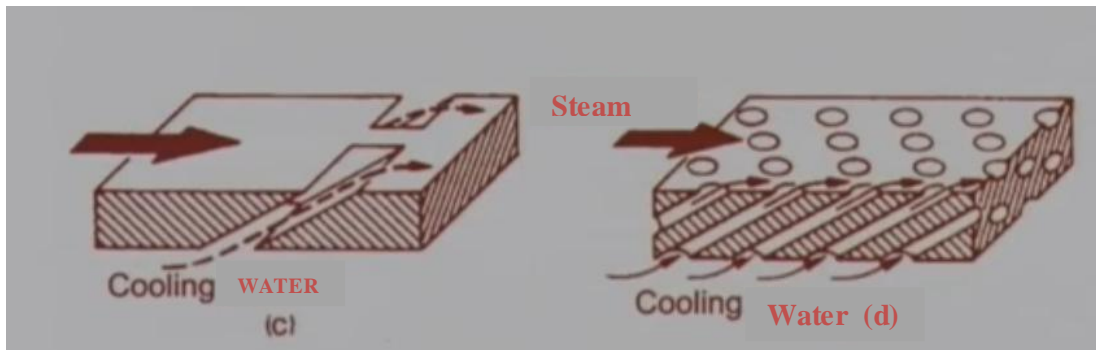


Fig 3.3: c) Discrete film cooling and d) Full blade film cooling (Roy B., 2015)

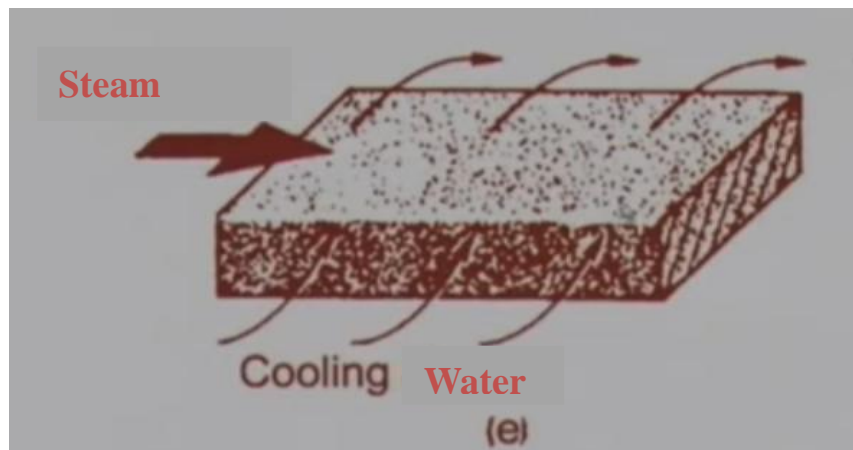


Fig 3.3: e) Full blade transpiration cooling (Roy B., 2015

)

3.5 FSI SIMULATION

Fluid Structure Interaction simulation is the process of simulating components or systems which involves interaction between fluid and solid surfaces. There are many applications in real life where fluid structure interaction takes place. Few examples are internal combustion engines, turbines, dams, airplanes, underwater vehicles, biomechanics, lubrication systems, hydraulic power systems etc. Fluids and solids have different structure at molecular level and behave differently. Performing FSI simulations require

understanding of both fluid mechanics and strength of materials. It requires both a combined approach of CFD and FEA. CFD software generally works on finite volume method and FEA software work on finite element method.

There are basically three ways to perform FSI simulations, namely, uncoupled, loosely coupled and fully coupled approach. In the uncoupled approach, first, one part of the problem is solved. Then the solutions of the first part are transferred to the other part and then the other part is solved. In loosely coupled approach, one way data transfer mechanism takes place between CFD and FEA part. Data is transferred from one software to another and not vice-versa. This means that if CFD part is solved first, then the pressure load is transferred to FEA part and FEA part is solved in every time step. Then the next step will be repeated in same manner. In fully coupled approach, two way data transfer mechanism takes place between CFD and FEA software. This means that if CFD part is being solved first, then the pressure load will be transferred to FEA part. FEA part will then be solved. Then displacement of structure will get transferred to CFD part. This completed one time step. After this, next time step will take place in same manner.

Different approaches are used for performing FSI simulations depending on the available computational resources. The FSI simulations are generally complex in geometries, physics and numerical modeling. The fully coupled approach requires more resources and time in comparison to coupled approach. The loosely coupled approach requires more resources and time in comparison to uncoupled approach.

3.5.1 Methodology

The FSI simulation performed in this chapter is for a steam turbine blade under steady state condition with uncoupled approach using Ansys R18.1 CFX and Ansys R18.1 Static Structural software.

The methodology used to solve this problem is shown in the form of flowchart in Figure 3.4. Firstly, the problem formulation is done. Then, the geometry is imported from CAD software to CAE software. Then meshing of the geometry is performed. After this CFD analysis is performed and CFD results are obtained. Then FEA analysis is performed and FEA results are obtained. Finally, CFD results and FEA results are combined to obtain FSI simulation results.

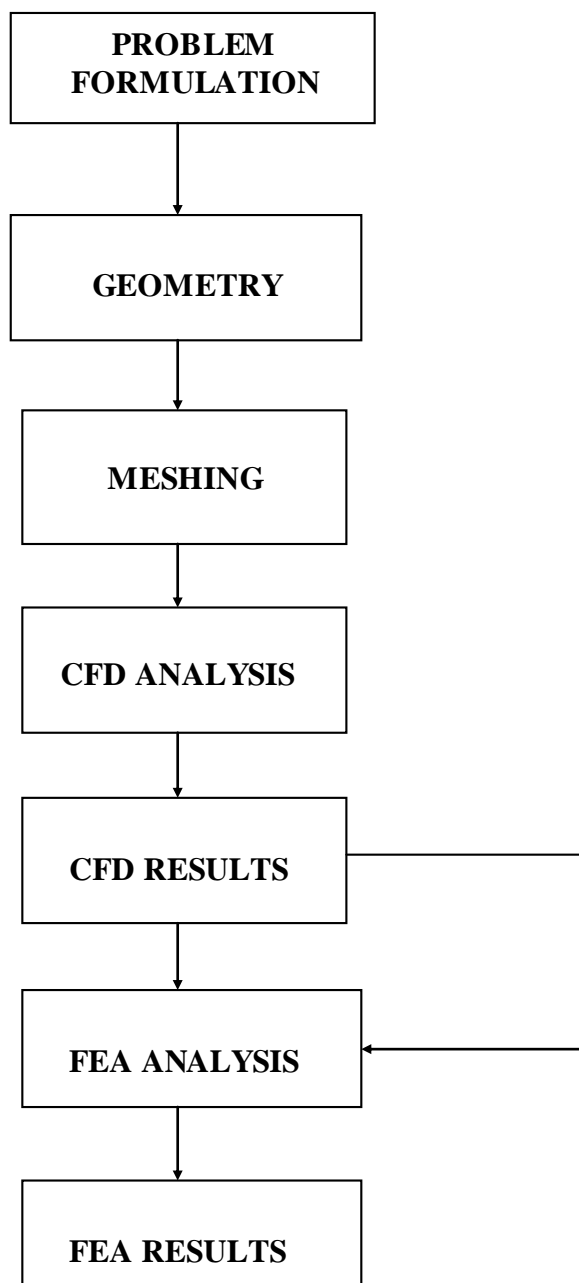


Fig 3.4: Methodology of the problem

3.5.2 Problem Formulation

The problem consists of a steam turbine blade under steady state condition. The turbine structure is of aerofoil type and is a hollow structure. Steam (steam) flows over the turbine blade in one direction and cold water flows through the hollow part of the turbine in the perpendicular direction. The cold water is used for cooling of turbine blade and steam is used for rotating the turbine. The flow of the fluides is assumed to be steady.

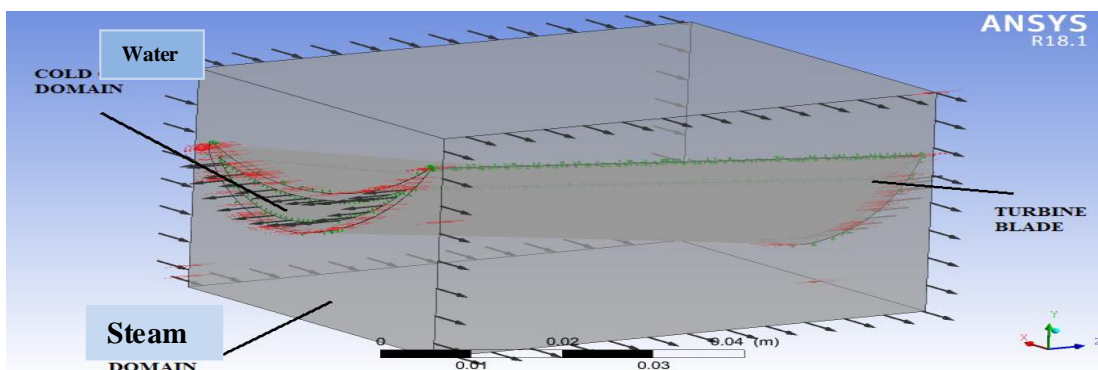


Fig 3.5: Problem domain and its components

3.5.3 CAD Model

The geometry is prepared with the help of computer aided design. The geometry is imported from a reliable source to Ansys R18.1 Geometry module. The geometry is 3D modeled. It consists of a hollow turbine blade with a rectangular flow domain. The geometry is then edited on DesignModeler software. The solid part of the blade is assigned solid domain and is named as blade. The hollow part of the blade is assigned fluid domain and is named cold domain. The rectangular flow domain is assigned fluid domain and is

named as hot domain. Also, it is to be noted that in practice, steam turbine has internal cooling passages for cooling, not a hollow part. An approximation is taken in this report that cold water passes through the hollow part of the blade. This has been done to make the geometry simpler and thereby reducing computational resources required in the analysis.

As shown in Figure 3.8, the volume and surface area of the cold domain are $7.9916 \times 10^{-6} \text{m}^3$ and $.0056769 \text{m}^2$. As shown in Figure 3.9, the volume and surface area of the hot domain are $.00011511 \text{m}^3$ and $.022094 \text{m}^2$. As shown in Figure 3.10, the volume and surface area of the blade are $8.5002 \times 10^{-6} \text{m}^3$ and $.012523 \text{m}^2$. As shown in Figure 3.11, the volume and surface area of complete CAD model are $.0001316 \text{m}^3$ and $.040294 \text{m}^2$.

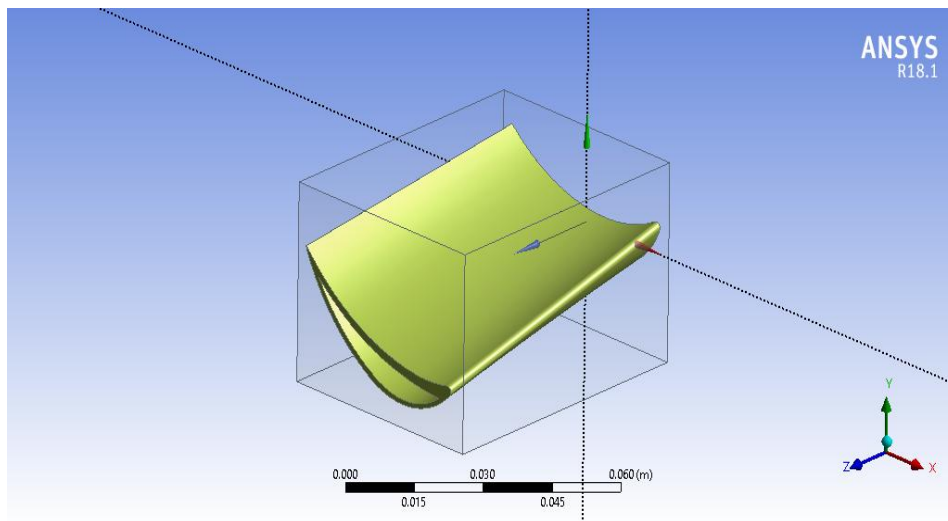


Fig 3.6: CAD model of the problem

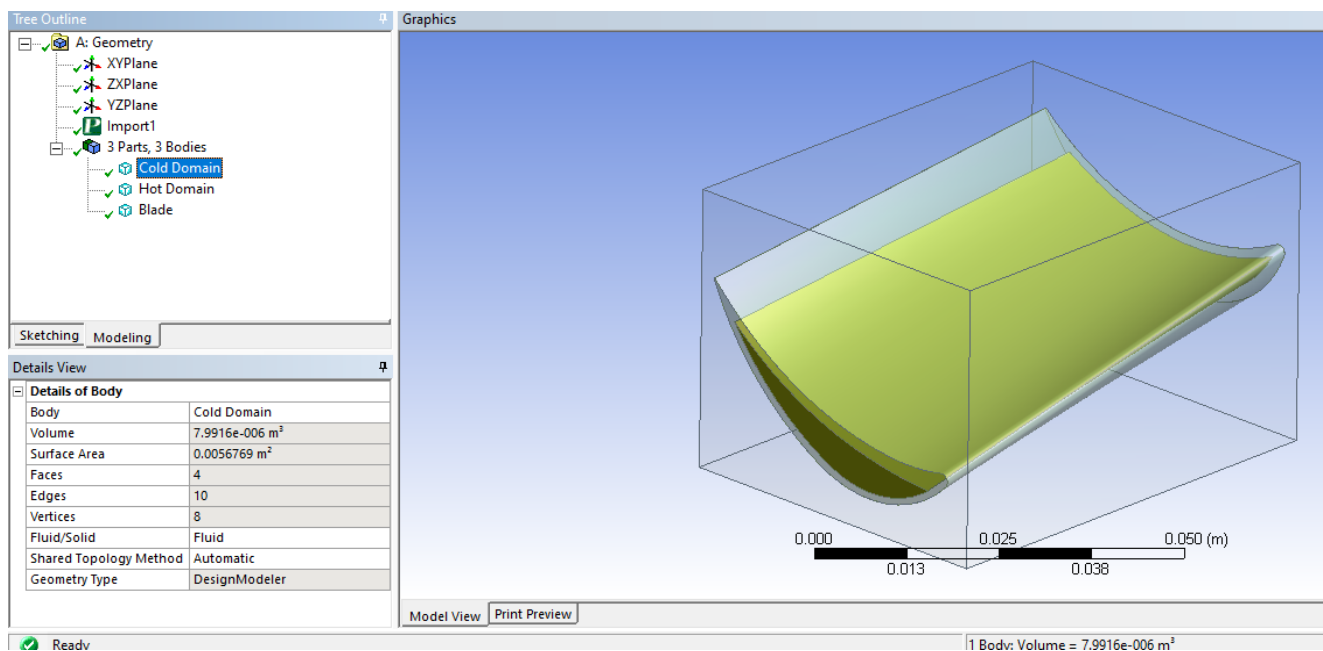


Fig 3.7: Cold domain and its properties

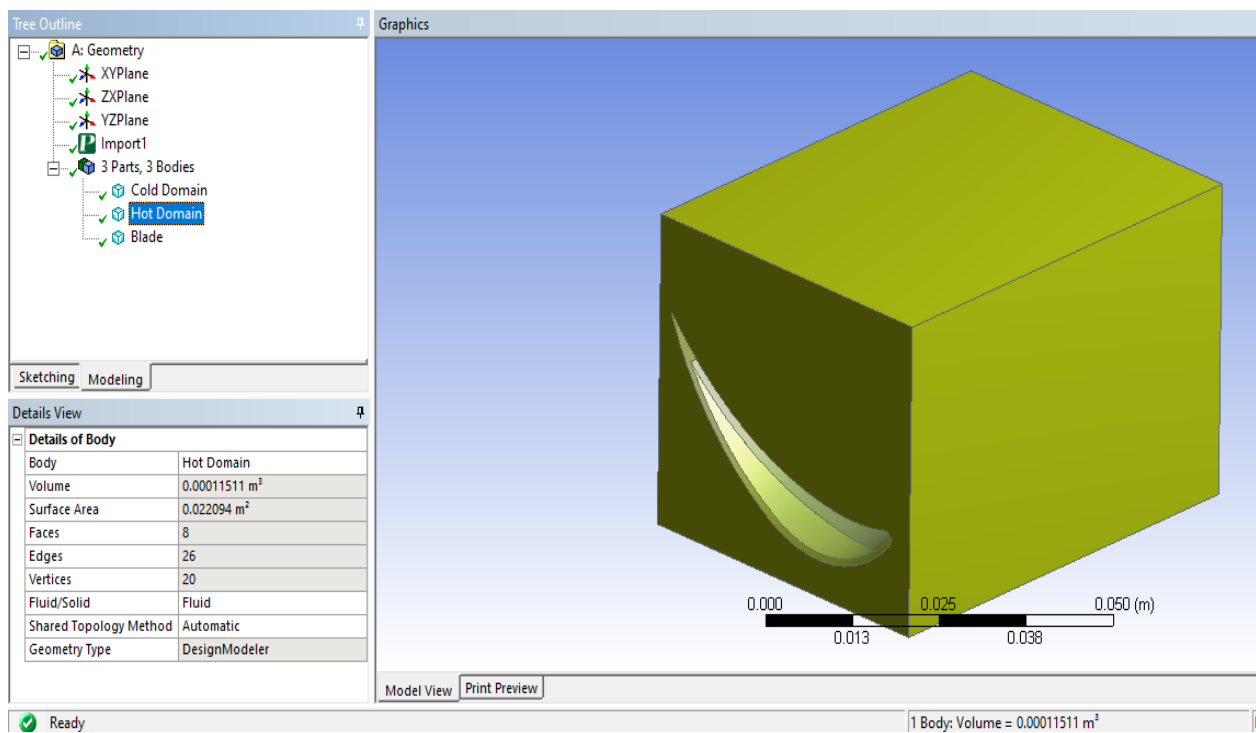


Fig 3.8: Hot domain and its properties

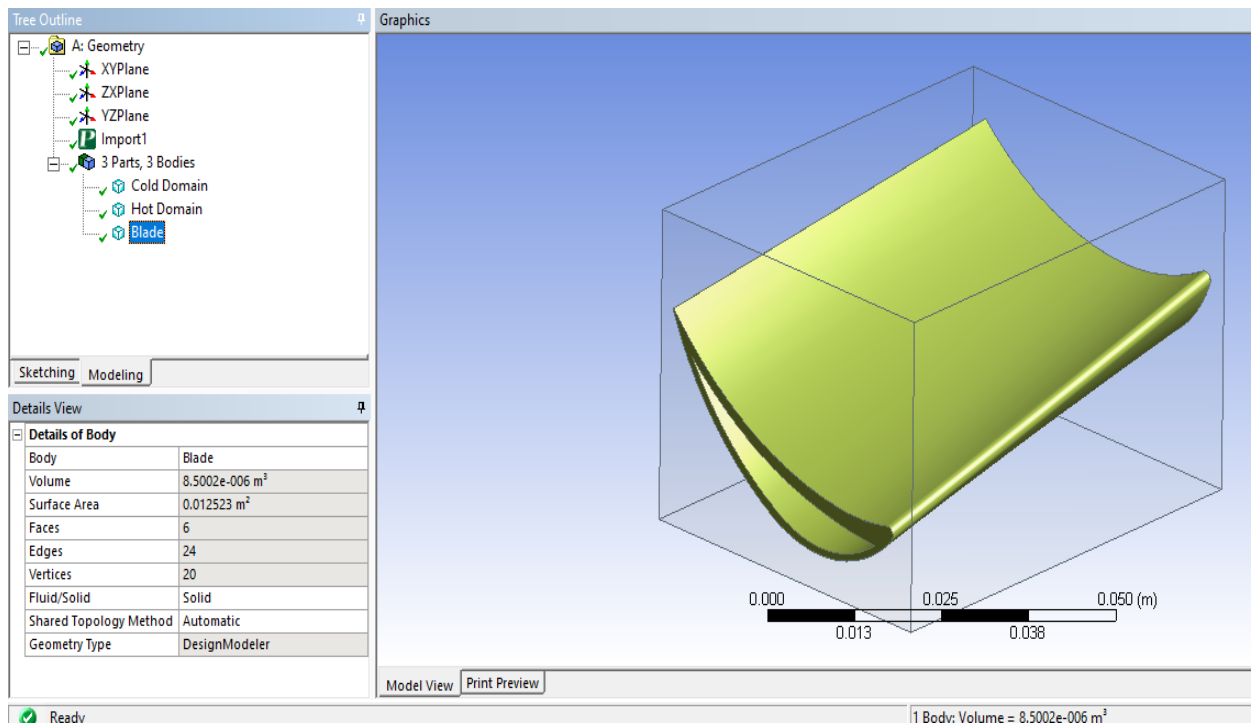


Fig 3.9: Blade and its properties

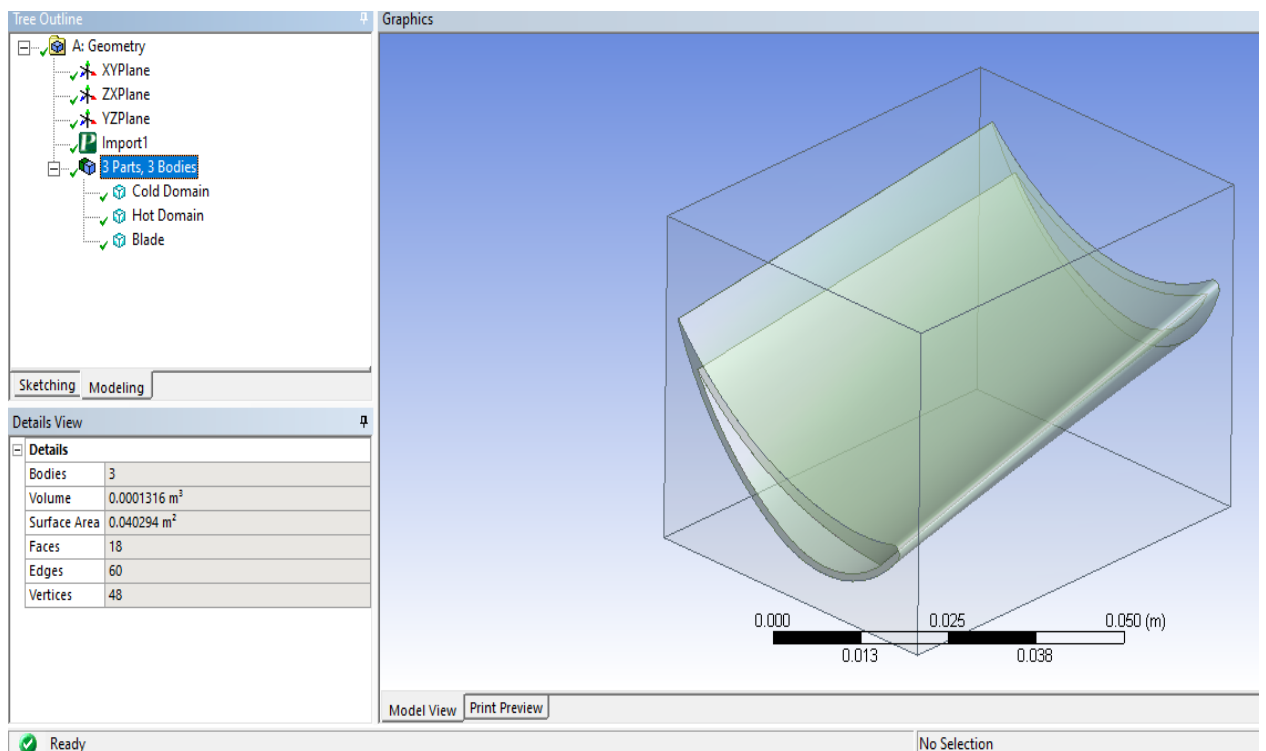


Fig 3.10: CAD model and its properties

3.5.4 Meshing

Meshing of the complete geometry (blade as well as flow domain) is performed on the mesh module of Ansys R18.1 CFX software. Physics preference is set to CFD and solver preference is set to CFX. Linear order elements are used for meshing. Target skewness is set to 0.9 for assuring quality of mesh created. The element type for the hot domain is set to 4 noded tetrahedron elements and for cold domain and blade is set to 4 noded tetrahedron elements. Minimum size of elements is set to 4.5456×10^{-5} m (default). Mesh is generated with 373651 nodes and 1335373 elements. All the surfaces and edges for defining boundary conditions in setup module are provided with names in mesh module only. The names provided to bodies, faces and edges are hot inlet, hot free surfaces, hot symmetry, hot outlet, hot side interface, steam, blade to hot interface, blade symmetry, blade to cold interface, blade, cold inlet, cold interface, cold outlet and cold water.

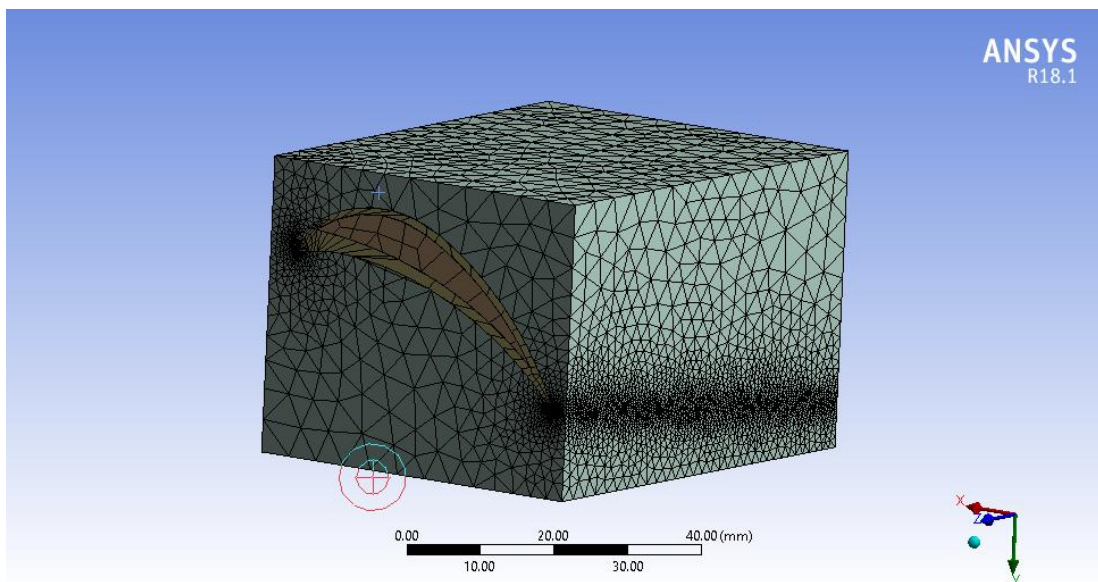


Fig 3.11: Meshing of model

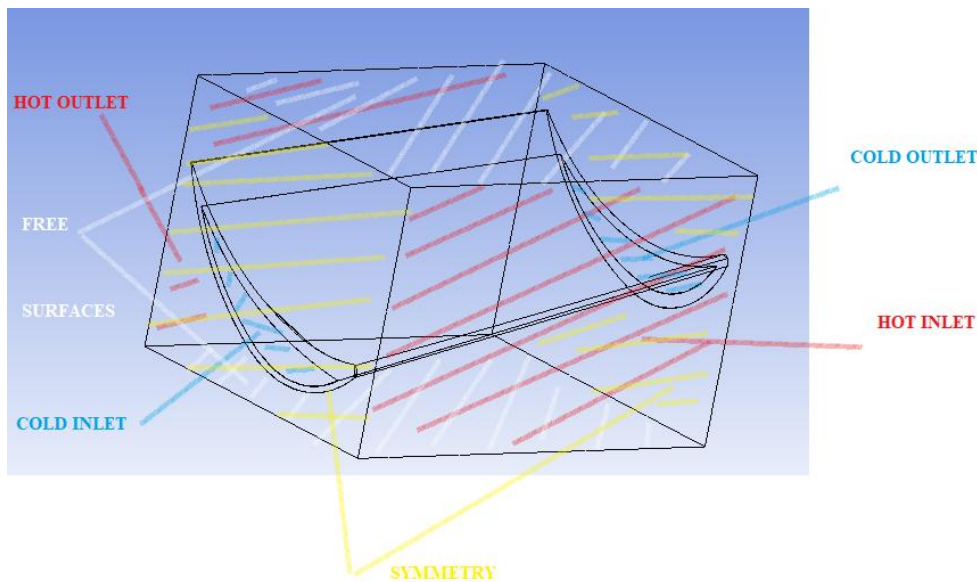


Fig 3.12: Named selections in geometry

3.5.5 CFD Analysis

As discussed in section 1.3.1, computational fluid dynamics is the branch of fluid dynamics in which problems of fluid dynamics are solved using software on computer. In this section, we have solved the fluid dynamics part of steam turbine blade under steady condition problem. The software used to solve CFD part of the problem is Ansys R18.1 CFX. Ansys R18.1 CFX is CFD software which is generally used for simulating turbo machineries such as compressors, rotors, propellers, pumps, fans, turbines etc.

3.5.5.1 Methodology

Solving any problem on Ansys R18.1 CFX consists of five steps. The five steps are geometry, mesh, setup, solution and results. Firstly, the geometry is created in geometry module. Then the geometry is meshed. After that, boundary conditions, material properties, analyzing procedure, time step of problem and other major steps are taken in setup module.

Then in solution module, the processing capabilities, initial point etc steps are taken. Then finally, in CFD post processor, the results are obtained in the results module.

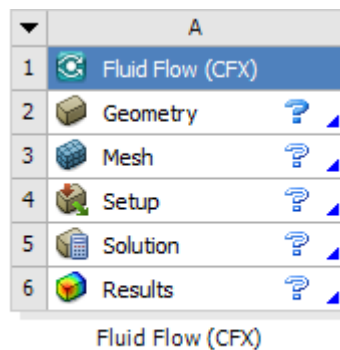


Fig 3.13: Ansys R18.1 CFX methodology

3.5.5.2 Setup

Most of the analysis part is done in setup module of Ansys R18.1 CFX software. Firstly, the analysis type is set to steady state, since the turbine is operating in steady state condition. After this, three domains are created for steam, cold water and blade. For steam domain, the fluid is taken as water vapor at 100°C . The domain type is defined as fluid domain. The domain is set to be stationary. The reference pressure is set to 1 atm. The heat transfer option is set to thermal energy. K-epsilon turbulence model is taken to define the turbulence of the fluid. Turbulence intensity is set to 5%. Domain initialization is done. For the cold water domain, all the parameters are same as steam domain except the fluid material. The fluid material is set to water vapor at 25°C . For the blade domain, the domain type is set to solid domain. The material of the blade is set to steel. The domain motion is set to rotating. The blade is assigned a relative velocity of 314 rad/s along the x axis passing through the remote point. Heat transfer model is set to thermal energy and domain initialization is performed.

Then boundary conditions are applied for each domain. The inlet velocity for steam is 15m/s and inlet temperature for steam is 650°C. The outlet pressure for steam is atmospheric pressure. In steam domain, also other boundary conditions are assigned. A free surface boundary condition is defined for up and down faces of the rectangular flow domain. Free slip wall condition is applied in free surface boundary condition. After this symmetry boundary condition is applied to the rest of the two faces of the rectangular flow domain.

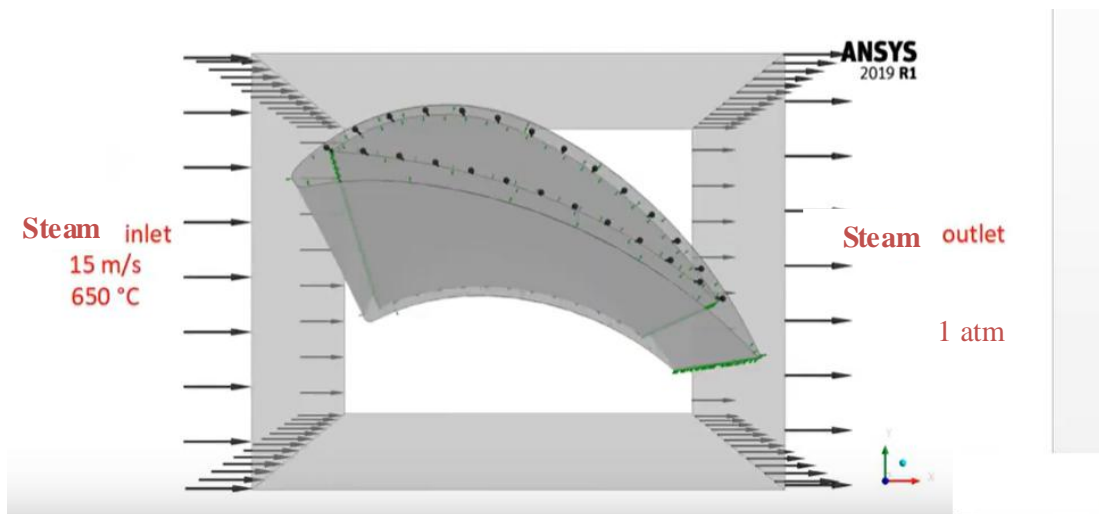


Fig 3. 14: Inlet and outlet boundary condition for steam

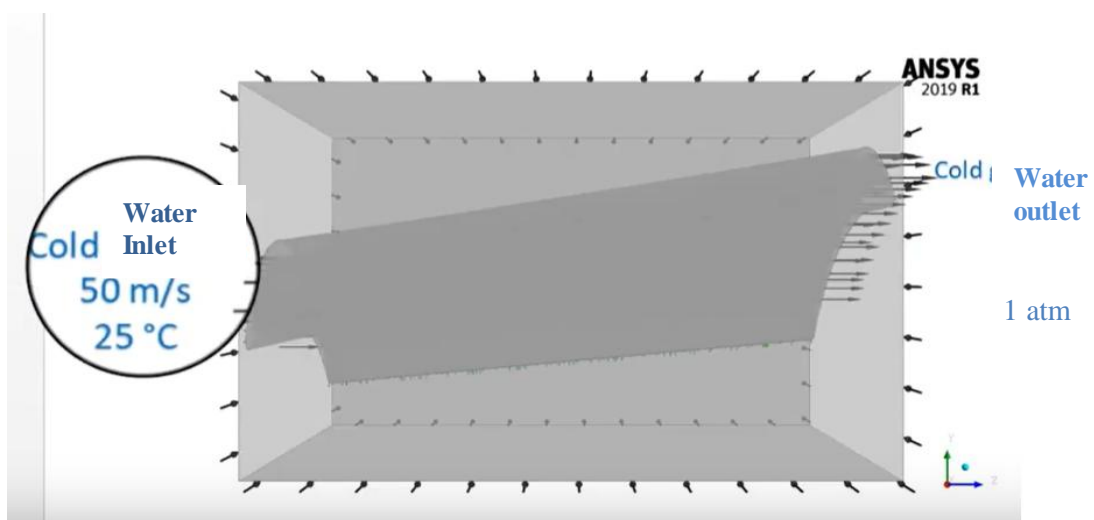


Fig 3. 15: Inlet and outlet boundary condition for cold water

The inlet velocity for cold water is 50m/s and the inlet temperature of cold water is 25⁰C. The outlet pressure for cold water is atmospheric pressure.

After defining the boundary conditions, the interfaces are defined between the blade and steam and blade and cold water. For defining the interfaces, the blade is considered to be a thin material of steel of thickness 0.1mm. In steam domain and blade domain, general connection interface is defined of fluid-solid interface type between surfaces already defined in mesh module. One interface is defined between surfaces of cold domain and blade already defined in mesh module with general connection and of fluid solid interface type.

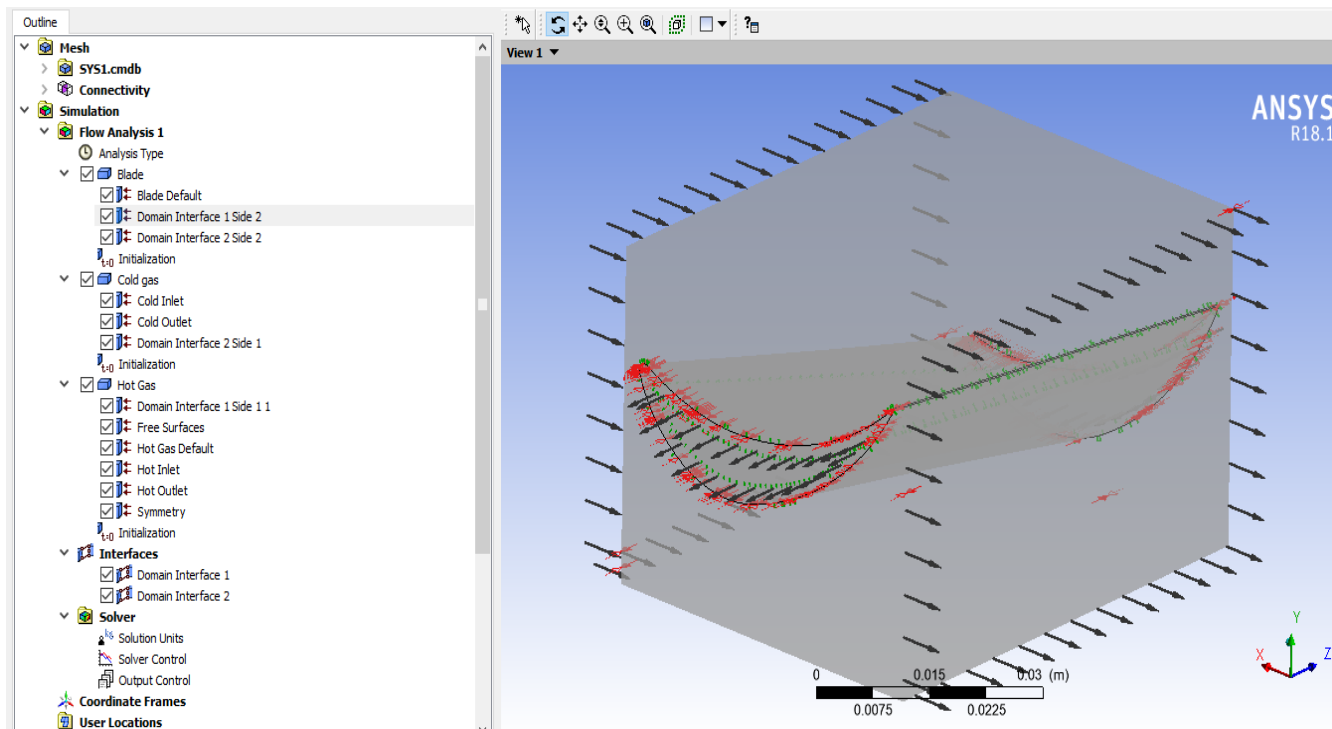


Fig 3.16: Setup module of the problem

For solving parameters, minimum number of iterations is set to 1 and maximum number of iterations is set to 1000. The residual type is set to RMS and residual target is set to 1e-4.

3.5.5.3 Solution

In solution module of Ansys R18.1 CFX software, double precision parameter is selected. Initial value is selected to current solution data (if possible). The problem is then run under solution module. The variables that were given a target residual of $1e-3$ are momentum and mass of cold water, momentum and mass of steam, heat transfer, turbulence kinetic energy for steam and turbulence kinetic energy for cold water.

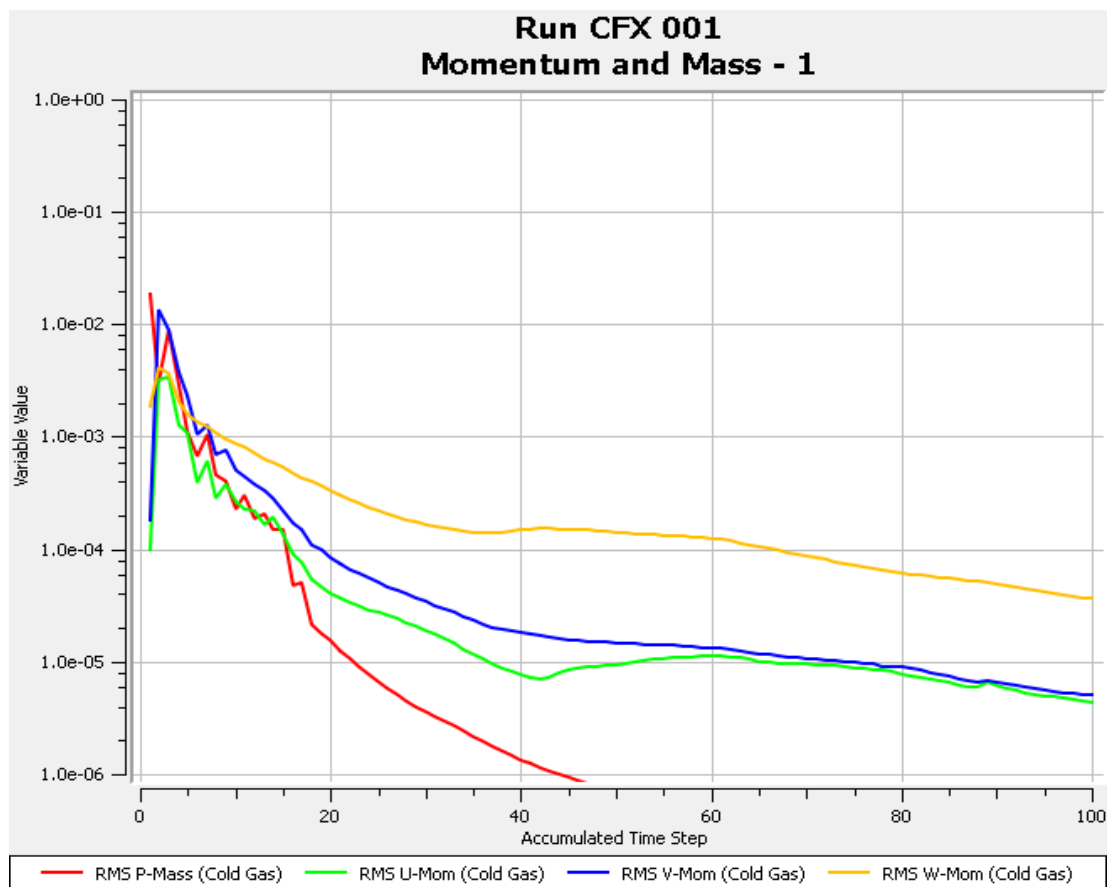


Fig 3.17: Momentum and mass residuals for cold water

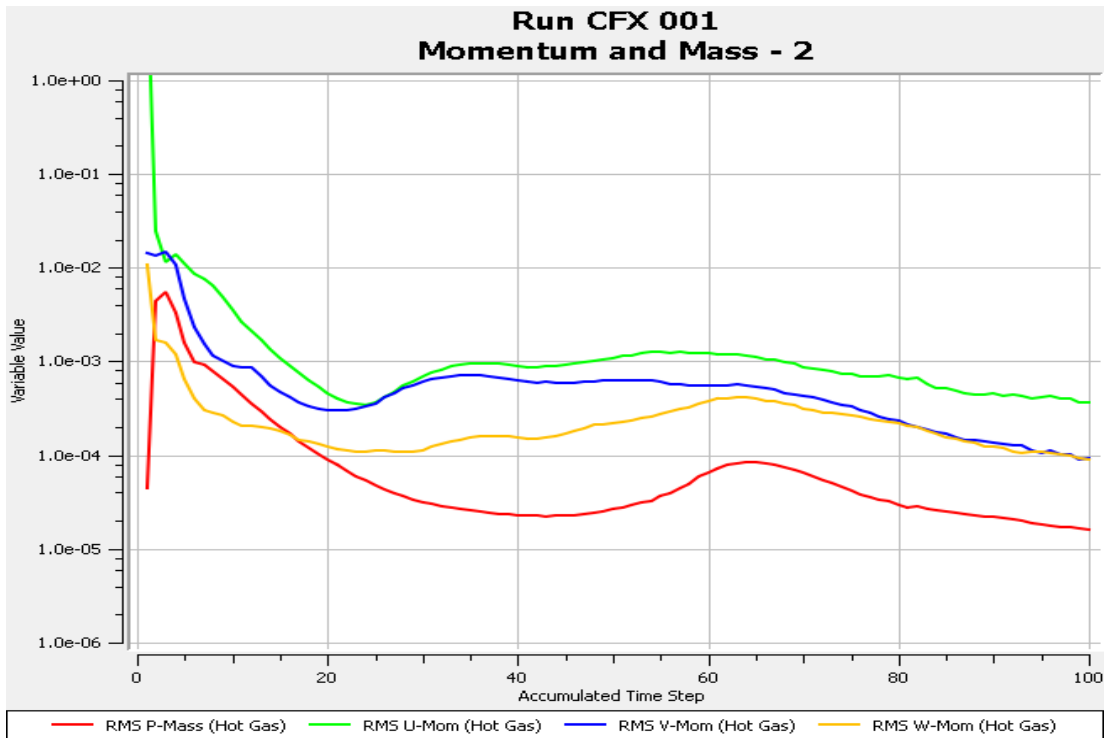


Fig 3.18: Momentum and mass residuals for steam

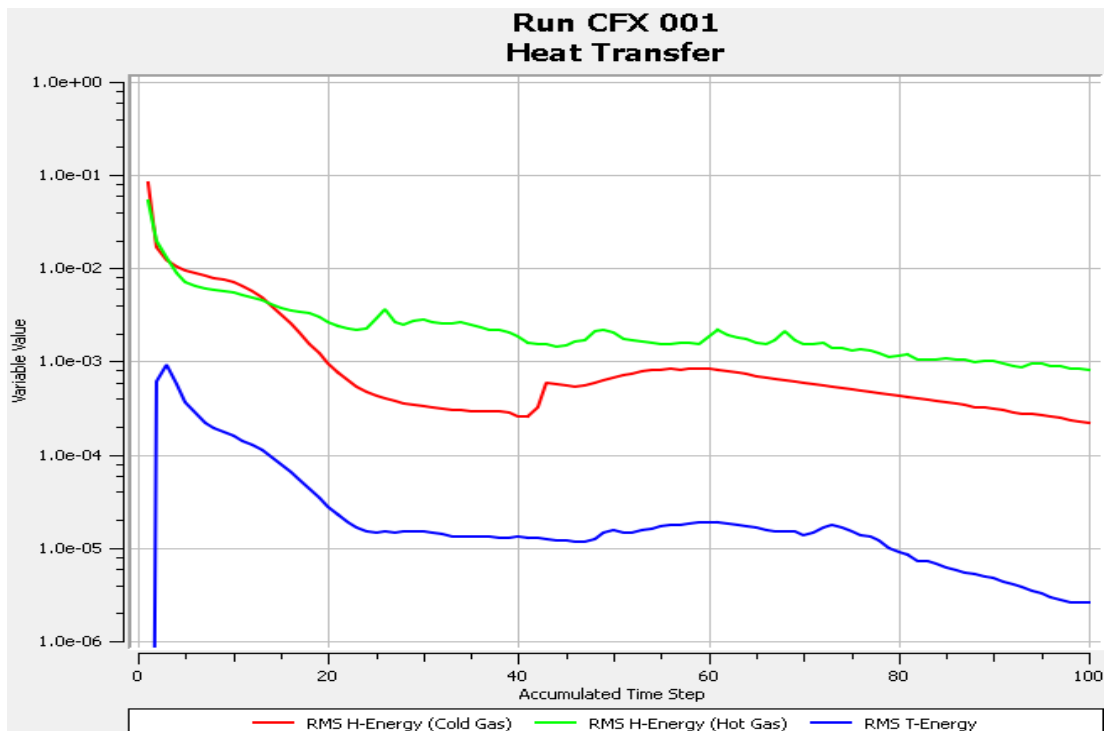


Fig 3.19: Heat transfer for cold water and steam

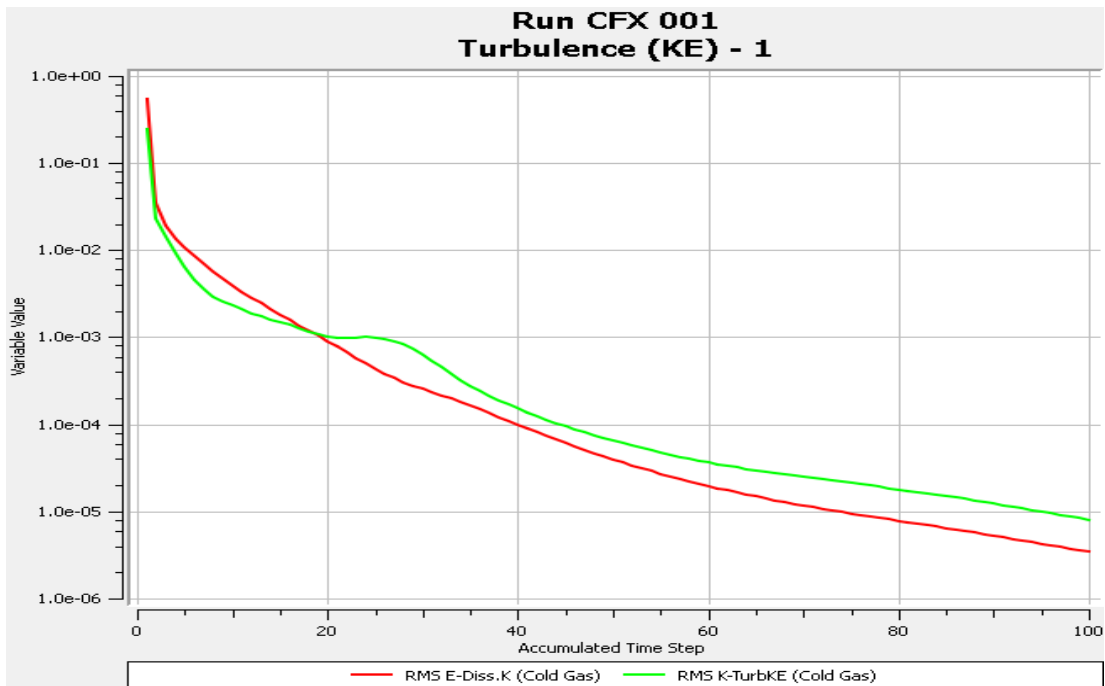


Fig 3.20: Turbulence kinetic energy residuals for cold water

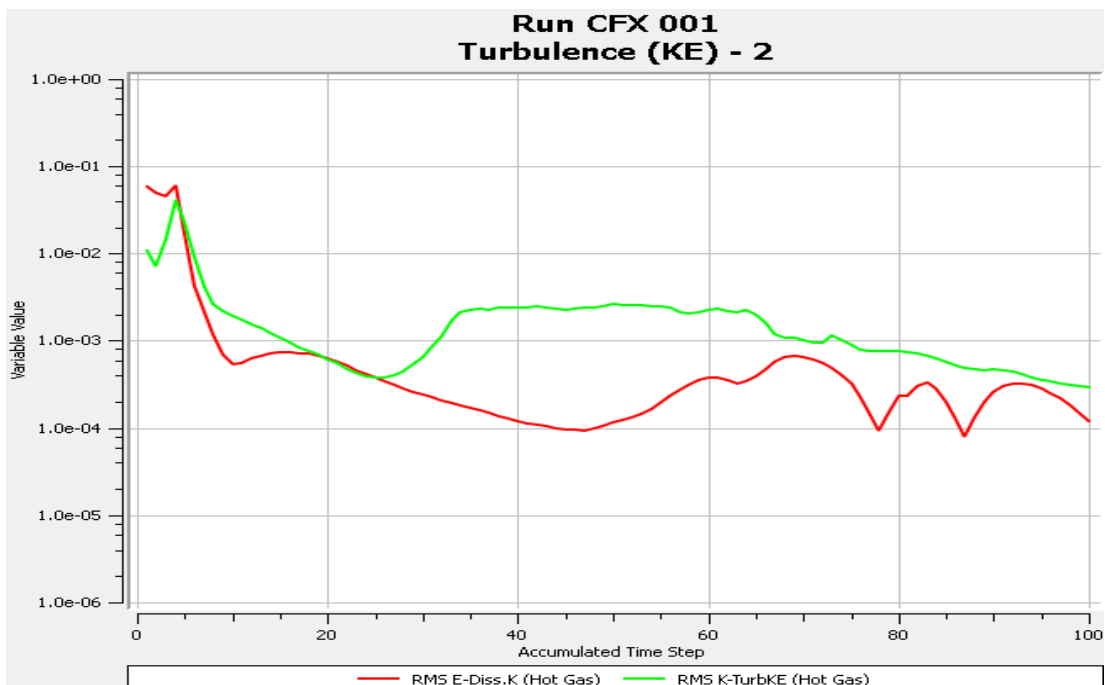


Fig 3.21: Turbulent kinetic energy residuals for steam

3.5.5.4 Results

The results are obtained in CFD-Post which is the post processor for Ansys R18.1 CFX software. Firstly, contours are obtained for different variables. For all the variables, domain is set to all domain type. Location is set to blade to hot interface. Range is set to global and number of contours is set to 101. The contours are obtained for temperature, pressure, and thermal gradient.

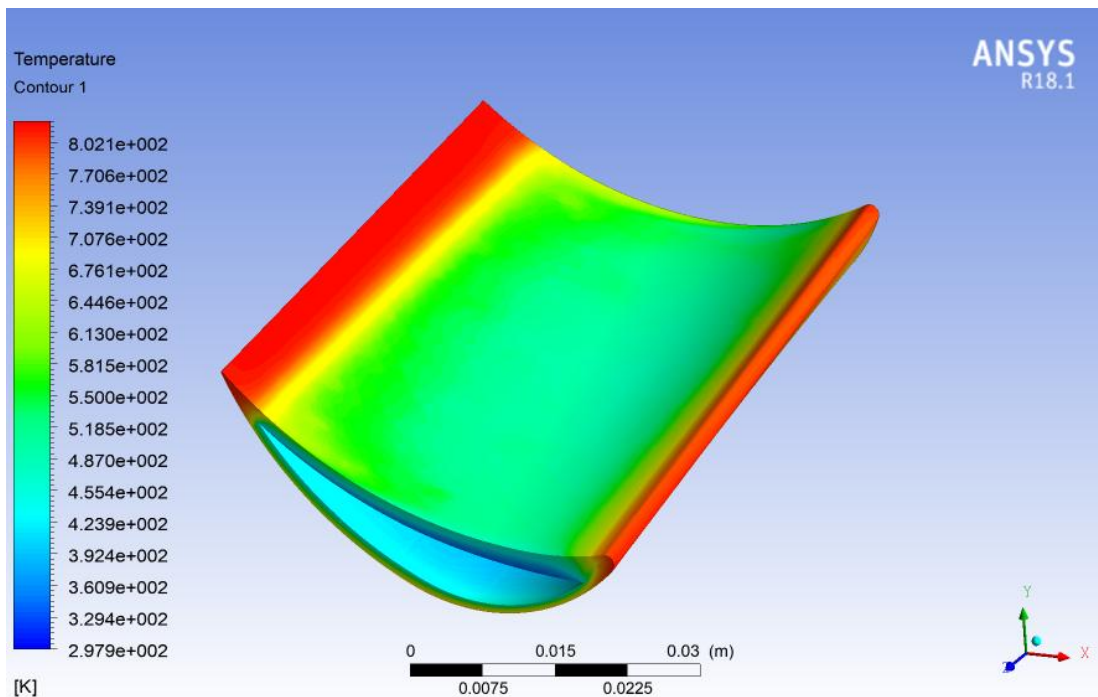


Fig 3.22: Temperature contour upper surface

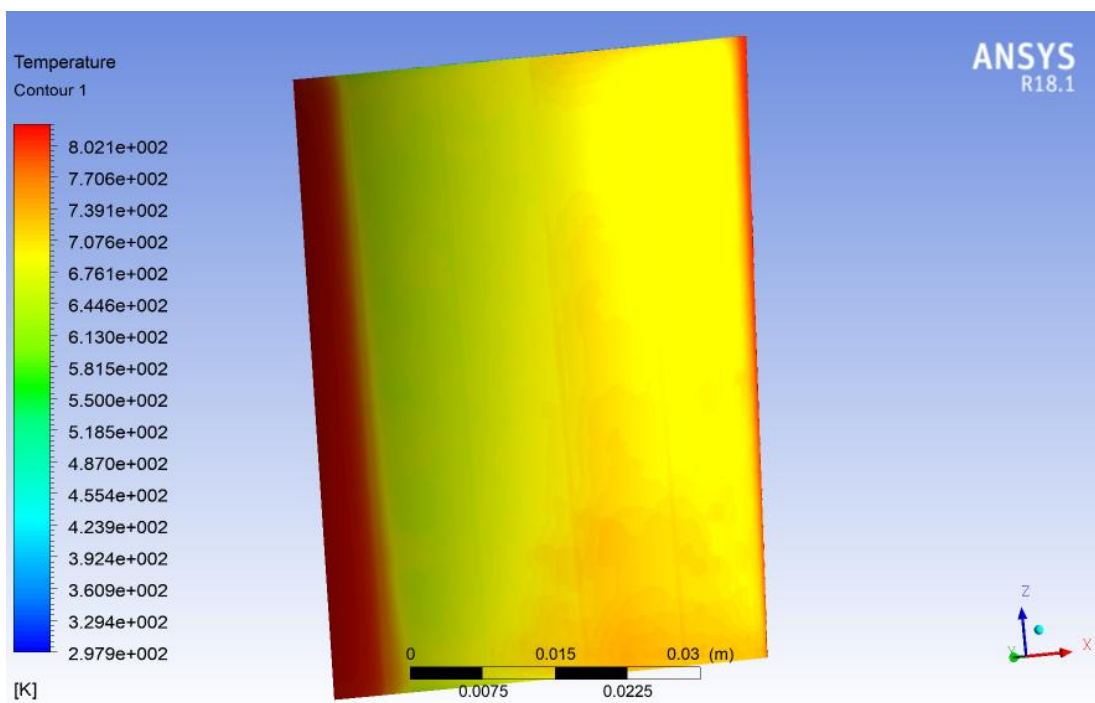


Fig 3.23: Temperature contour lower surface

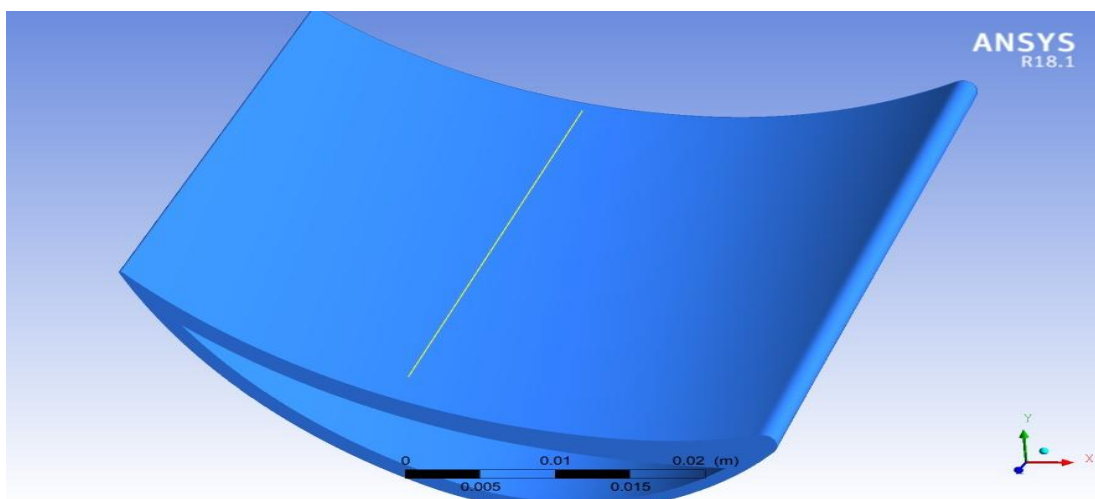


Fig 3.23(a): Line location in z direction on blade surface

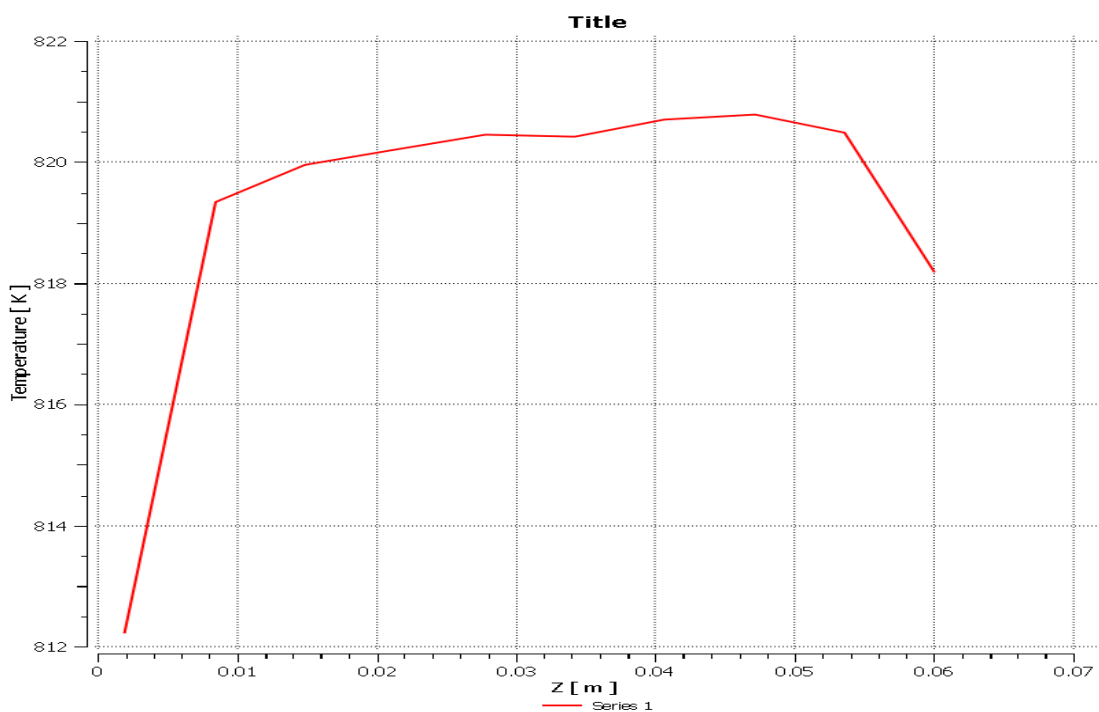


Fig 3.23(b): Temperature vs z graph along line in z direction on upper surface

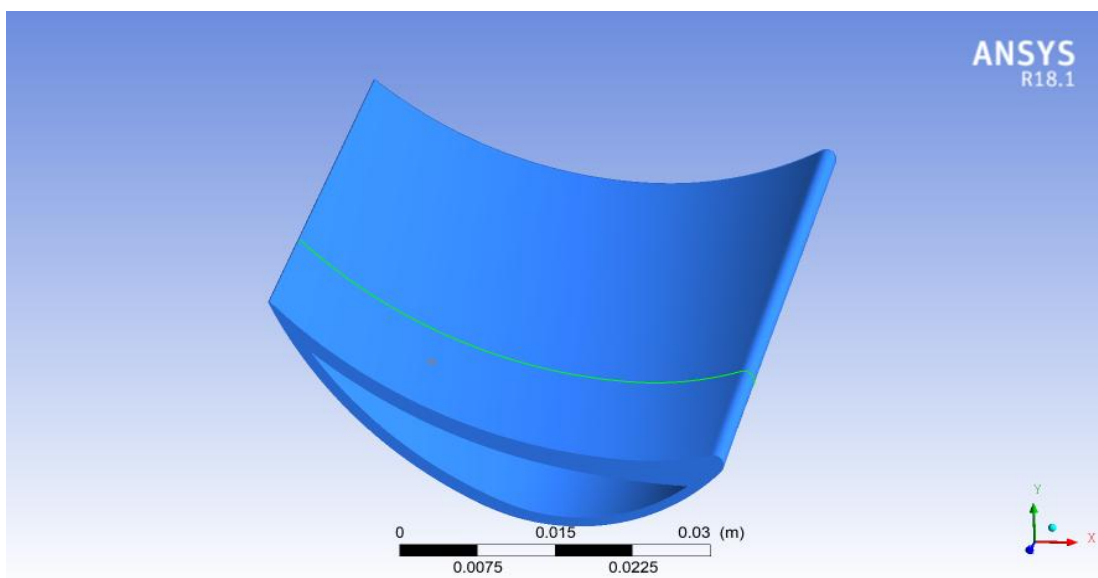


Fig 3.23(c): Polyline along x direction on blade surface

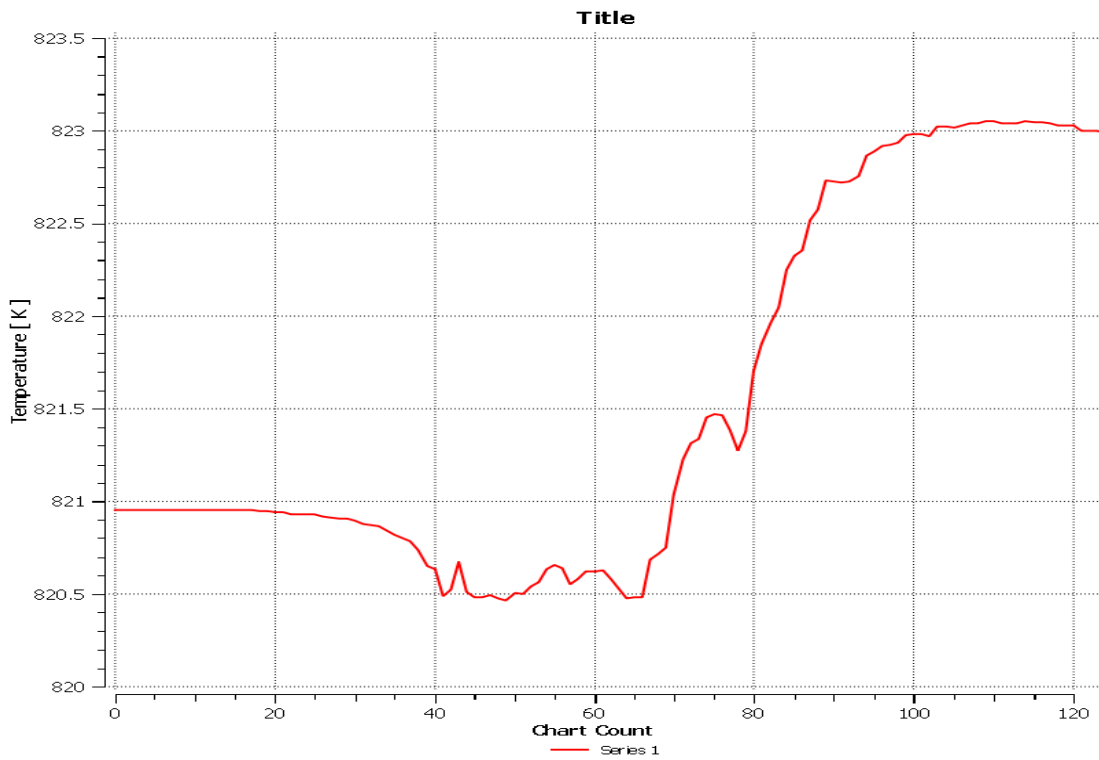


Fig 3.23(d): Temperature vs x graph on upper surface

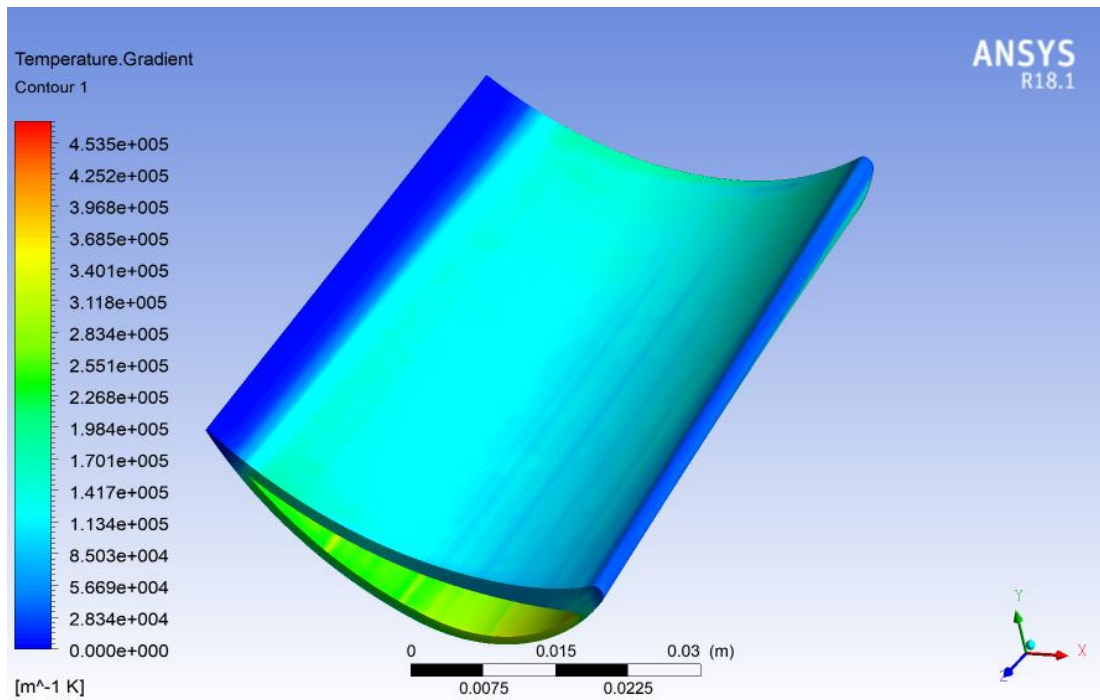


Fig 3.24: Temperature gradient contour on upper surface

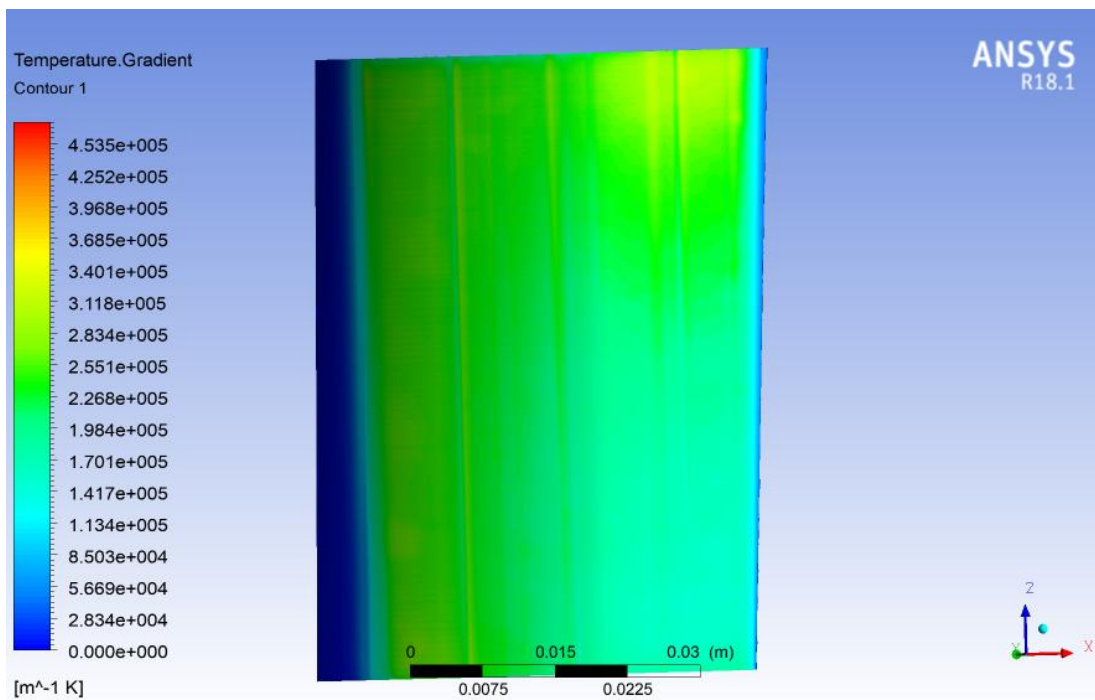


Fig 3.25: Temperature gradient contour on lower surface

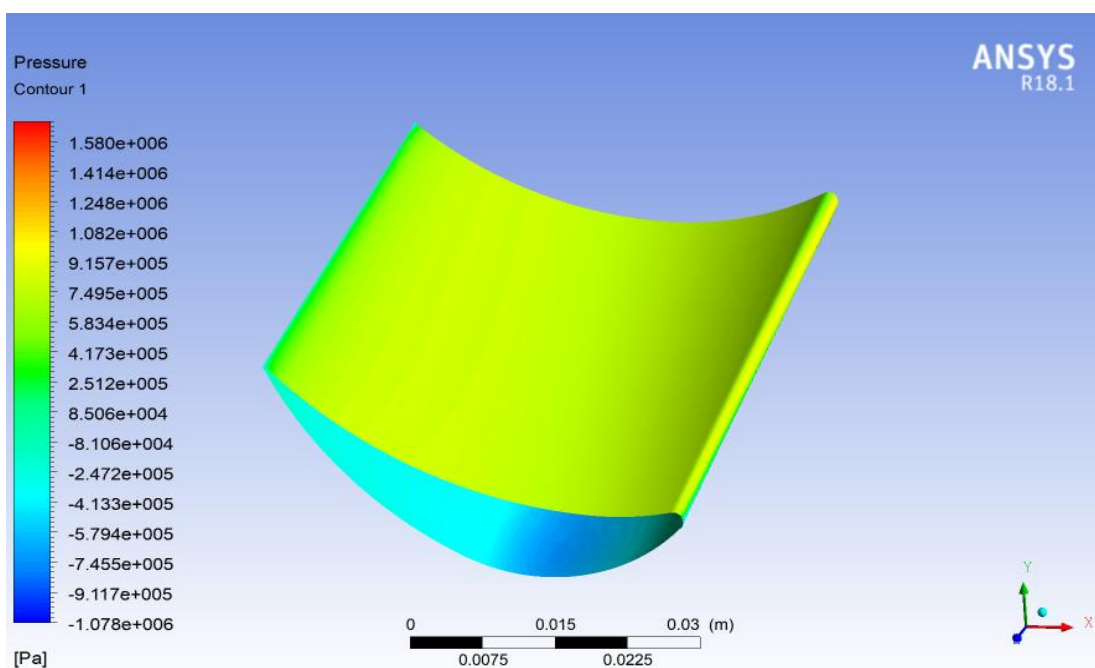


Fig 3.26: Pressure contour on upper surface

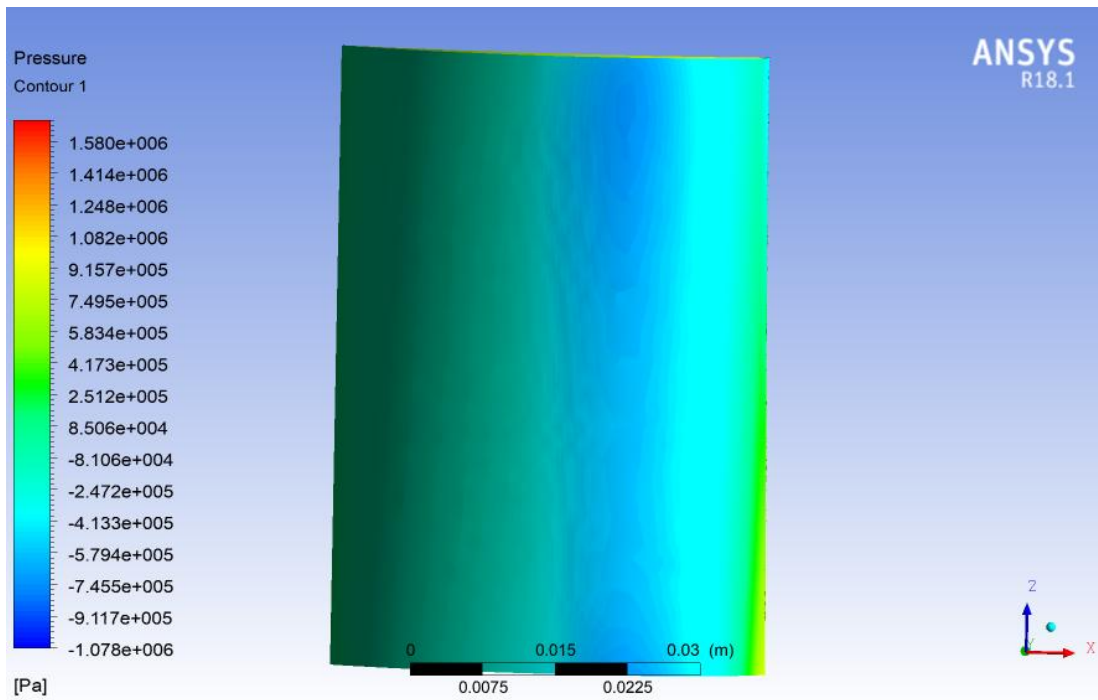


Fig 3.27: Pressure contour on lower surface

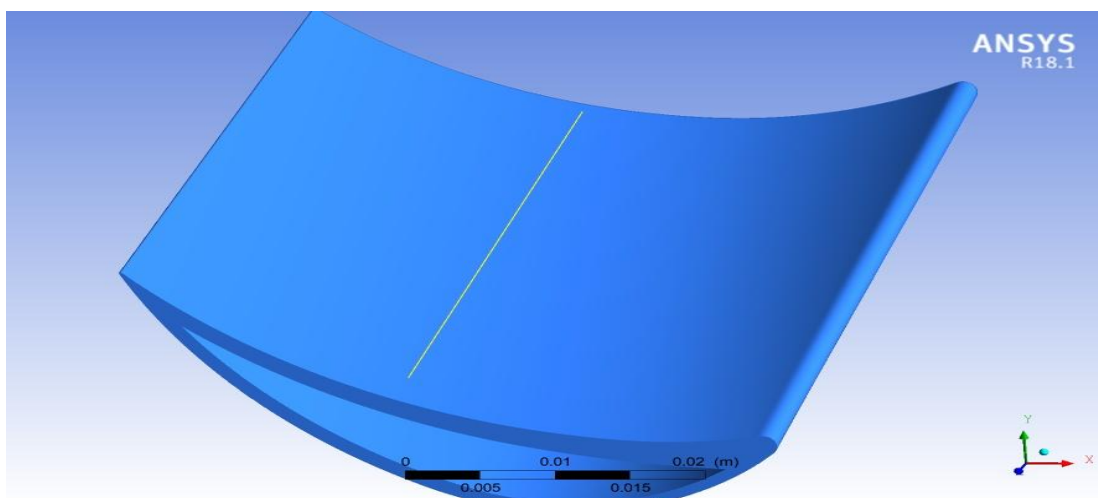


Fig 3.28: Line location on blade surface in z direction

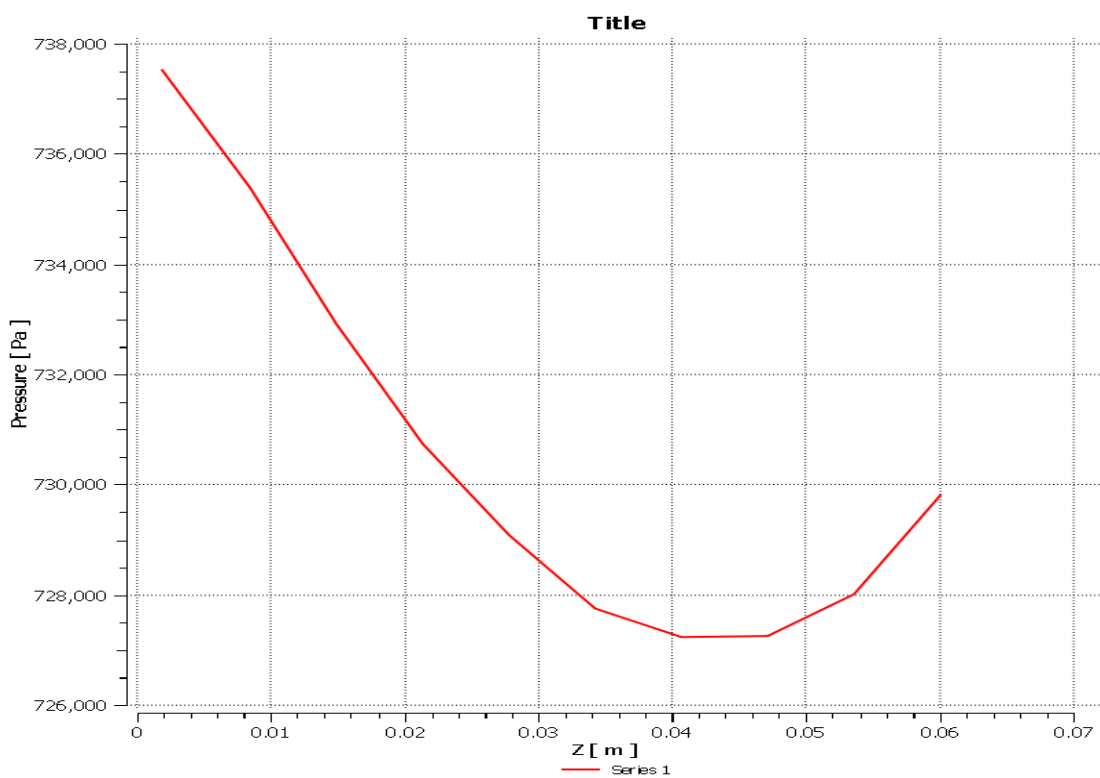


Fig 3.29: Pressure vs z curve along z direction on blade surface

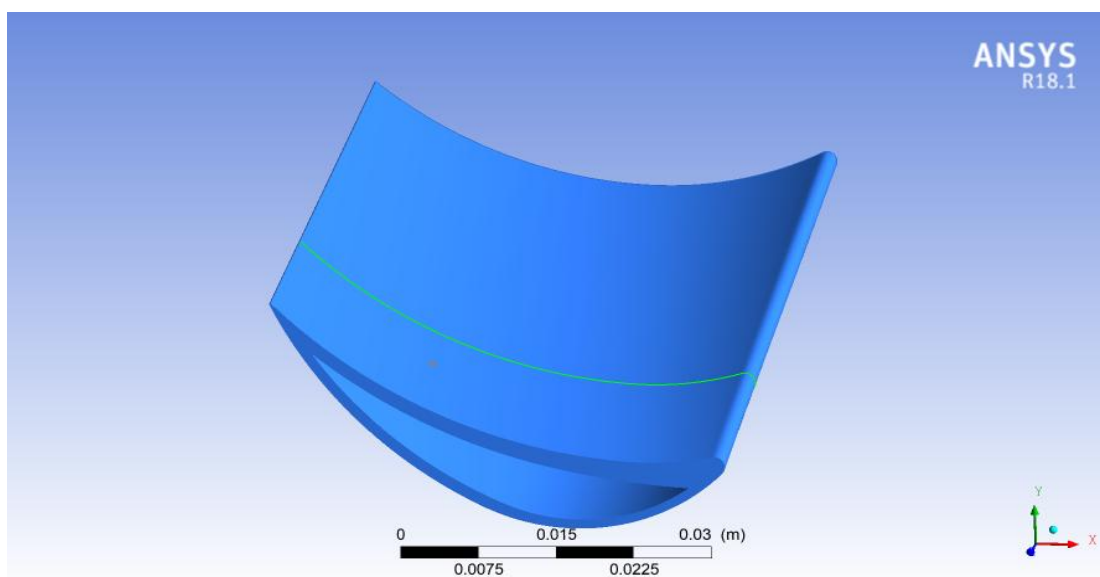


Fig 3.30: Line along x direction on blade surface

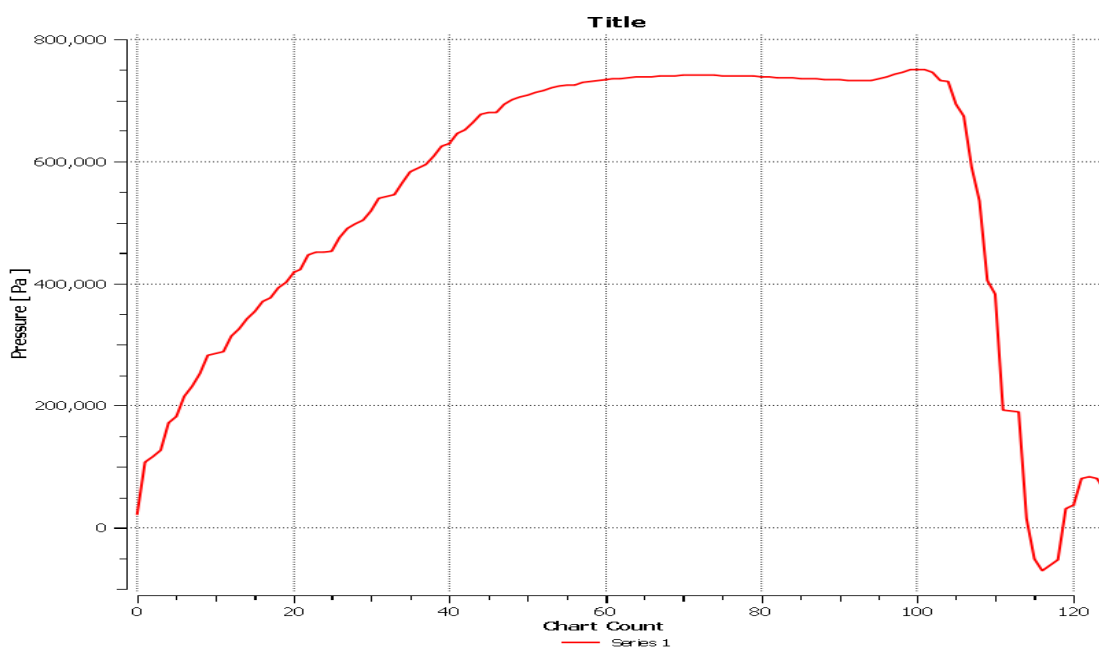


Fig 3.31: Pressure vs chart count along the line in x direction on upper blade surface

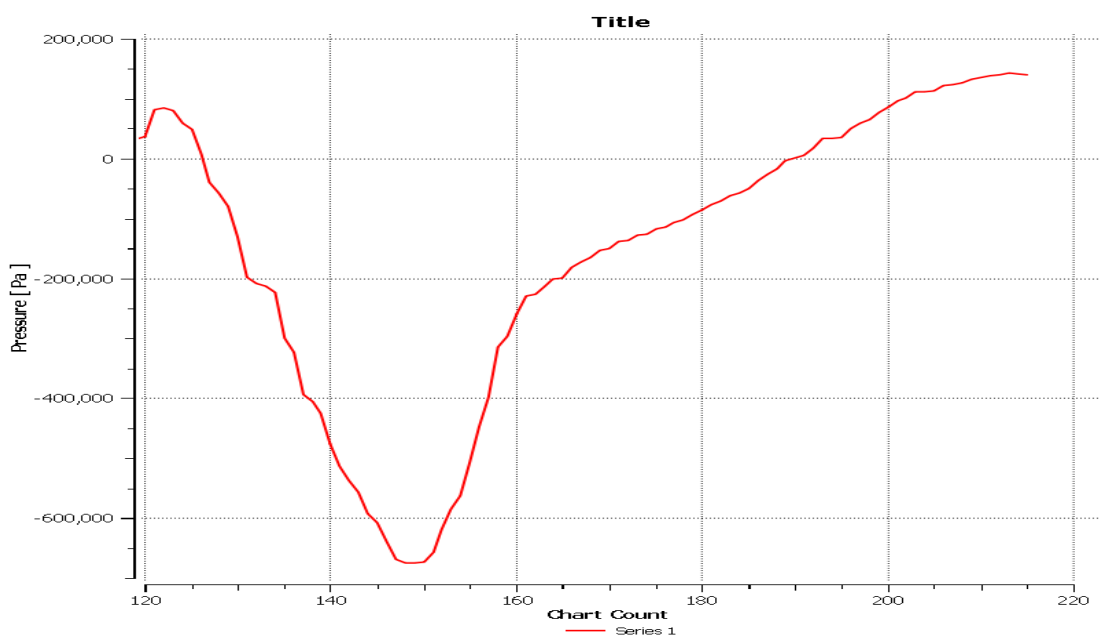


Fig 3.32: Pressure vs chart count along the line in x direction on lower blade surface

After this, an isosurface is defined passing through the blade in z direction in the steam domain. The isosurface is defined at a distance of .0223569m from the cold inlet surface. Contours for different variables are obtained on this isosurface. It is done to obtain the changes in those variables in the midway of their flow in the flow domain. Contour of pressure and vector of velocity is obtained on the isosurface formed.

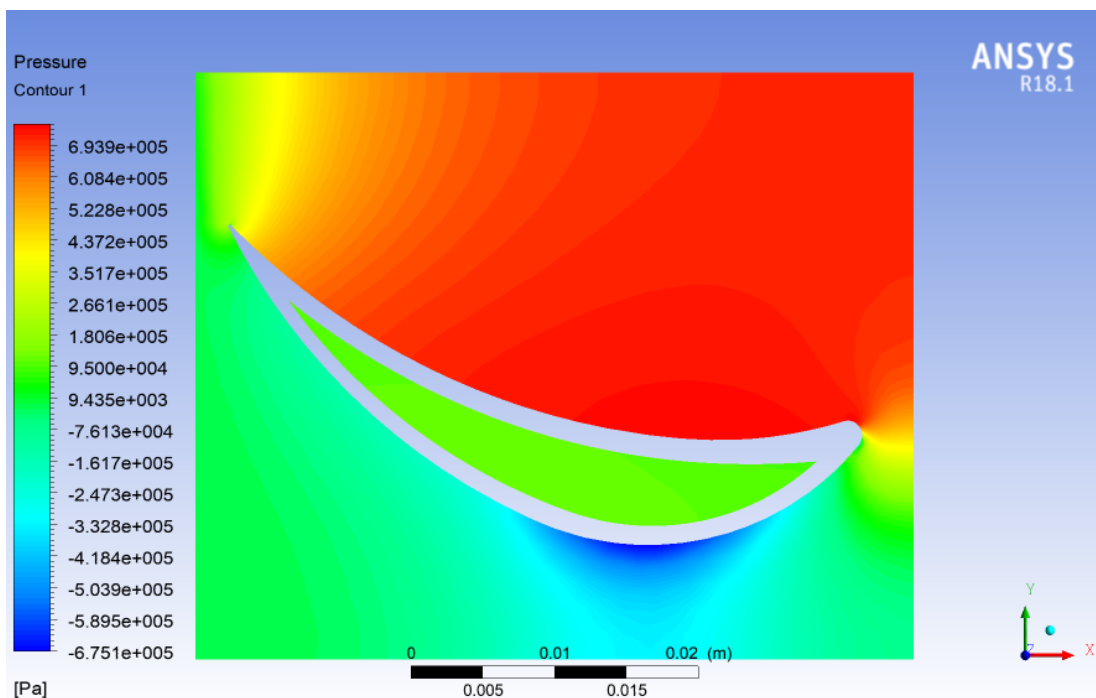


Fig 3.33: Pressure contour on a plane ($z = 0.0464391\text{m}$)

3.5.6 FEA Analysis

Finite Element Analysis is an analysis procedure used in different fields to solve physical problems using an algorithm on computer. As discussed in section 1.3.2, FEA is used in wide range of applications in different fields such as structural analysis, heat transfer analysis, modal analysis, dynamic and static analysis, electromagnetic, biomechanics etc.

For the problem of steam turbine blade under steady state condition, we have performed a structural analysis on Ansys R18.1 Static Structural software. Generally, Ansys R18.1 Static Structural software is used for performing linear static analysis, in which there are no dynamic forces and non linearity.

3.5.6.1 Methodology

In Ansys R18.1 Static Structural software, there are six modules, namely, engineering data, geometry, model, setup, solution and results. Firstly, the material is selected for the CAD model. Then, the geometry is created. After this, the geometry is meshed (divided into elements and nodes) in the model module. In the setup module, the analysis settings, boundary conditions, etc settings are assigned to the problem. In solution module, the software runs the simulation and results are obtained in results module.

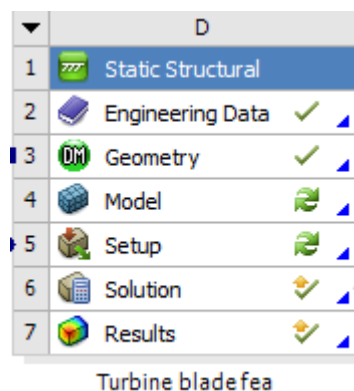


Fig 3.34: Ansys R18.1 Static Structural methodology

3.5.6.2 Engineering data

This module allows one to choose material properties from large number of predefined materials as well as create one's own material. Structural steel is assigned as the material

for turbine blade. This module automatically assigns different properties of the material selected such as density; coefficient of thermal expansion, young's modulus, bulk modulus, shear modulus, Poisson's ratio, tensile yield strength, compressive yield strength, tensile ultimate strength, compressive ultimate strength, strain life parameters etc.

Contents of Engineering Data		Source	Description
1			
2	Material		
3	Structural Steel	General	Fatigue Data at zero mean stress comes from 1998 ASME BPV Code
*	Click here to add a new material		

Properties of Outline Row 3: Structural Steel			
	A	B	
	Property	Value	
1	Material Field Variables	Table	
2	Density	7850	kg m ⁻³
3	Isotropic Secant Coefficient of Thermal Expansion		
4	Coefficient of Thermal Expansion	1.2E-05	C ⁻¹
5	Isotropic Elasticity	Tabular	
6	Derive from	Young's Modulus and Poisson's Ratio	
7	Interpolation Options	Table	
8	Alternating Stress Mean Stress	Tabular	
9	Strain-Life Parameters		
13	Tensile Yield Strength	2.5E+08	Pa
21	Compressive Yield Strength	2.5E+08	Pa
22	Tensile Ultimate Strength	4.6E+08	Pa
23	Compressive Ultimate Strength	0	Pa
74			

Fig 3.35: Engineering data module

3.5.6.3 Geometry

Since the geometry remains the same for FEA analysis as CFD analysis, geometry for the FEA analysis is directly imported from Ansys R18.1 CFX geometry module. After geometry is imported, it is then edited in DesignModeler. All the fluid domains, which are steam domain and cold water domain are suppressed for this analysis. Now, only the solid domain geometry, that is, blade is present for analysis. Then distributed mass is assigned to the blade over its entire body. The distributed mass is calculated using the Equation (3.7). Density is obtained from engineering data module and volume is obtained from geometry module. This is done in order to have better quality of mesh.

$$\text{Point mass} = \text{density} * \text{volume} \quad (3.7)$$

$$\text{density} = 7850 \text{ kg/m}^3$$

$$\text{volume} = 8.5002\text{e-}6 \text{ m}^3$$

$$\text{distributed mass} = 7859 \text{ kg/m}^3 * 8.5002\text{e-}6 \text{ m}^3$$

$$\text{distributed mass} = 6.6727\text{e-}2 \text{ kg}$$

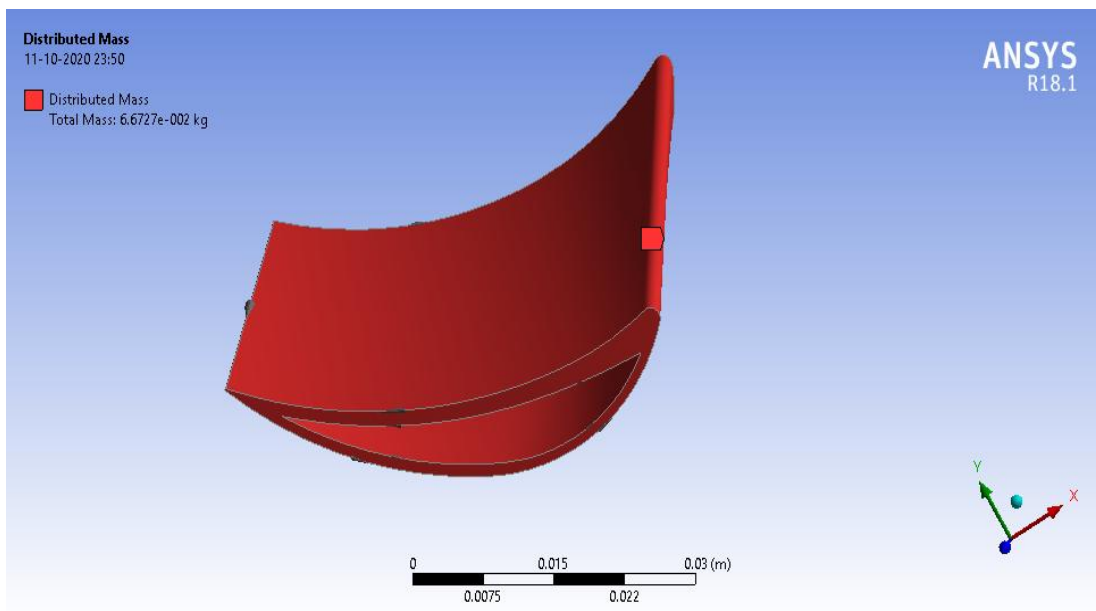


Fig 3.36: Distributed mass applied to blade

3.5.6.4 Model

In model module, firstly, a coordinate system is created apart from the default global coordinate system with coordinates of origin as (0, 0, 0). A remote point is defined for providing fixed support to the turbine blade. It is defined on the face of cold inlet fluid. Finally, the blade model is meshed with medium smoothing, target quality of 0.5 and adaptive size function. Physics preference is set to Mechanical and element order is program controlled. The mesh is developed with 10 noded tetrahedral elements on the blade. The mesh was successfully created with 131995 nodes and 78994 elements.

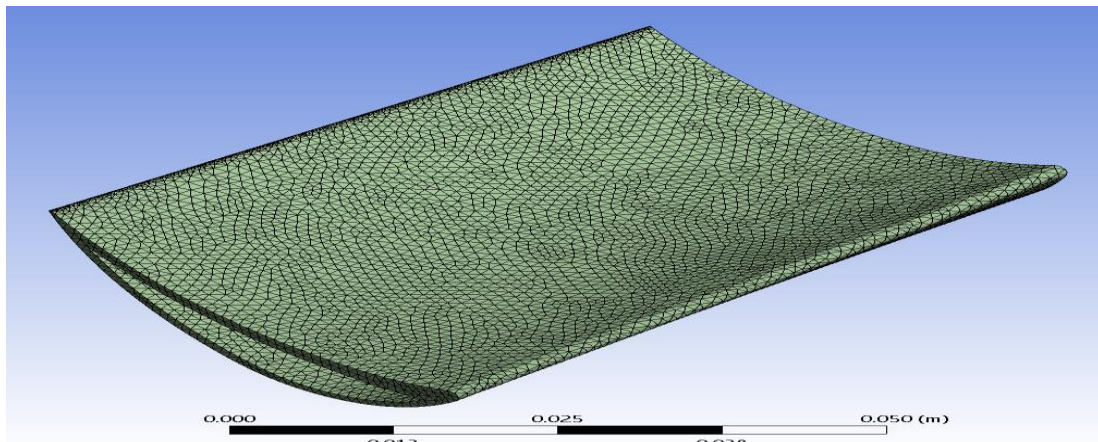


Fig 3.37: Meshed geometry for FEA analysis

3.5.6.5 Setup

In setup module, analysis setting is setup. The number of steps, current step number and step end time are set to 10, 1 and 1 respectively. In output control stress, strain and nodal forces are set to yes. After analysis settings, rotational velocity is provided to turbine blade. Rotational velocity is provided in x direction of magnitude 314 rad/s. The blade will rotate about x direction at a distance of 7.29×10^{-2} mm from the centre of mass in negative z direction. The centre of rotation is kept at an imaginary point from turbine blade in space, as that point is considered to be the centre of rotor to which turbine blade is attached. Then, fixed boundary condition is applied to remote point that is zero displacement in all directions and zero rotation in all directions.

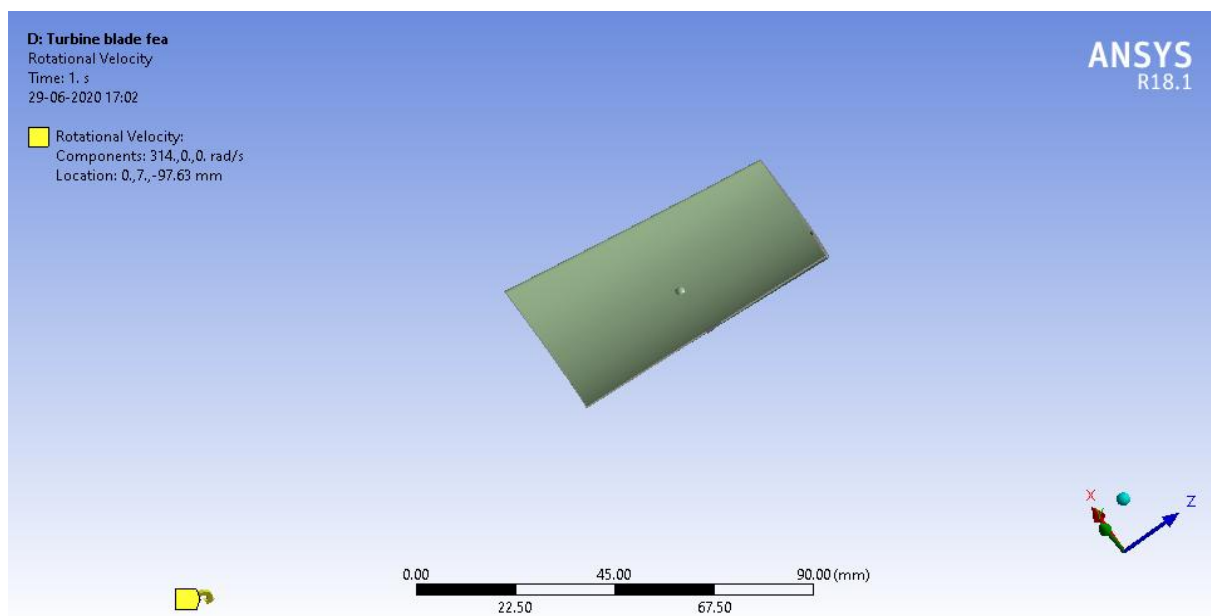


Fig 3.3

3.38: Rotational velocity applied to turbine blade

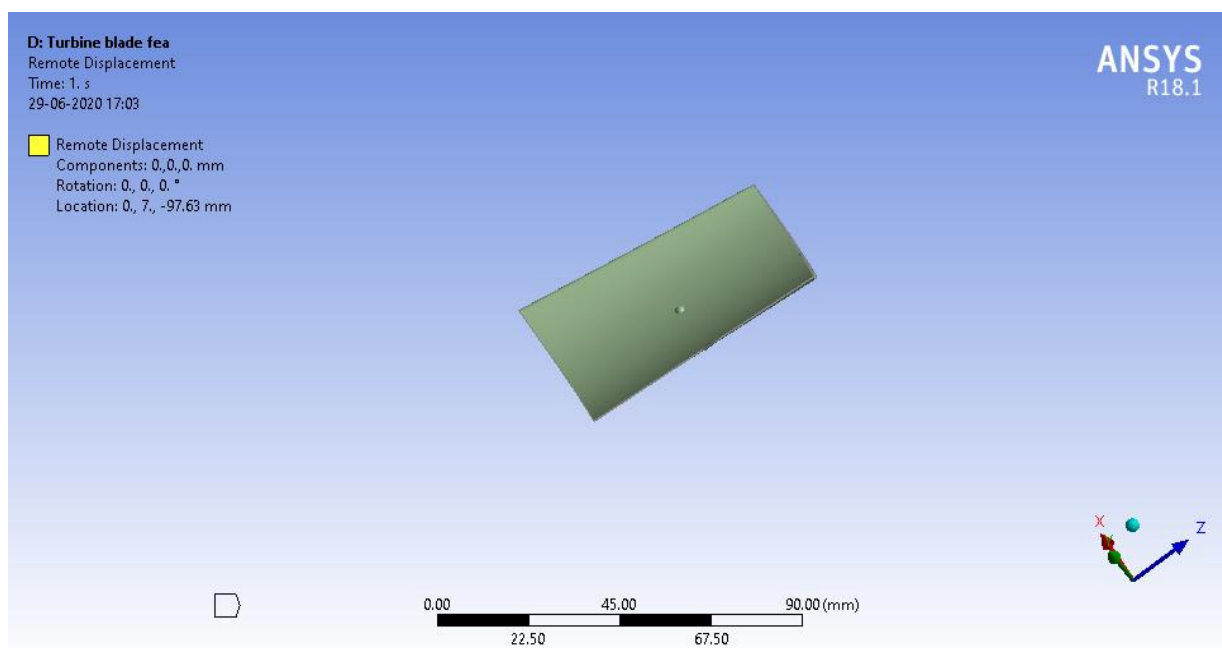


Fig 3.39: Fixed boundary condition at cold inlet surface

In CFD analysis performed earlier for the same problem, the steam was directly hitting the turbine blade to rotate the turbine, thus imparting pressure load on turbine blade. This pressure load and body temperature is imported from Ansys R18.1 CFX to Ansys R18.1 Static Structural. The pressure is imported on blade to hot interface surface. The body temperature is also imported on the blade which will act as thermal load in FEA analysis.

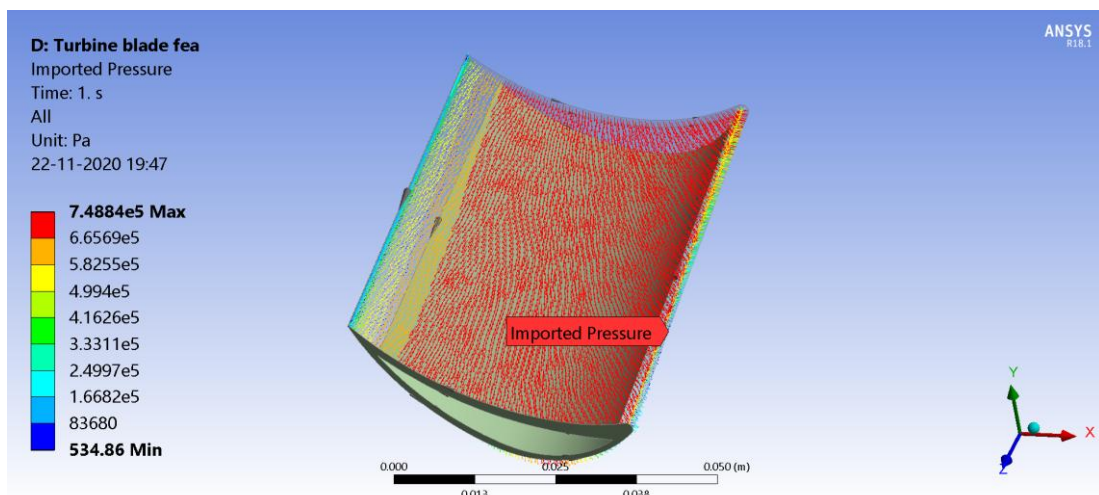


Fig 3.40: Pressure on turbine blade on upper surface

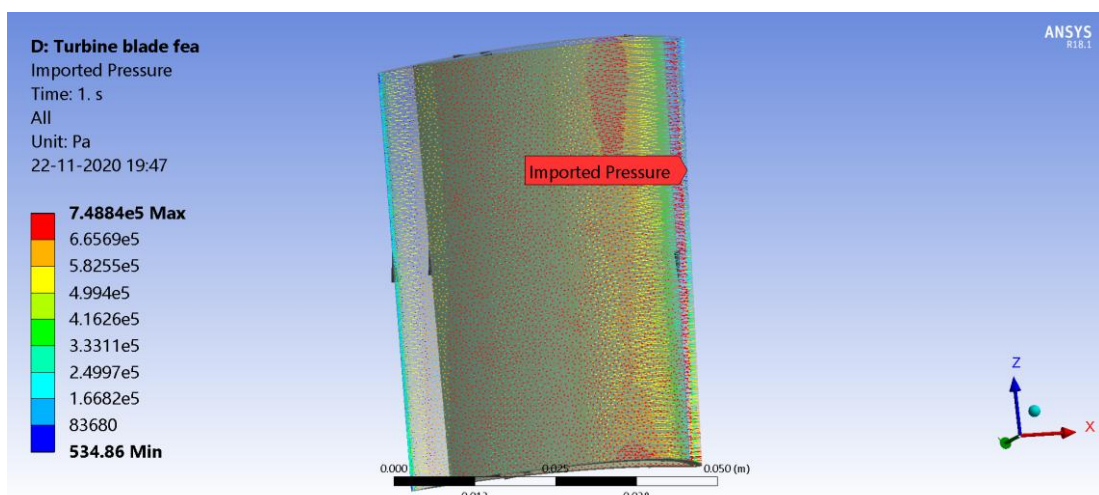


Fig 3.41: Pressure on turbine blade on lower surface

3.5.6.6 Solution and Results

In the solution module, the software runs the simulation and results module display the results. Contours of total deformation and equivalent von-mises stress are obtained for the turbine blade. Also, the values of force reaction and moment reaction are obtained at the fixed support of turbine blade. The simulation run took 33 sec to complete. The MAPDL memory used is 279 MB and the MAPDL result file size is 17.563 MB.

Contours of total deformation and equivalent von mises stress are obtained.

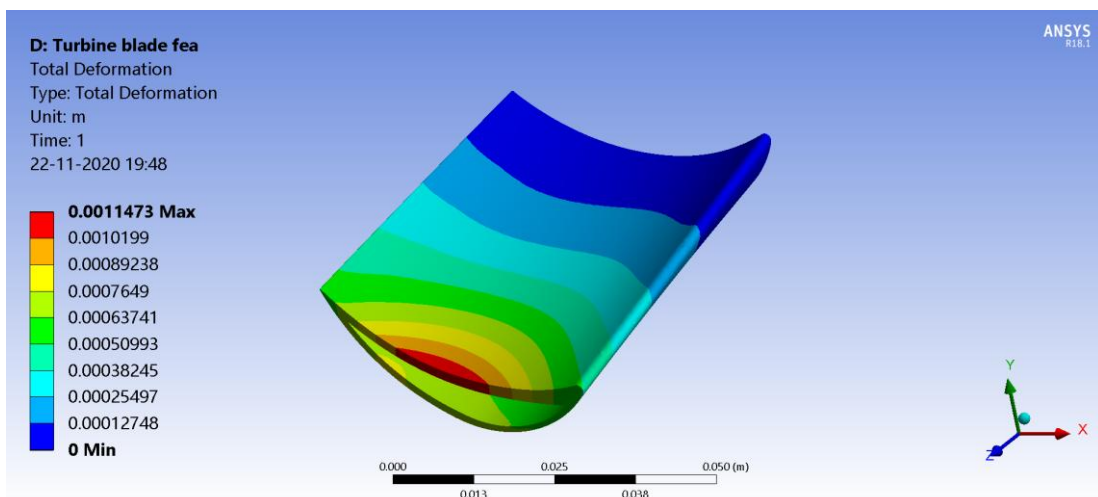


Fig 3.42: Total deformation contour on upper surface of the blade

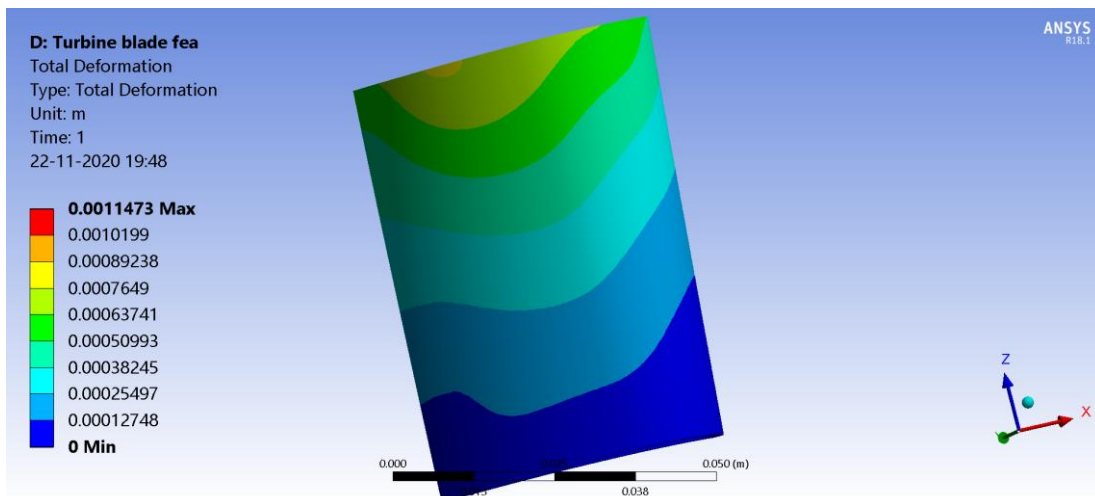


Fig 3.43: Total deformation contour on lower blade surface

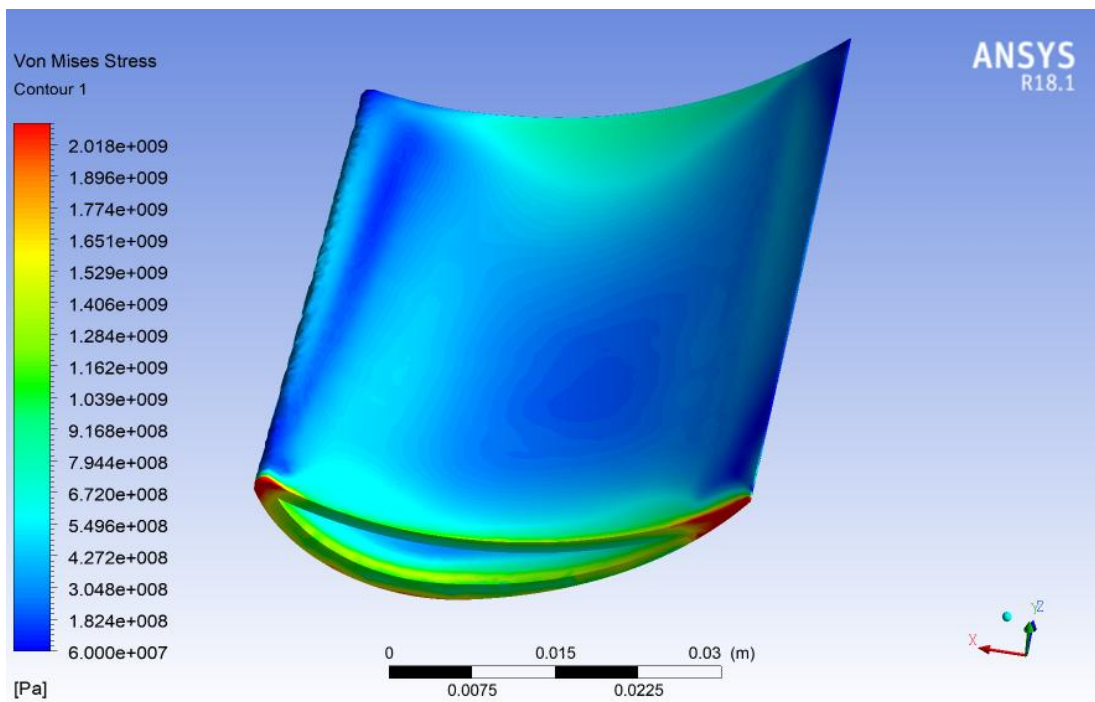


Fig 3.44: Equivalent stress contour on upper surface of the blade

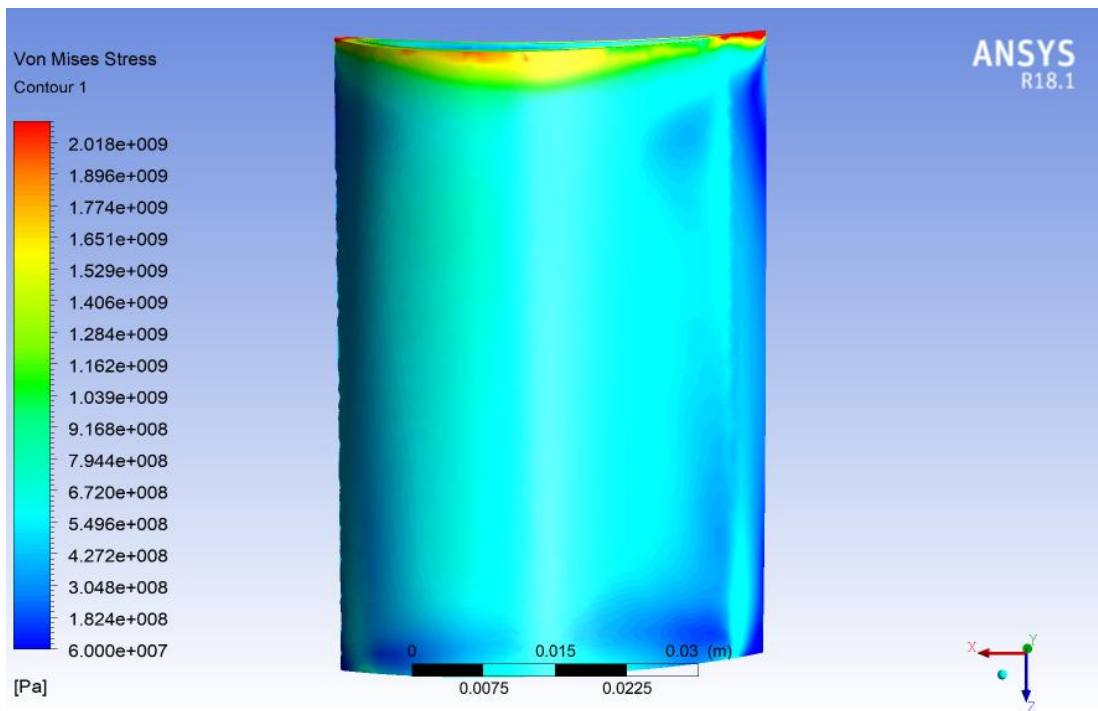


Fig 3.45: Equivalent stress contour on lower surface of the blade

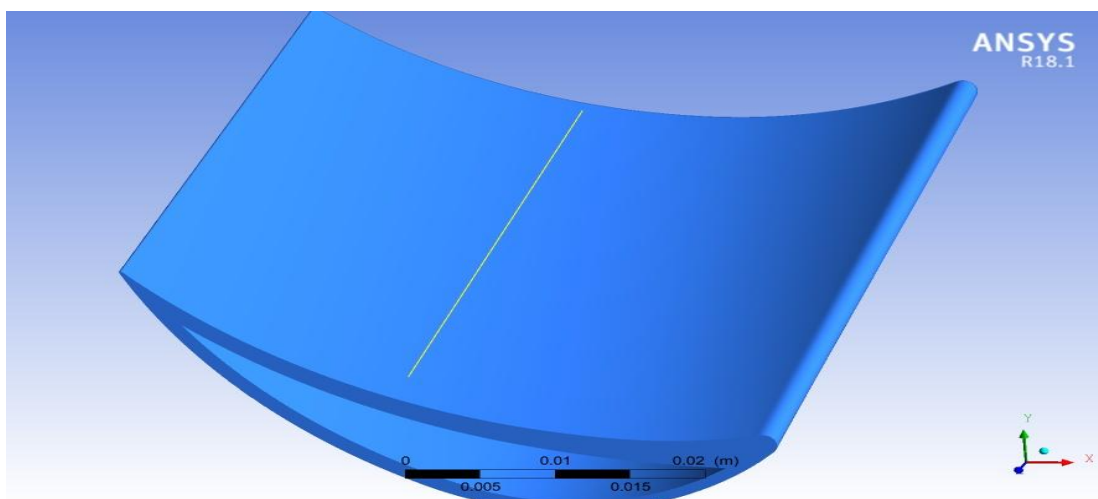


Fig 3.46: Line location along z direction

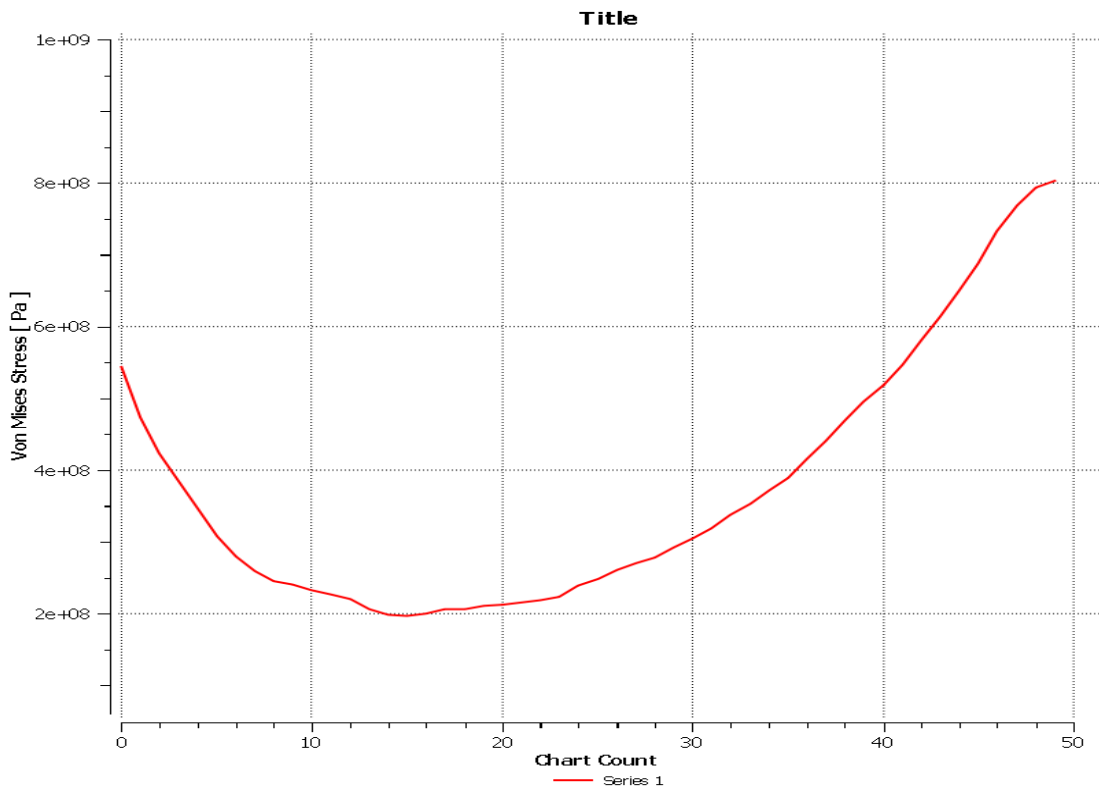


Fig 3.47: Stress vs z graph along line in z direction

After this, force reaction and moment reaction are also obtained at the remote point. The Figure 3.26 and Figure 3.27 represent the direction of force reaction and moment reaction.

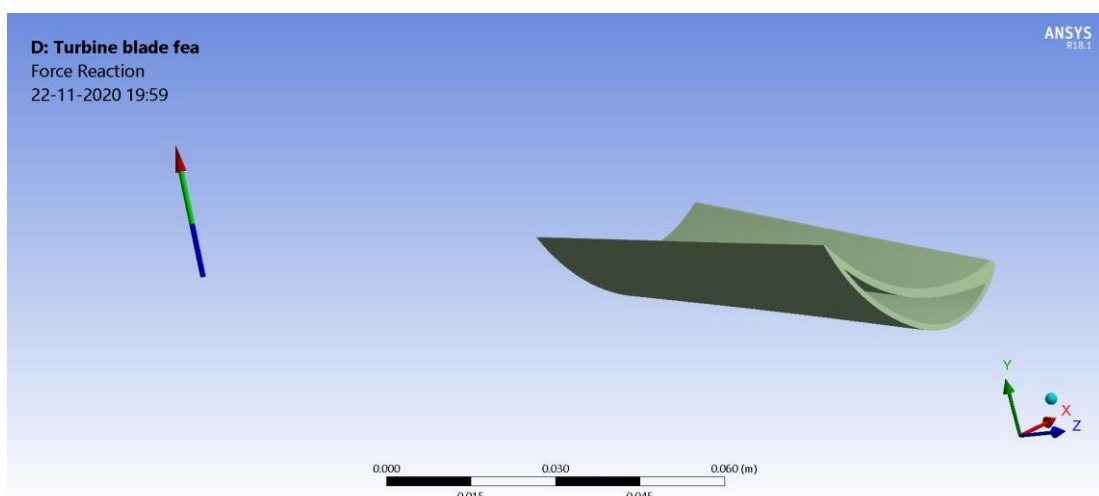


Fig 3.48: Force reaction direction and magnitude (3011.9 N)

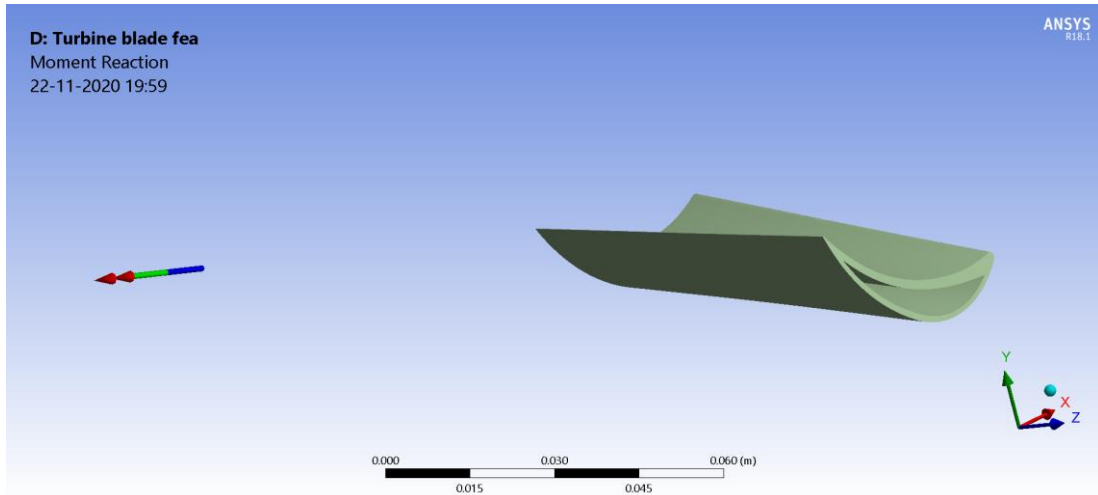


Fig 3.49: Moment reaction direction and magnitude (384.86 Nm)

CHAPTER 4: TRANSIENT FSI ANALYSIS

In this chapter, stress and strain analysis is performed for steam turbine blade under transient conditions. First of all, transient conditions are explained in this chapter. Then types of stress experienced by turbine blade during transient conditions are discussed. After this, damage caused to turbine blade due to these stresses is explained. Finally, complete FSI simulation is discussed performed on Ansys R18.1 software. It is also to be noted that only one transient event has been taken in this analysis that is start-up. Hence, at every point in this report, by transient event we mean start-up event.

4.1 TRANSIENT CONDITION

Transient conditions are those conditions in which the input parameters varies with time, the output parameters may or may not vary with time. In other words, one can say that transient conditions are time dependent. Generally, the output also varies with time in transient conditions. Also, transient conditions are dynamic conditions and are difficult to understand or capture. It also means that these conditions make transitions from one state to another. Also, transient conditions are difficult to solve both analytically and computationally in comparison to steady state conditions. If a steady state is reached after a transient condition, then first transient condition is solved and then, steady state is solved taking transient solution as initial value for steady state.

For steam turbine operation, there are various types of transient conditions that occur during a cycle. Transient conditions occur before as well as after steady state operation. Also, in this case, the output also varies with time during transient conditions. In steam turbine, transient condition is related to two aspects; one is transient condition of inlet steam and second is the transient condition of turbine in form of output. The various

transient events occurring in an operation cycle of steam turbine is start up, shut down, load changing events, speed changing events etc.

Start up, as the name suggests is used to start the steam turbine from halt condition. Shutdown is used to take the turbine from working condition to a halt condition. Due to change in output requirements from turbine, speed and load changes take place in between the operation cycle which are also included in transient events. During repair times, load change and speed change events takes place. During steady state, turbine workers require setting the system to steady state condition and thereafter, no more attention is required of the workers. Whereas, in transient conditions, regular attention of turbine workers is required since the parameters of turbines are required to be changed regularly. Shutdown needs to be performed with accurate procedure because steam turbines running at high rpm and at high temperatures need to be put to halt. If the turbines operating at high temperatures are suddenly put to halt, then large thermal gradients will be produced in the blade and rotor, leading to large thermal stresses, hence leading to damage of turbine components. Therefore, this process is performed gradually.

4.2 START UP

A start up is a process of moving turbine from a halt condition to a working steady state condition. Turbines are an important component of any big application they are a part of. Also, turbines are heavy and expensive machines, which require proper maintenance, repair and conditioning. Steam turbines deal with high temperature steam for their operation. The steam temperature at inlet may reach as high as 2000K. If a steam turbine has been in shutdown for certain period of time and suddenly, such high temperature steam is allowed to pass through it, it may lead to a lot of damage to the components of turbine. To avoid this damage, the steam turbine is firstly, made to rotate at an initial low speed with the help of turning gear. Then the inlet steam passes through turbine almost at half the value of steady temperature. The pressure and velocity is low at initial time stage. After

this, the inlet steam temperature, pressure and mass flow rate keeps on rising gradually until it reaches the steady state value. Then the start up phase is said to be over and after this, the turbine works under steady state condition.

As discussed in section 2.1, start up procedures are of three types, namely, cold start, hot start and warm start [Banaszkiewicz, 2014]. These start ups are classified based on the inner casing temperature by Banaszkiwicz(2014). In his research, he classified them as follow:

- Cold start – when HP inner casing temperature is lower or equal to 170°C
- Hot start – when HP inner casing temperature is greater than 430°C
- Warm start – when HP inner casing temperature is lower or equal to 430°C

Start-ups are also classified on the basis of steady state casing temperature (T_0) at initial stage of start-up. It is classified as:

- Cold start - $T_0 < 170^{\circ}\text{C}$
- Warm start – $170^{\circ}\text{C} < T_0 < 430^{\circ}\text{C}$
- Hot start – $T_0 > 430^{\circ}\text{C}$

The steam parameters during a start up mainly depend on the time period of standstill of the turbine [Banaszkiewicz, 2014]. The following parameters are observed by Banaszkiwicz(2014):

- 2 hour standstill – $p = 12 \text{ MPa}$, $T = 480\text{-}500^{\circ}\text{C}$
- 8 hour standstill – $p = 6 \text{ MPa}$, $T = 450\text{-}480^{\circ}\text{C}$
- 36 hour standstill – $p = 5 \text{ MPa}$, $T = 400\text{-}430^{\circ}\text{C}$

where p and T represent pressure and temperature of live steam.

Proper procedure needs to be followed while operating steam turbine during start up. Some of the instructions are given in turbine operations instructions and other parameters are

obtained from a visual graph called as start up curves [Banaszkiewicz, 2014]. These curves are prepared separately for each individual turbine. Figure 4.1 represents a start up curve for a cold start after standstill of 72 hours [Banaszkiewicz, 2014]. In his research paper, he states that start up curves include details of pressure, temperature, rotational speed, power output, mass flow rate etc. In his research paper, it is also mentioned that modern steam turbines are provided fast start ups of duration between 1 to 3 hours. Specific tools designed for an individual turbine is used to form the start up curve for that turbine [Banaszkiewicz, 2014]. Presently, start up curves is formed keeping in mind the stresses produced and the time taken. Hence starts up curves are formed optimally [Banaszkiewicz, 2014]. There are certain parameters such as temperature differential between steam and metal, temperature differential between upper and lower parts of casing etc are tested experimentally on turbines with designed start up procedure. Then depending on the experimental results and permissible values, modifications in start-up curves is done.

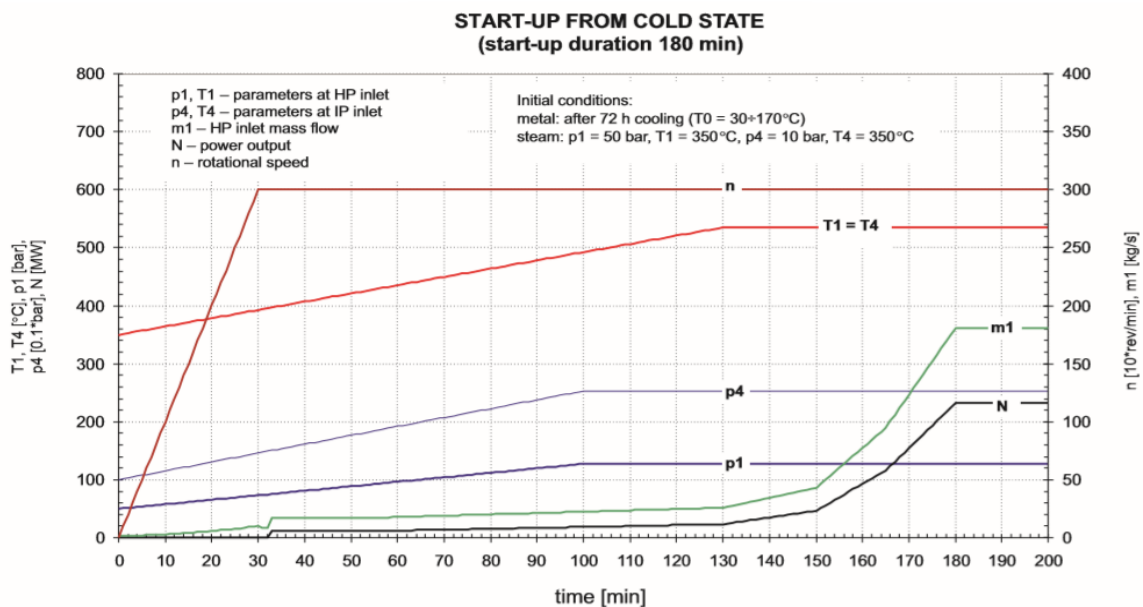


Fig 4.1: Start up curve (Banaszkiewicz M., 2014, p. 184)

4.3 TYPES OF STRESS

As discussed in section 3.2, the types of stresses induced in steam turbine due to external loads are thermal stress, centrifugal stress, vibratory stress, pressure and stress due to self weight. The magnitudes of these stresses vary from steady state condition. Also, during transient conditions, due to varying environment, these stresses also vary with time.

During a start-up, the inlet steam parameters changes from an initial value to a steady state value [Banaszkiewicz, 2014]. This leads to change in temperature of turbine components during a start-up. Due to change in temperature, there is non uniform heating of turbine components. Heat transfer takes place in turbine components from their outer surface to inner surface. The outer surface is more heated as it is in direct contact of hot steam, whereas the inner surface is less heated due to heat transfer through the material [Banaszkiewicz, 2014]. This leads to formation of thermal gradients, leading to high thermal stresses [Banaszkiewicz, 2014]. In his research paper, he also states that bigger and thicker the turbine components, higher will be the heating rate and higher will be the thermal stresses induced in component. For bigger and thicker turbine components, he gives example of rotor and turbine shaft. According to Banaszkiwicz(2014), another point that leads to high thermal stresses is the temperature differential between metal and inlet steam during initial stage of start up.

The vibratory stresses also produces more influence on turbine blades during transient events than steady state events. During steady states, the rotor rotational speed is constant and hence it is easy to handle vibratory stresses during steady state. During transient events, the rotor rotational speed keeps on varying. Banaszkiwicz (2014) tells that the vibrations produced in blades hinder the transient event operation. He also tells that the natural frequency of the HP and IP turbines is around thousand hertz and that of LP turbines is around hundred hertz. The turbine rotor rotational speed varies from 0-3000 rpm and it passes through all the natural frequencies of turbine blades, leading to resonance and hence large amplitudes [Banaszkiewicz, 2014]. According to Banaszkiwicz(2014),

the only way to reduce the damage is to pass through these critical frequencies as fast as possible, that is with acceleration range of 600-800rev/min².

The centrifugal load also varies with time during transient events because of varying rotational speed. As the rotor rotational speed increases to its steady state value, the centrifugal load also increase and therefore, the stress produced also increases. Equation (4.1), equation (4.2) and equation (4.3) prove variation of centrifugal load with time. ω is rotor rotational speed, m is the mass, R is radius, t is time and f is representation of a function.

$$\omega = f(t) \tag{4.1}$$

$$F = m * R * \omega^2 \tag{4.2}$$

$$F = f(t) \tag{4.3}$$

The pressure load also varies with time due to varying velocity. During a start-up, velocity of inlet steam varies with time. Hence, pressure load varies and stress due to pressure load also varies. Equation (4.4), equation (4.5) and equation (4.6) prove that vibratory load varies with time. V is velocity, F is vibratory load, ρ is density, A is area, t is time and f is representation of a function.

$$V = f(t) \tag{4.4}$$

$$F = \rho * A * V^2 \tag{4.5}$$

$$F = f(t) \tag{4.6}$$

The stress due to self weight remains constant in transient events since the self weight also remains constant approximately.

4.4 TYPES OF DAMAGE

As discussed in section 3.3, the damage or failure of a component occurs due to internal stresses which in turn take place due to external loads. The failure mechanisms occurring in turbine blades are fatigue, resonance, creep, elastic deformation, yielding and stress concentration.

When resonance takes place due to vibratory stresses, these stresses cross the yield strength of the material leading to yielding and also fatigue failure. During centrifugal loading of turbine blades, at fillets of blade root, stress concentration takes place leading to yielding. Nowadays, steam turbines are operated with fast start-ups procedures. During fast start-ups, in thick turbine components, high stresses are produced leading to both elastic deformation and yielding [Banaszkiewicz, 2014]. Also, the author states in his work that due to fast start-ups and shutdowns procedure, cycling loading of transient thermal stress takes place leading to thermal fatigue of the material. The thermal stresses being immense on turbine blades due to severe environments, is still less than yield point of the blades. This happens because of continuous improvement in blade material. Generally, super alloys are used for manufacturing of turbine blades. However, thermal stresses persisting in turbine blades for long periods of time leads to crack initiation in critical areas and ultimately leading to creep failure. Different material models used for studying these failure mechanisms are already mentioned in section 3.3.

All these failure and damage mechanisms are taken care of while designing turbine blade as well as other turbine components. Different computational analysis such as modal analysis, fatigue analysis, creep analysis, stress and strain analysis etc are performed for predicting the critical stress and damage regions. This study can then be used for optimization of design of turbine components. Also, the above mentioned computational failure analysis are used to predict the fatigue life, creep life etc of different turbine components, which provides an approximate idea about the useful life of turbines. This knowledge is then utilized to form operating procedure, scheduling and maintenance procedures. However, performing transient computational analysis is resource and time

intensive. Hence, experience is required for performing such analysis with optimal amount of resources and time. Apart from studying failure analysis and taking required steps, turbine cooling is performed for blades to reduce thermal stresses in blades. Turbine cooling has already been explained in section 3.4.

4.5 FSI SIMULATION

FSI simulation has already been explained in section 3.5. The methodology for stress and strain analysis of steam turbine blades during a start-up remains the same as it was in steady state analysis. The problem formulation for this problem also remains the same except that the flow of fluid will be transient. The parameters of fluid such as inlet pressure, inlet temperature, inlet velocity etc will also vary with time. The turbine blade parameters such as rotational speed will also vary with time. The CAD model used for this problem also remains same as steady state analysis.

4.5.1 Meshing

Complete meshing of the CAD model is performed on Ansys R18.1 software. Physics preference is set to CFD and solver preference is set to CFX. Linear order elements are used for mesh generation. No edge sizing or body sizing is performed for meshing. Default parameters have been used for meshing. This has been done to reduce the computational resources and time required to solve this problem. The curvature normal angle is 12^0 for the curved surfaces in CAD model. The element type for the hot domain is set to 4 noded tetrahedron elements and for cold domain and blade is set to 4 noded tetrahedron elements. Default size of element is $4.5456e-5m$. The size function is set to curvature. The target skewness is set to 0.9. The mesh is generated with 369925 nodes and 1328757 elements. After mesh generation, named selection is performed for the CAD model which are hot

inlet, hot free surfaces, hot symmetry, hot outlet, hot side interface, steam, blade to hot interface, blade symmetry, blade to cold interface, blade, cold inlet, cold interface, cold outlet and cold water.

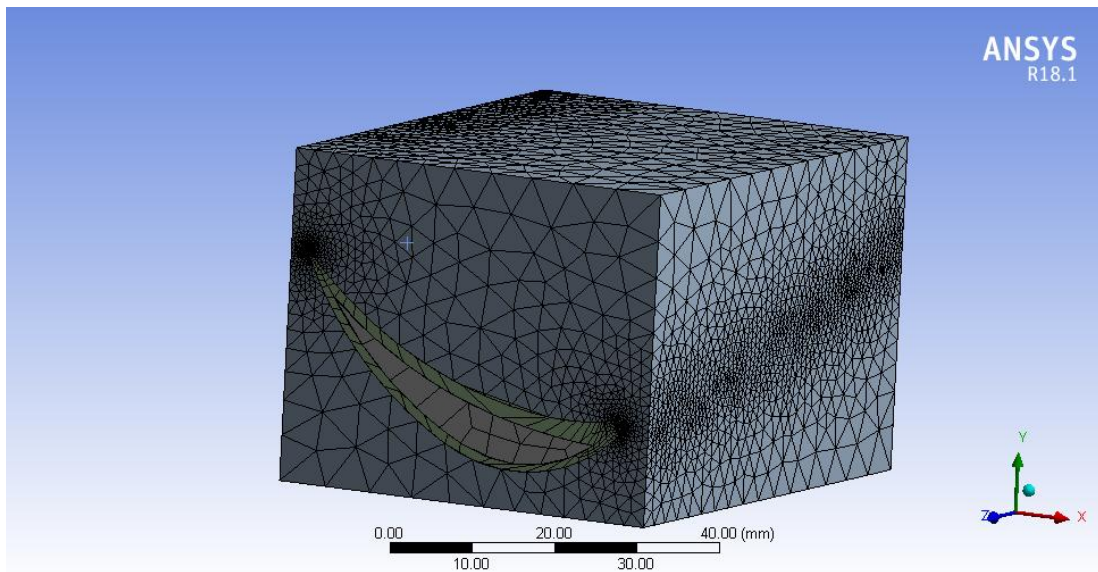


Fig 4.2: Meshed model

4.5.2 CFD Analysis

The methodology is same as explained earlier in section 3.5.4.1. The boundary conditions that we are going to set for this analysis are for a cold start procedure. Some of the parameters have been extracted from Figure 4.1 [Banaskeiwicz, 2014].

4.5.2.1 Setup

The parameters such as boundary conditions, analysis settings, solver control, domain settings etc are all performed in Ansys R18.1 CFX setup module. Firstly, analysis setting is set to transient. This setting is used while simulating transient events. Hence, this setting is

the most apt for this problem. After this, domains are formed termed as, blade, steam and cold water. For blade, it is defined as a solid domain with steel as the material. Heat transfer option is set to thermal energy. For cold water domain, it is defined as fluid domain with fluid as water vapor at 25⁰C. The reference pressure is set to 1 atm. Heat transfer setting is set to thermal energy and thermal radiation is set to none. Turbulence model for fluid is selected as shear stress transport (SST). For steam domain, the domain is defined as fluid domain and the fluid is set to water vapor at 100⁰C. The reference pressure is set to 1 atm. Turbulence model for the fluid is again set to shear stress transport (SST). All the domains are set as stationary domain.

After defining the domains, their initialization is done. Initialization is the process of defining the parameters of that domain at $t = 0$ sec. Blade domain is initialized with a temperature value of 200⁰C. For cold water domain, the initial velocity is set to 1.9443 m/s in z direction. The relative pressure is set to 0 atm and the initial temperature value is set to 50⁰C. The turbulence of fluid is set to low intensity (1%). For the steam domain, the initial velocity of fluid is set to -0.5833 m/s in x direction. The relative pressure is set to 4.9 MPa and inlet temperature is set to 350⁰C. The turbulence model is selected as low intensity (1%).

The blade is assumed to be of thickness of 0.1 mm. Then the interfaces are defined between the steam and blade and the cold water and blade. A general connection is defined between the blade to hot interface surface (blade) and hot side interface (steam). No slip condition is applied in this interface. Another general connection is defined between blade to cold interface (blade) and cold interface (cold water). Again, no slip condition is applied to this interface.

After defining the interfaces, boundary conditions are defined for all the domains. These boundary conditions define the values of parameters at the end of time of the simulation. The variation of these parameters with time is controlled by the software using the second order backward euler method. For the blade domain, blade surface at cold inlet and cold

outlet are set to adiabatic condition, so that no heat transfer takes place through those surfaces. For cold water domain, the cold inlet boundary condition is defined. The velocity at cold inlet is set to 50 m/s. The turbulence model I selected as low intensity (1%). The temperature is set to 30⁰C. Then the cold outlet boundary condition is defined. In this boundary condition, the relative pressure is set to 0. For steam domain, the hot inlet boundary condition is defined. The velocity is set to 15 m/s. The turbulence model is set to low intensity (1%). The total temperature is set to 650⁰C. Then hot outlet boundary condition is defined. The relative pressure is set to 0 atm. The surfaces adjacent to hot inlet and hot outlet are assigned symmetry boundary condition. The rest of the two surfaces in the rectangular hot domain are assigned wall type boundary condition. In this boundary condition, the surfaces are set to adiabatic and free slip condition. The blade is assigned relative velocity along the x axis passing through the remote point according to Table 1.

Table 4.1: Rotational velocity magnitude for transient analysis

Steps	Time (s)	X (rad/s)	Y (rad/s)	Z (rad/s)
1	0	0	0	0
1	1800	314	0	0
1	10800	314	0	0

For simulation run, the transient method is set to time integration. Time period is set to 180 min. Number of timesteps per period is 100, which makes each time step to be 108 secs. The number of periods per run is set to 1. The residual type is set to rms value and residual target I set to 1e-3.

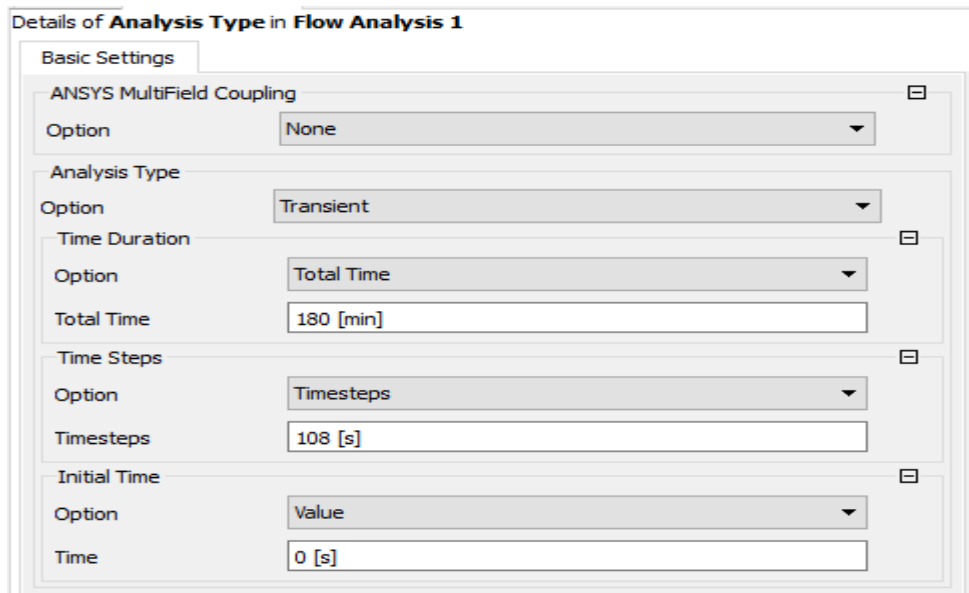


Fig 4.3: Transient model settings

4.5.2.2 Solution

The simulation is run under solution module of Ansys R18.1 CFX software. The initialization option I set to initial conditions. The parameters which require reaching a residual target of $1e-3$ are momentum and mass of cold water, momentum and mass of steam, heat transfer of steam, heat transfer of cold water, total energy, turbulence kinetic energy and turbulence frequency for steam and turbulence kinetic energy and turbulence frequency for cold water.

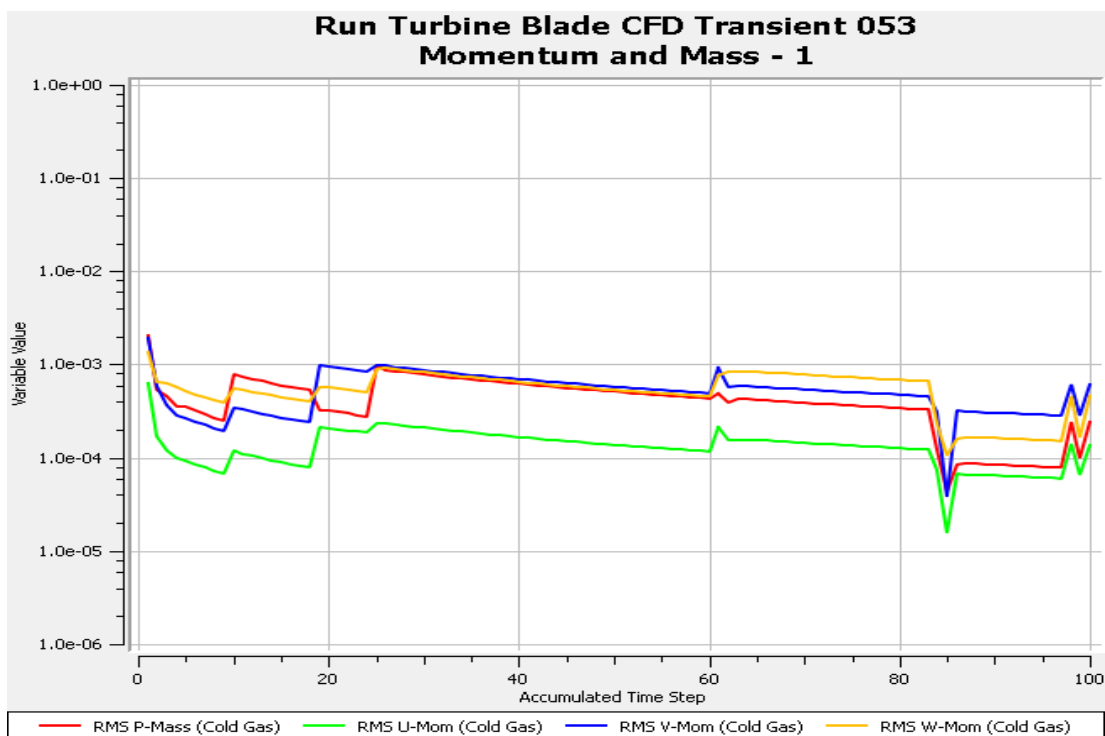


Fig 4.4: Residual target of mass and momentum for cold water

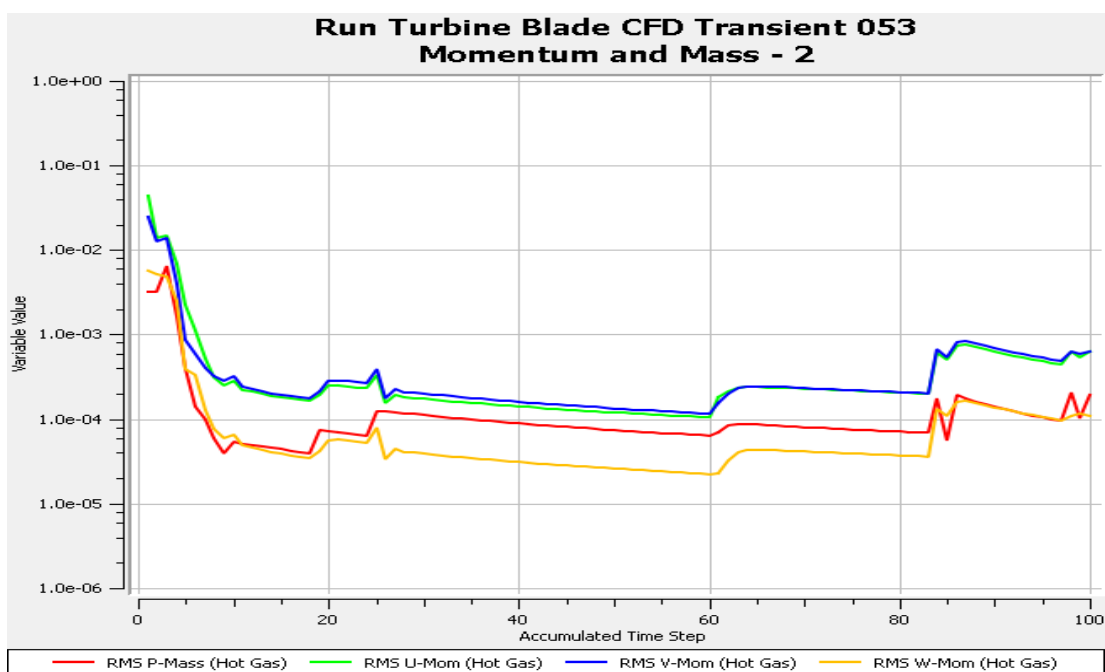


Fig 4.5: Residual target of mass and momentum for steam

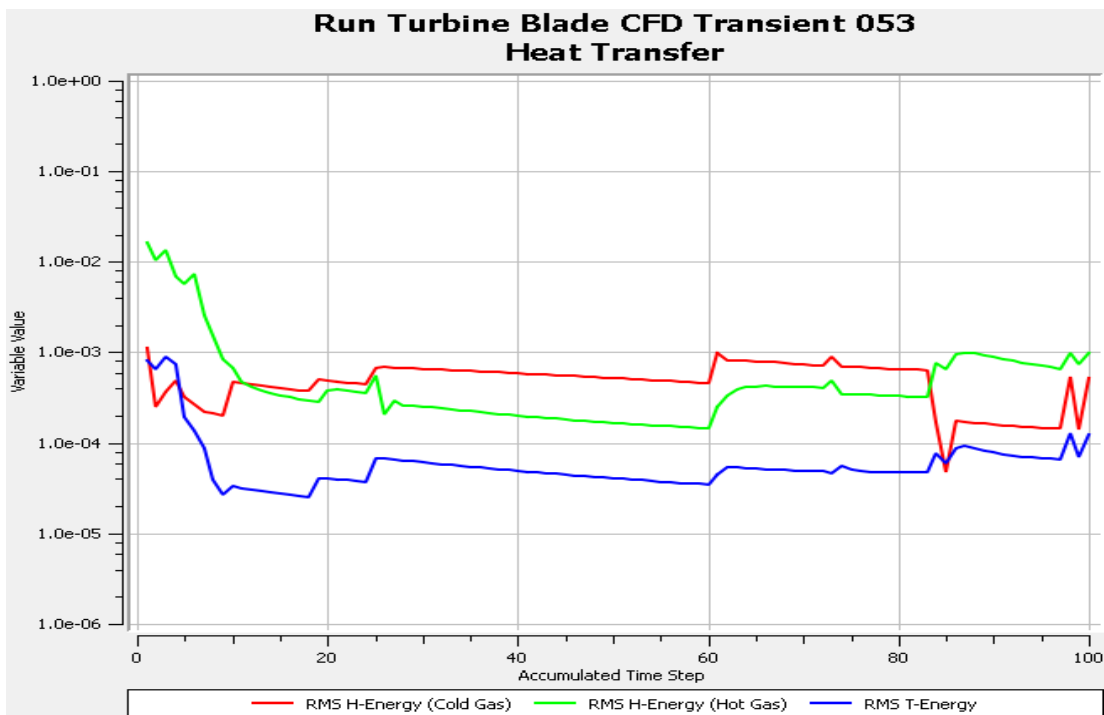


Fig 4.6: Residual target of heat transfer for steam and cold water

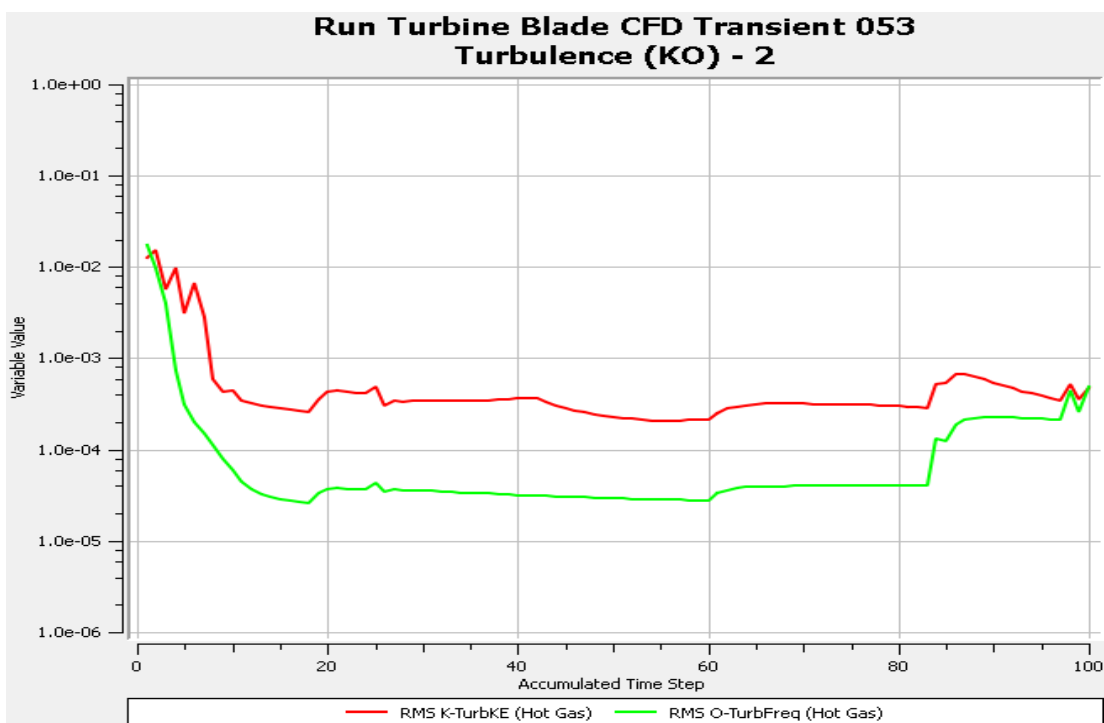


Fig 4.7: Residual target of turbulence kinetic energy and turbulence frequency for steam

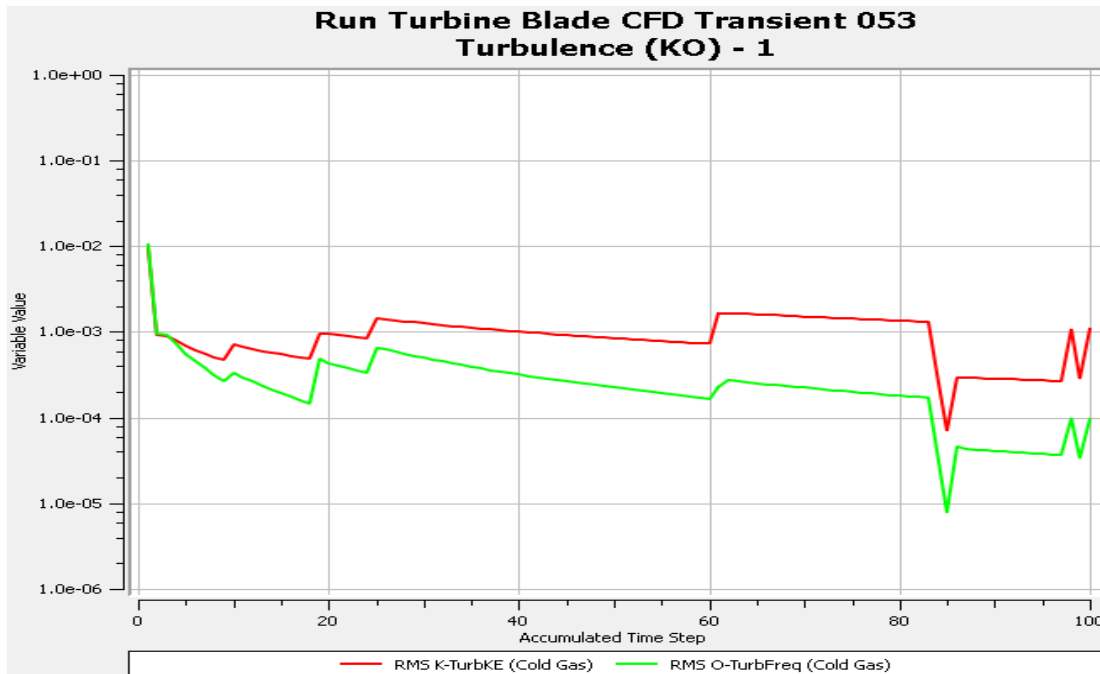


Fig 4.8: Residual target of turbulence kinetic energy and turbulence frequency for cold water

4.5.2.3 Results

Results for the CFD analysis are displayed in CFD-Post, which is the post processor for Ansys R18.1 CFX software. Contours are obtained for different variables, namely, temperature, pressure and temperature gradient.

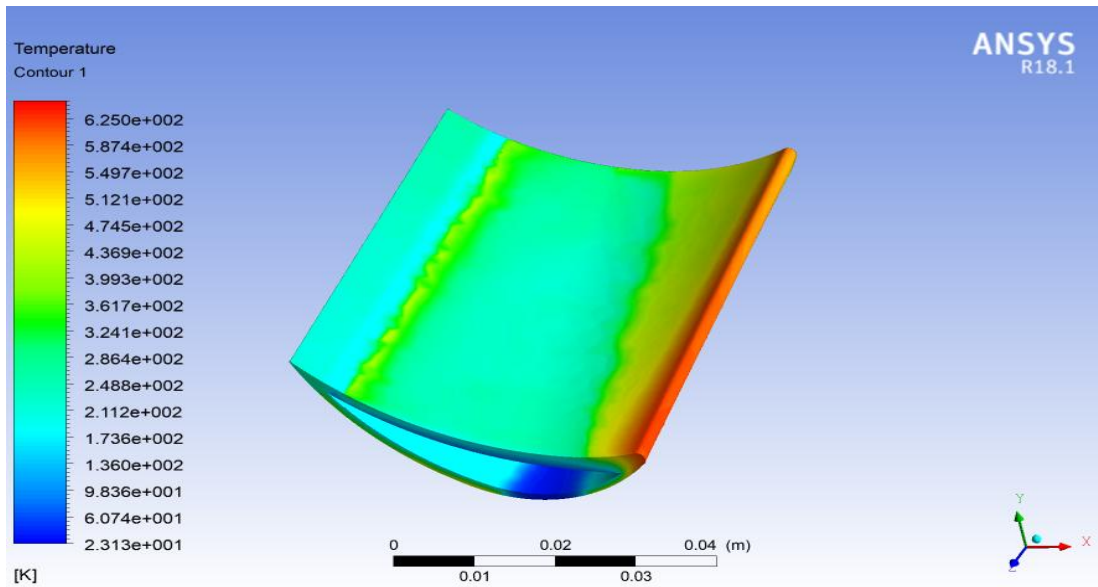


Fig 4.9: Temperature contour on upper surface of blade at $t = 10800s$

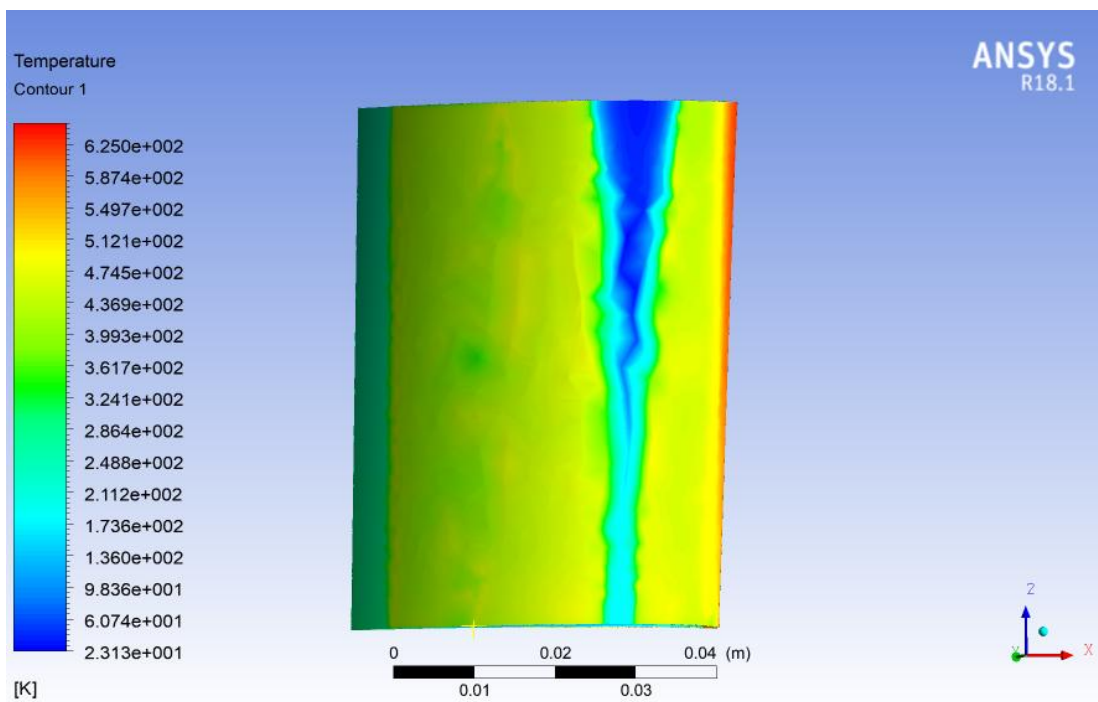


Fig 4.10: Temperature contour on lower surface of blade at $t = 10800 s$

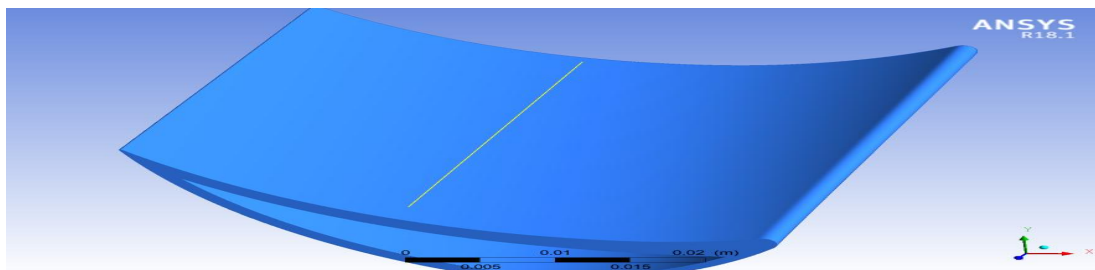


Fig 4.10(a): Line location in z direction on blade surface

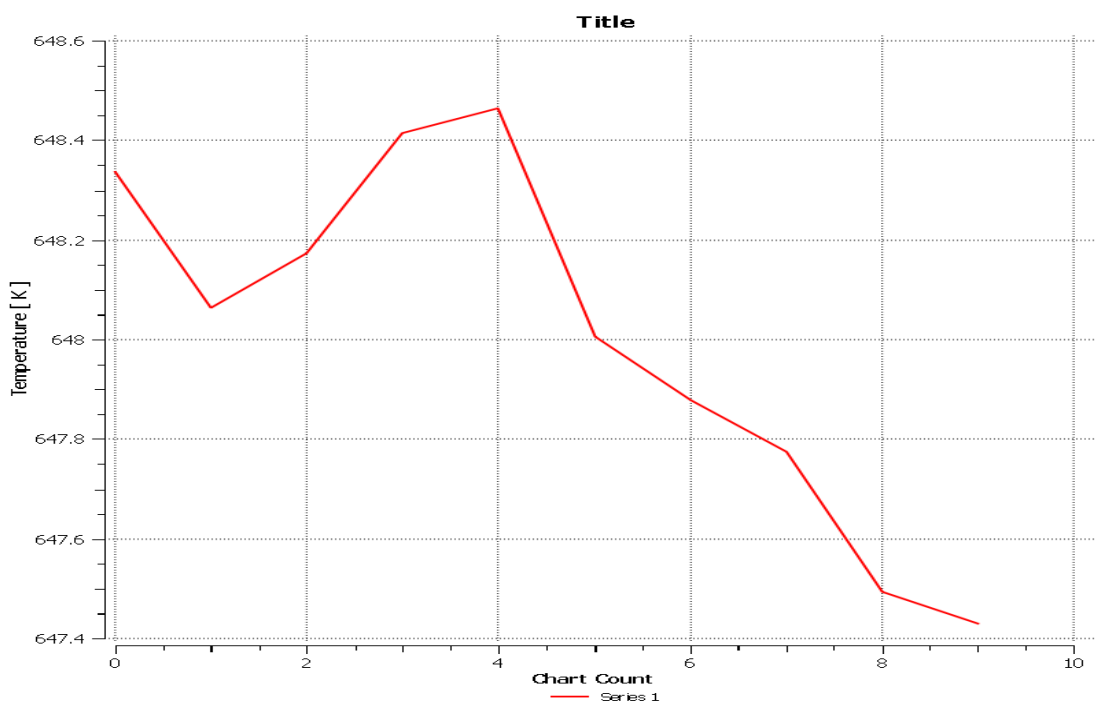


Fig 4.10(b): Temperature vs z graph along line in z direction on upper surface at $t = 10800s$

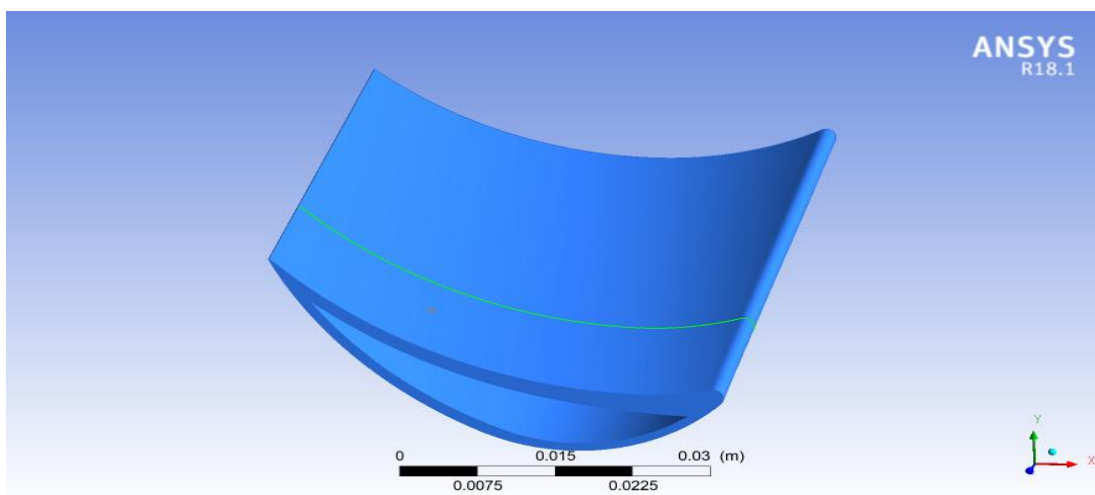


Fig 4.10 (c): Polyline location in x direction on blade surface

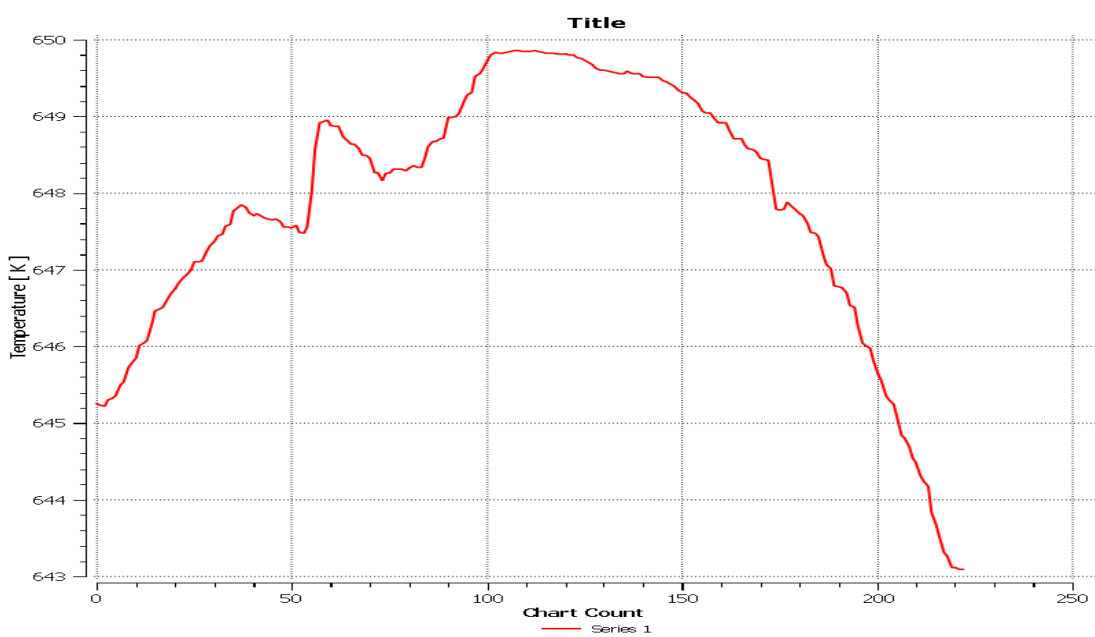


Fig 4.10 (d): Temperature vs x graph along line in x direction on upper surface at $t = 10800s$

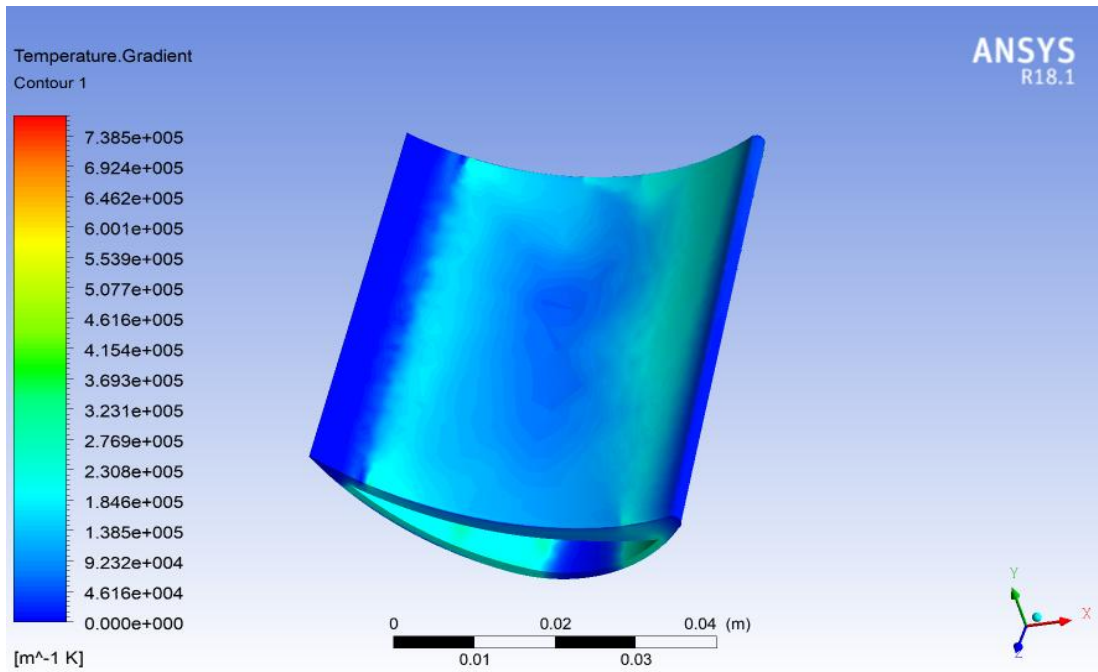
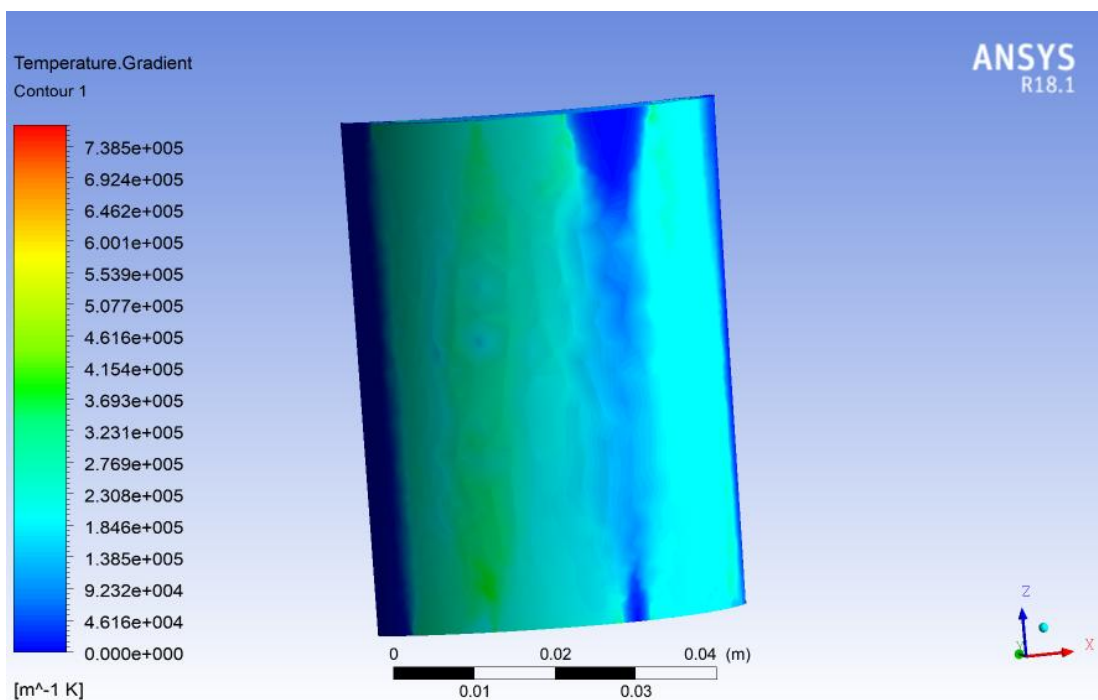
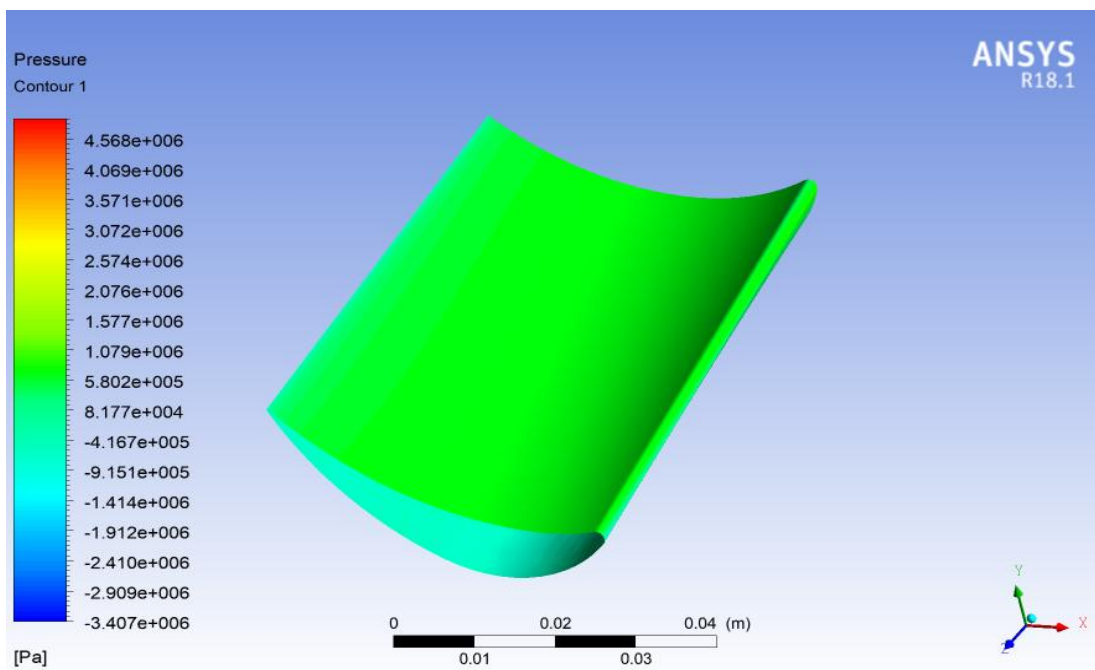
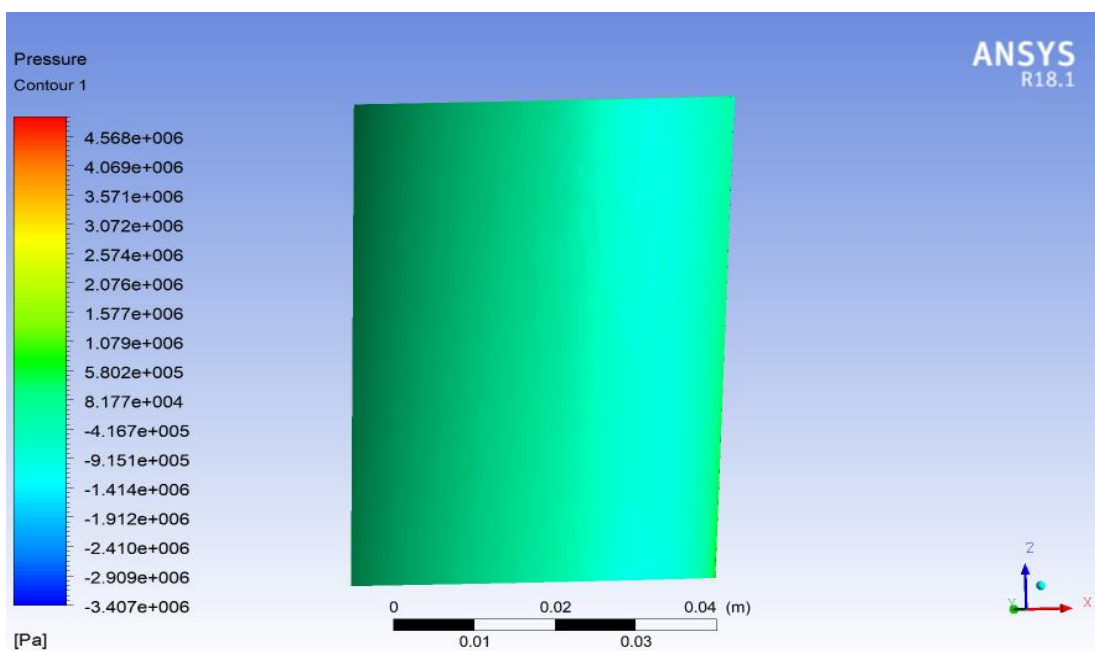


Fig 4.11: Temperature gradient contour on upper surface of blade at $t = 10800s$



a

Fig 4.12: Temperature gradient contour on lower surface of blade at $t = 10800s$ Fig 4.13: Pressure on upper surface contour at $t = 10800s$ Fig 4.14: Pressure on lower surface contour at $t = 10800s$

Then, an isosurface is created in same manner as it was created in steady state analysis. Contour of pressure and vector of velocity is obtained on this isosurface in order to study the change in pressure and velocity along a cross section of flow domain.

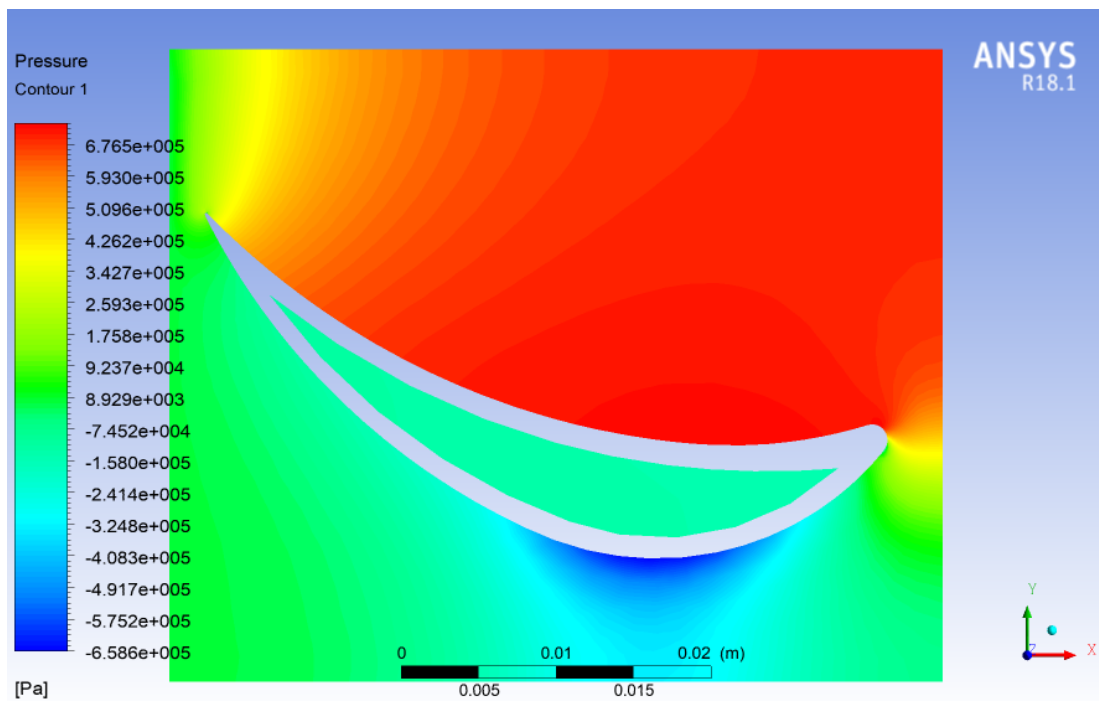


Fig 4.15: Pressure contour on a plane at $t = 10800s$

The pressure and temperature variation with time has been extracted during the start-up period.

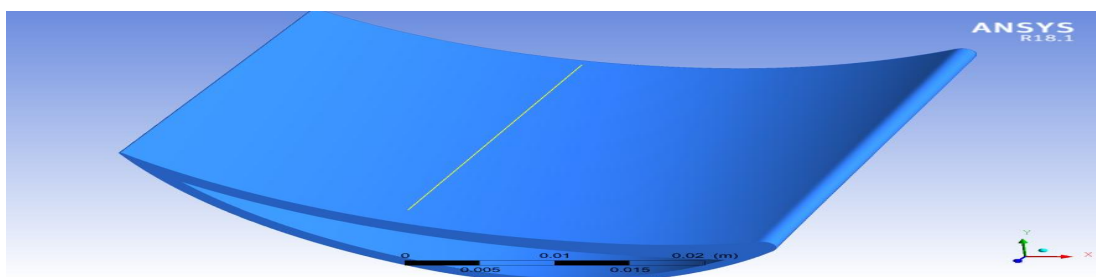


Fig 4.16: Line location on blade surface in z direction

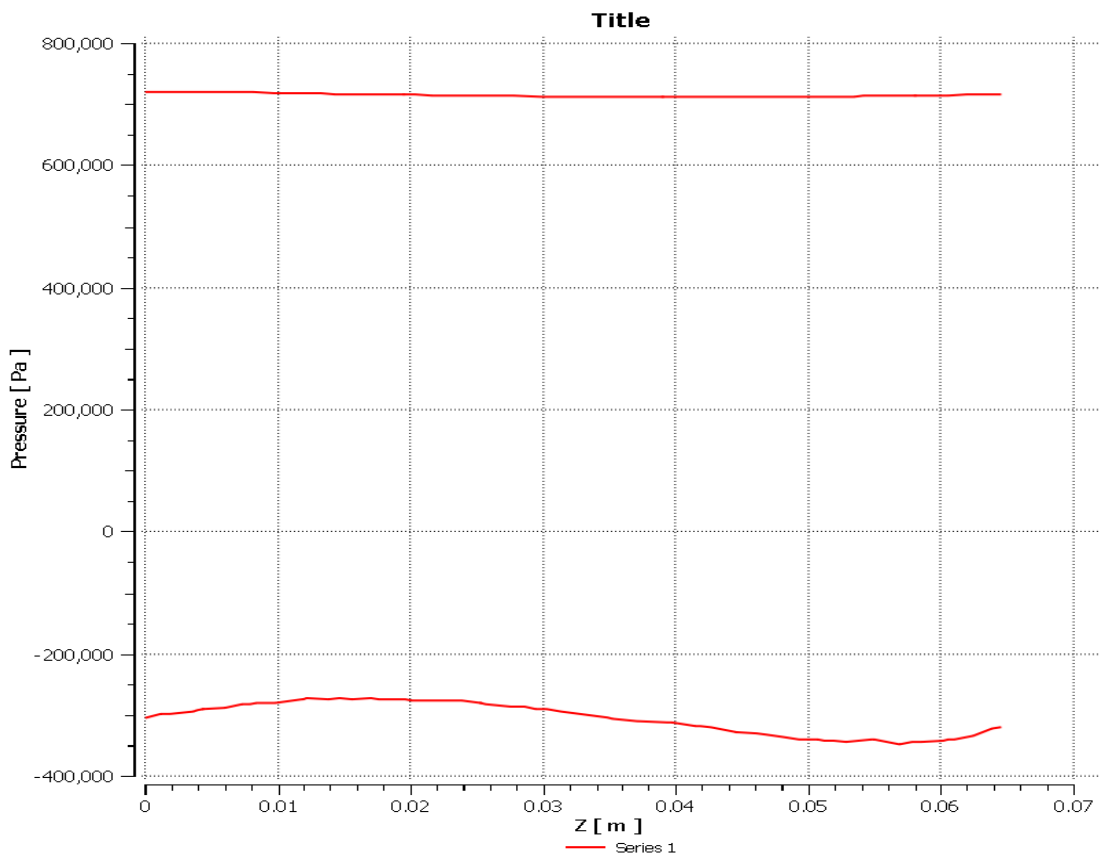


Fig 4.17: Pressure vs z graph along line in z direction on upper surface (upper line) and lower surface (lower line) at $t = 10800s$

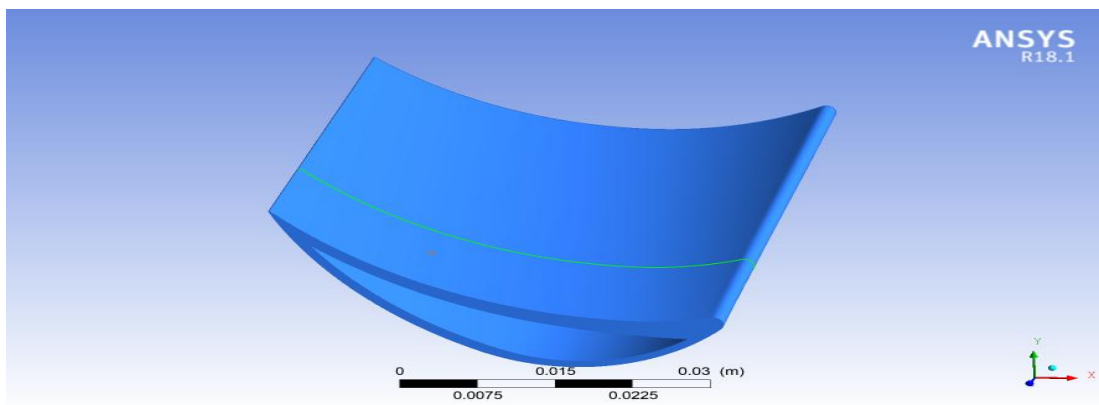


Fig 4.18: Line location on blade surface in x direction

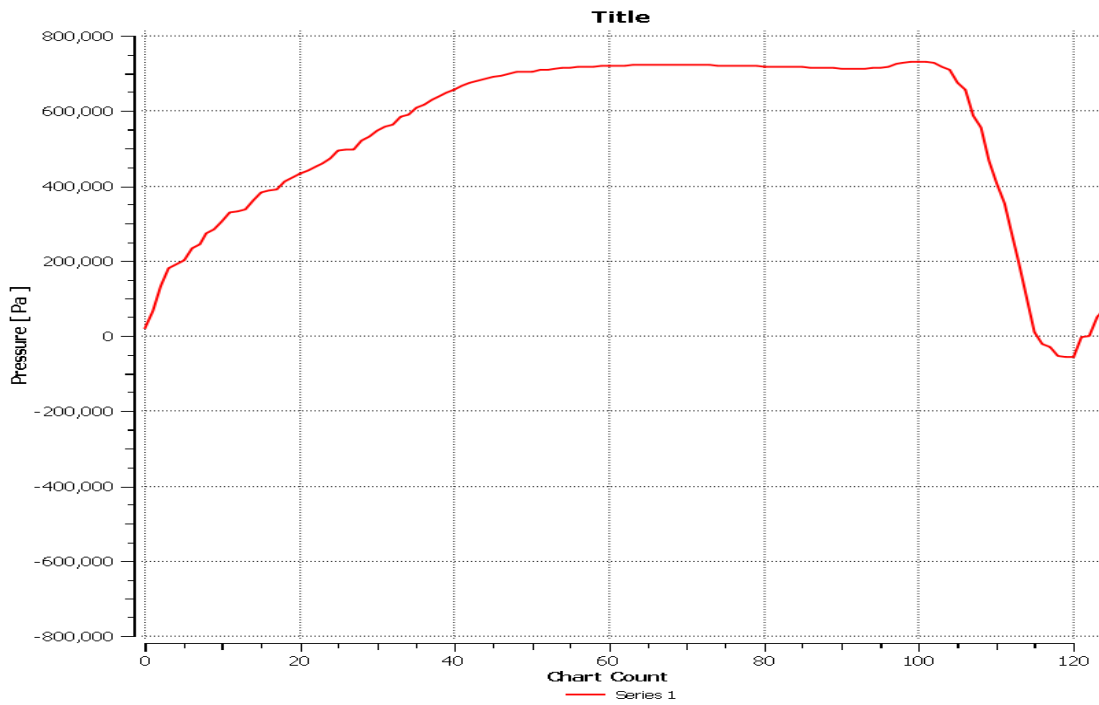


Fig 4.19: Pressure vs x graph along line in x direction on upper surface at $t = 10800s$

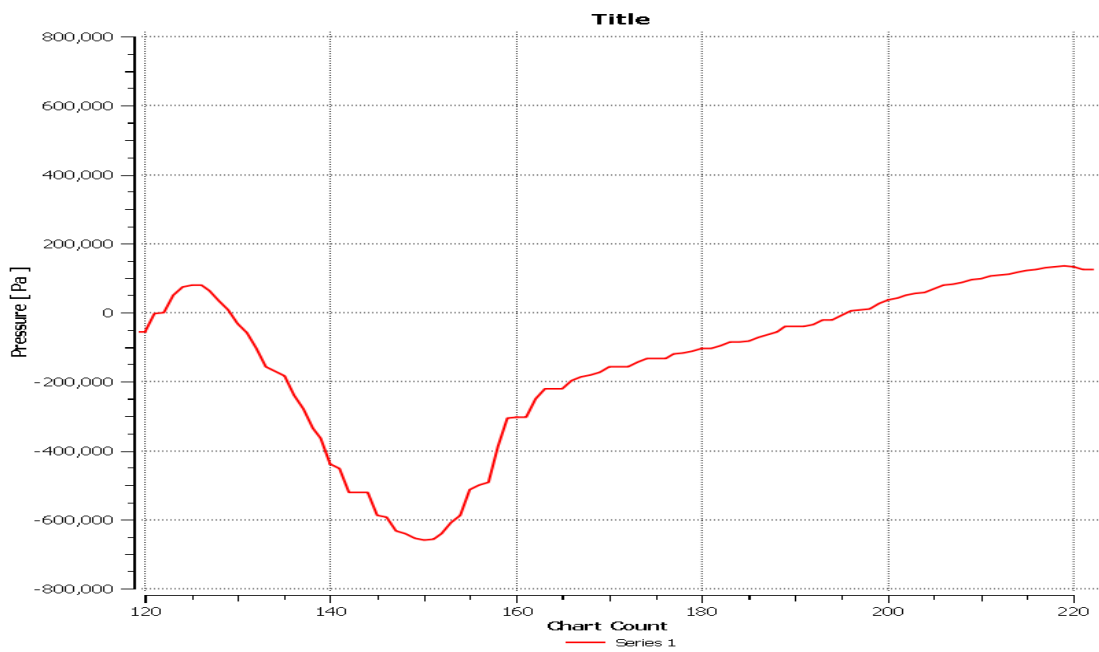


Fig 4.20: Pressure vs x graph along line in x direction on lower surface at $t = 10800s$

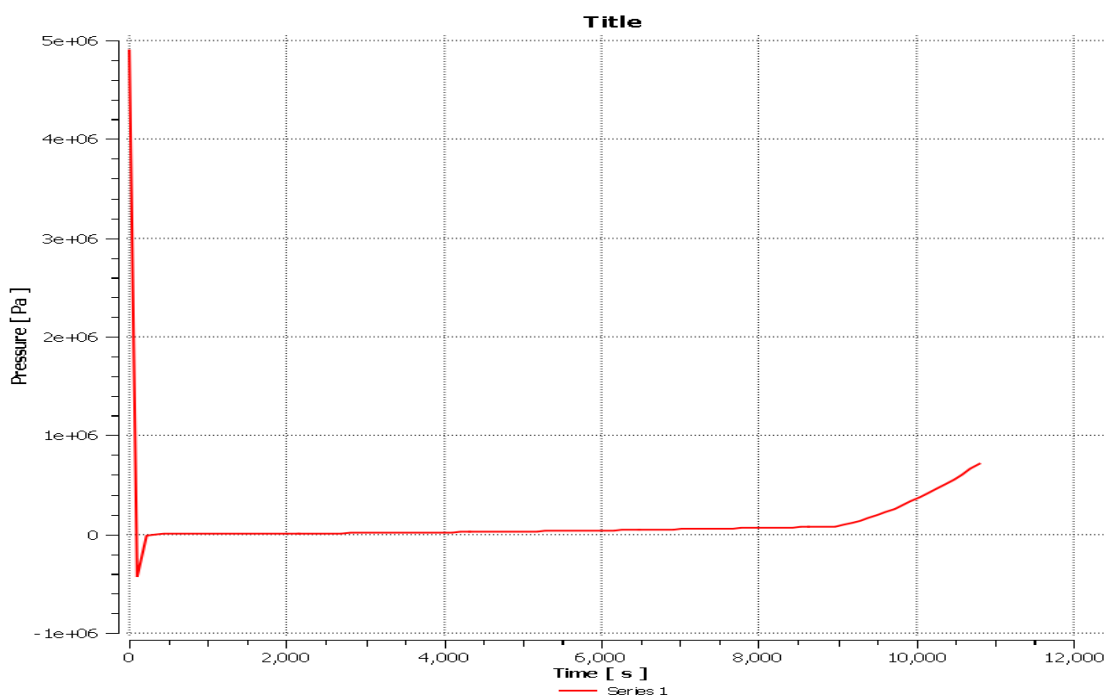


Fig 4.21: Pressure vs time during start-up at a point on blade surface

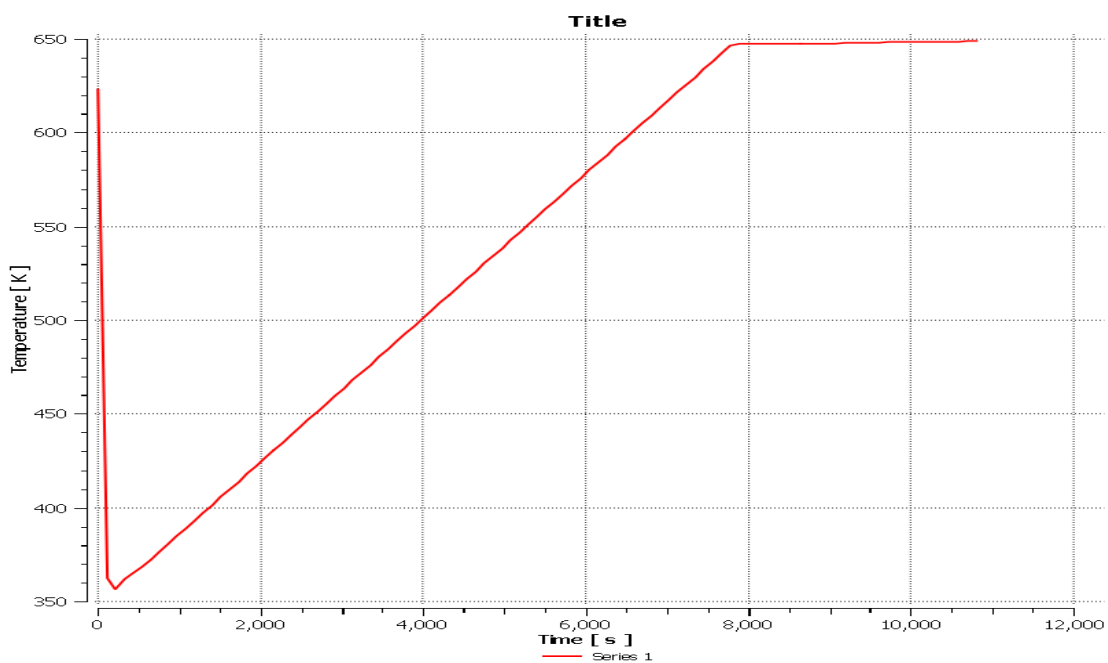


Fig 4.22: Temperature vs time during start-up

4.5.3 FEA Analysis

The FEA analysis for this problem is solved on Ansys R18.1 Transient Structural software. This software is used to solve transient structural problems. It is used for both linear and non linear analysis.

4.5.3.1 Methodology

All the steps followed in transient state analysis remains the same except that the software used here is Ansys R18.1 Transient Structural software. The modules are in the following order: engineering data, geometry, model, setup, solution, results. The difference from steady state analysis is that the code working behind the software changes here.

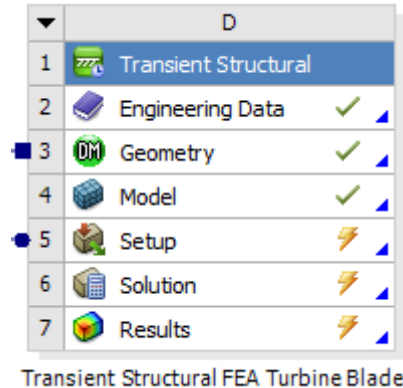


Fig 4.23: Methodology of FEA analysis

The engineering data remains the same as it was in steady state analysis, that is, the material selected for blade is structural steel. The geometry also remains the same as it was in steady state analysis, that is, the geometry consists of blade domain only. The steam domain and cold water domain are suppressed because they are fluid domains. A global coordination system is formed as done before in steady state analysis. Also, a remote point is created at which the boundary conditions will be assigned. The remote point is set at

location (0, 0.007, 0.09763) mm. The behavior of the remote point is rigid. The meshing of the model is performed with 10 noded tetrahedron elements. A meshed model is generated with 286449 nodes and 173489 elements. Named selection consists of complete body of the blade termed as blade.

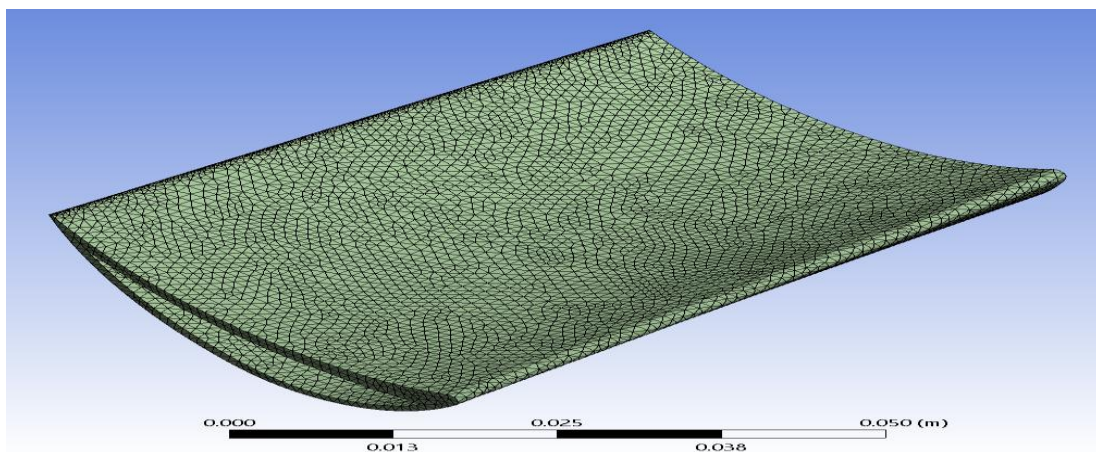


Fig. 4.24: Meshed model for FEA analysis

4.5.3.2 Setup

In setup module, analysis settings are setup. The physics type of the problem is set to structural. The analysis type is set to transient. Solver target is Mechanical APDL. No initial conditions have been setup for this problem. In analysis settings, the current step number and number of steps are set to 1. Step end time is set to 10800 sec. Initial time step and minimum time step are set to 100 sec. Large deflection setting is set to on.

After this, the rotational velocity of the blade is set up. The rotational velocity is set for the complete blade at remote point as it was set in steady state analysis. The difference here is the magnitude of rotational velocity. The rotational velocity magnitude for transient analysis is presented in Table 4.1.

Table 4.2: Rotational velocity magnitude for transient analysis

Steps	Time (s)	X (rad/s)	Y (rad/s)	Z (rad/s)
1	0	0	0	0
1	1800	314	0	0
1	10800	314	0	0

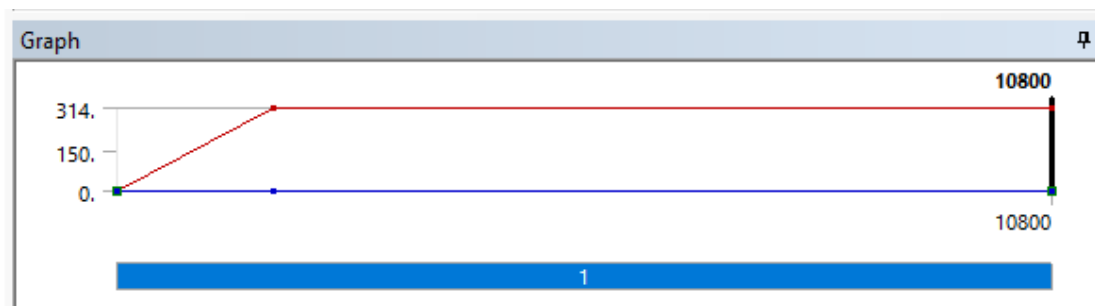


Fig 4.25: Graph of rotational velocity for transient analysis

The Table 4.1 and Figure 4.10 shows that the rotational velocity varies linearly between 0 sec to 1800 sec from 0 rad/s to 314 rad/s. Then the rotational velocity remains constant from 1800 sec to 10800 sec at 314 rad/s. This means that during the start-up, the steady state value of rotational velocity is reached at 1800 sec and then it remains constant.

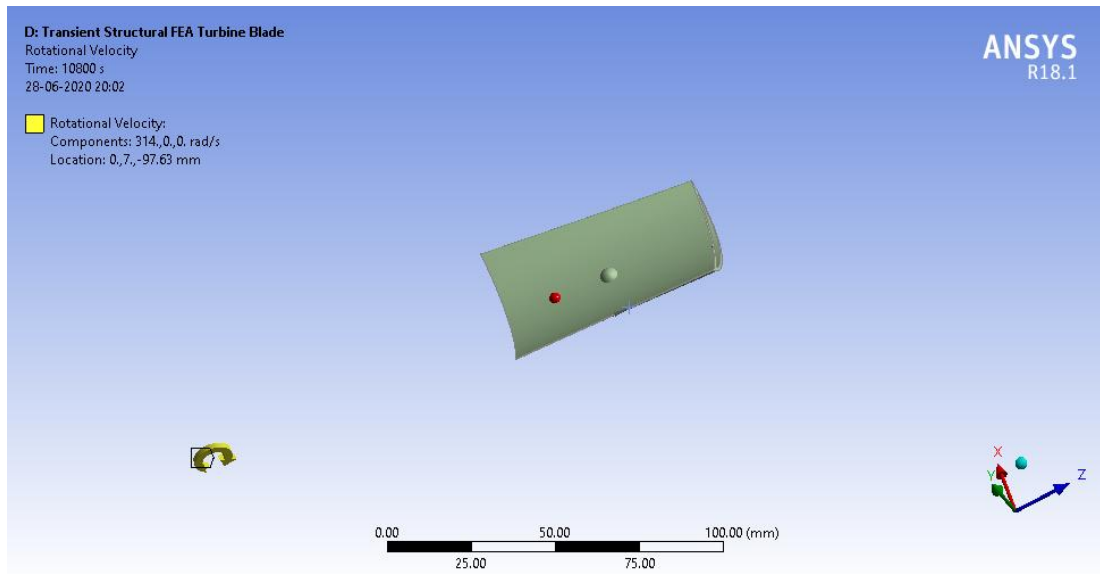


Fig 4.26: Rotational velocity boundary condition

After applying rotational velocity boundary condition, fixed support boundary condition is applied. This boundary condition is applied in same way as applied in steady state analysis. The remote point is completely fixed. After applying the boundary condition, pressure load and body temperature is imported from the results of CFD analysis.

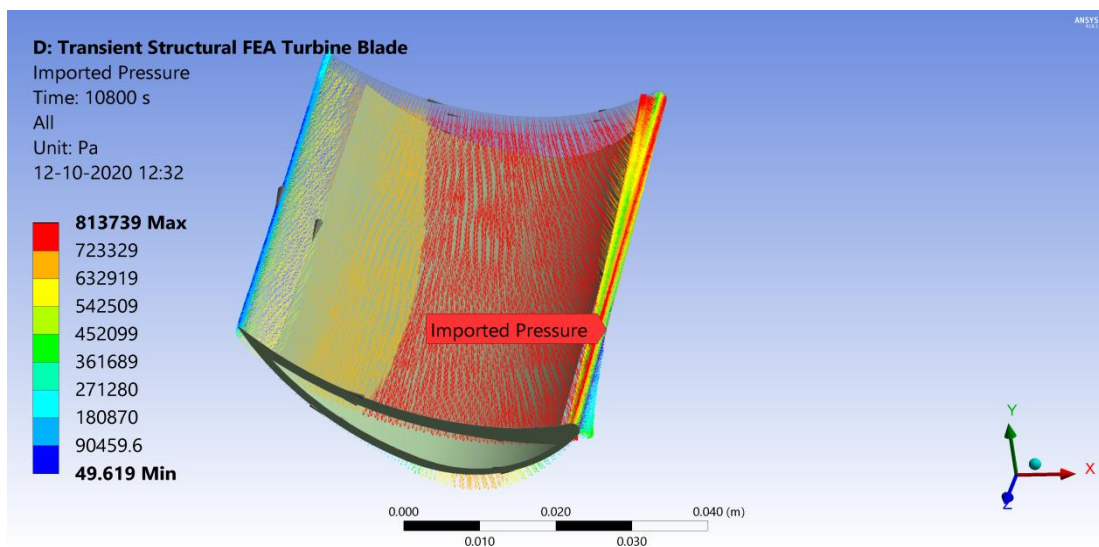


Fig 4.27: Absolute pressure load imported upper surface

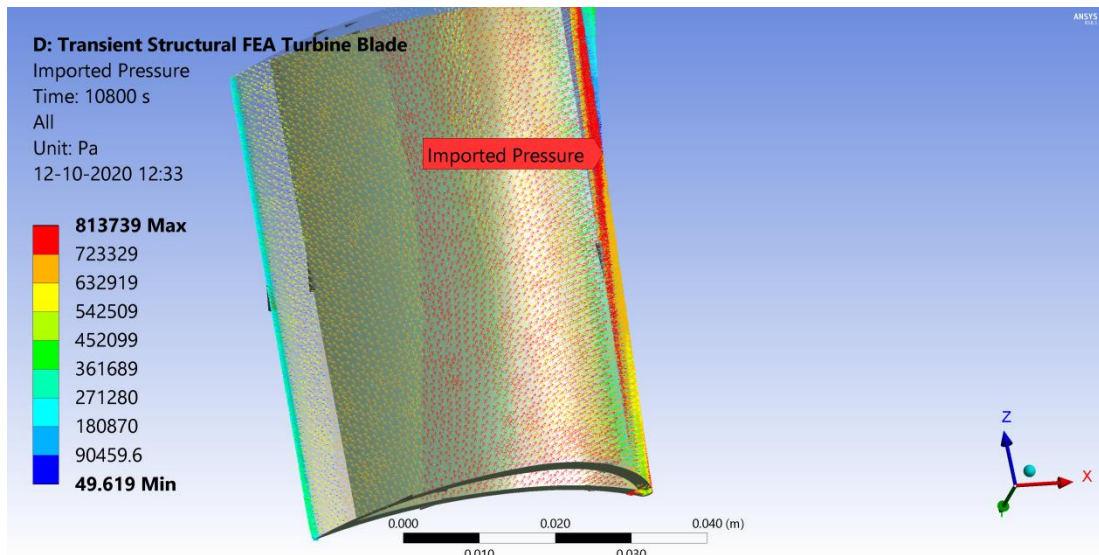


Fig 4.28: Absolute pressure load imported on lower surface

4.5.3.3 Solution and Results

The simulation is run and results are obtained in Ansys R18.1 Transient Structural software. The simulation run was completed successfully. The run took 2 hours and 26 minutes to complete. The MAPDL memory used is of size 2.5342 GB and the MAPDL result file size is of 9.0908 GB. In results section, contours of total deformation and equivalent von mises stress at $t = 108$ sec, $t = 1080$ s, $t = 4428$ s, $t = 8100$ s and $t = 10800$ s.

4.5.3.3.1 At $t = 108$ s

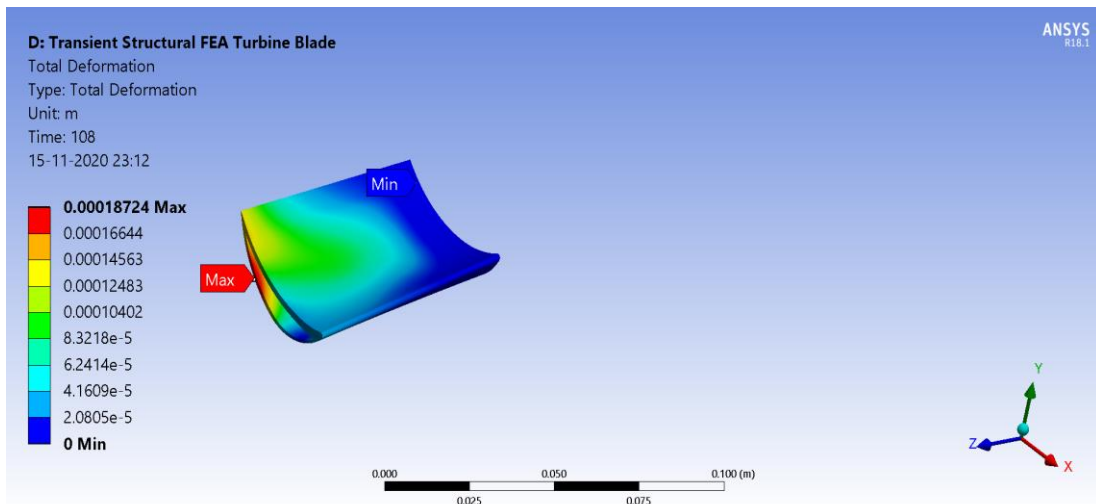


Fig 4.29: Total deformation contour at $t = 108$ s

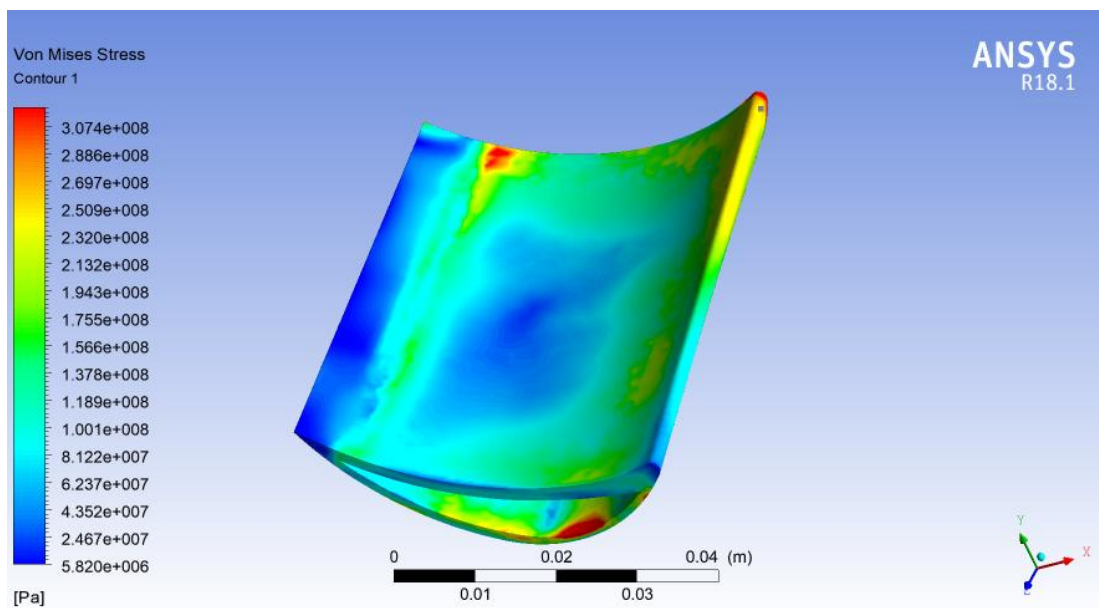


Fig 4.30: Von mises stress contour on upper surface at $t = 108$ s

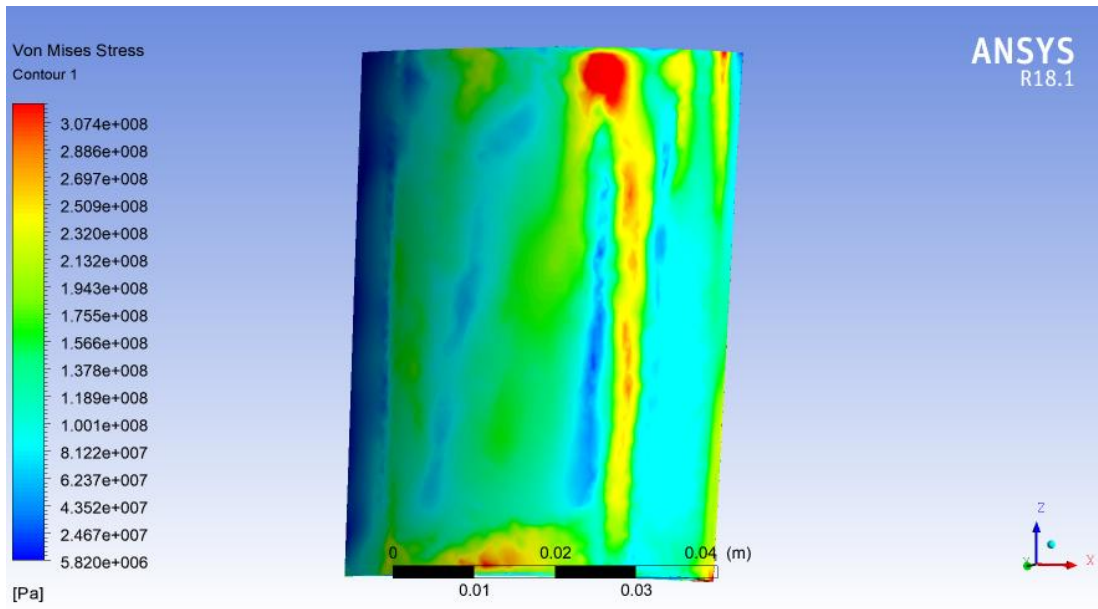


Fig 4.31: Von mises stress contour on lower surface at $t = 108s$

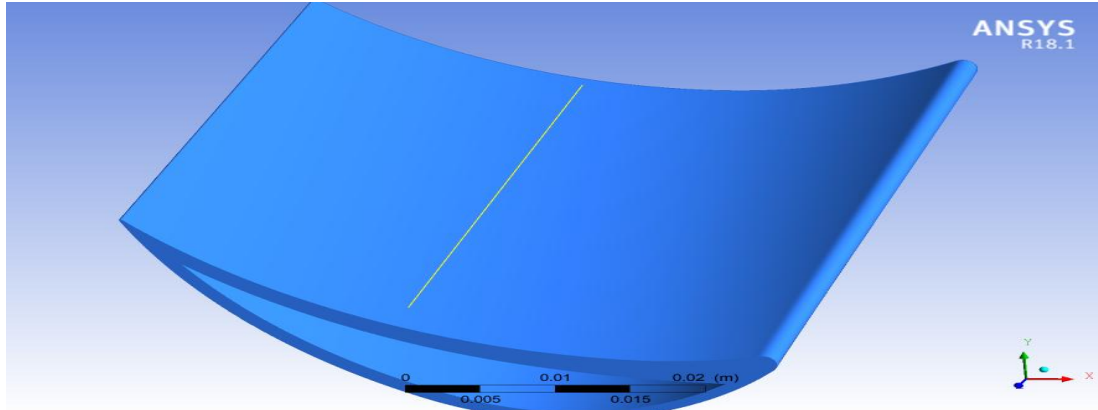


Fig 4.32: Line location on upper blade surface in z direction

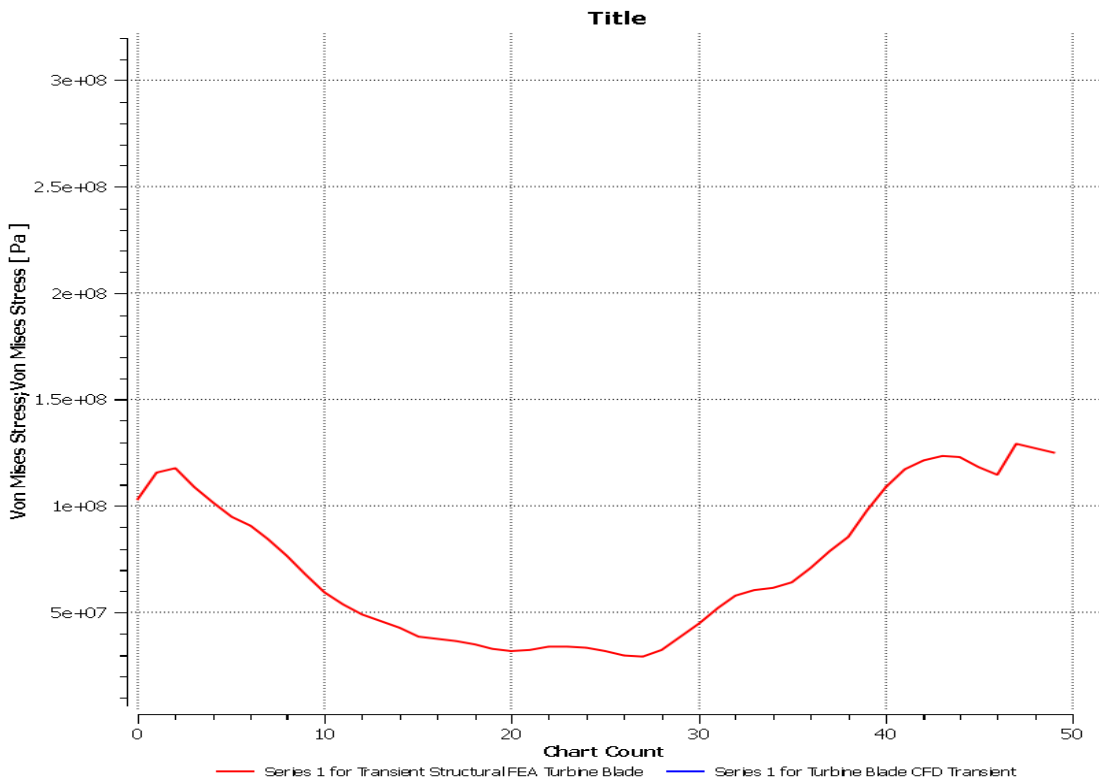


Fig 4.33: Stress vs z graph along a line in z direction at t = 108s

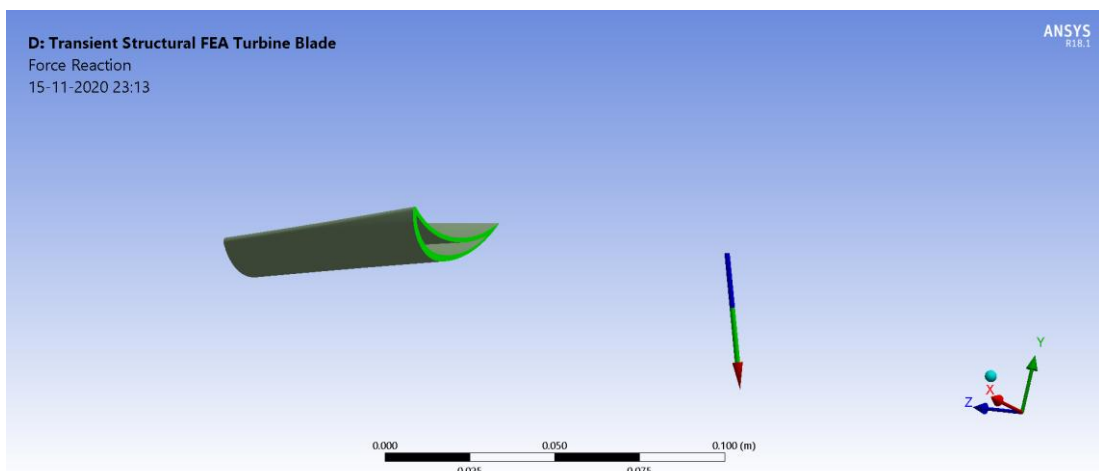


Fig 4.34: Force reaction direction and magnitude at remote point (Max: 491.55 N and Min: 491.3 N) at t = 108s

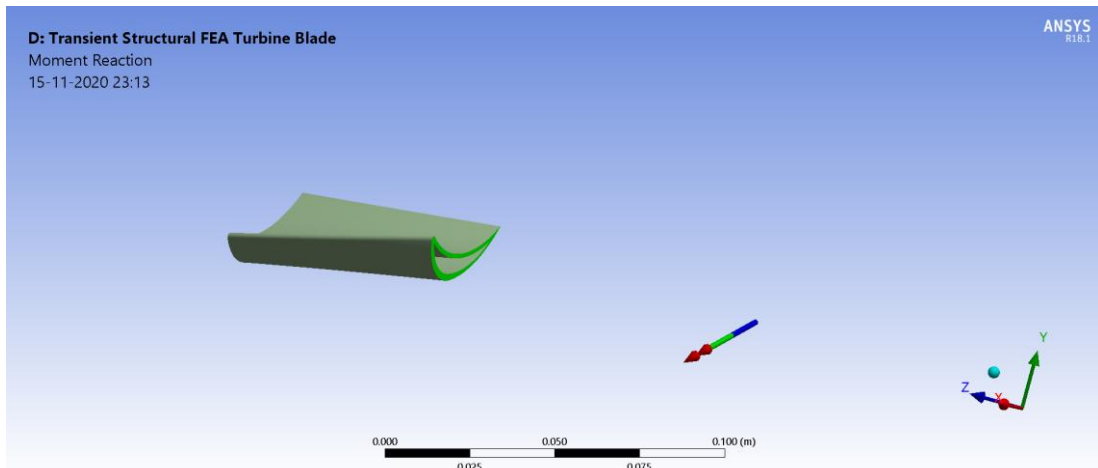


Fig 4.35: Moment reaction direction and magnitude at remote point (Max: 64.508 Nm and Min: 64.507 Nm) at $t = 108s$

4.5.3.3.2 At $t = 1080 s$

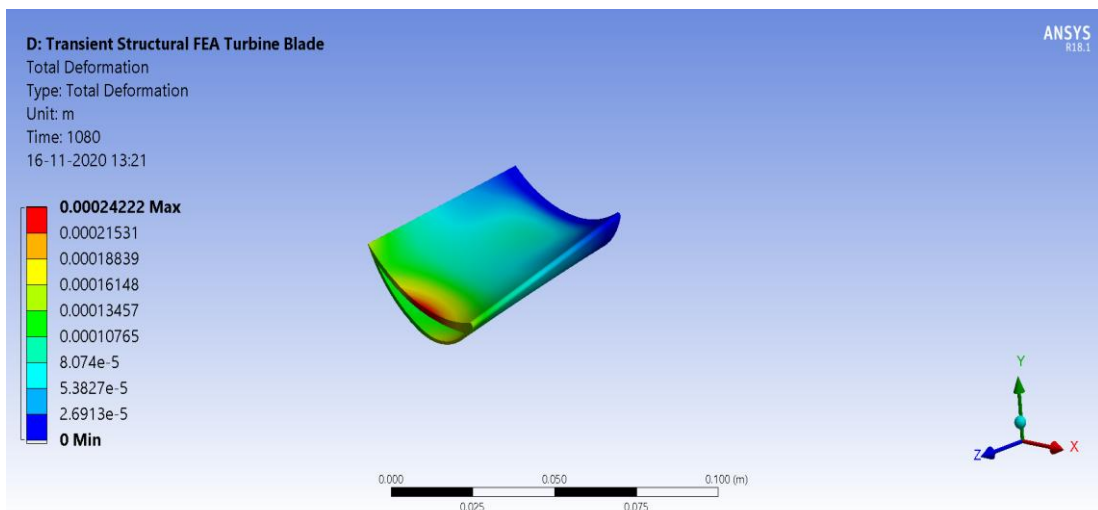
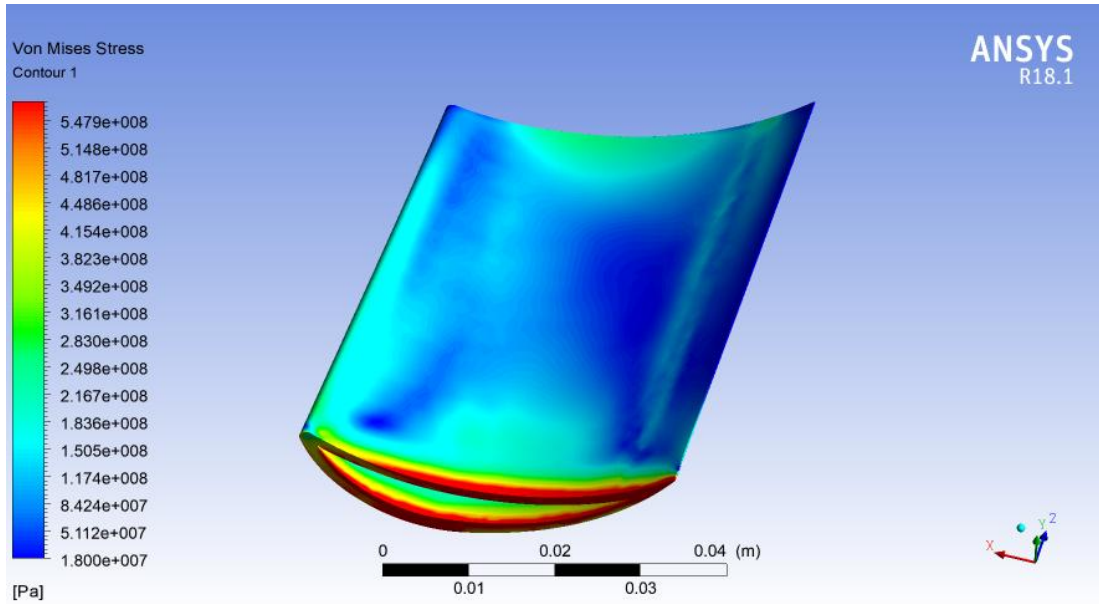
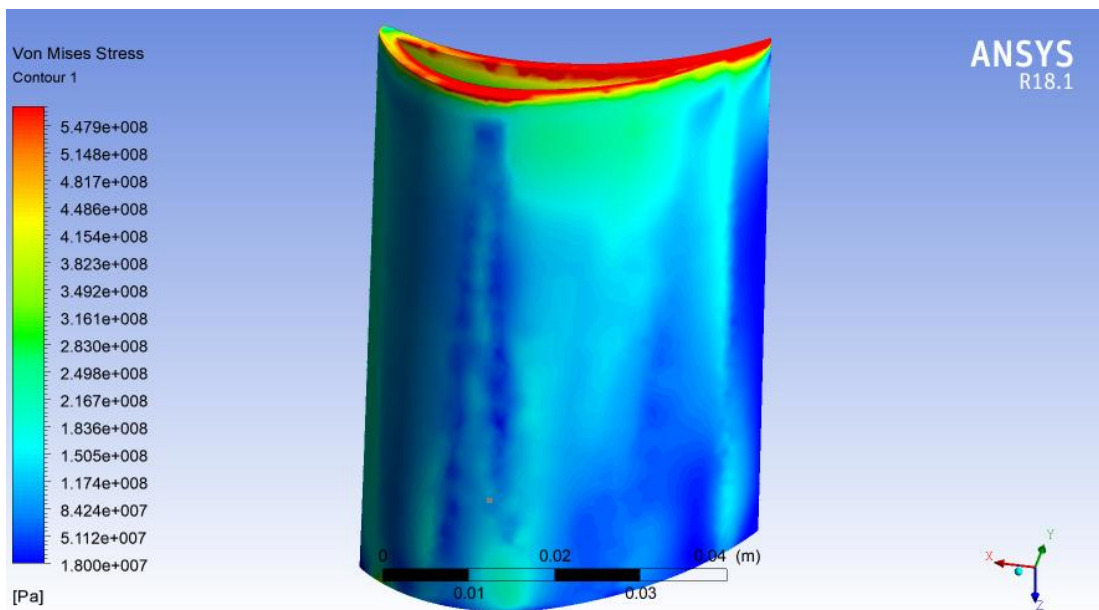


Fig 4.36: Total deformation contour on blade's upper surface at $t = 1080s$

Fig 4.37: Equivalent stress on upper surface contour at $t = 1080s$ Fig 4.38: Equivalent stress contour on lower surface at $t = 1080s$

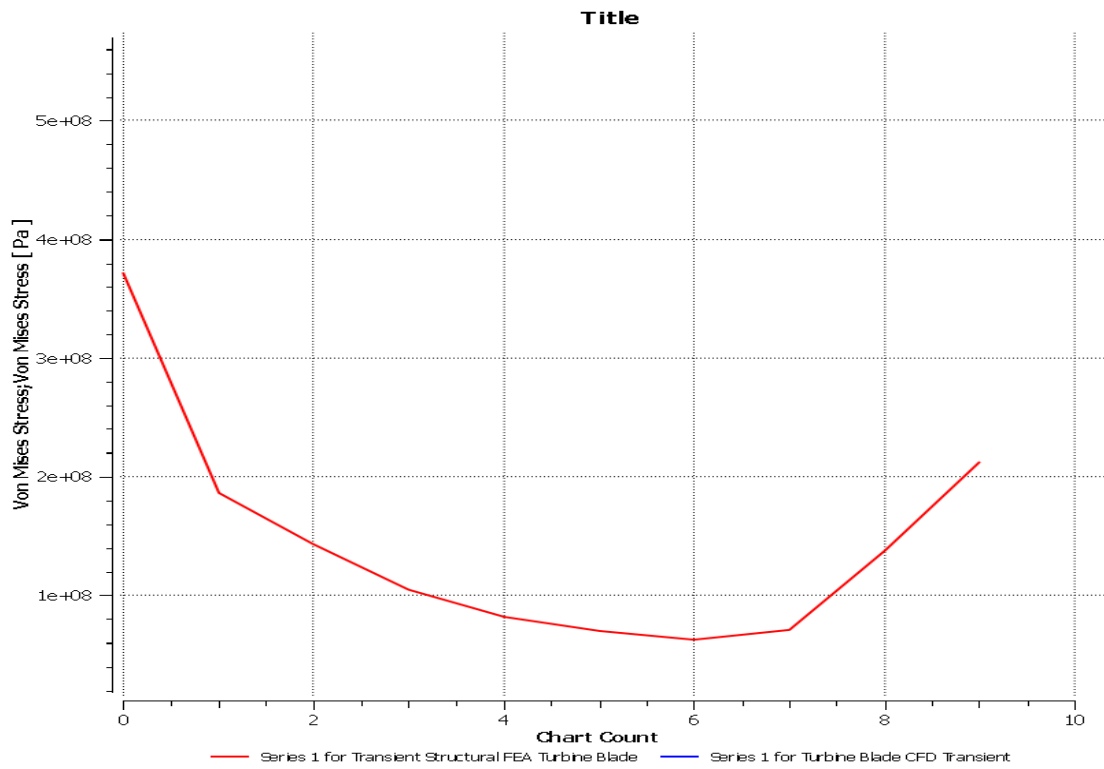


Fig 4.39: Stress vs z graph on line along z direction at t = 1080s

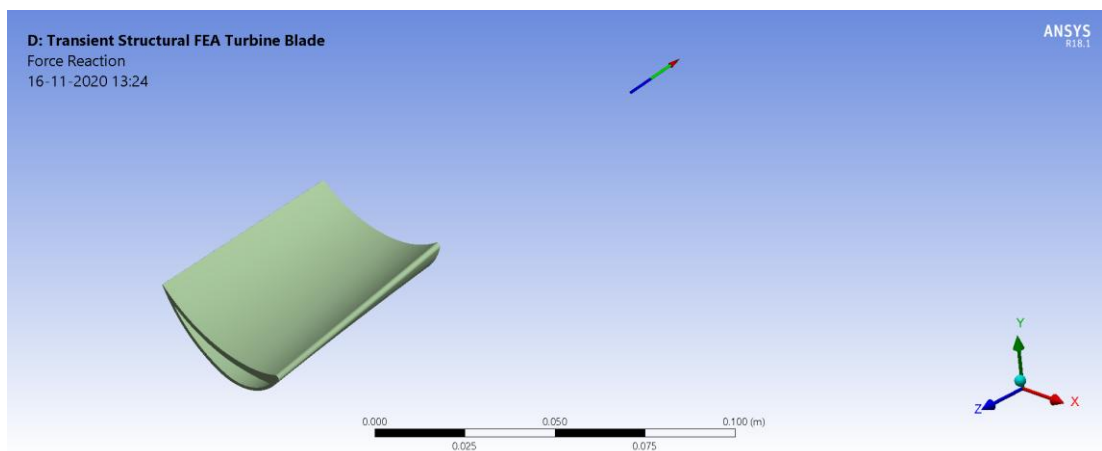


Fig 4.40: Force reaction direction and magnitude at remote point (Max: 307.06 N and Min: 16.795 N) at t = 1080s

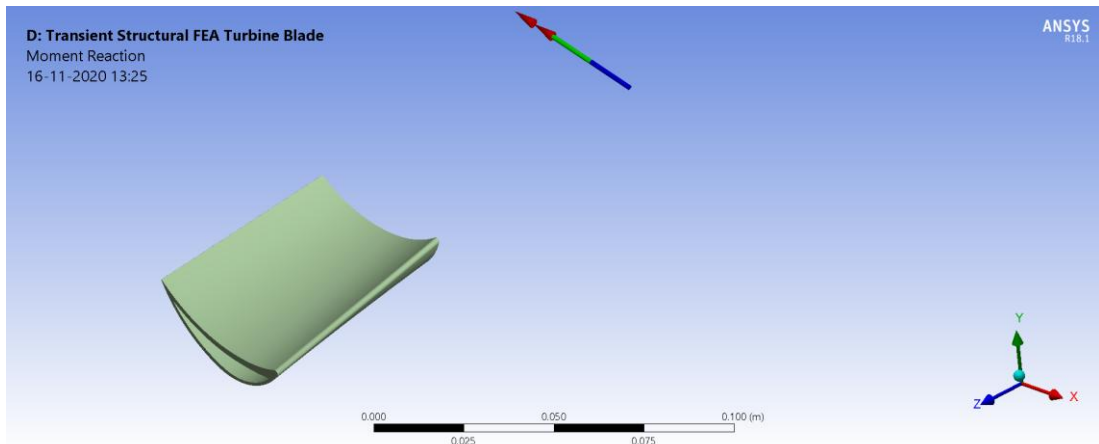


Fig 4.41: Moment reaction direction and magnitude at remote point (Max: 2.2608 Nm and Min: 2.1919 Nm) at t = 1080s

4.5.3.3.2 At t = 4428 s

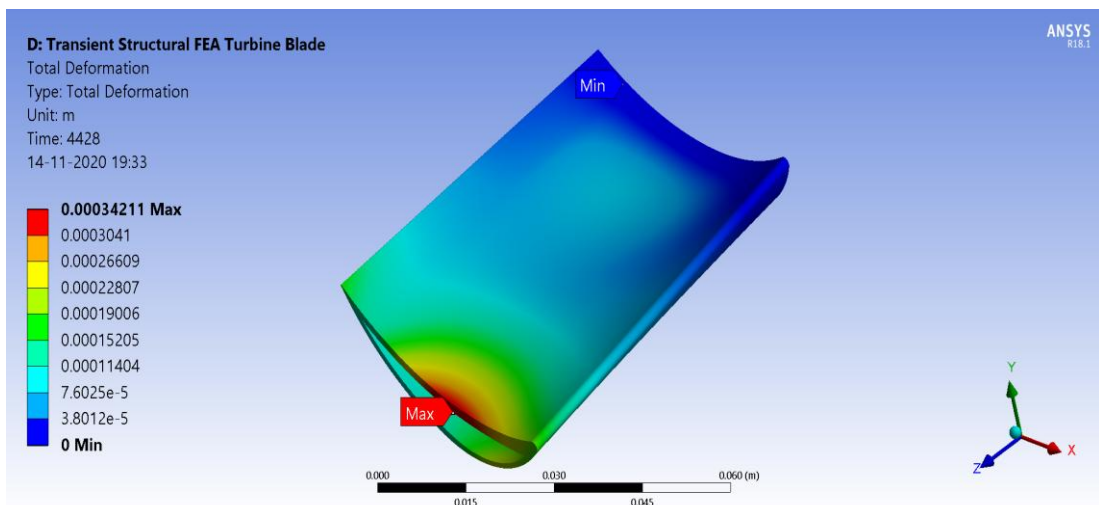
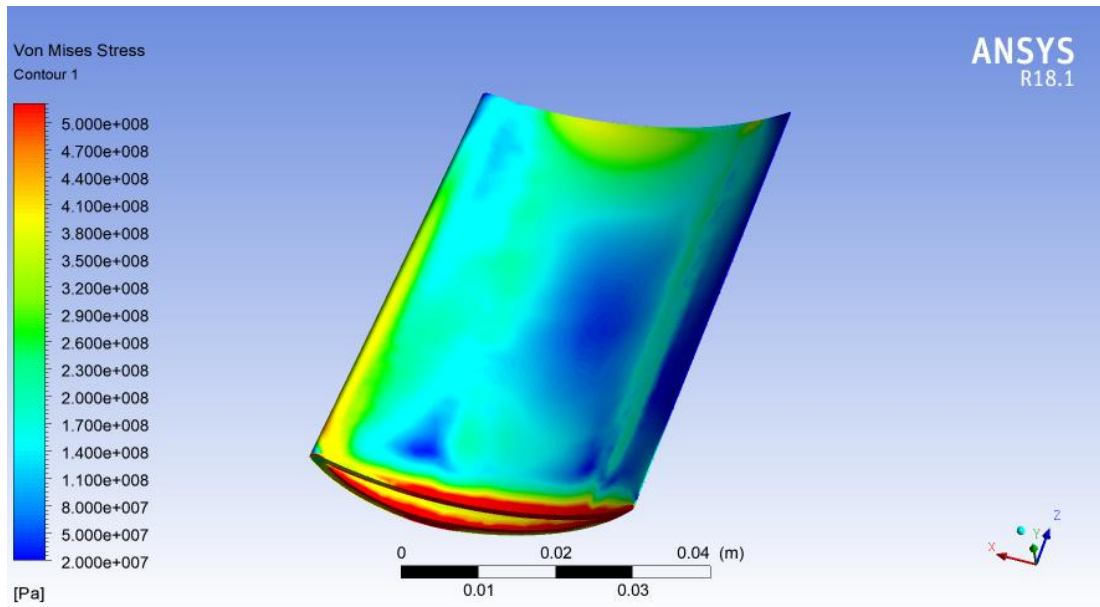
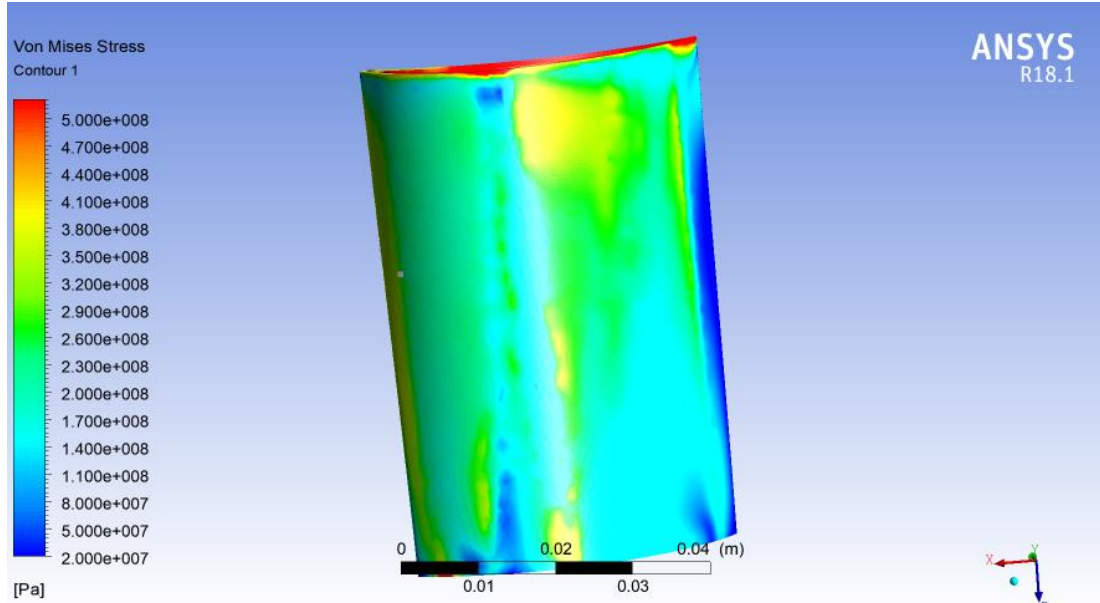


Fig 4.42: Total deformation contour at t = 4428s

Fig 4.43: Von mises stress contour on upper surface at $t = 4428s$ Fig 4.44: Von mises stress contour on lower surface at $t = 4428s$

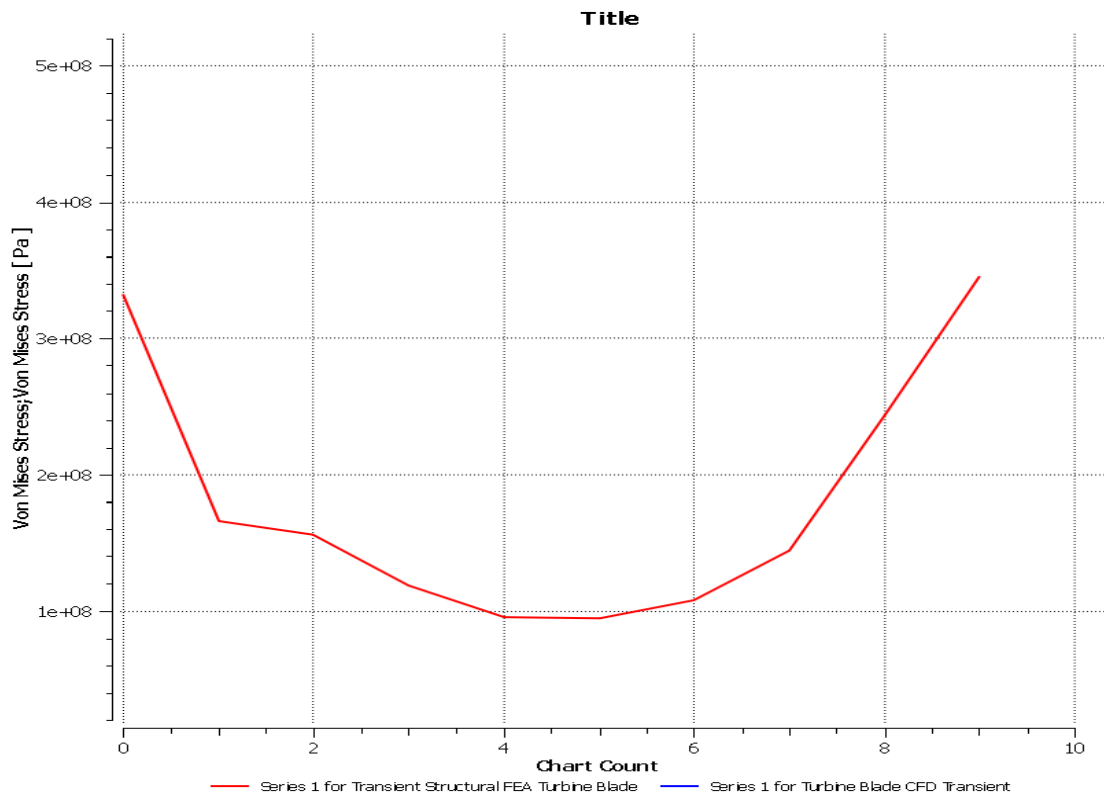


Fig 4.45: Von mises stress vs z graph along line in z direction at t = 4428s

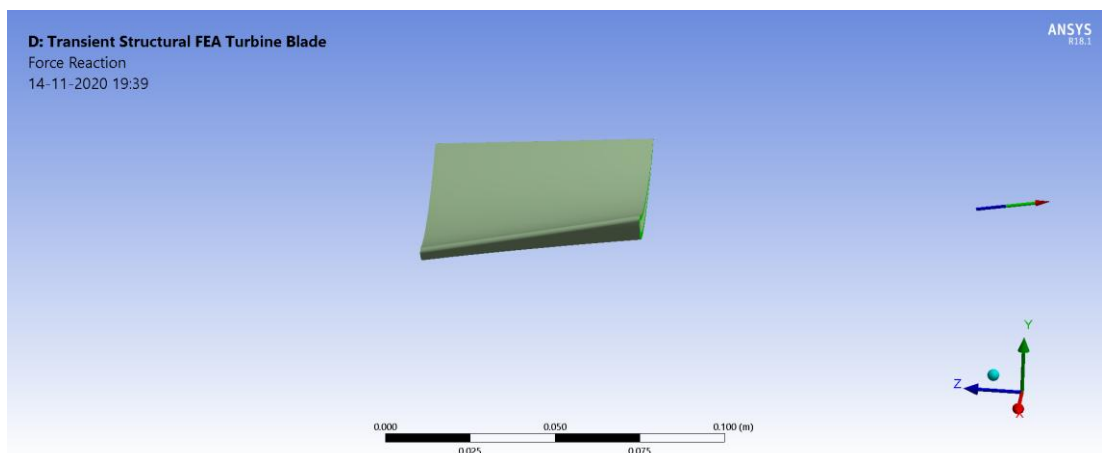


Fig 4.46: Force reaction direction and magnitude (Max: 852.82 N and Min: 98.743 N) at t = 4428s

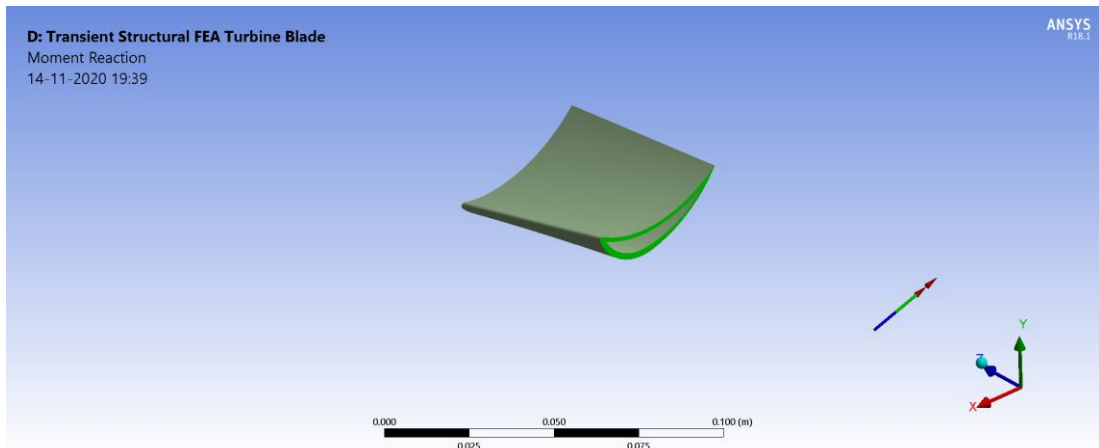


Fig 4.47: Moment reaction direction and magnitude (Max: 12.914 Nm and Min: 12.739 Nm) at t = 4428s

4.5.3.3.4 At t = 8100s

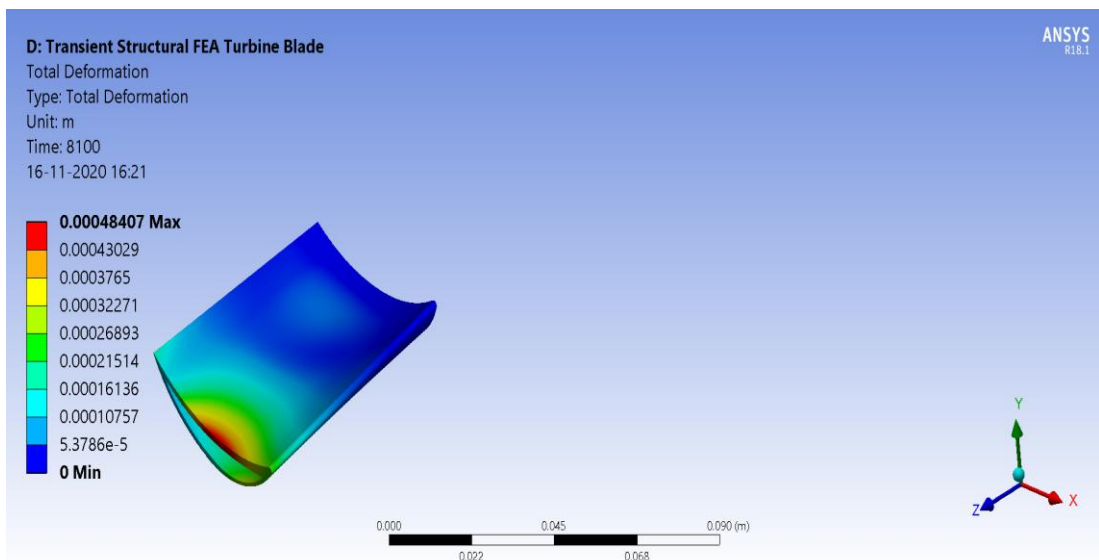


Fig 4.48: Total deformation contour at t = 8100s

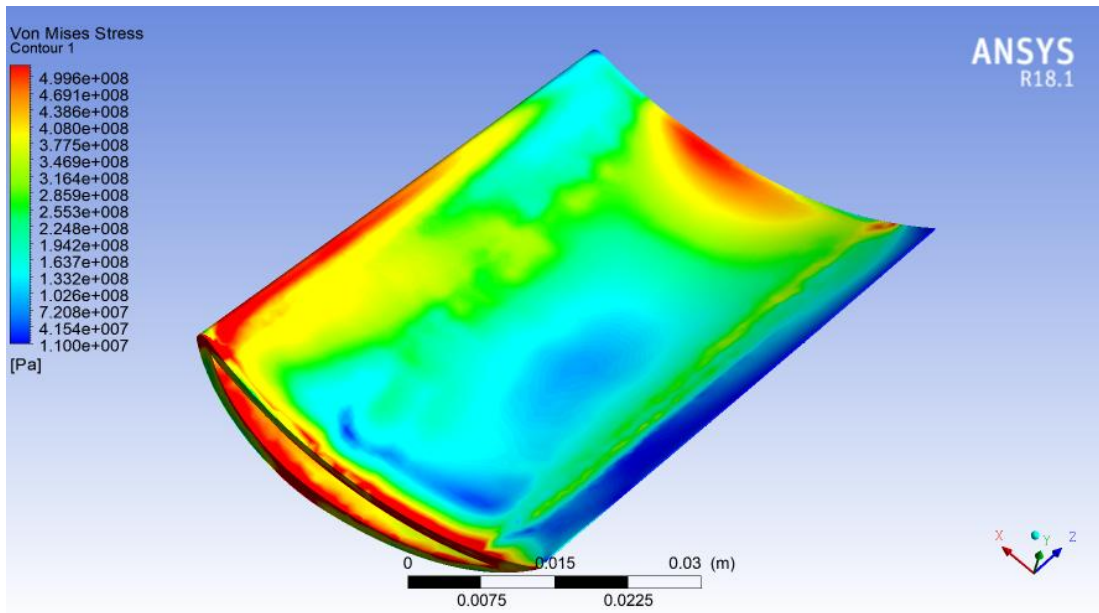


Fig 4.49: Von mises stress contour on upper surface at t = 8100s

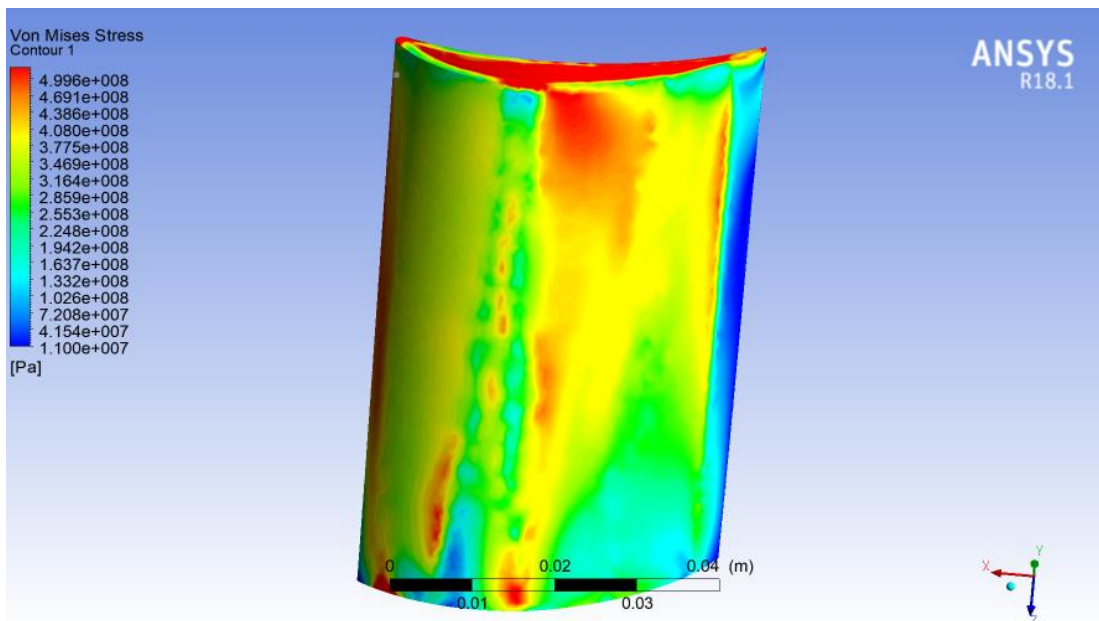


Fig 4.50: Von mises stress contour on lower surface at t = 8100s

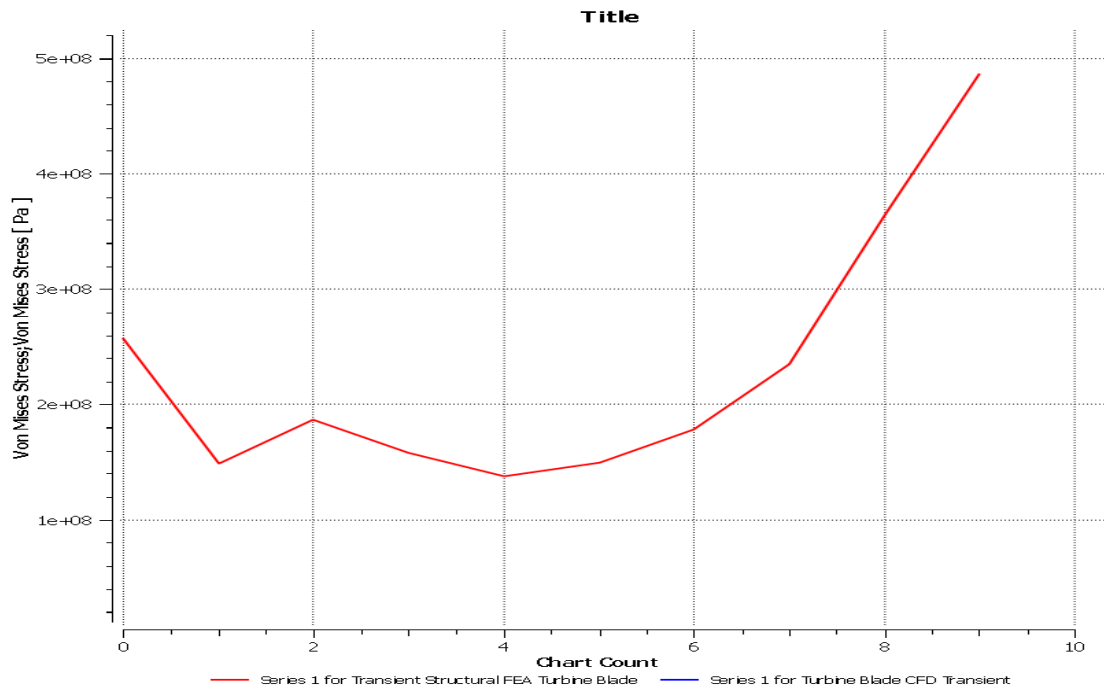


Fig 4.51: Von mises stress vs z graph on upper blade surface at t = 8100s

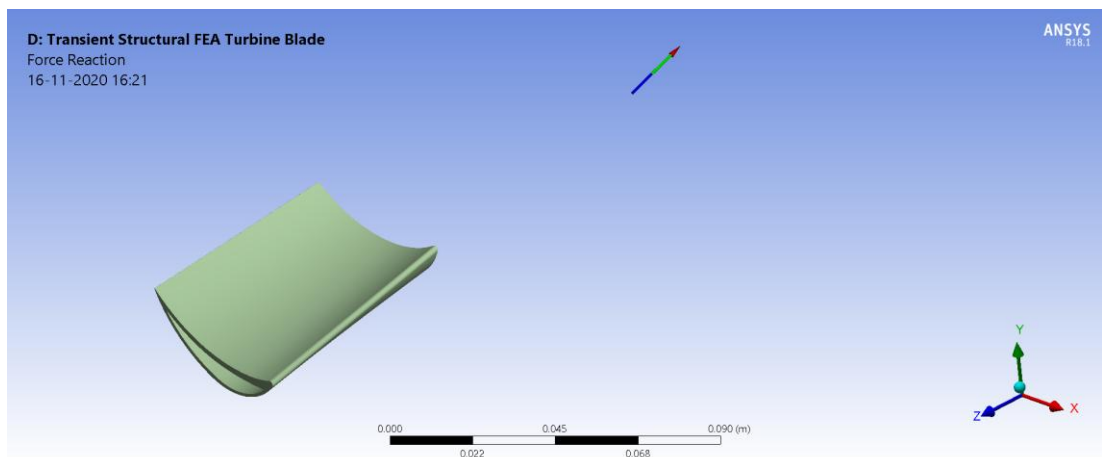


Fig 4.52: Force reaction direction and magnitude at remote point (Max: 874.99 N and Min: 265.42 N) at t = 8100s

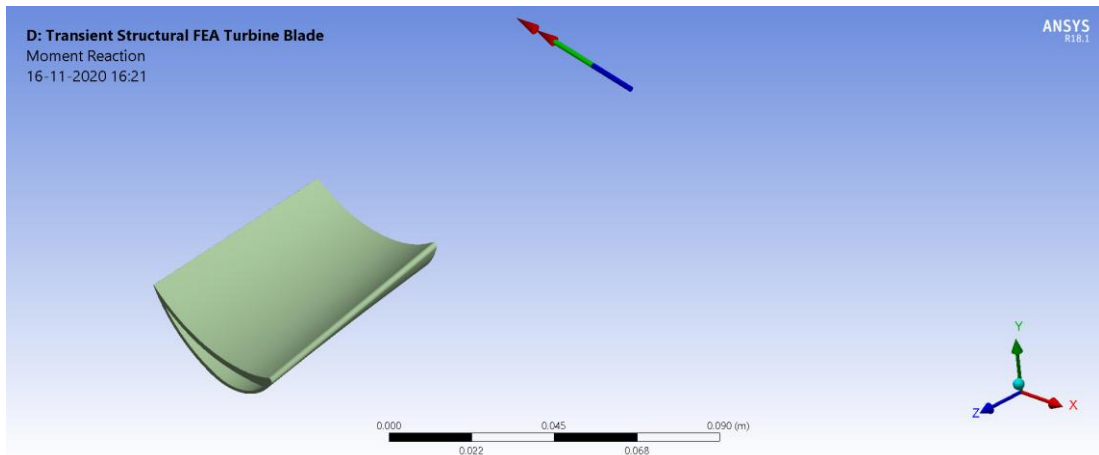


Fig 4.53: Moment reaction direction and magnitude at remote point (Max: 34.817 Nm and Min: 34.654 Nm) at $t = 8100s$

4.5.3.3.5 At $t = 10800s$

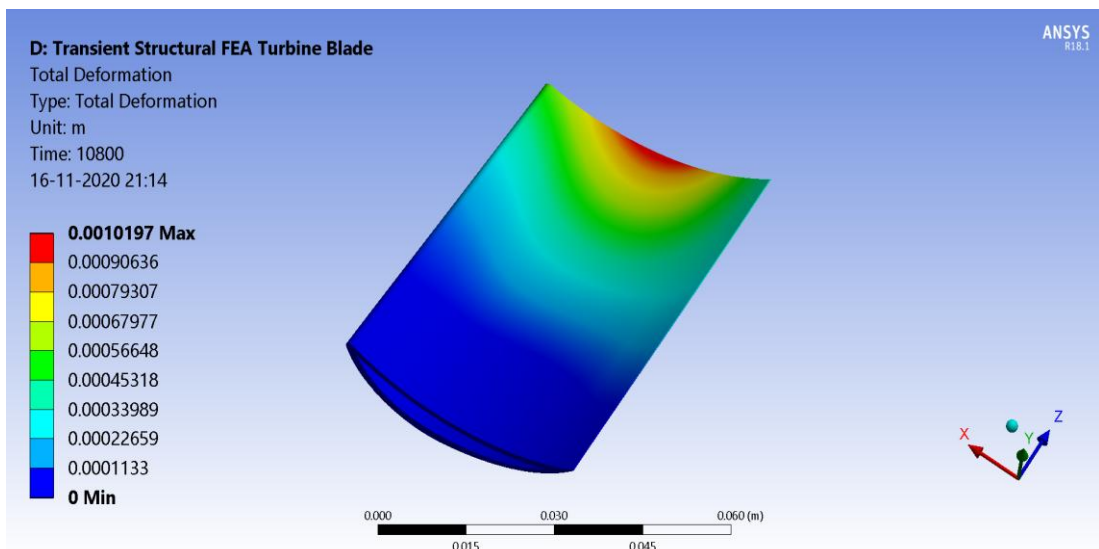


Fig 4.54: Total deformation contour at $t = 10800s$

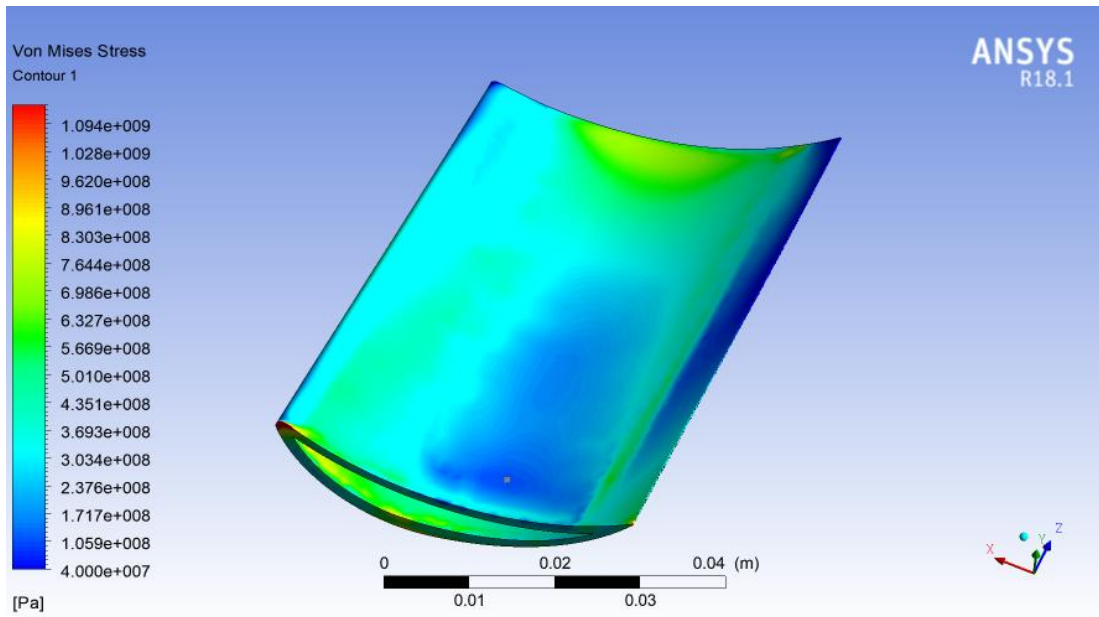


Fig 4.55: Von mises stress contour on upper surface at t = 10800s

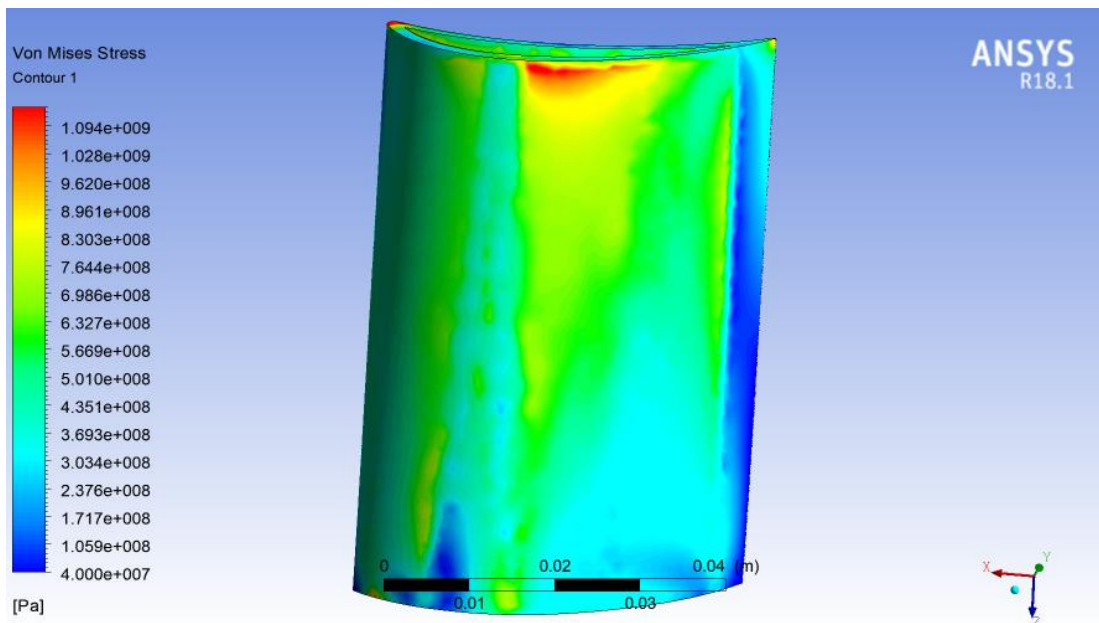


Fig 4.56: Von mises stress contour on lower surface at t = 10800s

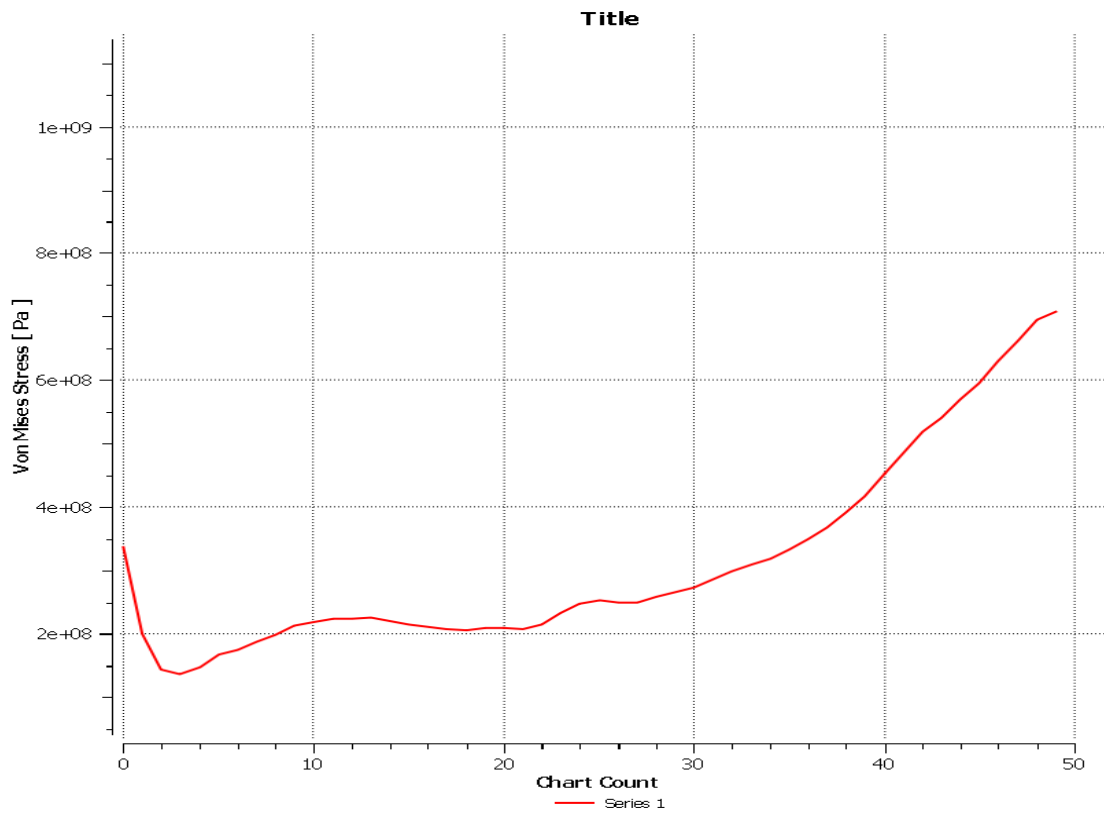


Fig 4.57: Von mises stress vs z graph on line in z direction on blade surface at t = 10800s

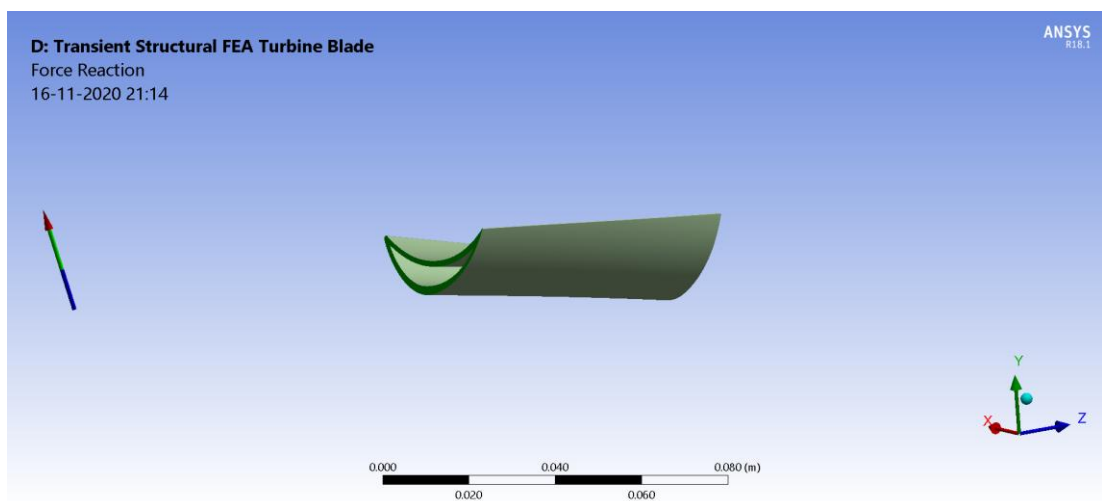


Fig 4.58: Force reaction direction and magnitude at remote point (Max: 2933.1 N and Min: 2865.8 N) at t = 10800s

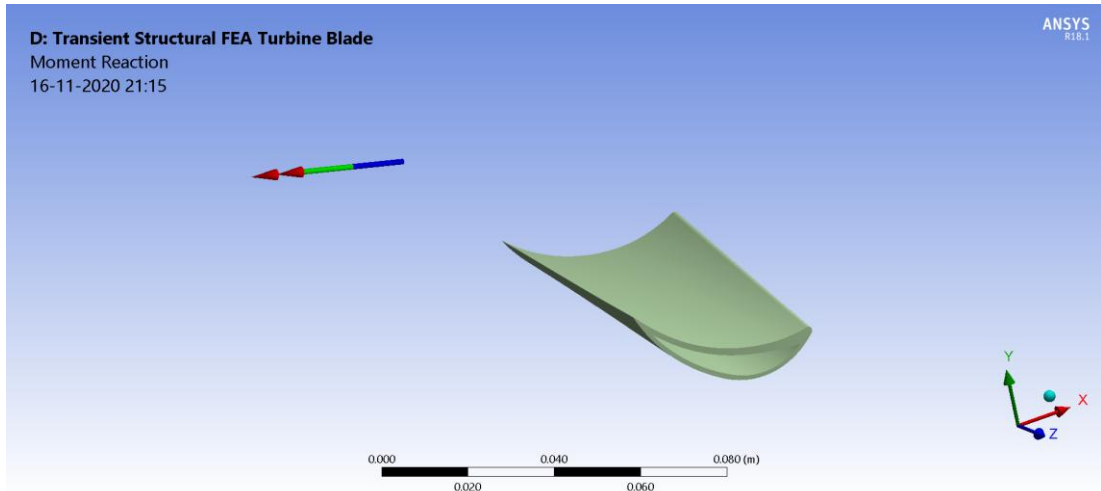


Fig 4.59: Moment reaction direction and magnitude at remote point (Max: 374.3 Nm and Min: 374.15 Nm) at t = 10800s

The variation of stress with time is shown in the form of graph in Figure 4.31.

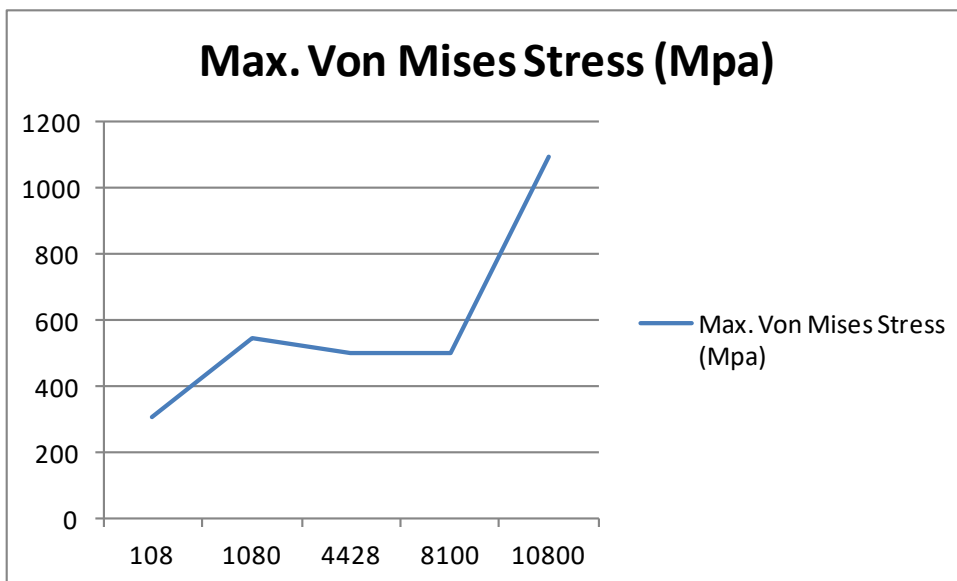


Fig 4.60: Von mises stress vs time during start-up

We have also obtained force reaction and moment reaction values at fixed point. The

direction as well as the magnitude of force reaction and moment reaction is shown in Figure 4.16 and Figure 4.17 respectively.

Table 4.3: Force reaction vs time

Time (s)	Max. Force Reaction (N)
108	491.55
1080	307.06
4428	852.82
8100	874.99
10800	2933.1

Table 4.4: Moment reaction vs time

Time (s)	Max. Moment Reaction (Nm)
108	64.508
1080	2.2608
4428	12.914
8100	34.817
10800	374.3

CHAPTER 5: RESULTS

This chapter deals with the discussion of the results displayed in Chapter 3 and Chapter 4 for steady state analysis and transient analysis respectively. After discussion of results for both the problems, comparison between the two has been done.

5.1. STEADY STATE ANALYSIS

5.1.1 CFD Results

The temperature contour in Figure 3.22 shows that blade temperature is maximum at the leading and trailing edge, equal to 802.1 K. The hollow side of the blade has constant temperature, equal to 300 K. The lower side of the blade has higher temperature than the upper side. On the lower surface also, the leading and trailing edge has the highest temperature. In figure 3.24, the trailing edge and leading edge have lesser value of temperature gradient than the rest of the blade. The magnitude of thermal gradient varies between 0 K/m to 453500 K/m on the blade's surface. The hollow surface and the lower surface of the blade have higher thermal gradients. The pressure is above atmospheric pressure on the upper surface of the blade and hollow part of the blade as shown in fig 3.26. The maximum magnitude of pressure is at upper surface of the blade with magnitude reaching as high as 1.7 MPa. The pressure on the lower surface of the blade is below atmospheric pressure with lowest magnitude of 0 Pa. The pressure difference between upper and lower surface creates a lift force in -Y direction. Due to pressure difference between upper and lower surfaces of the blade, lift force is produced on the blade which causes rotation of the blade.

A line location is formed in the z direction on the upper surface of the blade as shown in figure 3.28. The plot of pressure vs z along this line is shown in figure 3.29. From the

graph, it can be depicted that the pressure is plotted from cold outlet section to cold inlet section. Pressure magnitude along the line first decreases and then increases. A polyline location is formed in the x direction on the blade's surface. The pressure plot is created along the polyline on the upper surface and lower surface of the blade.

5.1.2 FEA Results

In Figure 3.42, total deformation contour is shown. The total deformation keeps on decreasing from free end to fixed end of the blade. The maximum magnitude of total deformation is 1.1473 mm. In Figure 3.43, the total deformation on the lower surface of the blade can be observed. In Figure 3.44, equivalent von mises stress is maximum at the fixed end of the blade near the leading edge and trailing edge. Maximum value of von mises stress is 2.1×10^9 Pa. Also, the free end at the trailing edge has minimum von mises stress equal to 6×10^7 Pa.

Figure 3.47 shows the graph of Stress vs z along the line location on upper surface of the blade. Figure 3.48 shows force reaction at fixed point. The total force reaction is 3011.9 N with direction as shown in the figure. Figure 3.49 depicts moment reaction. The total magnitude of moment reaction is 384.86 Nm with direction as shown in the figure.

5.2 TRANSIENT STATE ANALYSIS

5.2.1 CFD Results

In figure 4.9, temperature contour is represented. Temperature is maximum at the leading edge and below the leading edge. The maximum value of temperature is 625 K. In Figure 4.11, contour of temperature gradient is varying over the entire surface of the blade. The maximum magnitude is $7.367 \times 10^5 \text{ m}^{-1} \text{ K}$. The minimum magnitude of thermal gradient is on

the leading and trailing edge of the blade. Figure 4.13 and figure 4.14 shows the pressure distribution on the upper and lower surface of the blade respectively. The maximum magnitude of pressure is 4.545 MPa. The pressure is more at the upper surface than at the lower surface. The pressure difference between lower and upper surface creates a lift force on the blade in -Y direction. The lowest magnitude of pressure is 0 Pa. The pressure is above the atmospheric pressure on the upper surface of the blade and it is below than the atmospheric pressure on the lower surface of the blade.

In figure 4.17, the pressure vs z graph is plotted along the line location on both the upper surface and lower surface of the blade. Similarly, figure 4.19 and figure 4.20 shows pressure vs x graph along polyline on the upper and lower surface of the blade respectively. Figure 4.21 shows variation of pressure during the transient analysis at a point location on the blade surface. The variation of temperature with time is shown in figure 4.22 at a point location on the blade surface.

5.2.2 FEA Results

In Figure 4.54, the total deformation decreases from fixed end to free end of the blade. The maximum magnitude of total deformation is at the centre of the free end. In figure 4.55, the equivalent von mises stress is maximum at the fixed end on the lower side of the blade. The trailing edge on both sides of the blade has the lowest magnitude of equivalent stress. The equivalent von mises stress is more on the lower side of the blade than on the upper side of the blade. Figure 4.57 shows von mises stress vs z curve along the line location on upper surface of the blade. Figure 4.58 and figure 4.59 discusses the magnitude and direction of force reaction and moment reaction respectively. The results discussed above are at $t = 10800$ s. Similarly, the results are obtained at four other time steps which are discussed below.

Table 5.1: Total deformation vs time during start-up

Time (s)	Total Deformation (mm)
108	0.18724
1080	0.24222
4428	0.34211
8100	0.48407
10800	1.0197

Table 5.2: Von mises stress vs time during start-up

Time (s)	Von Mises Stress (MPa)
108	307.4
1080	547.9
4428	500
8100	499.6
10800	1094

Figure 4.24 shows force reaction at fixed point. Due to varying loads, force reaction also varies with time. Figure 4.25 represents moment reaction at the remote point.

Table 5.3: Maximum force reaction vs time during start-up

Time (s)	Max. Force Reaction (N)
108	491.55
1080	307.06
4428	852.82
8100	874.99

10800	2933.1
-------	--------

Table 5.4: Maximum moment reaction vs time during start-up

Time (s)	Max. Moment Reaction (Nm)
108	64.508
1080	2.2608
4428	12.914
8100	34.817
10800	374.3

Figure 4.60 depicts von mises stress variation on the turbine blade with time during the start-up process. It can be interpreted that the maximum value of von mises stress first increases with time, then remains constant and in the end again increases with time.

5.3 COMPARISON OF RESULTS

The maximum temperature of blade is 802.1 K and 625 K for steady state and transient state analysis. The maximum value of thermal gradient occurs at the lower surface and hollow surface, equal to $4.535e5$ K/m. The thermal gradient is varying over the entire surface of the blade for transient state analysis with maximum magnitude of $7.367e5$ K/m. The leading edge and trailing edge of the blade has the lowest thermal gradients for both the analysis. The pressure is above the atmospheric pressure on the upper surface of the blade and below the atmospheric pressure on the lower surface of the blade for both the analysis. The maximum magnitude of pressure is 1.7 MPa and 4.545 MPa for steady state and transient state analysis respectively.

The total deformation is highest at the free end and decreases gradually as we move towards the fixed end of the blade. The total deformation is 0.1276 mm higher for steady state analysis than in transient state analysis. For steady state analysis, the von mises stress is maximum at the fixed end of the blade near the leading and trailing edge of the blade. In transient state analysis, the von mises stress is maximum at the fixed end on the lower side of the blade. The maximum magnitude of von mises stress is 2.1×10^9 Pa and 1.094×10^9 Pa for steady state and transient state analysis respectively. The values of force reaction and moment reaction remains constant for steady state analysis but varies in transient state analysis. The maximum magnitude of force reaction is 3011.9 N and 2933.1 N for steady state and transient state analysis respectively. The maximum magnitude of moment reaction is 384.86 Nm and 374.3 Nm for steady state and transient state analysis respectively.

CHAPTER 6: CONCLUSION

The stress analysis is performed for steam turbine blade during steady state and transient state (start-up). The maximum temperature achieved in the steady state and transient state analysis differs by 177.1 K with former one being more. The thermal gradient produced in the blade is 1.62 times more in transient state analysis than in steady state analysis. Therefore, the stress produced due to thermal load in the blade in transient state analysis is more than in steady state analysis. Due to higher stress due to thermal load in transient state analysis, creep damage of the blade can take place during the start-up. Due to the pressure differential between upper and lower surface of the blade, a lift force is produced in the -Y direction in both the analysis. The total deformation is 0.1276 mm higher in steady state analysis than in transient state analysis. The equivalent stress due to all the loads applied is higher in steady state than in transient state analysis. The maximum magnitude of force reaction in steady state analysis is almost same to that in transient state analysis. The maximum magnitude of moment reaction in steady state analysis is also similar to that in transient state analysis. But there magnitudes varies in transient state condition due to varying loading conditions.

Power produced by single blade, $P = \text{Torque} * \text{Angular Velocity}$ (6.1)

$$P = 384.86 * 314$$

$$P = 120.846 \text{ kW.}$$

Finally, it is concluded that the thermal stresses in turbine blade during the start-up is very high and may lead to fatigue or creep failure of the blade. Hence, care needs to be taken while designing the start-up procedure for a steam turbine. Also, one can further study the creep life prediction for a steam turbine blade. It is also concluded that the area on the blade's surface at the trailing edge, leading edge and centre of the fixed end is the critical area as the maximum stress is induced in this part during the start-up process. The stress in this critical area has crossed the tensile yield strength and tensile ultimate strength of

blade's material which might lead to plastic deformation and fracture of the blade in that part. In future, one can perform fatigue analysis of the turbine blade to evaluate its fatigue life.

APPENDIX

A.1 PROBLEMS SOLVED ON ANSYS R18.1

This section consists of different problems solved on Ansys R18.1 software. All these problems helped to achieve the main problem which is presented in the report. Every problem in this list presents the problem formulation, boundary condition and results. The problems solved have been showcased pictorially in proper sequence.

1. Unsteady Flow Over a Cylinder

Consider the unsteady state case of a fluid flowing past a cylinder, as illustrated above. For this tutorial we will use a Reynolds Number of 120. In order to simplify the computation, the diameter of the cylinder is set to 1 m, the x component of the velocity is set to 1 m/s and the density of the fluid is set to 1 kg/m³. Thus, the dynamic viscosity must be set to 8.333x10⁻³ kg/m*s in order to obtain the desired Reynolds number. Compared to the steady case, the unsteady case includes an additional time-derivative term in the Navier-Stokes equation.

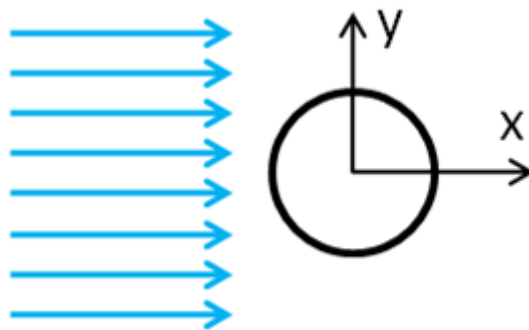


Fig A.1: Schematic diagram

The methods implemented by FLUENT to solve a time dependent system are very similar to those used in a steady-state case. In this case, the domain and boundary conditions will be the same as the Steady Flow Past a Cylinder. However, because this is a transient

system, initial conditions at $t=0$ are required. To solve the system, we need to input the desired time range and time step into FLUENT. The program will then compute a solution for the first time step, iterating until convergence or a limit of iterations is reached, then will proceed to the next time step, "marching" through time until the end time is reached.

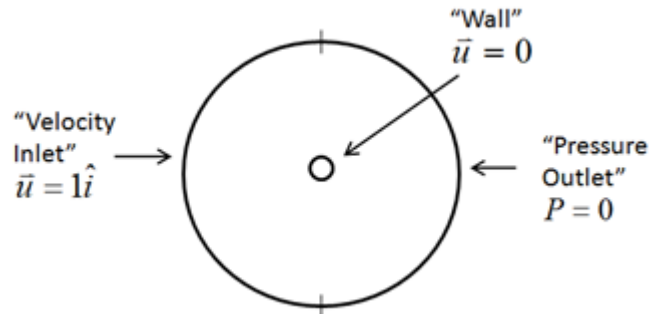


Fig A.2: Boundary condition

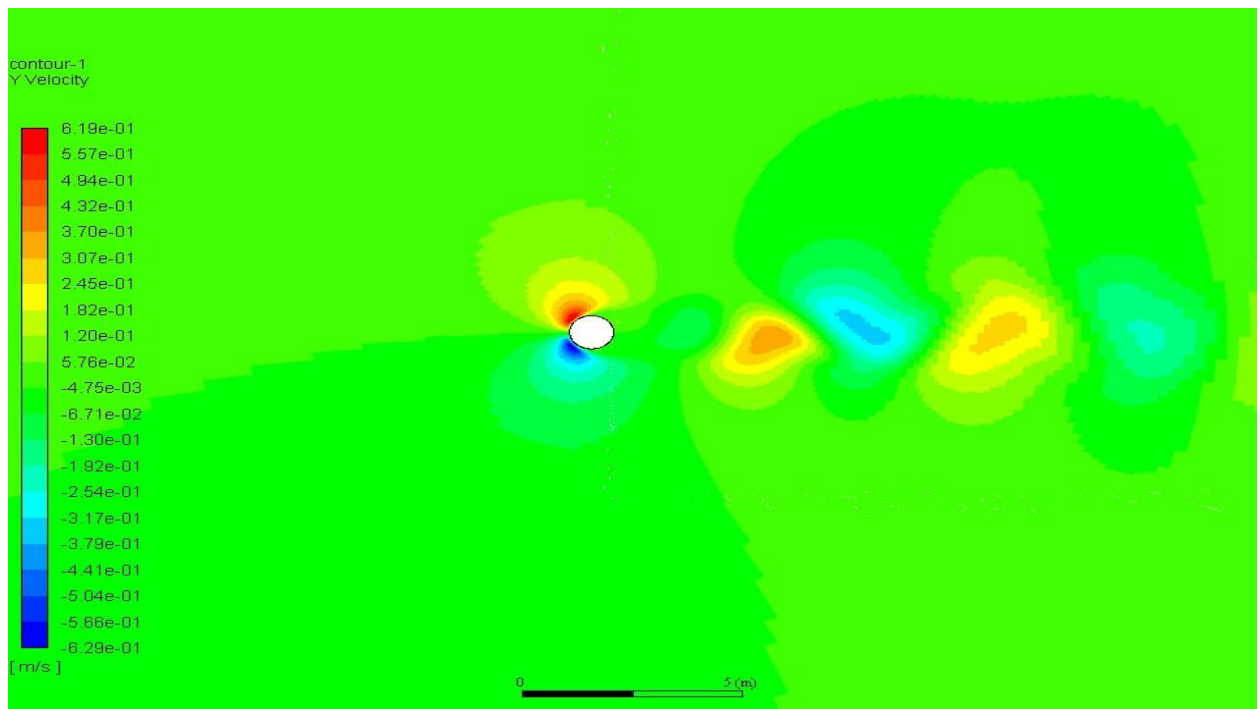


Fig A.3: Velocity contour in Y direction

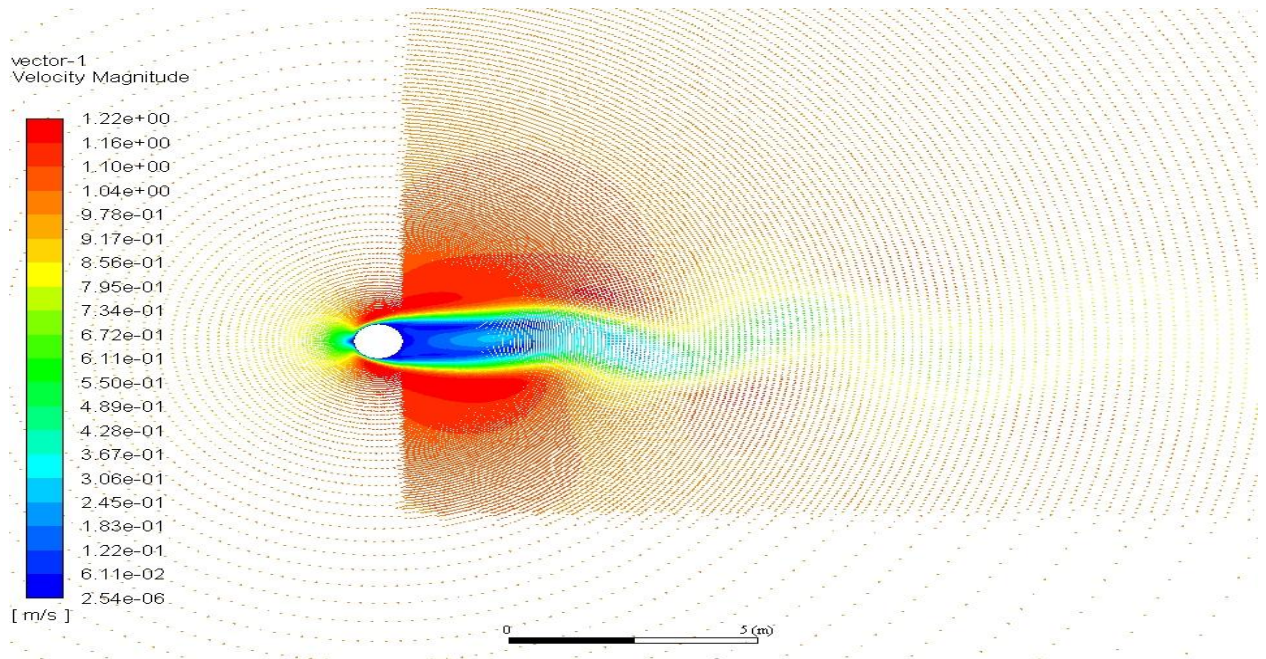


Fig A.4: Velocity magnitude vector

2. Turbulent Pipe Flow

The inlet velocity is 1 m/s, the fluid exhausts into the ambient atmosphere and density is 1 kg/m^3 . For $\mu = 2 \times 10^{-5} \text{ kg/(ms)}$, the Reynolds no. based on the pipe diameter and average velocity at the inlet is 10000. This change of viscosity has taken us from a Reynolds number of 100 to 10,000. At this Reynolds number, the flow is usually completely turbulent.

A turbulent flow exhibits small-scale fluctuations in time. It is usually not possible to resolve these fluctuations in a CFD calculation. So the flow variables such as velocity, pressure, etc. are time-averaged. Unfortunately, the time-averaged governing equations are not closed. (i.e. They contain fluctuating quantities which need to be modeled using a turbulence model.)

In this problem, $k-\varepsilon$ model is used for numerical representation of turbulent flow. $k-\varepsilon$ models consist of two differential equations: one each for the turbulent kinetic energy k and turbulent dissipation ε . These two equations have to be solved along with the time-averaged continuity, momentum and energy equations. So turbulent flow calculations

are much more difficult and time-consuming than laminar flow calculations.

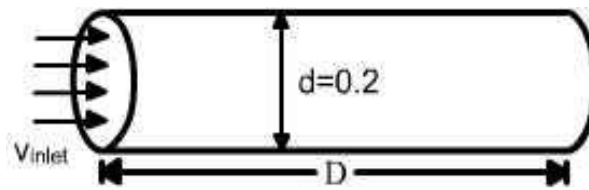


Fig A.5: Schematic Diagram

The boundary conditions and the geometry remains the same as the previous problem.

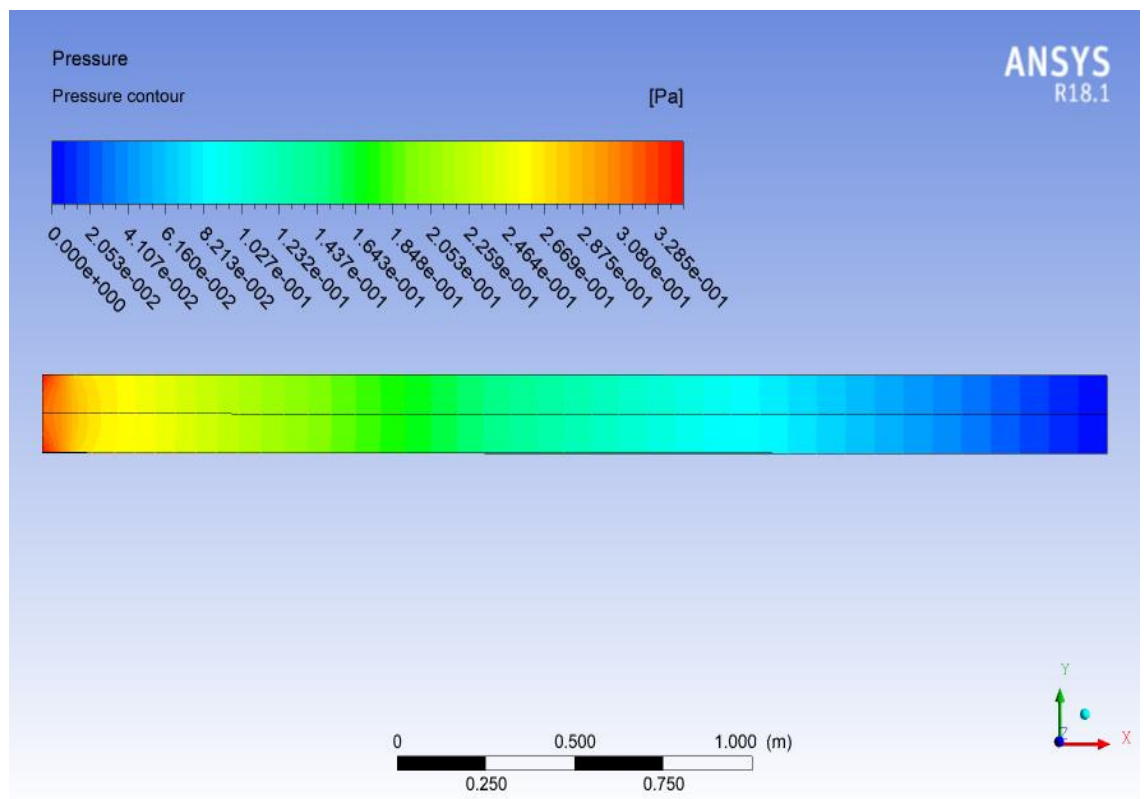


Fig A.6: Pressure contour

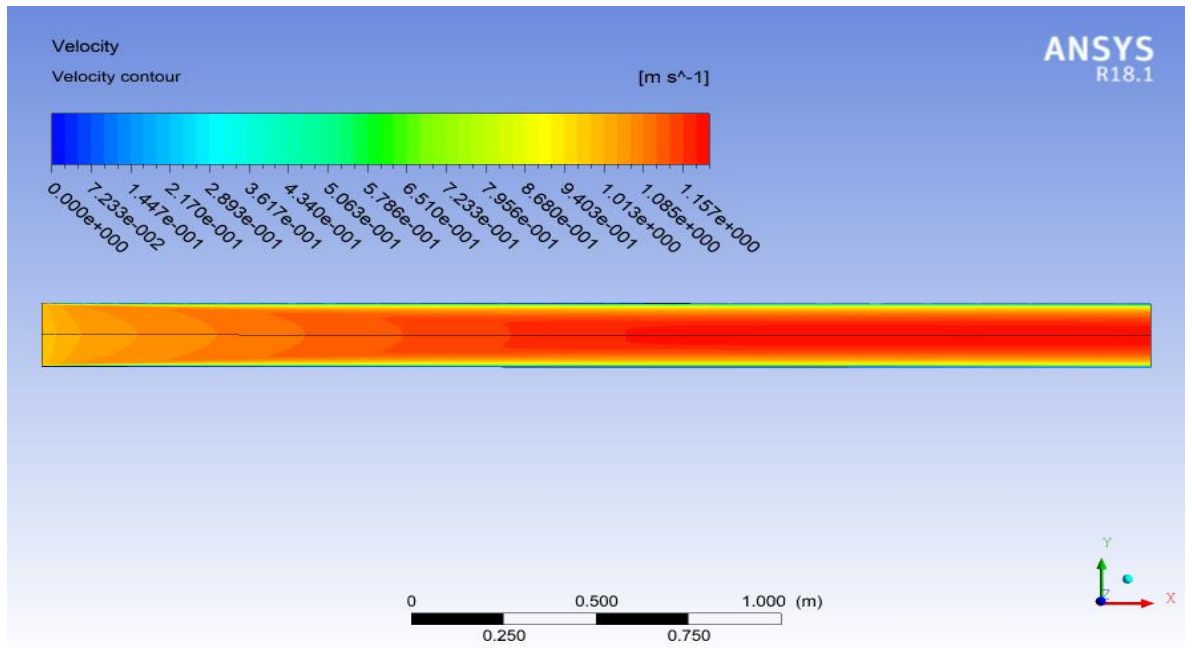


Fig A.7: Velocity contour

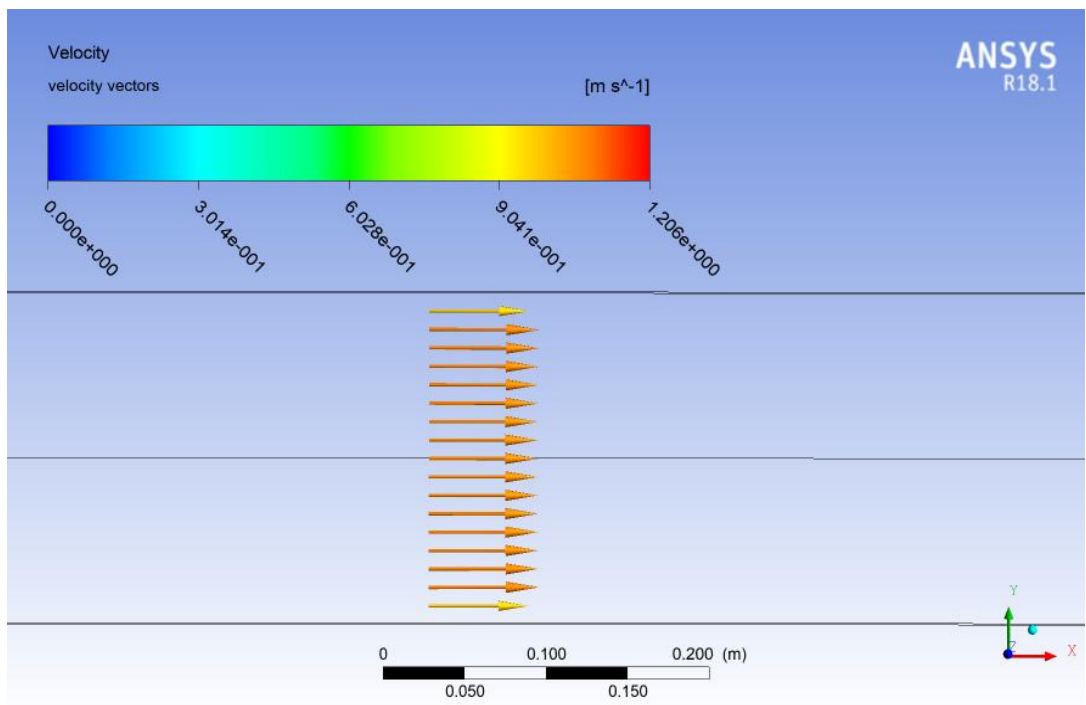


Fig A.8: Velocity vector

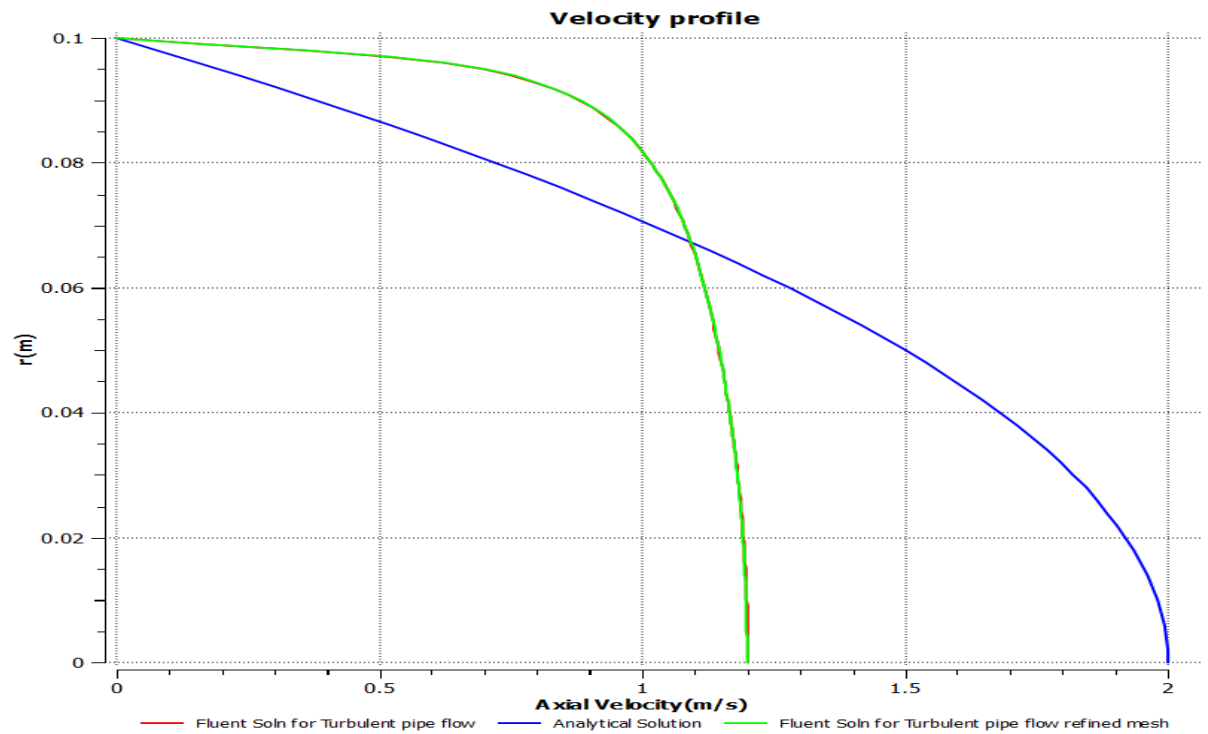


Fig A.9: Velocity profile

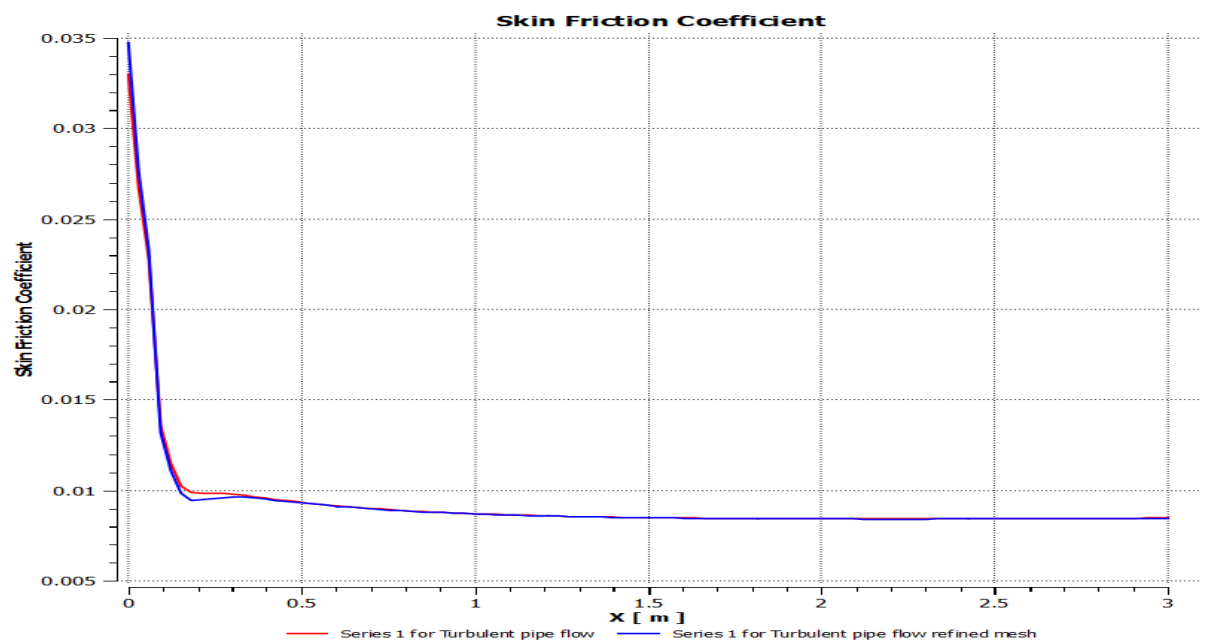


Fig A.10: Skin friction coefficient along the length of pipe

3. Flat Plate Boundary Layer

Consider a fluid flowing across a flat plate, as illustrated above. Obtain the velocity and pressure distribution when the Reynolds number based on the plate length is 10,000. This Reynolds number is obtained by using the following settings. The plate length is 1 m. The

incoming fluid is flowing in the x-direction with a velocity of 1 m/s. The density of the fluid is 1 kg/m^3 and the viscosity is $1 \times 10^{-4} \text{ kg/(m-s)}$.

$$\frac{\delta_{99}}{x} = \frac{5}{\sqrt{Re_x}} \quad (\text{A.1})$$

When $x = L$, $\delta_{99} = 0.05 \text{ m}$. The height of the domain will be set to ten times the boundary layer thickness. Thus, the height of the boundary will be set to 0.5 m .

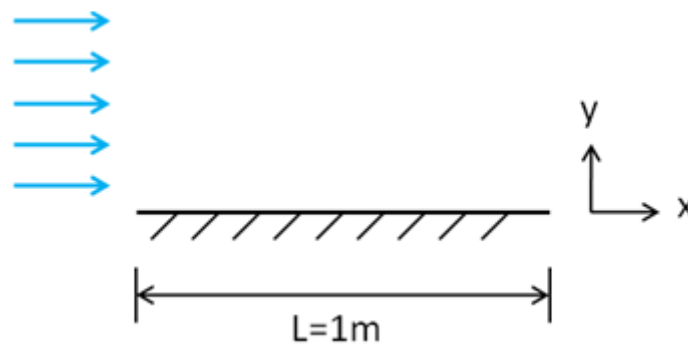


Fig A.11: Schematic diagram

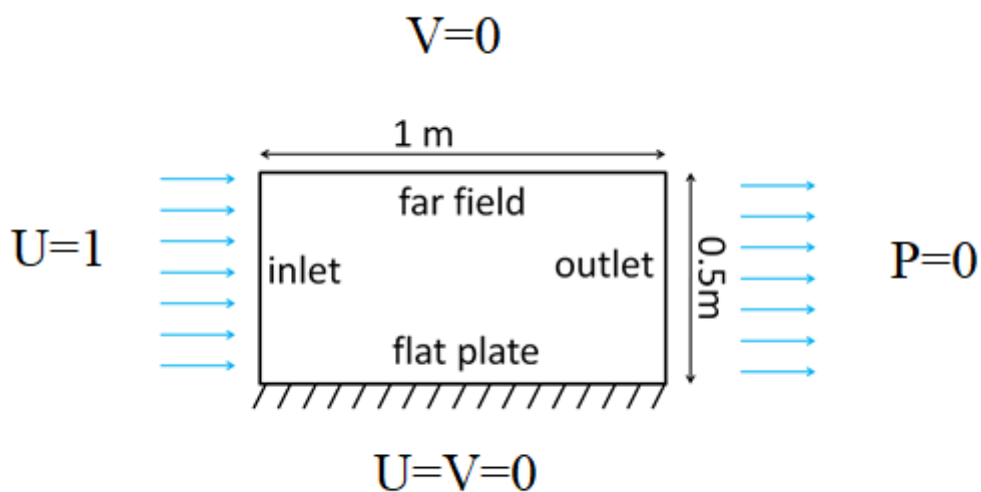


Fig A.12: Boundary condition

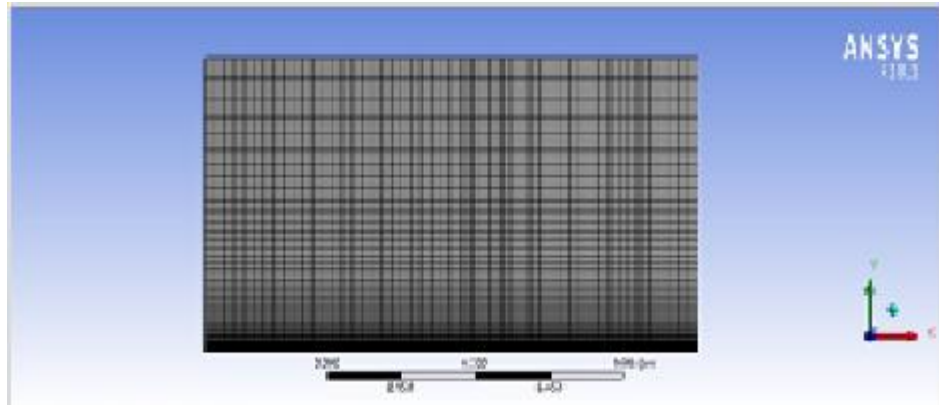


Fig A.13: Meshed model

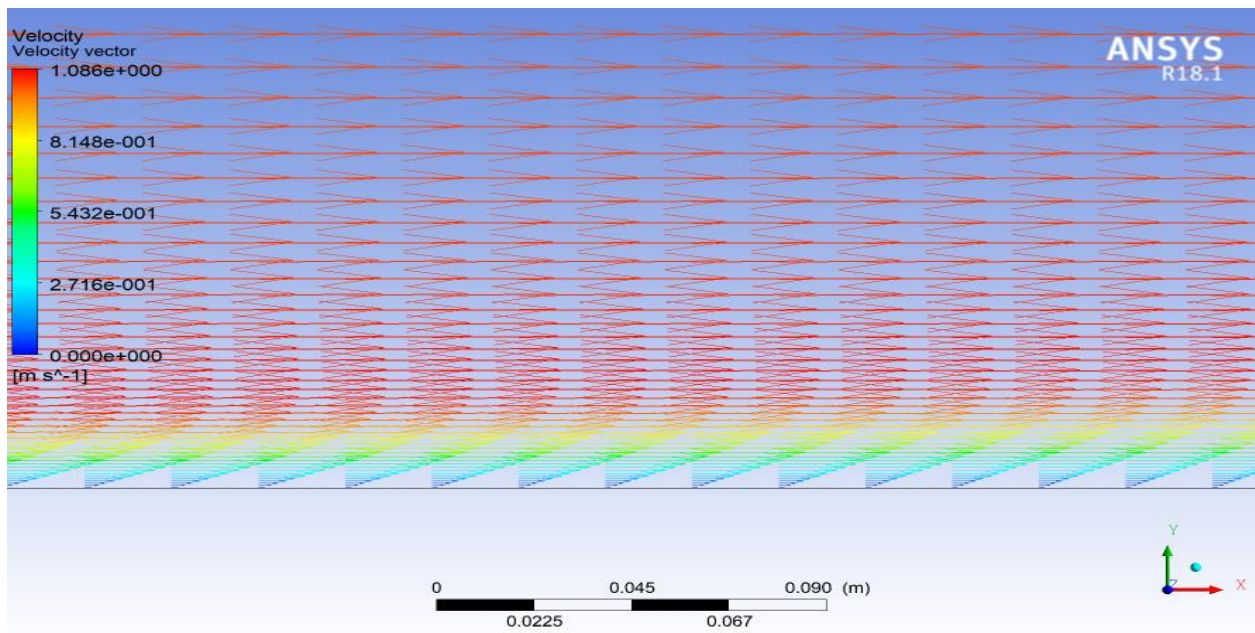


Fig A.14: Velocity vector

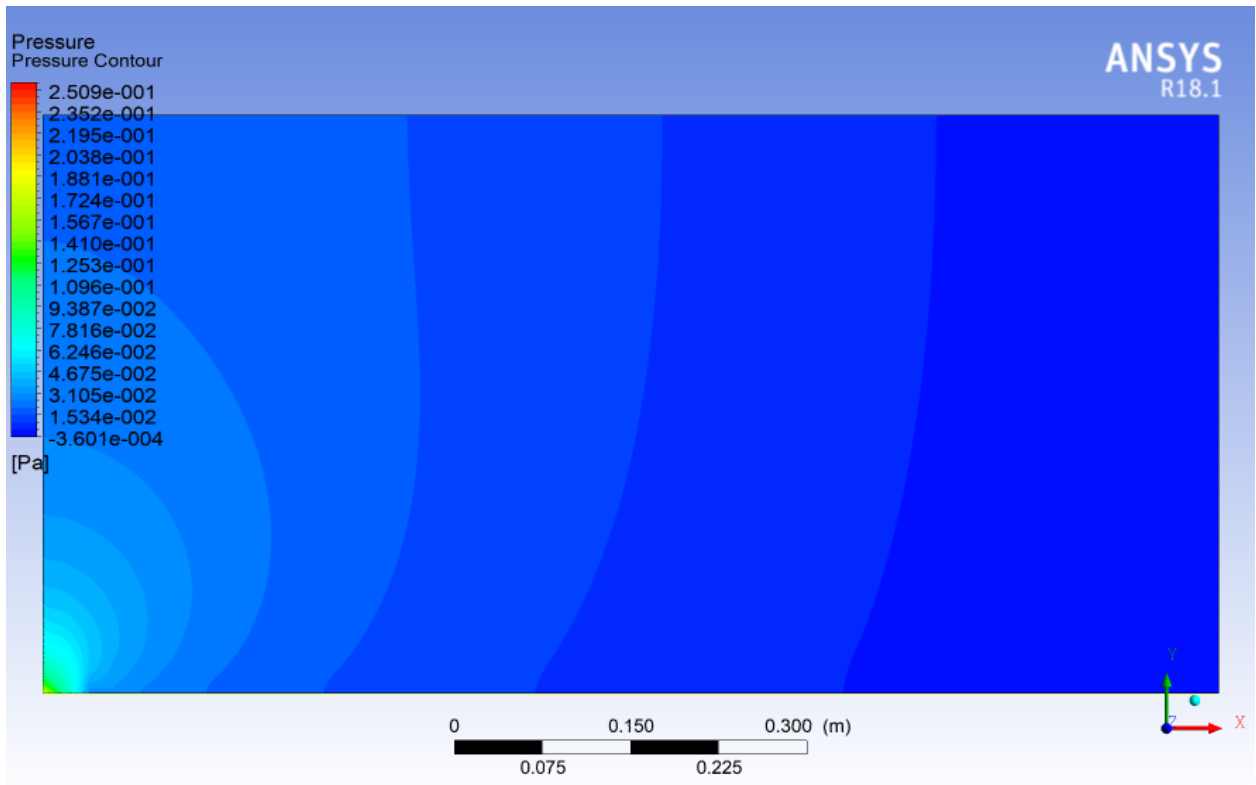


Fig A.15: Pressure contour

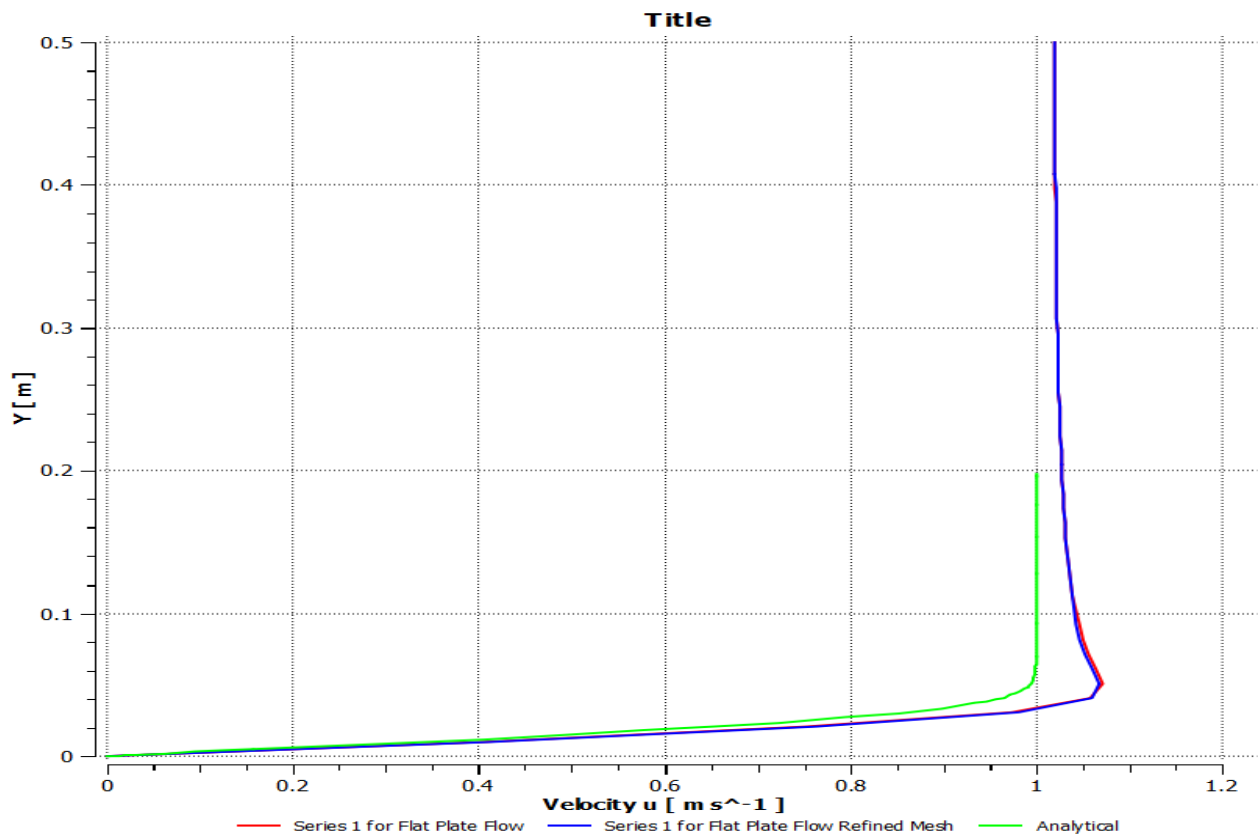


Fig A.16: Velocity in Y direction

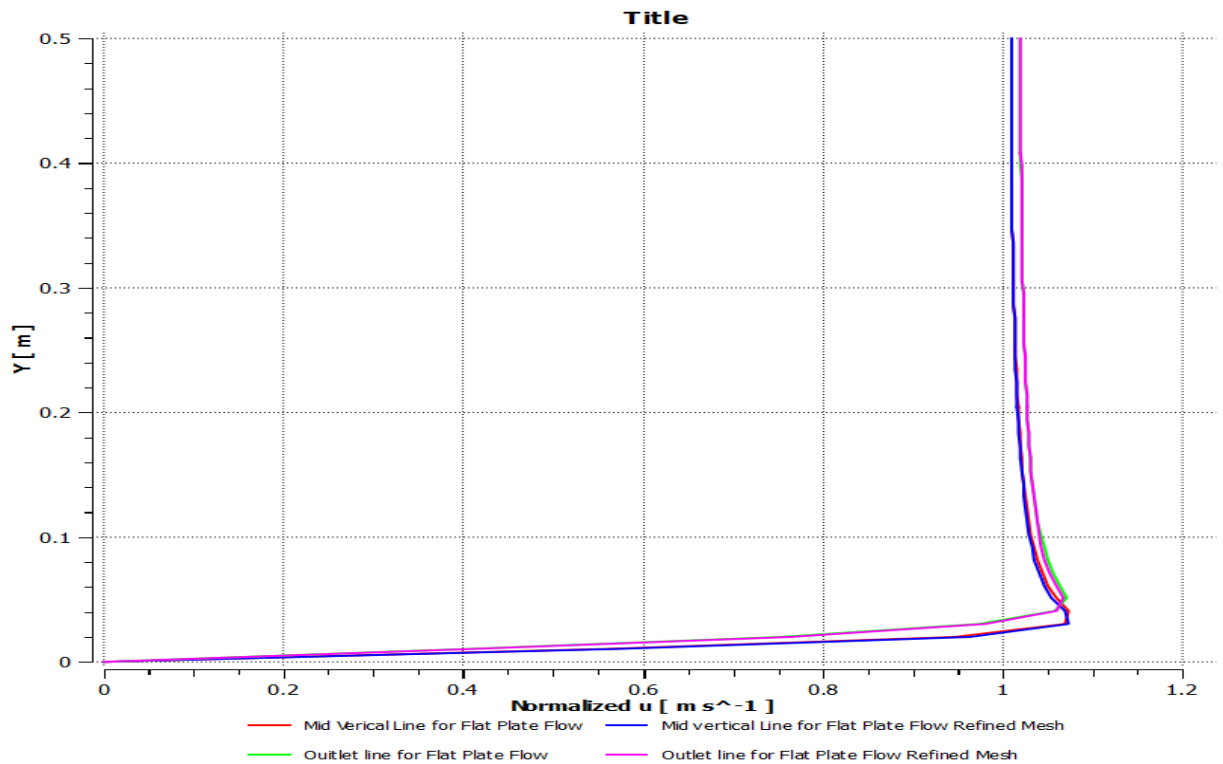


Fig A.17: Normalised velocity in Y direction

4. Wind Turbine Blade FSI (CFD)

The blade is 43.2 meters long and starts with a cylindrical shape at the root and then transitions to the airfoils S818, S825 and S826 for the root, body and tip, respectively. This blade also has pitch to vary as a function of radius, giving it a twist and the pitch angle at the blade tip is 4 degrees.

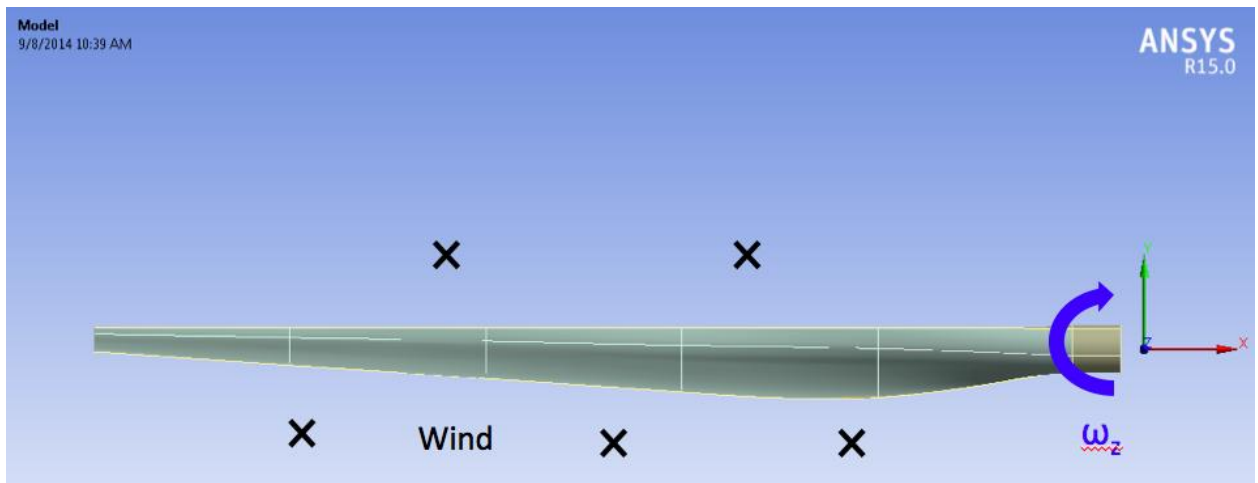


Fig A.18: Blade CAD geometry

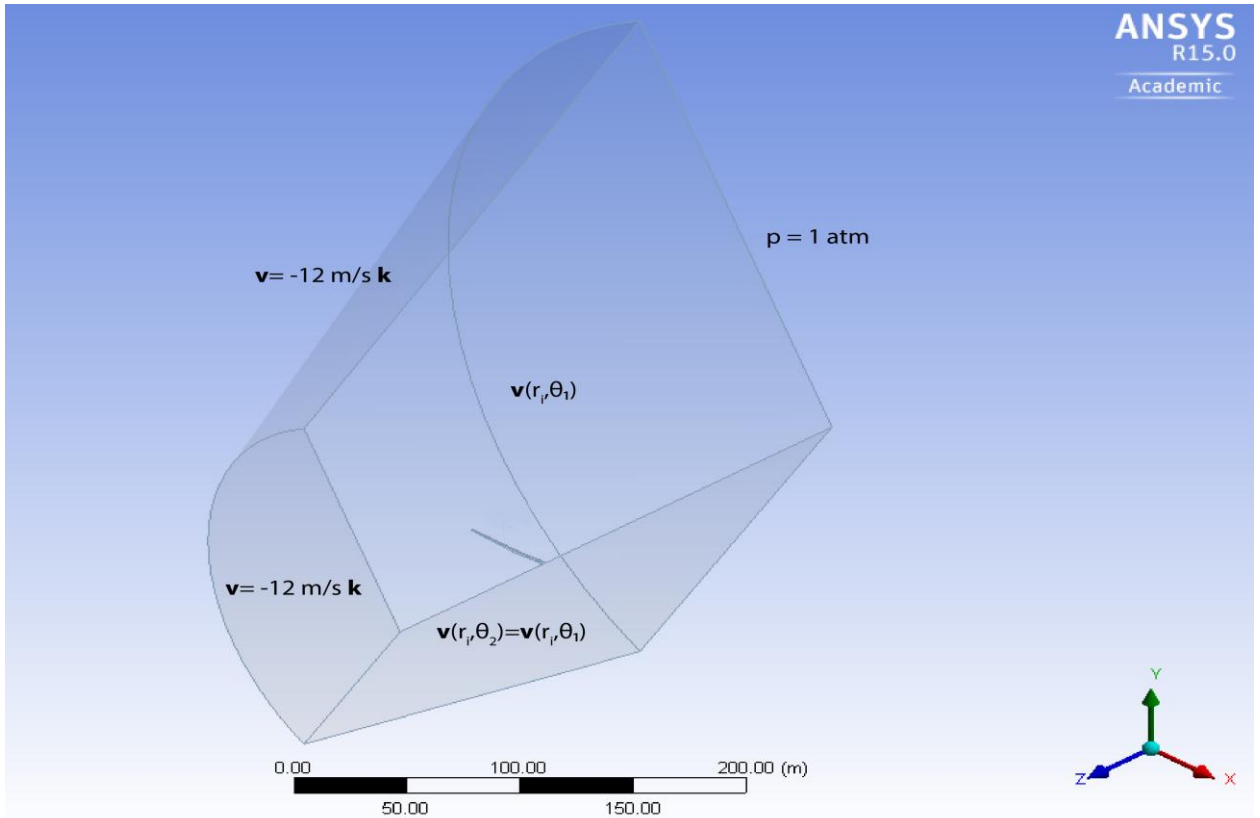


Fig A.19: Complete CAD geometry

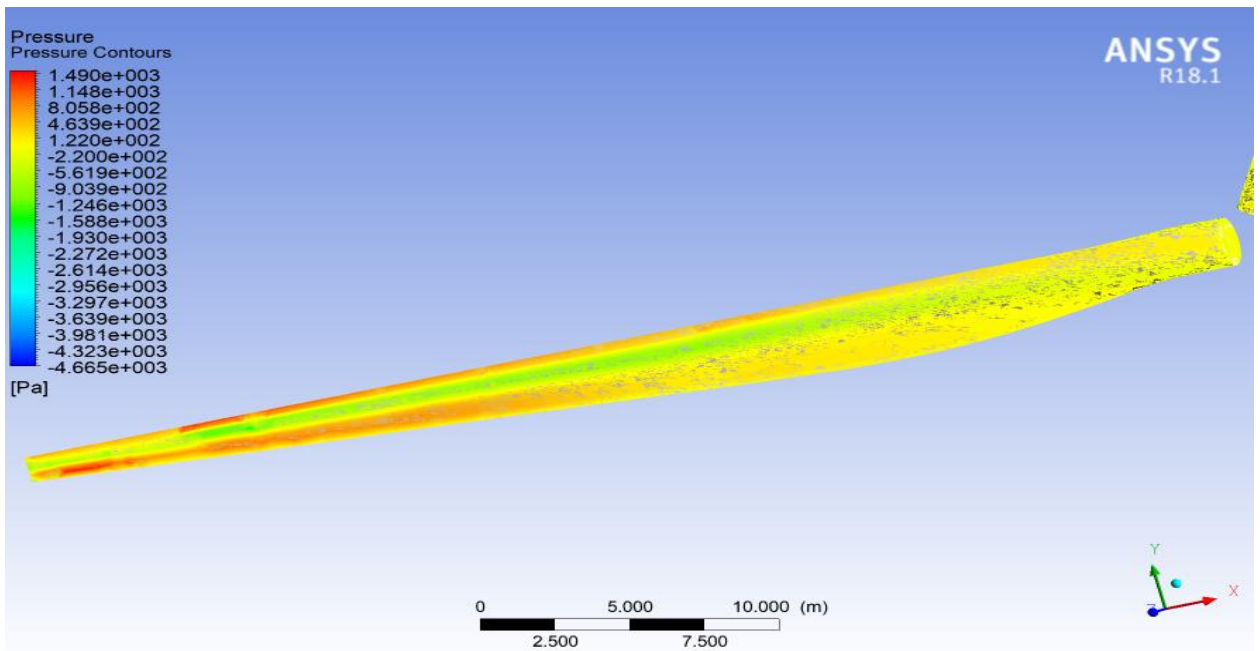


Fig A.20: Pressure contour

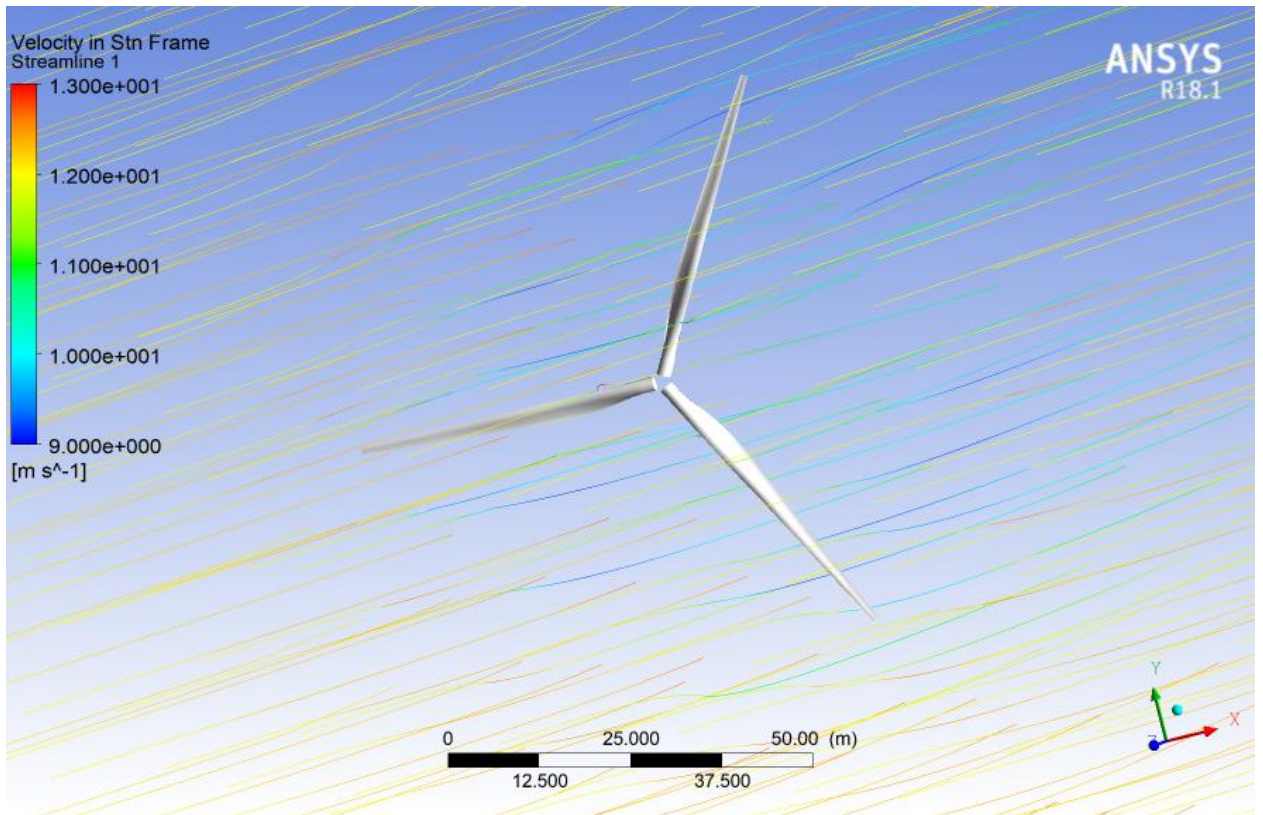


Fig A.21: Velocity streamline

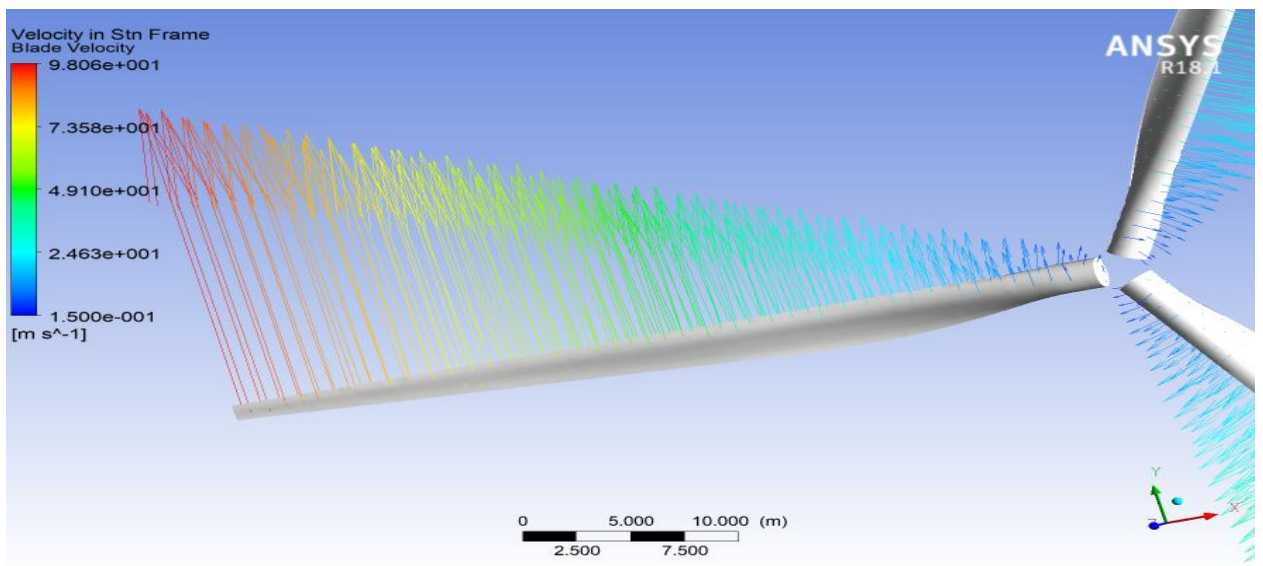


Fig A.22: Blade velocity vector

5. Wind Turbine Blade FSI (FEA)

The pressures on the wetted areas of the blade are passed as pressure loads to ANSYS Mechanical to determine stresses and deformations on the blade.

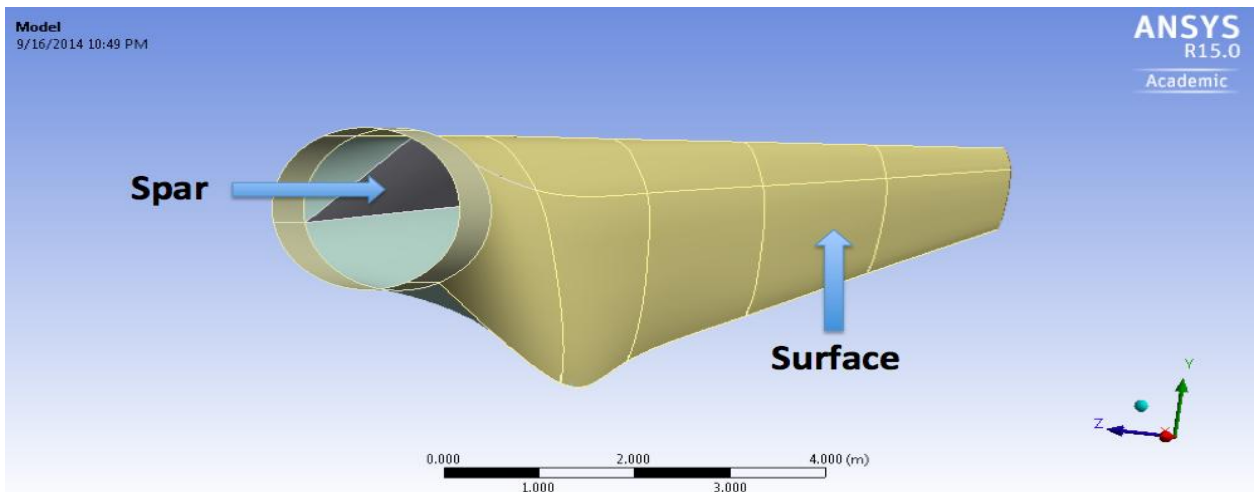


Fig A.23: CAD geometry

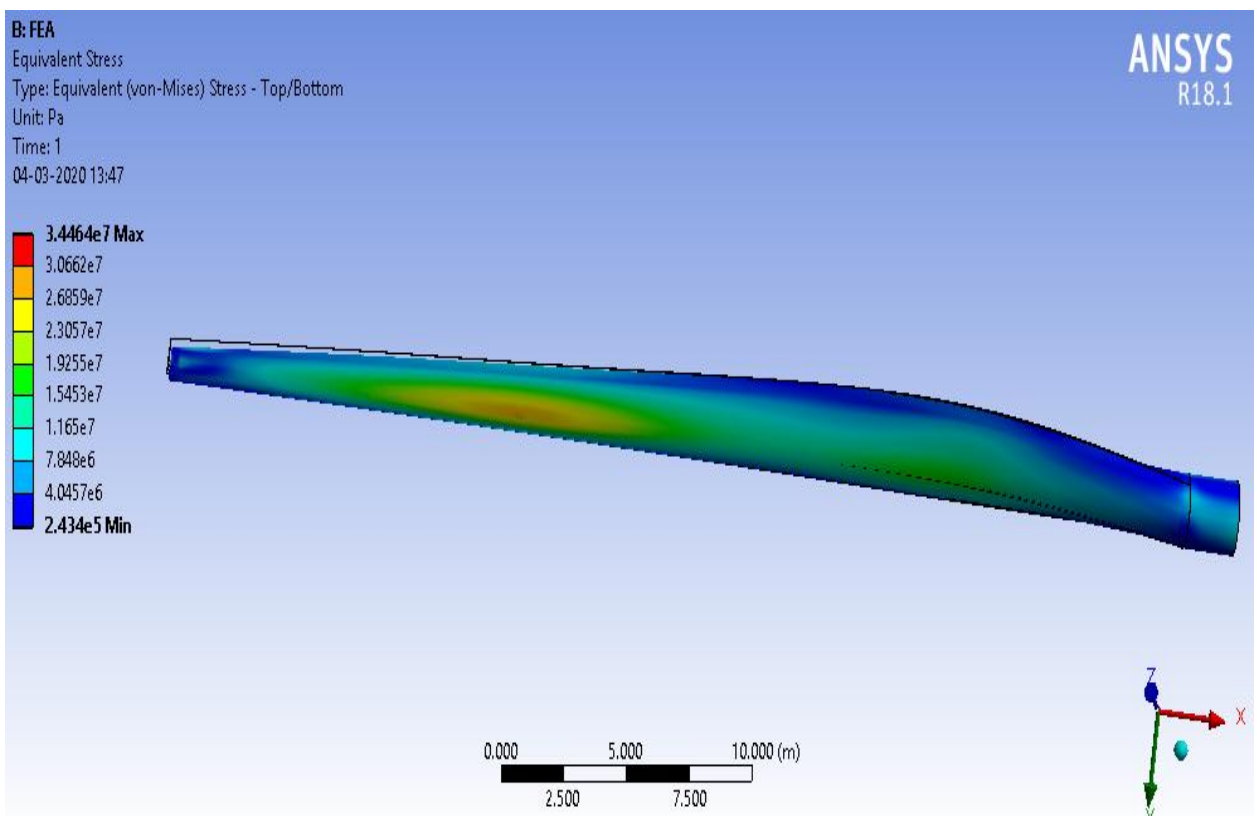


Fig A.24: Equivalent von mises stress contour

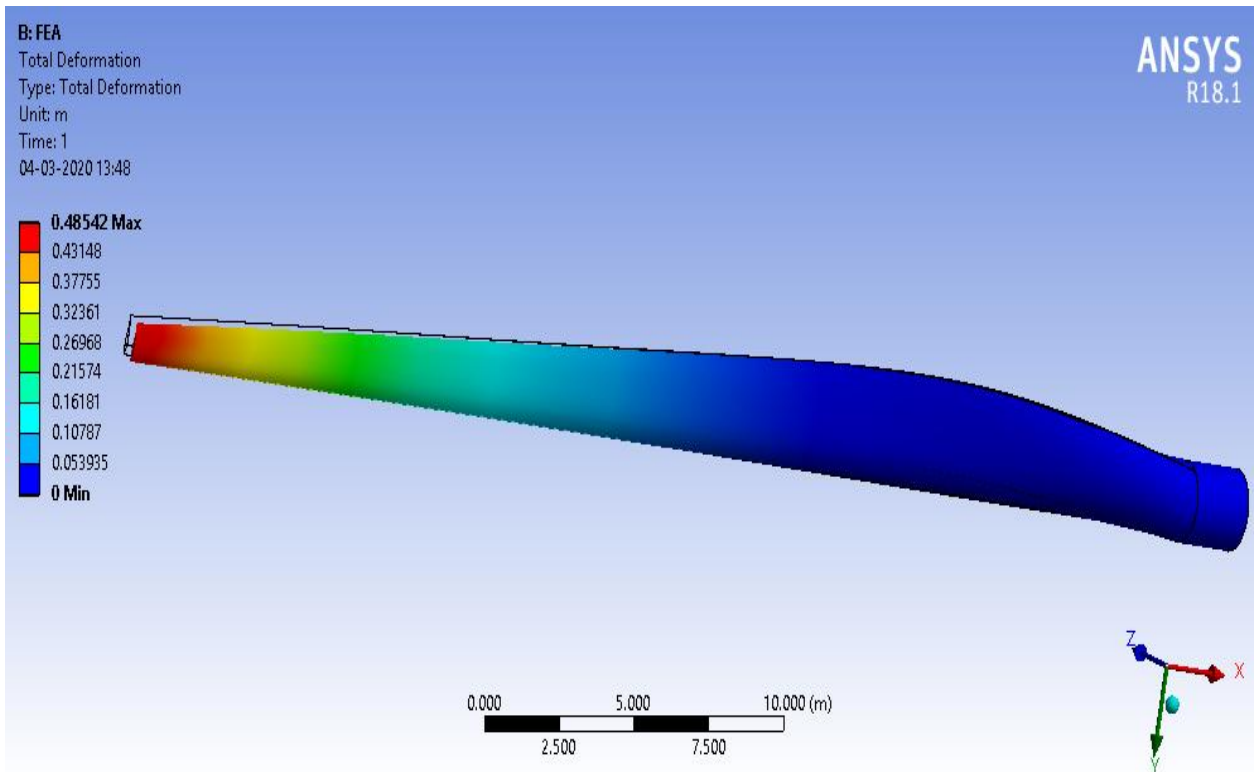


Fig A.25: Total deformation contour

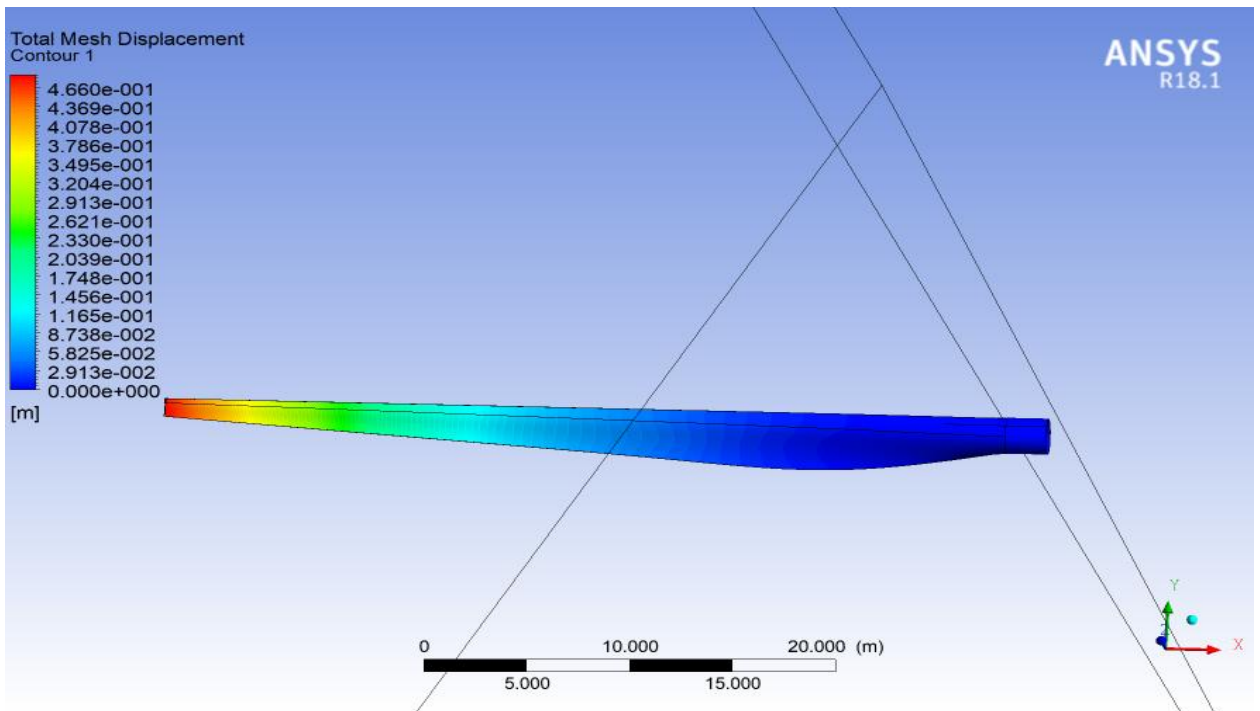


Fig A.26: Total mesh displacement contour

6. 2D Steady Laminar Convection

A fluid enters a pipe of radius 0.06 meters at a constant velocity of 0.1 m/s. The fluid has a density of 1.2 kg/m^3 , a thermal conductivity of 0.02 W/mK , a specific heat of 1000 J/kgK , and a viscosity of $1.8 \times 10^{-5} \text{ kg/ms}$. The first 5.76 meters of the pipe are isothermal, held at 300 K . The remaining 2.88 meters of the pipe have a constant heat flux of 37.5 W/m^2 added at the wall.

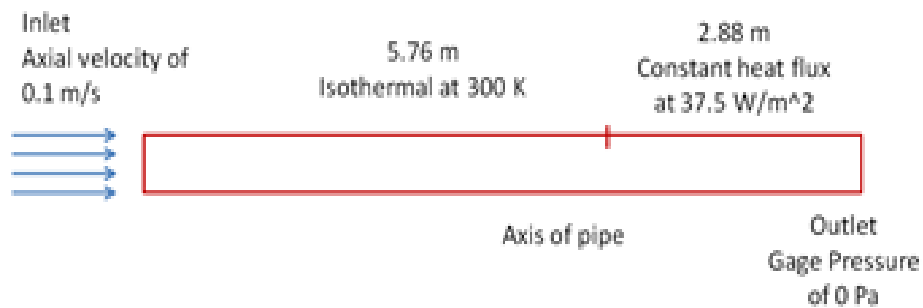


Fig A.27: Schematic diagram

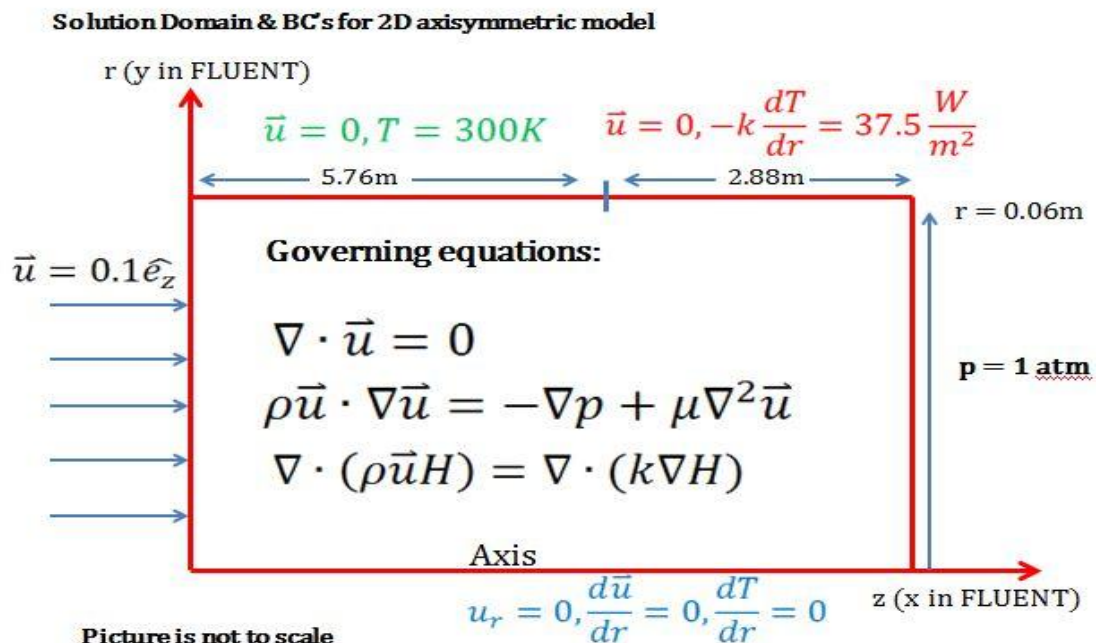


Fig A.28: Boundary condition

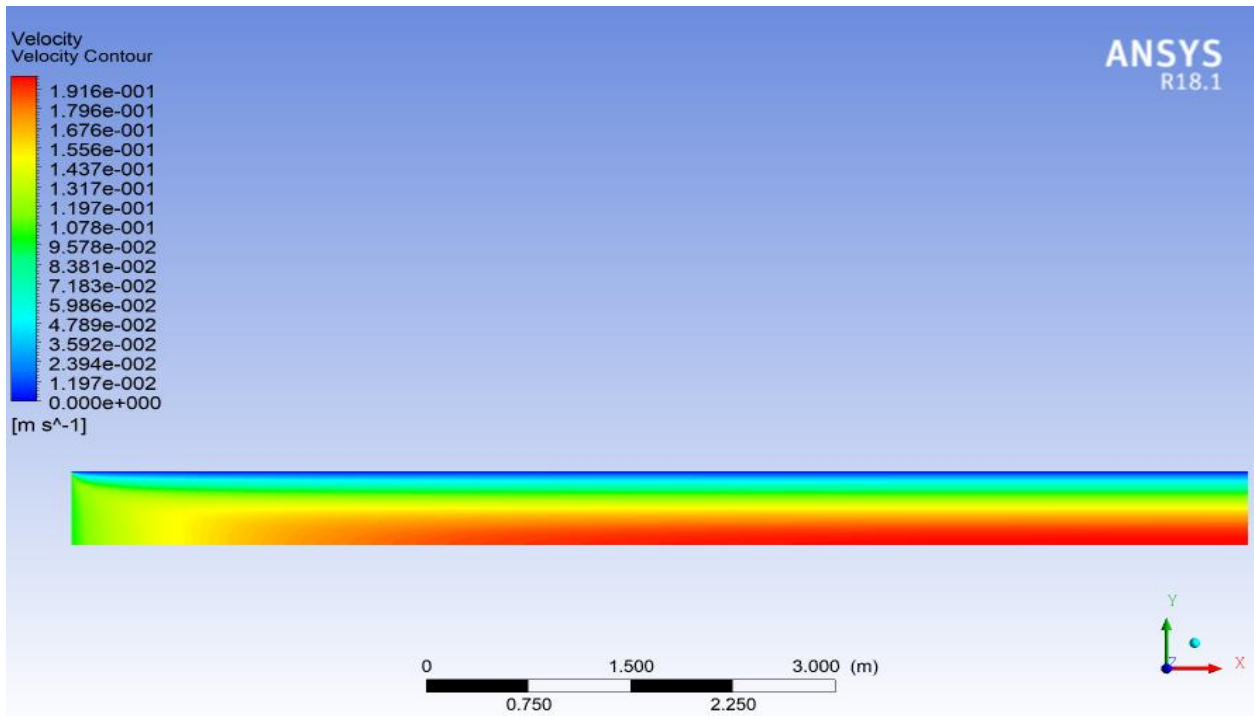


Fig A.29: Velocity contour on half cross section of the pipe

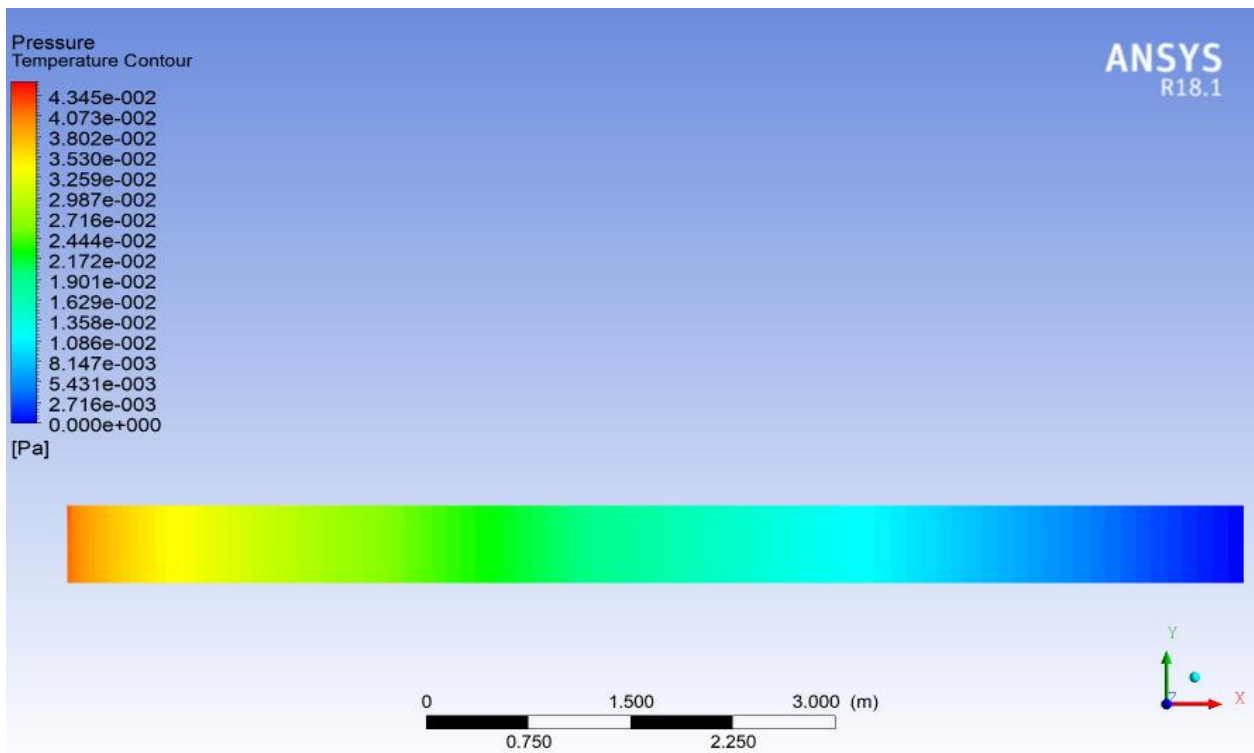


Fig A.30: Pressure contour

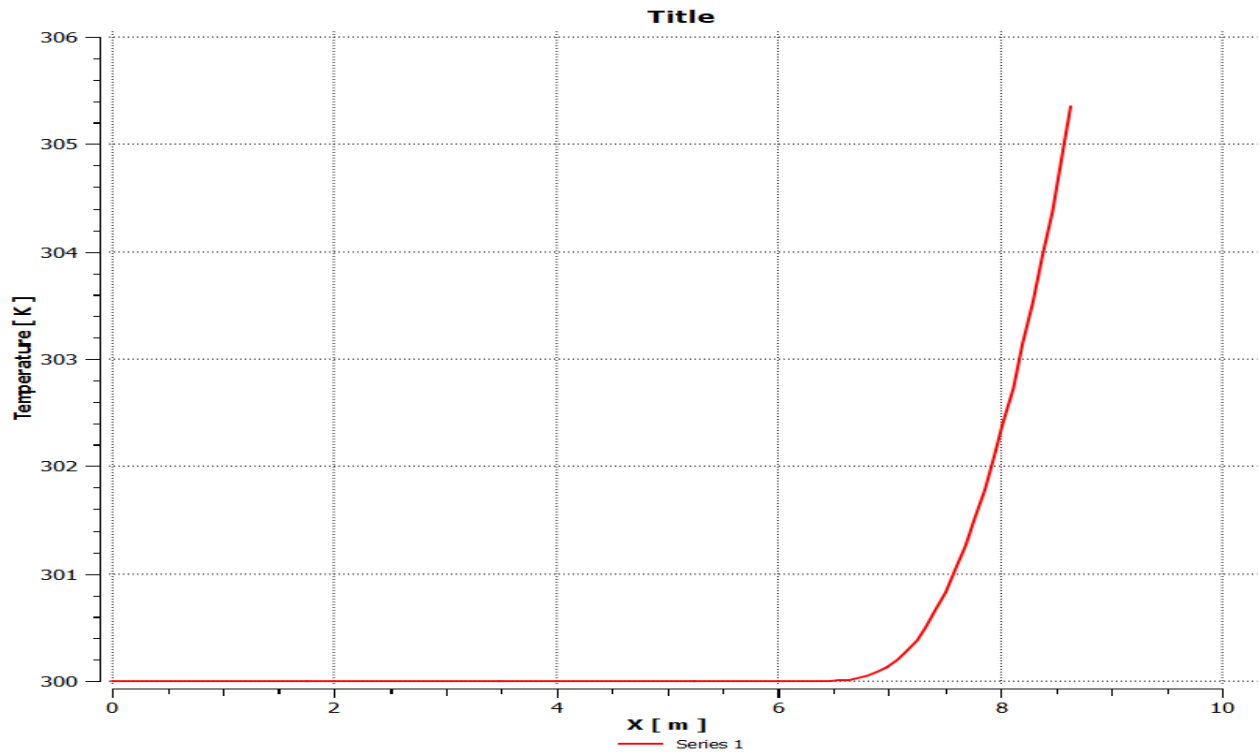


Fig A.31: Temperature along length of the pipe

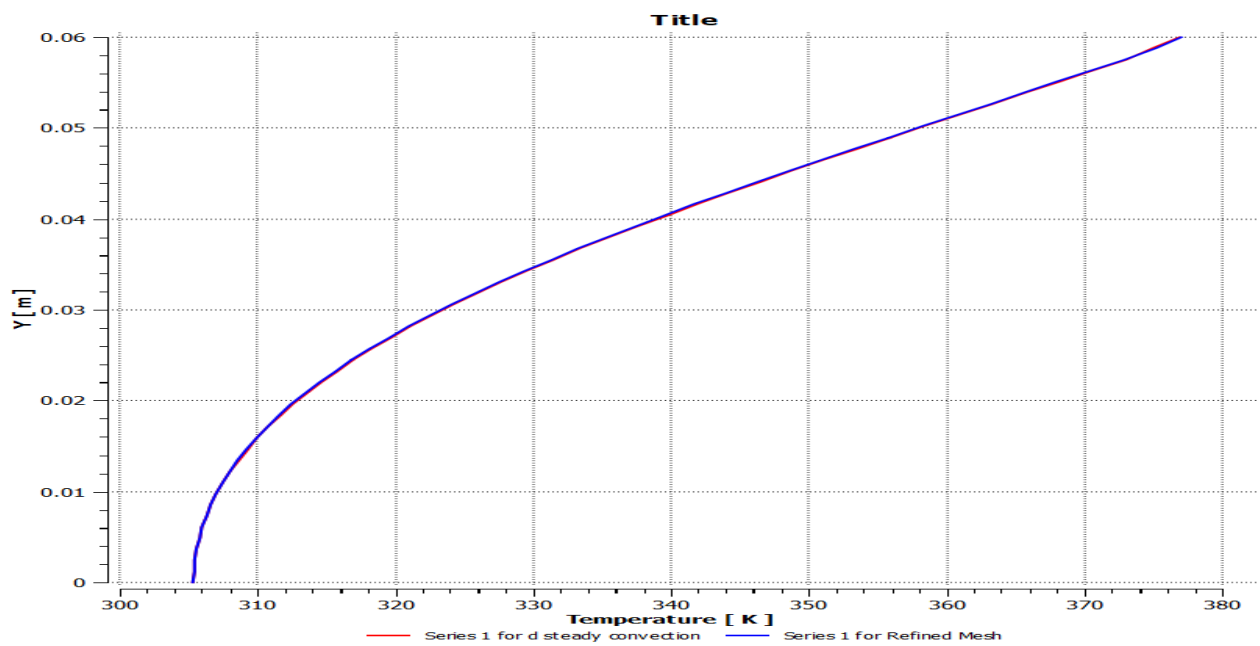


Fig A.32: Temperature across the cross section

7. Sudden Expansion in Laminar Pipe Flow

Consider a fluid flow through a sudden expansion in an axisymmetric pipe. The flow is laminar and axisymmetric. Due to symmetry, the computational domain covers only half of the pipe. BD is the axis of symmetry. The radius $R_1 = 1\text{ m}$ and $R_2/R_1 = 2$. $L_1/R_1 = 20$ and $L_2/R_2 = 50$. The inlet velocity at AB is uniform, $U_1 = 0.277\text{ m/s}$. The fluid exhausts into the ambient atmosphere which is at a pressure of 1 atm at CD. The density $\rho = 1\text{ kg/m}^3$, and the dynamic viscosity is: $\mu = 0.01\text{ kg/(ms)}$.

The Reynolds number Re at AB = $(2 R_1 \rho U_1) / \mu = 55.4$.

The computational domain consists of 2 parts: one for the small pipe and the other for the larger pipe. In the small pipe, the viscous boundary layer grows along the pipe wall starting at the inlet, and eventually a fully-developed velocity profile forms provided that the small pipe is long enough. As that flow passes through the expansion entrance, a recirculation zone forms in the corner of the larger pipe. The flow will become fully developed again after sufficient distance downstream from the recirculation zone.

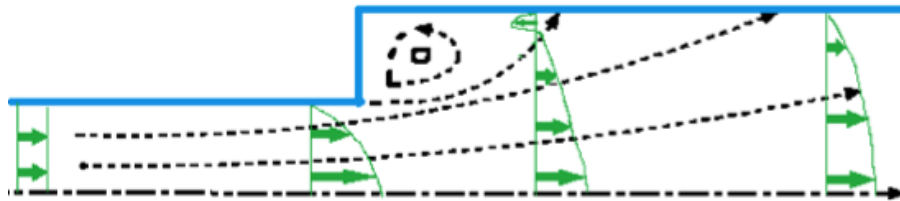


Fig A.33: Schematic diagram

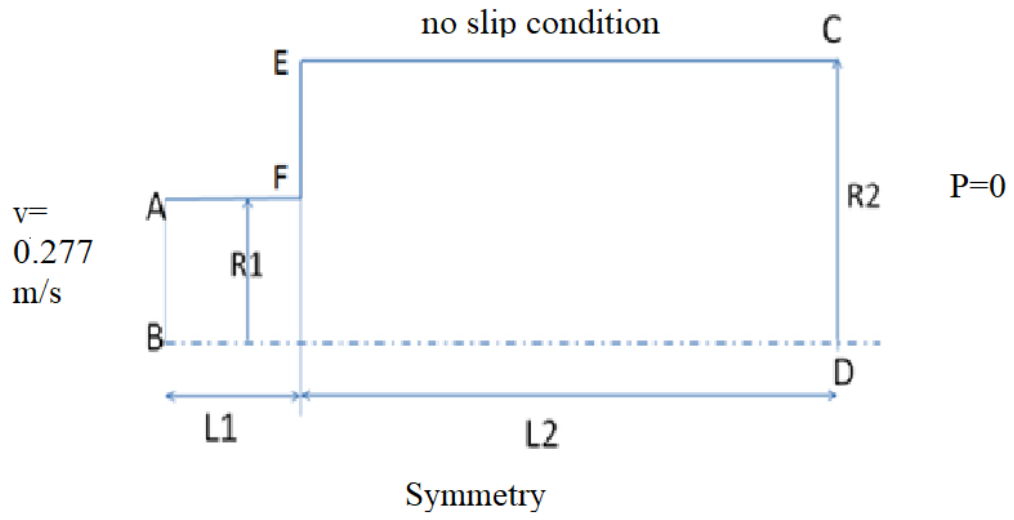


Fig A.34: Bounadry condition

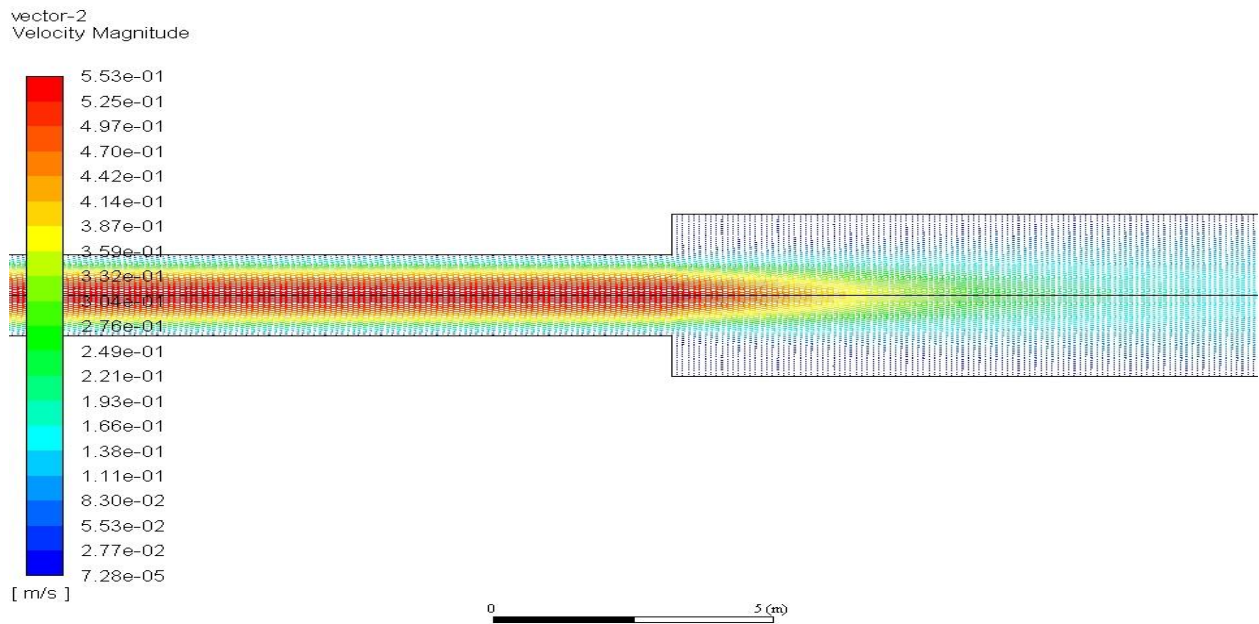


Fig A.35: Velocity vector

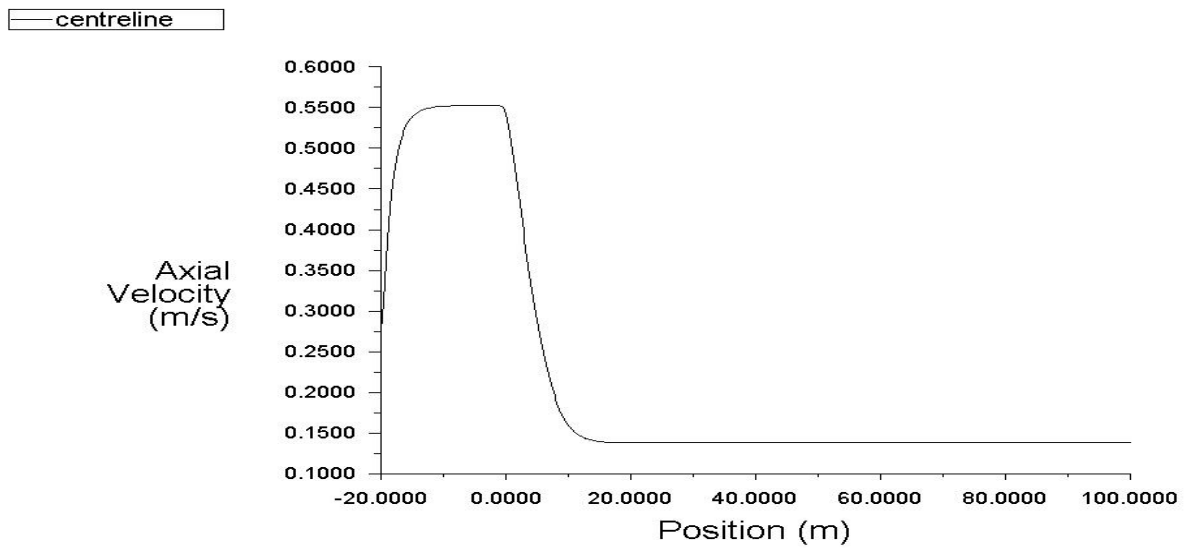


Fig A.36: Velocity along the length of pipe

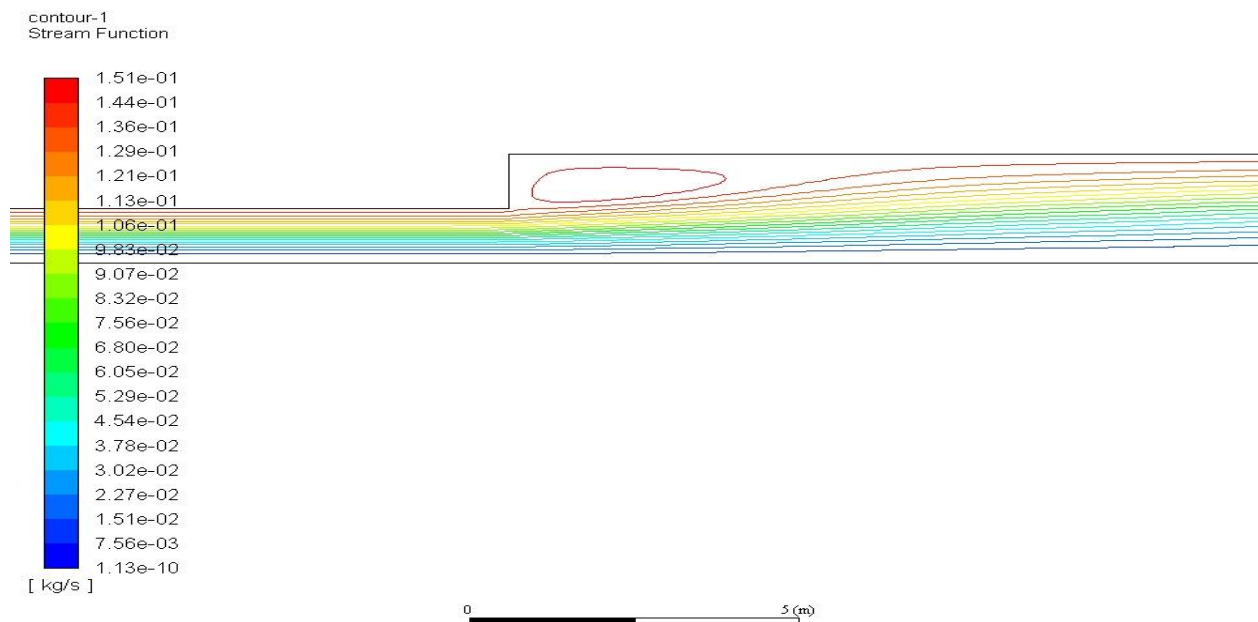


Fig A.37: Stream function across the pipe

8. Flow over an Aerofoil

A NACA 0012 Airfoil at a 6 degree angle of attack placed in a wind tunnel will be simulated in this problem.

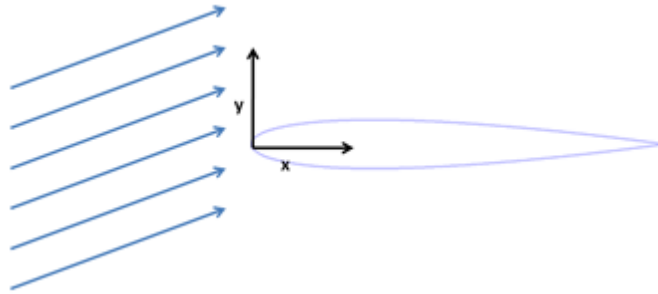


Fig A.38: Schematic diagram

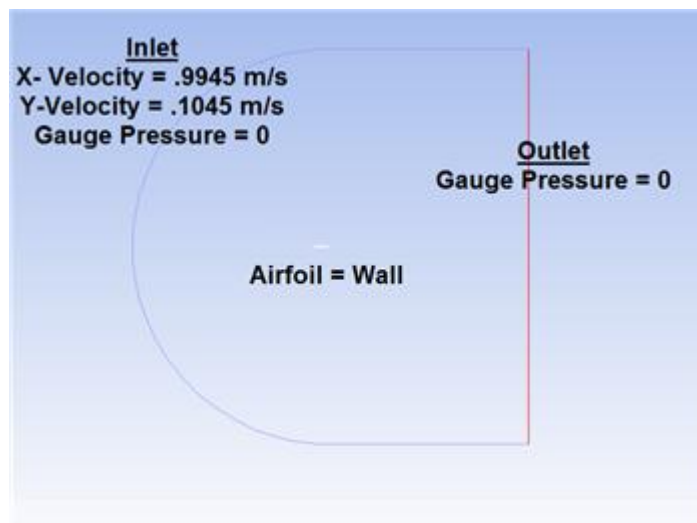


Fig A.39: Boundary condition

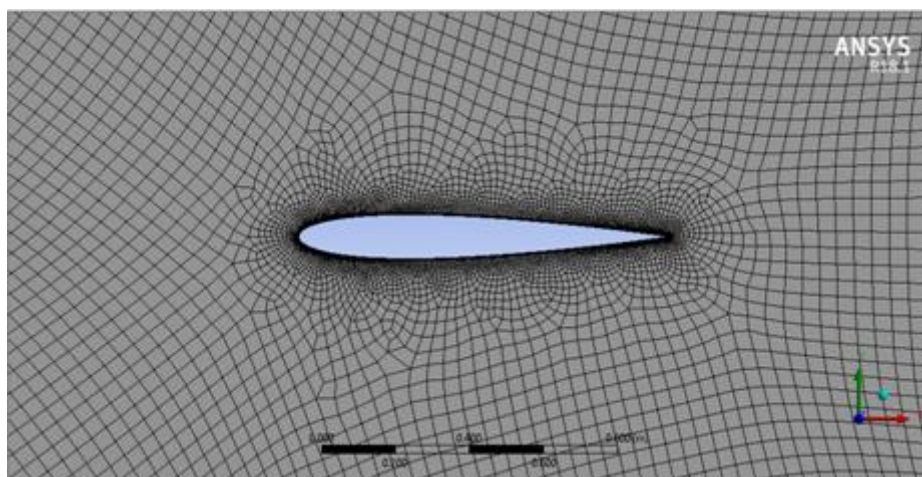


Fig A.40: Meshed model

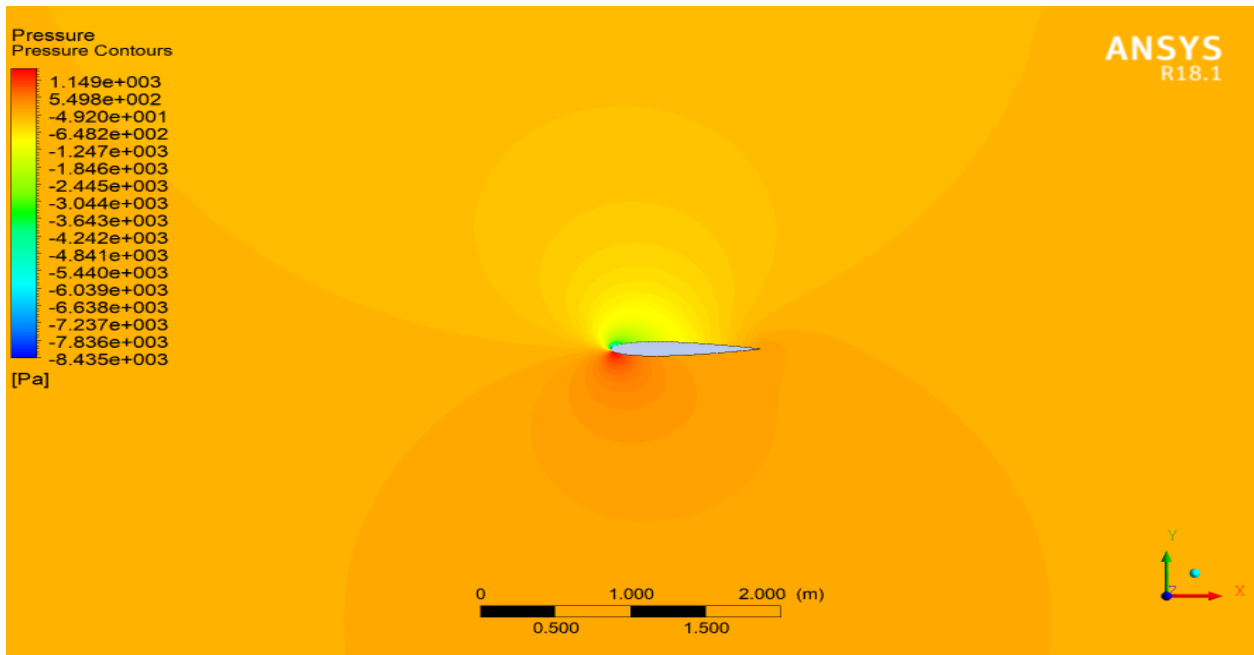


Fig A.41: Pressure contour

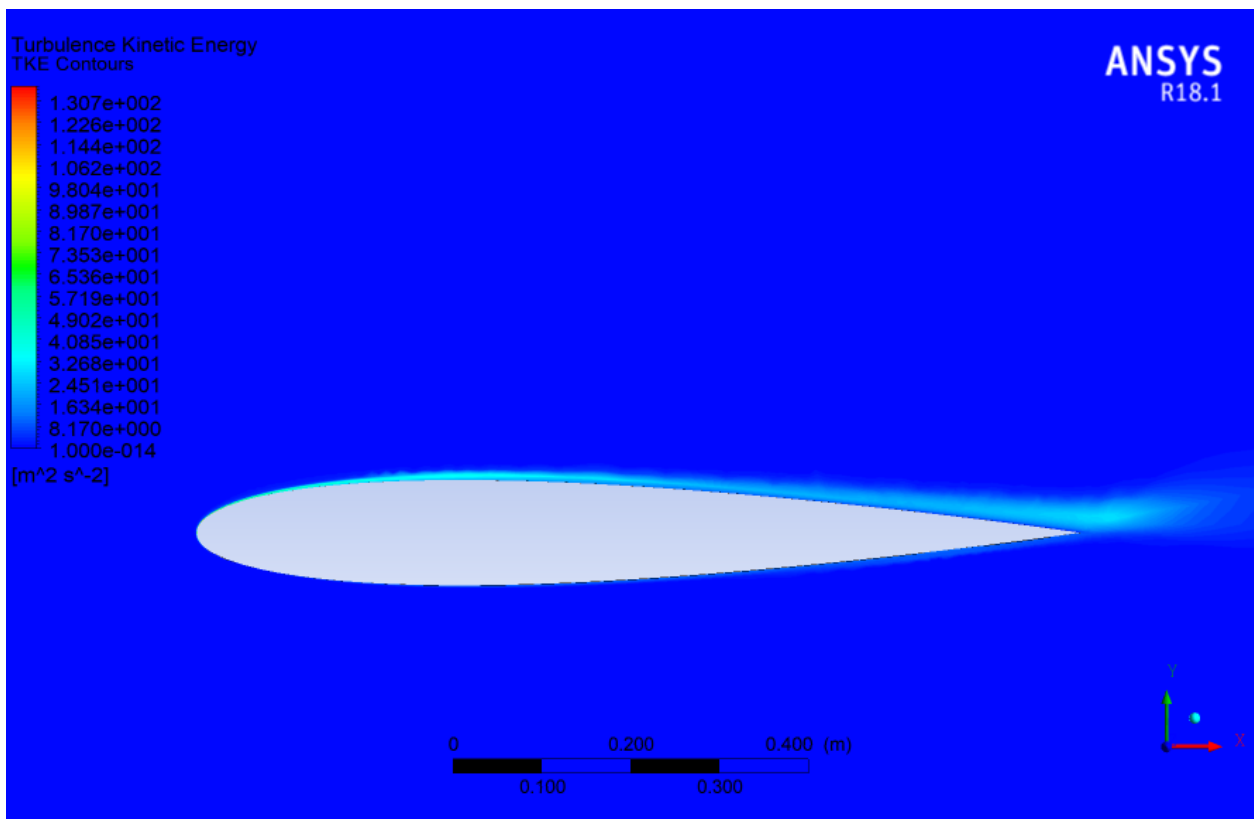


Fig A.42: Turbulence kinetic energy contour

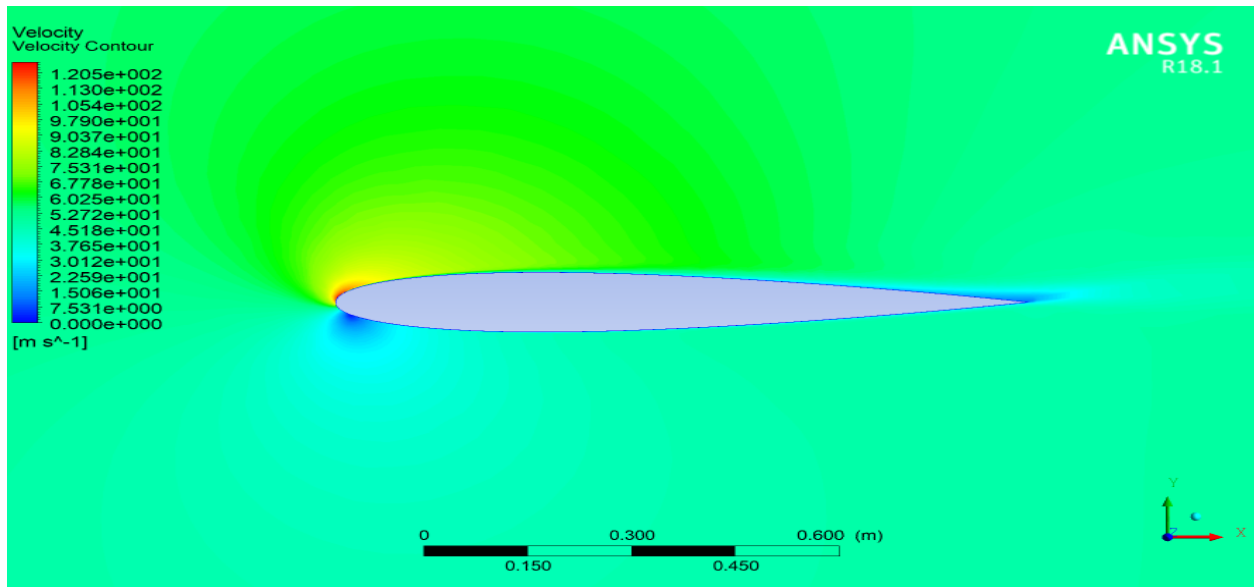


Fig A.43: Velocity contour

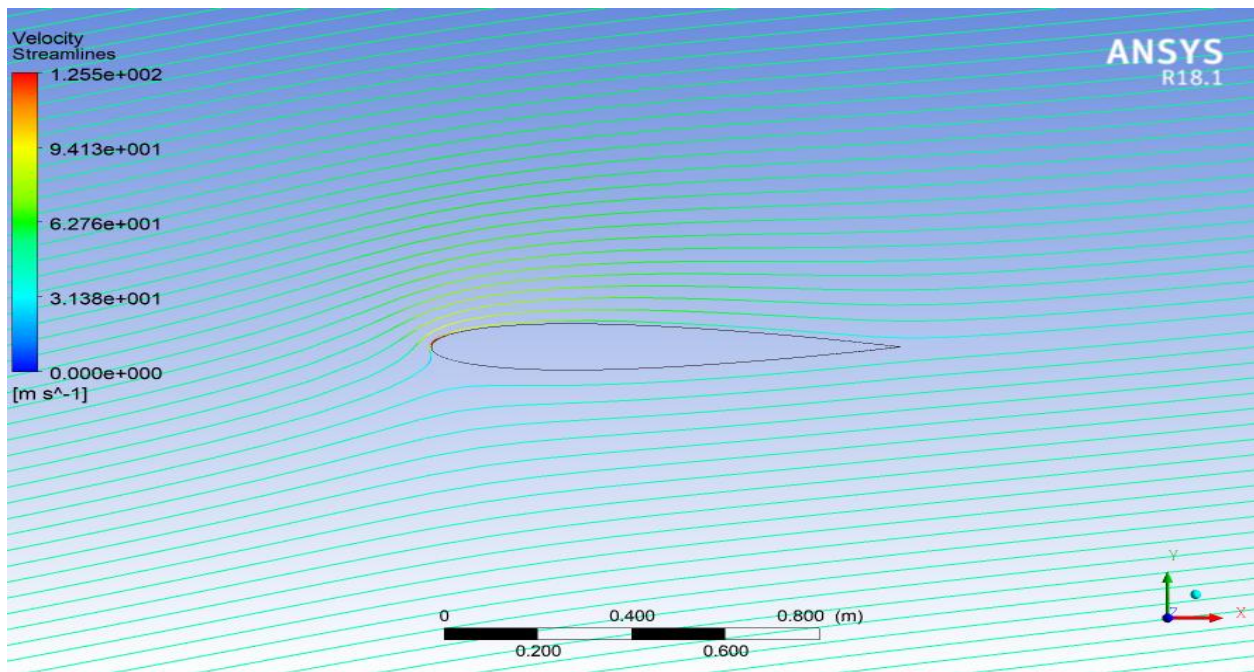


Fig A.44: Velocity streamline

A.2 Problems Solved and Important Concepts

This section consists of a table representing the problem solved and the important concepts learned in that problem. Apart from the above seven listed problems in the above section, seven more problems have been solved which have been stated in this table.

Table A.1: Problems vs. concepts

S.No.	Problem	Concepts Learned
1	Laminar pipe Flow	<ul style="list-style-type: none"> • Conservation of Mass • Conservation of Momentum • Drag Coefficient • No Slip Boundary Condition
2	Laminar Channel Flow	<ul style="list-style-type: none"> • Conservation of Mass • Conservation of Momentum • Drag Coefficient
3	Turbulent Pipe Flow	<ul style="list-style-type: none"> • Time Averaged Governing Equations • K-Epsilon Turbulence Model • Turbulent Viscosity • Skin Friction Coefficient • Non Dimensional Variables
4	Flat Plate Boundary Layer	<ul style="list-style-type: none"> • Boundary Layer Thickness • Flow Domain Control Volume • Normalized Velocity Variable • Overshoot in Velocity Profile • Blasius Boundary Layer Solution
5	Compressible Flow in a Nozzle	<ul style="list-style-type: none"> • Inviscid Flow • Conservation of Energy • Mach Number • Static Pressure
6	2D Steady Laminar Convection	<ul style="list-style-type: none"> • Convection Coefficient • Nusselt Number • Mixed Mean Temperature • Fourier's Law
7	Turbulent Forced Convection	<ul style="list-style-type: none"> • Fourier's Law • Wall Shear Force • Time Averaged Governing Equations

		<ul style="list-style-type: none"> • K-Epsilon Turbulence Model • Fanning Friction Factor
8	Supersonic Flow Over a Wedge	<ul style="list-style-type: none"> • Static Temperature • Theta-Beta-M Chart • Shock Angle • Far Field Boundary Condition • 2D Inviscid Compressible Flow Equations • Normal Shock Relations
9	Sudden Expansion in Laminar Pipe Flow	<ul style="list-style-type: none"> • Recirculation Zone • Stream Function
10	Steady Flow Over a Cylinder	<ul style="list-style-type: none"> • Streamlines
11	Unsteady Flow Over a Cylinder	<ul style="list-style-type: none"> • Navier Stokes Equation for Unsteady Flow • Lift Coefficient • Strouhal Number • Time Marching Solution
12	Flow Over an Aerofoil	<ul style="list-style-type: none"> • Angle of attack • Turbulence Kinetic Energy • Pressure Coefficient • Stagnation Point
13	Wind Turbine Blade FSI (CFD)	<ul style="list-style-type: none"> • Pitch Angle • Tip Speed Ratio • SST K-Omega Turbulence Model • Periodic Boundary Condition • Turbulent Intensity • Blade Velocity • Quality Parameters of Meshing
14	Wind Turbine Blade FSI (FEA)	<ul style="list-style-type: none"> • Spar of a Blade • Equivalent Von Mises Stress • Total Deformation • Reaction Force • Total Mesh Disp.

REFERENCES

- [1] Dr. Leonid Moroz, “Steam Turbine Thermal Stress Online Monitoring Technology”, 17th EPRI Steam Turbine Generator Workshop, Turbine Generator Users Group Meeting & Vendor Exhibition, Pittsburgh, PA August 15, 2017
- [2] Dr. Leonid Moroz, Glenn Doerksen, Fernando Romero, Dr. Roman Kochurov, Dr. Boris Frolov, “Integrated Approach for Steam Turbine Thermo-Structural Analysis and Lifetime Prediction at Transient Operations”, Proceedings of ASME Turbo Expo 2017: Turbomachinery Technical Conference and Exposition GT2017 June 26-30, 2017, Charlotte, NC, USA
- [3] Robust Design in Less Time INDUSTRIAL EQUIPMENT—TURBOMACHINERY
- [4] Pawel Borkowski, Dominik Glowacki, Agnieszka Nowakowska, Jakub Pawlicki, Janislaw Zwolinski, “FE Analysis of a Steam Turbine HP Rotor Blade Stage Concerning Material Effort, Dynamic Properties and Creep Damage Assessment”, Archive of Mechanical Engineering, VOL. LXIII 2016 Number 1
- [5] Michal Hoznedl and Ladislav Tajč, “Flow parameter changes in steam turbine 10 MW during start-up and heating”, AIP Conference Proceedings 1889, 020010 (2017); Published Online: 25 September 2017
- [6] Mujahid Badshah , Saeed Badshah , James VanZwieten , Sakhi Jan , Muhammad Amir and Suheel Abdullah Malik, “Coupled Fluid-Structure Interaction Modelling of Loads Variation and Fatigue Life of a Full-Scale Tidal Turbine under the Effect of Velocity Profile”, Energies 2019, 12, 2217; doi:10.3390/en12112217
- [7] “ANSYS R18.1 CFX-Pre User's Guide”, ANSYS R18.1, Inc. Southpointe 275 Technology Drive Canonsburg, PA 15317 , November 2011
- [8] “ANSYS R18.1 CFX Reference Guide”, ANSYS R18.1, Inc. Southpointe 275 Technology Drive Canonsburg, PA 15317, November 2013
- [9] “ANSYS R18.1 CFX-Solver Modeling Guide”, ANSYS R18.1, Inc. Southpointe 275 Technology Drive Canonsburg, PA 15317, November 2011
- [10] “ANSYS R18.1 CFX-Solver Theory Guide”, ANSYS R18.1, Inc. Southpointe 275 Technology Drive Canonsburg, PA 15317, November 2011
- [11] Mingyu Zhu, “Design and analysis of steam turbine blades”, IOP Conf. Series:

Journal of Physics: Conf. Series 1300 (2019) 012056, IOP Publishing doi:10.1088/1742-6596/1300/1/012056c

- [12] Somashekar S, Prem Chand R, Chandrashekar K M, Sachin D, “Design and Structural Analysis of Turbine Blades”, International Journal for Research in Applied Science & Engineering Technology (IJRASET) ISSN: 2321-9653, Volume 5 Issue VII, July 2017
- [13] D.Jojappa, K.Naresh babu, K.krishnaveni, “Fatigue Failure Analysis of steam Turbine Shaft using FEM Technique”, International Journal of Research and Innovation on Science, Engineering and Technology (IJRISET), Year of publication: 2016 Review Type: peer reviewed Volume: III, Issue : I
- [14] S.Naveen kumar, Konduru Sivaprasad Raju, S.Bhakiyaraja, Dr.D .Vijayaganapathy, “Static and Design Analysis of a Steam turbine Blade”, International Journal of Pure and Applied Mathematics, Volume 120 No. 6 2018, 3989-3996
- [15] Ms. Mohini R. Kolhe, Prof. A. D. Pachchhao, Prof. H.G.Nagpure, “Thermal stress Analysis in Steam Turbine Rotor-A Review”, IOSR Journal of Mechanical and Civil Engineering (IOSR-JMCE) e-ISSN: 2278-1684, p-ISSN: 2320-334X PP 83-86
- [16] Kumar Kenche Gowda and Santhosh M. Kumar, “Avoiding Stressed-Out Steam Turbines”, Triveni Engineering and Industries Ltd and Ansys R18.1 India
- [17] F Ogunbiyi , S A Salifu, T Jamiru, , E R Sadiku, O T Adesina, “Thermo-mechanical simulation of steam turbine blade with spark plasma sintering fabricated Inconel 738LC superalloy properties”, Conference of the South African Advanced Materials Initiative (CoSAAMI 2019) IOP Conf. Series: Materials Science and Engineering655 (2019) 012046, IOP Publishing doi:10.1088/1757-899X/655/1/012046
- [18] Tulsidas.D, Shantharaja.M, Bharath..V.G, “Life Estimation of a Steam Turbine Blade using Low Cycle Fatigue Analysis”, International Conference on Advances in Manufacturing and Materials Engineering, AMME 2014
- [19] Mali, S.D., Rathod, G.P, Joshi, D.H., “Start-up Analysis of 125MW Steam Turbine at Different Condition”, International Journal of Advance Engineering and Research Development Volume 2,Issue 12,December -2015
- [20] Iroizan Adasi Ubulom, “Fluid-structure and Thermal Interactions Modelling for an HP Turbine Blade Fatigue Life Evaluation”, School of Engineering and Information Technology, UNSW Canberra

- [21] Chi-Loong Chow, “Computation of Transient Temperatures and Stresses in Steam Turbine Rotors”, May, 1965, Mechanical Engineering Department, Imperial College of Science and Technology, London.
- [22] Harshit Sharma, Hrishikesh Mishra, Madhav Gupta, Neelam Baghel, “Demonstrating and Analysis of Turbine Blade”, International Journal of Recent Technology and Engineering (IJRTE) ISSN: 2277-3878, Volume-8, Issue-1, May 2019
- [23] Ratna Burugu, Vallem Kiran Kumar, “Analysis of Steam turbine Blade and Shaft Assembly using Coating Materials”, International Journal of Research and Innovation, Volume-4/Issue-2/IJRI-04-120
- [24] Majid Reza zadeh Reyhani, Mohammad Alizadeh, Alireza Fathi, Hiwa Khaledi, “Turbine blade temperature calculation and life estimation-a sensitivity analysis”, Propulsion and Power Research, 2013
- [25] Mariusz Banaskeiwicz, “Steam turbines start-ups”, Transactions of the Institute of Fluid-Flow Machinery, No. 126, 2014, 169–198
- [26] Mariusz Banaskeiwicz, Wojciech Radulski, Krzysztof Dominiczak, “Advanced lifetime Assessment of Steam Turbine Components based on Long Term Operating Data”, Archive of mechanical Engineering, VOL.LXV 2018 Number4
- [27] Mariusz Banaskeiwicz, “Numerical Modeling of Cyclic Creep-Fatigue Damage Development for Lifetime Assessment of Steam Turbine Components”, <https://www.intechopen.com/books/thermal-power-plants-new-trends-and-recent-developments/numerical-modeling-of-cyclic-creep-fatigue-damage-development-for-lifetime-assessment-of-steam-turbine>
- [28] Donghuan Liu, Haisheng Li and Yinghua Liu, “Numerical Simulation of Creep Damage and Life Prediction of Superalloy Turbine Blade”, Hindawi Publishing Corporation Mathematical Problems in Engineering Volume 2015, Article ID 732502, 10 pages
- [29] Sushila Rani, “Failure Analysis of First Stage Fluid Turbine Blade”, Mechanical, Production & Industrial and Automobile Engineering Department, Delhi Technological University, Delhi, August 2017
- [30] Gordana Baki, Vera Šijačković, Miloš Đukić, Bratislav Rajčić, Marko Tasić, “Remaining Life Assessment of a High Pressure Turbine Casing in Creep and Low Cycle Service regime” THERMAL SCIENCE: Year 2013, Vol. 17, Suppl. 1, pp. S127-S138

- [31] B.V. Ilchenko, R.R. Yarullin, A.P. Zakharov , R.Z. Gizzatullin, “Residual life prediction of power steam turbine disk with fixed operating time”
- [32] Mior Azman Meor Said, Muhammad Hafizuddin Osman, Puteri Sri Melor Megat Yusoff, Shaharin Anwar Sulaiman and Syed M Afdhal Syed Ahmed Ghazali, “ Determination of Remaining Useful Life of Fluid Turbine Blade”, MATEC Web of Conferences38, 01011 (2016) , DOI: 10.1051/mateconf/21063801011
- [33] Munson, Bruce Roy, T. H. Okiishi, and Wade W. Huebsch. "Turbomachines." Fundamentals of Fluid Mechanics. 6th ed. Hoboken, NJ: J. Wiley & Sons, 2009
Stodola, Aurel, “Steam and Fluid Turbines: With a Supplement on the Prospects of the Thermal Prime Mover”, McGraw-Hill, 1927
- [34] Bhagi LK, Rastogi V, Gupta P, “Study of Corrosive Fatigue and Life Enhancement of Low Pressure Steam Turbine Blade using Friction dampers”, Journal of Mechanical Science and Technology, **31**: 17–27. doi:10.1007/s12206-016-1203-5 , 2017
- [35] Abu A.O., Eshati S., Laskaridis P., Singh R.: Aero-engine turbine blade life assessment using the Neu/Sehitoglu damage model, International Journal of Fatigue, 61, 2014, 160-169
- [36] Ritesh Patil. (2017, September 22). Thermo Mechanical fatigue Lecture [Video]. YouTube.
https://www.youtube.com/watch?v=8X_wsocvNuM&list=WL&index=117&t=0s
- [37] Saud T.Al Jadir. (2019, September 12). Turbine Blade/Heat Transfer Analysis By Using Fluid-Solid Interfaces with ANSYS R18.1 CFX [YouTube].
<https://www.youtube.com/watch?v=zvpt9PjterM>
- [38] Reina Trevino. (2019, May 19). Analysis of a Fluid Turbine Blade with Nb5Si3 [YouTube]. <https://www.youtube.com/watch?v=IBOt7vqM4Nc>
- [39] KRISHNA.SUSHMITHA Aeronautical Engineering. (2019, May 9).
<https://www.youtube.com/watch?v=b3YG165celM&pbjreload=101>
- [40] Ravi Kumar (Steam and Fluid power Systems). (2017, Feb 20). Steam and Fluid Power systems (Lecture 21-30) [YouTube].
<https://www.youtube.com/channel/UCx1eYCS080c5r4Z4nghCwzQ>
- [41] Bhaskar Roy (nptelhrd). (2015 mar 12). Mod-01 Lec-28 Turbine Blade Cooling technologies [YouTube].
<https://www.youtube.com/watch?v=knnNYBZbjPw&list=PLbMVogVj5nJSXjTminozHE>

[FZJkN_ojx_e&index=29&t=0s](#)